Graduate Theses, Dissertations, and Problem Reports

2022

Amelioration of Mitochondrial Bioenergetic Dysfunction in Diabetes Mellitus: Delving into Specialized and Non-specific Therapeutics for the Ailing Heart

Andrya Jean Durr
West Virginia University, ajdurr@hsc.wvu.edu

Follow this and additional works at: https://researchrepository.wvu.edu/etd

Part of the Cardiovascular Diseases Commons, Exercise Physiology Commons, Molecular Biology Commons, Molecular Genetics Commons, and the Nutritional and Metabolic Diseases Commons

Amelioration of Mitochondrial Bioenergetic Dysfunction in Diabetes Mellitus: Delving into Specialized and Non-specific Therapeutics for the Ailing Heart

Andrya Jean Durr

Dissertation submitted to the School of Medicine at West Virginia University

in partial fulfillment of the requirements for the degree of

Doctor of Philosophy in
Exercise Physiology; Cardiovascular and Metabolic Diseases

John Hollander, Ph.D., Chair
Mark Olfert, Ph.D.
Emidio Pistilli, Ph.D.
Paul Lockman, Ph.D.
David Klinke, Ph.D.

Department of Human Performance, Division of Exercise Physiology

West Virginia University, Morgantown, WV, USA
2022

ABSTRACT

Amelioration of Mitochondrial Bioenergetic Dysfunction in Diabetes Mellitus: Exploring Specialized and Non-specific Therapeutics for the Ailing Heart

Andrya Jean Durr

Morbidity and mortality of the diabetic population is influenced by many confounding factors, but cardiovascular disease (CVD), remains the leading cause of death. Mitochondrial dysfunction is central in the development of cardiac contractile dysfunction, with decreased mitochondrial bioenergetic function, increased dependence on free fatty acid utilization, and a decrease in glucose utilization having been shown to contribute to contractile dysfunction. Strategies targeting the amelioration of mitochondrial bioenergetic function are attractive for limiting diabetes-induced heart failure, and preserving health-span. The goals of this dissertation were to assess two mitochondrial-centric approaches for the amelioration of mitochondrial and cardiac contractile dysfunction in diabetes mellitus. Our laboratory previously identified microRNA-378a (miR-378a) as a regulator of mitochondrially encoded ATP synthase membrane subunit 6 (mt-ATP6) mRNA, a component of the ATP synthase F_0 complex. More recently, a second class of non-coding RNAs, long non-coding RNAs (lncRNA), have been proposed to regulate microRNA activity. LncRNA potassium voltage-gated channel subfamily Q member 1 overlapping transcript 1 (Kcnq1ot1), is predicted to bind miR-378a. Chapter 2 aimed to determine if inhibition of miR-378a could ameliorate cardiac contractile dysfunction in type 2 diabetes mellitus (T2DM), and to ascertain whether Kcnq1ot1 interacts with miR-378a to impact ATP synthase functionality by preserving mt-ATP6 levels. MiR-378a genomic loss, and inhibition by Kcnq1ot1, improved ATP synthase functionality, and preserved cardiac contractile function. Together, Kcnq1ot1 and miR-378a may act as constituents in an axis that regulates mt-ATP6 content. By acting as therapeutic targets, their manipulation may provide benefit to ATP synthase functionality in the heart during T2DM. A second method of ameliorating mitochondrial dysfunction is mitochondrial transplantation. Current literature suggests that mitochondrial transplantation may be of benefit to the diabetic heart. Chapter 3 aimed to assess mitochondrial transplantation as a prophylactic method of treating mitochondrial dysfunction in the diabetic heart. Following mitochondrial transplantation *in vivo* using ultrasound-guided echocardiography, mitochondrial signal was detectable in at least 30% of the left ventricle myocardium, primarily within and near injection sites. Poor mitochondrial distribution indicated a need for a more focused injection strategy aimed at targeting a cardiac region or segment of interest. Speckle tracking echocardiography has been utilized to evaluate spatial and progressive

alterations in the diabetic heart independently, but the spatial and temporal manifestation of cardiac dysfunction remain elusive. Therefore, the objectives of Chapter 4 were to elucidate if cardiac dysfunction associated with T2DM occurs spatially, and if patterns of regional or segmental dysfunction manifest in a temporal fashion. Non-invasive echocardiography datasets were utilized to segregate mice into two pre-determined groups, wild-type and *Db/Db*, at 5, 12, 20, and 25 weeks. Machine learning was used to identify and rank cardiac regions, segments, and features by their ability to identify cardiac dysfunction. Overall, the Septal region, and the AntSeptum segment, best represented cardiac dysfunction associated with the diabetic state at 5, 20, and 25 weeks, with the AntSeptum also containing the greatest number of features which differed between diabetic and non-diabetic mice. These results suggested that cardiac dysfunction manifests in a spatial and temporal fashion, and is defined by patterns of regional and segmental dysfunction in the diabetic heart. Further, the Septal region, and AntSeptum segment, may provide a locale of interest for therapeutic interventions aimed at ameliorating cardiac dysfunction in T2DM.

DEDICATION

To my family and my love:

Without your faith and confidence in my ability to push myself beyond my comfort zone again and again, this dissertation would be just a dream. A tremendous amount of thanks for always being there to support me.

ACKNOWLEDGEMENTS

They say it takes a village, but it was more like an army. I want to take a moment to thank all those who helped me along the way.

Firstly, I wish to thank my laboratory mentor and committee chair, John M. Hollander, Ph.D., for his guidance and support to help me develop both personally and professionally as a scientist. I would also like to thank my committee members: Mark Olfert, Ph.D., Emidio Pistilli, Ph.D., Paul Lockman, Ph.D., and David Klinke, Ph.D., for continuously asking the hard questions and forcing me to delve deeper into my work.

To the current and previous laboratory members, we spent a lot of time in the weeds, but we had some really great times too. Dr. Quincy Hathaway and Dr. Danielle Shepherd, you guys made my early time in the lab fun and full of adventure. I never expected to have such good friends, or to have the adventures we did. Danielle, you're truly a friend for life and I am beyond grateful for our friendship. Dr. Amina Kunovac, when you joined the lab, I was thrilled to have another woman around, thank you for your friendship and support, and always being willing to help out when I needed another pair of eyes. Andrew Taylor, thank you from the bottom of my heart for your help in finishing the miR-378a/Kcnq1ot1 project, you may or may not know how much help you were my last few years. Mark Pinti, you were the man with a mitochondrial function plan, thank you for your help in running my mitochondrial assays and being there to help tease out experimental details. Saira Rizwan and Ethan Meadows, you guys have been wonderful colleagues and friends, I wish you all luck.

I would also like to acknowledge Rebecca A. Radabaugh, HT (ASCP) QIHC, Robert L. Crickard, MT (ASCP), Jacqueline Karakiozis, BS, MLT (ASCP), and Deborah Mclaughlin, HT (ASCP) of the Electron Microscopy, Histopathology and Tissue Bank Core Research Facility and the Department of Pathology at WVU

for their expertise in sample processing and imaging, and their help with experimental design.

I wish to thank the ladies of the Animal Models and Imaging Facility and Microscope Imaging Facility, Sarah McLaughlin and Dr. Amanda Ammer, for all of your help with my experiments. Even more so, thank you for all the times I was able to hide in your office, chat, and drink some coffee. Those were some of my favorite times, and helped me to keep going when I got stuck.

Thank you to Dr. Ariel Thomas and Anna Korol, for being such wonderful and supportive friends. Ariel, you are one of the most genuine, hardworking people I have ever met. Here's to many more years of friendship, and a lot more free time. Anna, I am so glad that you rotated in my lab and that I have got to know you. You are one of my dearest friends. I can't wait to see what you come up with during your time at WVU.

Finally, thank you to my fiancé and my family for your love and support. Thank you for listening to my experiment woes over and over again, but also celebrating the wins with me, even when it was something as simple as a western blot. I could write three pages describing how much I appreciate all of you, but I don't think I will. I hope you all already know.

TABLE OF CONTENTS

Chapter 2: Specific Aim 1

Manipulation of the MiR-378a/mt-ATP6 Regulatory Axis Rescues ATP Synthase in the Diabetic Heart and Offers a Novel Role for LncRNA Kcnq1ot1

Chapter 3: Specific Aim 2

Chapter 4: Specific Aim 2

LIST OF TABLES

Supplemental Table S4.4: Performance of supervised machine learning SVM models for segmental datasets at 5, 12, 20, and 25 weeks of age.

LIST OF FIGURES

Chapter 2

PostWall, Anterior Free, and Posterior Free datasets at 5, 12, 20, and 25 weeks of age.

LIST OF ABBREVIATIONS AND DEFINITIONS

ATCC	American Type Culture Collection
AntFree	Anterior free segment
AntSeptum	Anterior septal segment
Ago2	Argonaute 2
BN-PAGE	Blue native polyacrylamide gel electrophoresis
CO	Cardiac output
CVD	cardiovascular disease
CD	Circumferential displacement
CS	Circumferential strain
CSR	Circumferential strain rate
CV	Circumferential velocity
ATP synthase	Complex V
CLIP	Cross-linked immunoprecipitation
Ct	Delta threshold
DCM	Diabetic cardiomyopathy
LVAW;d	Diastolic LV anterior wall thickness
LVPW;d	Diastolic LV posterior wall thickness
EF	Ejection fraction
ETC	Electron transport chain
FS	Fractional shortening
HR	Heart rate

HL-1-378a	HL-1 miR-378a overexpressing cell line
IHC	Immunohistochemistry
InfFreeWall	Inferior free segment
IFM	Interfibrillar mitochondria
KO	Knockout
LatWall	Lateral segment
LSD	Least significant difference
LV	Left ventricle
Kcnq1ot1	LncRNA potassium voltage-gated channel subfamily Q member 1 overlapping transcript 1
LD	Long diastolic
lncRNA	Long non-coding RNAs
LS	Long systolic
LVED;d	LV end-diastolic diameter
LVEV;d	LV end-diastolic volume
LVED;s	LV end-systolic diameter
LVEV;s	LV end-systolic volume
MALAT1	Metastasis associated lung adenocarcinoma transcript 1
miR	MicroRNA
miR-378a	microRNA-378a
mt-ATP6	Mitochondrially encoded ATP synthase membrane subunit 6

MI	Myocardial infarction
MPI	Myocardial performance index
ncRNA	Non-coding RNA
ND	Non-diabetic
NucDNA	Nuclear DNA
Neat1	Nuclear Enriched Abundant Transcript 1
PDCD4	Programmed Cell Death 4
PPAR	Peroxisome proliferator activator receptor
ppargc1b	Peroxisome proliferator-activated receptor gamma coactivator 1 beta
PostWall	Posterior segment
PostSeptal	Posterior septal segment
PGC-1	PPARγ coactivator-1
PWD	Pulse wave-doppler
RD	Radial Displacement
RS	Radial strain
RSR	Radial strain rate
RV	Radial velocity
RIPA	Radioimmunoprecipitation assay
RISC	RNA-induced silencing complex
SD	Short diastolic
SS	Short systolic
SSG	Short systolic global

STE	Speckle tracking strain-based echocardiography
SEM	Standard error of the mean
SV	Stroke volume
SSM	Subsarcolemmal mitochondria
SVM	Support vector machine
LVAW;s	Systolic LV anterior wall thickness
LVPW;s	Systolic LV posterior wall thickness
TE	Tris-EDTA
T1DM	Type 1 diabetes mellitus
T2DM	Type 2 diabetes mellitus
WVU	West Virginia University
WT	Wild-type
XIAP	X-linked inhibitor of apoptosis

LIST OF MULTIMEDIA OBJECTS AND FILES

Chapter 2

Supplementary Material: (http://doi.org/10.6084/m9.figshare.18940262)

Supplemental Data Methods:
(http://doi.org/10.6084/m9.figshare.18940262)

Supplemental Tables: (http://doi.org/10.6084/m9.figshare.18940262)

Supplemental Figures: (http://doi.org/10.6084/m9.figshare.18940262)

Un-edited Western blot images:
(http://doi.org/10.6084/m9.figshare.18940262)

Un-edited blue-native PAGE images:
(http://doi.org/10.6084/m9.figshare.18940262)

Chapter 3

Supplemental Video S3.1: Injection of mKate2 positive mitochondria into the left ventricular myocardial wall using ultrasound-guided echocardiography (https://figshare.com/s/48e1bcd943be9452c64c)

Supplemental Video S3.2: Video of HL-1 cardiomyocyte interactions with mKate2 positive mitochondria over a 24-hour period at 30-minute intervals (https://figshare.com/s/48e1bcd943be9452c64c)

Chapter 4

All datasets used for machine learning analyses and related code: (https://doi.org/10.5281/zenodo.6391011)

SPECIFIC AIMS

Cardiovascular disease (CVD) is the leading cause of mortality in the diabetic population, with diabetics having up to a four times greater risk of death from a cardiovascular event when compared to their healthy counterparts (1). Concomitantly, 322 billion dollars are spent on medical care for pre-diabetes and diabetes mellitus patients annually in the Unites States, as medical costs are estimated to be 2.3 times greater for those with diabetes mellitus than those without (2, 3). As diabetes mellitus incidence continues to grow exponentially, medical costs, reduced health-span, and increased risk of mortality will continue to rise as well (4). Diabetic patients experience a large number of macrovascular and microvascular complications, but CVD is the leading cause of mortality and can intensify other comorbidities. Decreases in mitochondrial bioenergetic function, increased dependence on free fatty acid utilization, and a decrease in glucose utilization have all been shown to contribute to the functional deficits observed in the diabetic heart (5-8).

Research focused on the prevention, management, and restoration of cardiac contractile function fills a ***critical need*** in the diabetic population by reducing the financial burden associated with management and treatment, preventing the development of cardiovascular dysfunction in those at risk, and improving health-span by improving health outcomes in those already afflicted. The current landscape of mitochondrially targeted therapeutics aimed at the diabetic heart are limited, and their advancement is necessary to improve the treatment of cardiac contractile and mitochondrial bioenergetic dysfunction. The studies outlined in this dissertation address these ***gaps in knowledge***. The studies outlined in *Specific Aim I* are designed to determine if loss or inhibition of microRNA-378a (miR-378a) can ameliorate mitochondrial bioenergetic and cardiac contractile dysfunction in the (type 2 diabetes mellitus) T2DM heart. The studies outlined in *Specific Aim II* are designed to determine the efficacy of mitochondrial transplantation as a method of mitochondrial bioenergetic rescue for

diabetes mellitus, in which mitochondrial transplantation can be achieved in a minimally invasive manner using ultrasound-guided injections, and enhanced using machine learning analysis to determine locales of interest. The ***long-term goals*** of this dissertation are to advance our knowledge of mitochondrially targeted therapeutics through the evaluation of non-coding RNA (ncRNA) targets and mitochondrial transplantation for the amelioration of reduced mitochondrial ATP generating capacity and cardiovascular contractile dysfunction in diabetes mellitus.

The ***objectives*** of this dissertation are to determine the efficacy of two mitochondrial-centric therapeutic approaches for their efficacy in the diabetic heart; (1) miR-378a inhibition and (2) mitochondrial transplantation. The ***central hypothesis*** of this dissertation is that both the inhibition of miR-378a, and mitochondrial transplantation may be two very different, yet conceivable methods of ameliorating mitochondrial bioenergetic dysfunction and cardiovascular contractile dysfunction in the diabetic heart. To test our central hypothesis, we propose two *Specific Aims:*

Specific Aim I: Determine whether loss of miR-378a restores ATP generating capacity of the type 2 diabetic heart through improved mitochondrial genome-encoded mt-ATP6 translation and ATP synthase functionality*.* Using a miR-378a knockout/*Db/Db* murine model and an *in vitro* model of miR-378a overexpression, we will test our ***working hypothesis*** that inhibition of miR-378a could ameliorate cardiac contractile dysfunction in T2DM through preservation of mitochondrially encoded ATP synthase membrane subunit 6 (mt-ATP6) and ATP synthase content and ATP synthase activity. Further, we will evaluate the role of long non-coding RNA (lncRNA) potassium voltage-gated channel overlapping transcript 1 (Kcnq1ot1) as a regulator of miR-378a, in which Kcnq1ot1 overexpression can influence miR-378a mediated downregulation of mitochondrial genome encoded protein mt-ATP6. *Specific Aim I* is focused at the molecular and genomic levels, where ncRNAs provide a wide array of potential therapeutic

targets for the treatment and preservation of cardiac contractile function. *Specific Aim I* includes three objectives:

1.1 Confirm the presence of the miR-378a/mt-ATP6 regulatory axis in the T2DM phenotype

1.2 Evaluate the impact of genomic loss of miR-378a on ATP synthase functionality and cardiac contractile dysfunction in a murine model of T2DM

1.3 Determine whether Kcnq1ot1 interacts with miR-378a in a sponging mechanism to influence mitochondrial genome-encoded mt-ATP6 and ATP synthase functionality.

The *expected outcomes* of *Specific Aim I* are that cardiac contractile dysfunction will be ameliorated though the restoration of mitochondrial ATP generating capacity in a murine model of T2DM. We anticipate that reducing the amount of miR-378a available to localize within the mitochondria may amend mitochondrial bioenergetic dysfunction through restoration of ATP generating capacity, indicated by increased translation of mt-ATP6 protein, and preserved ATP synthase content and activity. Further, we anticipate that inhibition of miR-378a by lncRNA Kcnq1ot1 will provide a therapeutic benefit to the T2DM heart through improved ATP synthase functionality.

Specific Aim II: Evaluate mitochondrial transplantation as a therapeutic approach for the amelioration of mitochondrial bioenergetic dysfunction in the diabetic heart*. Specific Aim II* aims to ascertain the efficacy of mitochondrial transplantation, a macroscale approach to the amelioration of mitochondrial dysfunction in diabetes mellitus through mitochondrial replacement, to preserve mitochondrial bioenergetic function in diabetes mellitus. In Specific Aim II, we will test our ***working hypothesis*** that mitochondrial transplantation can be applied to the diabetic heart in a prophylactic manner using minimally invasive ultrasound-

guided intracardiac injections, and that the specificity of mitochondrial transplantation may be enhanced using machine learning methodologies. We further hypothesized that spatial and temporal patterns of cardiac dysfunction exist in the diabetic heart, and could be identified in a murine model of T2DM using non-invasive echocardiography data and machine learning methodologies. *Specific Aim II* includes three objectives:

2.1 Assess the efficacy of ultrasound-guided injections as a minimally invasive method of mitochondrial transplantation for the diabetic heart

2.2 Determine the spatial and temporal progression of cardiac contractile dysfunction, and identify locales of interest for mitochondrial transplantation using a murine model of T2DM.

2.3 Evaluate the ability of machine learning to provide a more descriptive and thorough approach to efficiently managing large amounts of contractile data

The *expected outcomes* of *Specific Aim II* are that mitochondrial transplantation is adaptable for prophylactic use in diabetes mellitus using minimally invasive ultrasound-guided intracardiac injections. We expect that mitochondrial transplantation performed using ultrasound-guided injections will result in poor distribution of mitochondria within the left ventricular myocardium, therefore we anticipate the need to determine a locale of interest for targeted mitochondrial transplantation. We expect that machine learning methodologies will provide a more descriptive and thorough approach to efficiently managing large amounts of data for the evaluation of cardiac dysfunction, and that it can be used to evaluate cardiac contractile dysfunction associated with the T2DM murine heart. Lastly, we expect cardiac dysfunction to manifest in a spatial and temporal fashion, and be defined by patterns of regional and segmental dysfunction.

With respect to ***overall expected outcomes***, successful completion of *Specific Aim I* studies will provide a novel genomic pathway that could be leveraged for the amelioration of cardiac contractile dysfunction in T2DM. The successful completion of *Specific Aim II* studies will determine if mitochondrial transplantation may provide a method of replacing damaged mitochondria in the diabetic heart, which could be applied as prophylactic against mitochondrial bioenergetic dysfunction. Further, the identification of spatial and temporal patterns of cardiac dysfunction in the diabetic heart will aid in the determination of a locale of interest for both precise mitochondrial transplantation, and the identification of regions and segments of interest for experimental, clinical, and therapeutic purposes.

RESEARCH STRATEGY

SIGNIFICANCE. Diabetes mellitus is the world's fastest growing disease, affecting 347 million people worldwide (9, 10). Cardiovascular complications, including the development of diabetic cardiomyopathy (DCM), remain the leading cause of mortality in the diabetic population (10, 11). The pathophysiology of DCM is well characterized by mitochondrial dysfunction (5, 12). The mitochondrion is a critical producer of ATP, and bioenergetic disruption is central to the development of cardiac contractile dysfunction and heart failure, emphasizing its importance as a target for therapeutic intervention (13, 14). Interventions targeting mitochondrial function may include those aimed at preservation or rescue of bioenergetic function via improvements in respiratory capacity and ATP generating ability (15). Overall, improved methods of preserving mitochondrial bioenergetic function would reduce mortality rates in the diabetic population, and provide an essential treatment for DCM. As a result, strategies targeting preservation of bioenergetic function and ATP generating capacity, including those directed at the ATP synthase complex of the mitochondrial electron transport chain, are attractive for limiting diabetes-induced heart failure and disease burden.

Previous studies provide the ***scientific premise*** for the proposed experimentation. Our laboratory was the first to demonstrate that miR-378a enhancement in diabetic mitochondria leads to downregulation of mt-ATP6, a critical component of the ATP synthase F_0 complex, therefore reducing mt-ATP6 protein content and ATP synthase activity (15, 16). A second lncRNA, Kcnq1ot1, has been shown to be altered in the diabetic heart, and has been suggested to interact with target microRNAs to influence translation of protein (17, 18). As a predicted regulator of miR-378a, Kcnq1ot1 provided an additional layer of regulation for the mitochondrial genome, in which pathological overexpression of miR-378a may be quelled. Mitochondrial transplantation has been studied extensively in murine models of ischemia reperfusion, and has demonstrated significant benefits (19-22), but has been minimally explored in diabetes mellitus

(22-25). Current literature suggests that the transplantation of mitochondria from a non-allogeneic source, or from a different individual of the same species, demonstrated no negative inflammatory or rejection like consequences following transplantation (20, 25, 26). These reports demonstrate that mitochondrial transplantation may be of benefit to the diabetic heart, and would allow for the use of mitochondria collected from a healthy donor.

The research generated from this dissertation is ***significant*** because it aims to ameliorate cardiac contractile dysfunction associated with the diabetes mellitus pathology through assessment and implementation of novel mitochondrial-centric therapeutic strategies. This work was ***conceptually*** and ***mechanistically*** innovative because it utilized novel mouse models, including a miR-378a KO/*Db/Db* mouse, and manipulation of the mitochondrial ncRNA profile. The proposed research is ***technically*** *innovative* in its application of mitochondrial replacement strategies, and the use of echocardiography for the assessment of spatial and temporal patterns of dysfunction in the T2DM murine heart. Deepening our understanding of the influence of the ncRNA profile on regulation of the mitochondrial genome enhances the ***impact*** of these studies by providing new and innovative therapeutic targets for the amelioration of cardiac dysfunction. Further, the prophylactic application of mitochondrial transplantation in the diabetic heart aims to preserve mitochondrial bioenergetic function and prolong the development of cardiac contractile dysfunction.

References

1.   Raghavan S, Vassy JL, Ho YL, Song RJ, Gagnon DR, Cho K, et al. Diabetes Mellitus-Related All-Cause and Cardiovascular Mortality in a National Cohort of Adults. J Am Heart Assoc. 2019;8(4):e011295. doi:10.1161/JAHA.118.011295

2.   Dall TM, Yang W, Halder P, Pang B, Massoudi M, Wintfeld N, et al. The Economic Burden of Elevated Blood Glucose Levels in 2012: Diagnosed and Undiagnosed Diabetes, Gestational Diabetes Mellitus, and Prediabetes. Diabetes Care. 2014;37(12):3172-3179. doi:10.2337/dc14-1036

3.   Einarson TR, Acs A, Ludwig C, Panton UH. Economic Burden of Cardiovascular Disease in Type 2 Diabetes: A Systematic Review. Value Health. 2018;21(7):881-890. doi:10.1016/j.jval.2017.12.019

4.   McBrien KA, Manns BJ, Chui B, Klarenbach SW, Rabi D, Ravani P, et al. Health Care Costs in People with Diabetes and Their Association with Glycemic Control and Kidney Function. Diabetes Care. 362013. p. 1172-1180.

5.   Hathaway QA, Pinti MV, Durr AJ, Waris S, Shepherd DL, Hollander JM. Regulating Microrna Expression: At the Heart of Diabetes Mellitus and the Mitochondrion. Am J Physiol Heart Circ Physiol. 2018;314(2):H293-H310. doi:10.1152/ajpheart.00520.2017

6.   Verma SK, Garikipati VNS, Kishore R. Mitochondrial Dysfunction and Its Impact on Diabetic Heart. Biochimica et biophysica acta. 2017;1863(5):1098-1105. doi:10.1016/j.bbadis.2016.08.021

7.   Kota SK, Kota SK, Jammula S, Panda S, Modi KD. Effect of Diabetes on Alteration of Metabolism in Cardiac Myocytes: Therapeutic Implications. Diabetes Technol Ther. 2011;13(11):1155-1160. doi:10.1089/dia.2011.0120

8.   Rindler PM, Crewe CL, Fernandes J, Kinter M, Szweda LI. Redox Regulation of Insulin Sensitivity Due to Enhanced Fatty Acid Utilization in the

Mitochondria. Am J Physiol Heart Circ Physiol. 2013;305(5):H634-643. doi:10.1152/ajpheart.00799.2012

9.   Danaei G, Finucane MM, Lu Y, Singh GM, Cowan MJ, Paciorek CJ, et al. National, Regional, and Global Trends in Fasting Plasma Glucose and Diabetes Prevalence since 1980: Systematic Analysis of Health Examination Surveys and Epidemiological Studies with 370 Country-Years and 2.7 Million Participants. Lancet. 2011;378(9785):31-40. doi:10.1016/S0140-6736(11)60679-X

10.   Einarson TR, Acs A, Ludwig C, Panton UH. Prevalence of Cardiovascular Disease in Type 2 Diabetes: A Systematic Literature Review of Scientific Evidence from across the World in 2007-2017. Cardiovascular diabetology. 2018;17(1):83. doi:10.1186/s12933-018-0728-6

11.   Dal Canto E, Ceriello A, Ryden L, Ferrini M, Hansen TB, Schnell O, et al. Diabetes as a Cardiovascular Risk Factor: An Overview of Global Trends of Macro and Micro Vascular Complications. Eur J Prev Cardiol. 2019;26(2_suppl):25-32. doi:10.1177/2047487319878371

12.   Athithan L, Gulsin GS, McCann GP, Levelt E. Diabetic Cardiomyopathy: Pathophysiology, Theories and Evidence to Date. World J Diabetes. 2019;10(10):490-510. doi:10.4239/wjd.v10.i10.490

13.   Salvatore T, Pafundi PC, Galiero R, Albanese G, Di Martino A, Caturano A, et al. The Diabetic Cardiomyopathy: The Contributing Pathophysiological Mechanisms. Front Med (Lausanne). 2021;8:695792. doi:10.3389/fmed.2021.695792

14.   Brown DA, Perry JB, Allen ME, Sabbah HN, Stauffer BL, Shaikh SR, et al. Expert Consensus Document: Mitochondrial Function as a Therapeutic Target in Heart Failure. Nat Rev Cardiol. 2017;14(4):238-250. doi:10.1038/nrcardio.2016.203

15.   Jagannathan R, Thapa D, Nichols CE, Shepherd DL, Stricker JC, Croston TL, et al. Translational Regulation of the Mitochondrial Genome Following Redistribution of Mitochondrial Microrna in the Diabetic Heart. Circ Cardiovasc Genet. 2015;8(6):785-802. doi:10.1161/CIRCGENETICS.115.001067

16.   Shepherd DL, Hathaway QA, Pinti MV, Nichols CE, Durr AJ, Sreekumar S, et al. Exploring the Mitochondrial Microrna Import Pathway through Polynucleotide Phosphorylase (Pnpase). J Mol Cell Cardiol. 2017;110:15-25. doi:10.1016/j.yjmcc.2017.06.012

17.   Yang F, Qin Y, Wang Y, Li A, Lv J, Sun X, et al. Lncrna Kcnq1ot1 Mediates Pyroptosis in Diabetic Cardiomyopathy. Cell Physiol Biochem. 2018;50(4):1230-1244. doi:10.1159/000494576

18.   Yang F, Qin Y, Lv J, Wang Y, Che H, Chen X, et al. Silencing Long Non-Coding Rna Kcnq1ot1 Alleviates Pyroptosis and Fibrosis in Diabetic Cardiomyopathy. Cell Death Dis. 2018;9(10):1000. doi:10.1038/s41419-018-1029-4

19.   Emani SM, Piekarski BL, Harrild D, Del Nido PJ, McCully JD. Autologous Mitochondrial Transplantation for Dysfunction after Ischemia-Reperfusion Injury. J Thorac Cardiovasc Surg. 2017;154(1):286-289. doi:10.1016/j.jtcvs.2017.02.018

20.   Masuzawa A, Black KM, Pacak CA, Ericsson M, Barnett RJ, Drumm C, et al. Transplantation of Autologously Derived Mitochondria Protects the Heart from Ischemia-Reperfusion Injury. Am J Physiol Heart Circ Physiol. 2013;304(7):H966-982. doi:10.1152/ajpheart.00883.2012

21.   Blitzer D, Guariento A, Doulamis IP, Shin B, Moskowitzova K, Barbieri GR, et al. Delayed Transplantation of Autologous Mitochondria for Cardioprotection in a Porcine Model. Ann Thorac Surg. 2020;109(3):711-719. doi:10.1016/j.athoracsur.2019.06.075

22.   McCully JD, Levitsky S, Del Nido PJ, Cowan DB. Mitochondrial Transplantation for Therapeutic Use. Clin Transl Med. 2016;5(1):16. doi:10.1186/s40169-016-0095-4

23.   Roushandeh AM, Kuwahara Y, Roudkenar MH. Mitochondrial Transplantation as a Potential and Novel Master Key for Treatment of Various Incurable Diseases. Cytotechnology. 2019;71(2):647-663. doi:10.1007/s10616-019-00302-9

24.   Doulamis IP, Guariento A, Duignan T, Orfany A, Kido T, Zurakowski D, et al. Mitochondrial Transplantation for Myocardial Protection in Diabetic Hearts. Eur J Cardiothorac Surg. 2020;57(5):836-845. doi:10.1093/ejcts/ezz326

25.   Hayashida K, Takegawa R, Shoaib M, Aoki T, Choudhary RC, Kuschner CE, et al. Mitochondrial Transplantation Therapy for Ischemia Reperfusion Injury: A Systematic Review of Animal and Human Studies. J Transl Med. 2021;19(1):214. doi:10.1186/s12967-021-02878-3

26.   Ramirez-Barbieri G, Moskowitzova K, Shin B, Blitzer D, Orfany A, Guariento A, et al. Alloreactivity and Allorecognition of Syngeneic and Allogeneic Mitochondria. Mitochondrion. 2019;46:103-115. doi:10.1016/j.mito.2018.03.002

BACKGROUND AND SIGNFICANCE

Diabetes mellitus is a prolific disease characterized by a complex set of pathological insults which impact all of the biological systems of the body. Pathophysiological changes can be observed at the level of the genome, and traced throughout the cellular, organellar, and tissue levels, culminating in what is ultimately a systemic disease (1, 2). Of the associated co-morbidities, cardiovascular disease (CVD) accounts for the greatest mortality rate in the diabetic population (3). Though CVD is rampant and only becoming more prevalent, gaps remain in our knowledge regarding its development and progression. Mechanistically, the pathophysiology of CVD in diabetes mellitus is a continuously evolving subject. While many mechanisms have yet to be fully elucidated, a large volume of research is available to support a significant role for mitochondrial dysfunction, and related abnormalities, in cardiac contractile dysfunction (4-7). The foremost role of mitochondria in the heart is to produce ATP for contraction. Due to the role of mitochondrial dysfunction in CVD pathophysiology, mitochondrial targeted therapeutics are attractive for the amelioration of cardiac contractile dysfunction in diabetes mellitus, but their efficacy is not well established. The projects discussed in this dissertation focus extensively on the amelioration of mitochondrial dysfunction as a method to improve contractile ability of the diabetic heart. The aims of this research were to assess the efficacy of two mitochondrial-centric therapeutic approaches for the treatment of diabetic cardiac contractile dysfunction. Contributing studies are provided in *chapter 2*, "Manipulation of the MiR-378a/mt-ATP6 Regulatory Axis Rescues ATP Synthase in the Diabetic Heart and Offers a Novel Role for LncRNA Kcnq1ot1", *chapter 3*, "Evaluation of Myocardial Mitochondrial Transplantation for Application in the Diabetic Heart", and *chapter 4*, "Machine Learning for Spatial Stratification of Progressive Cardiovascular Dysfunction in a Murine Model of Type 2 Diabetes Mellitus". A summary and future directions are provided in **chapter 5**, "General Discussion".

References

1.   Hathaway QA, Pinti MV, Durr AJ, Waris S, Shepherd DL, Hollander JM. Regulating Microrna Expression: At the Heart of Diabetes Mellitus and the Mitochondrion. Am J Physiol Heart Circ Physiol. 2018;314(2):H293-H310. doi:10.1152/ajpheart.00520.2017

2.   Einarson TR, Acs A, Ludwig C, Panton UH. Prevalence of Cardiovascular Disease in Type 2 Diabetes: A Systematic Literature Review of Scientific Evidence from across the World in 2007-2017. Cardiovascular diabetology. 2018;17(1):83. doi:10.1186/s12933-018-0728-6

3.   McEwen LN, Kim C, Haan M, Ghosh D, Lantz PM, Mangione CM, et al. Diabetes Reporting as a Cause of Death: Results from the Translating Research into Action for Diabetes (Triad) Study. Diabetes Care. 2006;29(2):247-253. doi:10.2337/diacare.29.02.06.dc05-0998

4.   Makrecka-Kuka M, Liepinsh E, Murray AJ, Lemieux H, Dambrova M, Tepp K, et al. Altered Mitochondrial Metabolism in the Insulin-Resistant Heart. Acta Physiol (Oxf). 2020;228(3):e13430. doi:10.1111/apha.13430

5.   Jia G, Hill MA, Sowers JR. Diabetic Cardiomyopathy: An Update of Mechanisms Contributing to This Clinical Entity. Circ Res. 2018;122(4):624-638. doi:10.1161/CIRCRESAHA.117.311586

6.   Bugger H, Abel ED. Mitochondria in the Diabetic Heart. Cardiovasc Res. 2010;88(2):11. doi:10.1093/cvr/cvq239

7.   Cortassa S, Caceres V, Tocchetti CG, Bernier M, de Cabo R, Paolocci N, et al. Metabolic Remodelling of Glucose, Fatty Acid and Redox Pathways in the Heart of Type 2 Diabetic Mice. The Journal of physiology. 2020;598(7):1393-1415. doi:10.1113/JP276824

Chapter 1:

Literature Review

1.1 Diabetes Mellitus

1.1a Significance

The frequency of diabetes mellitus has continued to increase worldwide, with current prevention strategies failing to quell the surge. Previous reports from the World Health Organization and others documented 422 million cases worldwide in 2014, and estimate a rise to 642 million by 2040 (1, 2). More recent reports cite worsening statistics, and document 451 million diagnoses in 2017, with a projected increase to 693 million by 2045 (3). Diabetes mellitus results from a complex array of metabolic and physiological changes, and is often associated with multiple comorbidities, or health conditions that are associated with, but not a symptom of, the primary disease. In conjunction with the typical presentation of diabetes mellitus, patients may develop other conditions including but not limited to ocular myopathy, kidney failure, cardiovascular disease (CVD), stroke, and lower limb amputation (4, 5). Together, this systemic insult results in notably reduced health-span, reduced life-span, and higher mortality rates in the diabetic population (2, 5).

Diabetes mellitus was listed as the seventh leading cause of death in the United States in 2016 (2), but the number of people who pass from diabetes mellitus is likely higher than reported due to a lack of emphasis on the primary disease when reporting on death certificates (6, 7). As a result, people who pass from diabetes mellitus associated comorbidities, such as CVD or stroke, may not be documented as dying from diabetes mellitus, making the real death toll difficult to identify (8). Moreover, nearly 80,000 death certificates list type 2 diabetes mellitus (T2DM) as the primary cause of death, but over 250,000 death certificates list diabetes mellitus as underlying or contributing to cause of death (9). Hence, reporting differences in the primary versus secondary or underlying cause of death influences mortality statistics by separating deaths from diabetes mellitus and those attributed to comorbidities, resulting in diabetes mellitus appearing less

deadly than it would otherwise. When viewed as a whole, the inclusion of all diabetes mellitus related deaths places it as the 3rd leading cause of death in the United States, only behind heart disease (647,457 deaths) and cancer (599,108 deaths) (10). In reality, diabetes mellitus has the second greatest contribution to reduced global life expectancy, even when adjusted for comorbidities and other confounding factors (3, 11). There are three foremost types of diabetes mellitus; type 1 diabetes mellitus (T1DM), T2DM, and gestational diabetes. Of note, Alzheimer's Disease has recently garnered the description of "type 3 diabetes mellitus," due to the interrelationship of key features shared by the two pathologies, but this connection is currently under evaluation and is only mentioned as a note for the reader (12). For the scope of this dissertation, T2DM is the primary target of potential research advances, and will be discussed.

1.1b Type 2 Diabetes Mellitus

The prevalence of T2DM is far higher than T1DM, accounting for over 90% of diagnoses (1, 13). T2DM is often described as adult-onset or non-insulin-dependent diabetes mellitus because of its primary manifestation in adulthood, and high base-line levels of insulin. In fact, non-insulin dependent refers to the body's inability to effectively use insulin for blood glucose regulation, rather than an inability to produce it (2, 14). As the epidemic of obesity continues, the use of "adult-onset" as a descriptor of T2DM is lessening due to an increased prevalence of T2DM in children and adolescents. The pathophysiology of T2DM is characterized by hyperinsulinemia and hyperglycemia, or excessive insulin and glucose in the blood, and insulin resistance (14, 15). The dysregulation of insulin and blood glucose levels, whether due to poor management of the condition or because the condition went undiagnosed, can lead to a decline in pancreatic beta cell function and result in the need for glucose management through exogenous insulin supplementation (14, 15). Though this type of diabetes mellitus is often thought to be the result of obesity and physical inactivity, current literature suggests that an underlying cornucopia of physiological changes sets the stage

for T2DM development (2). Symptoms accompanying T2DM may go undetected for long periods of time prior to a diagnosis, and underlying comorbidities, such as CVD, may have already developed (2). As a result, patients with T2DM may be living with unmanaged hyperglycemia and hyperinsulinemia for extended periods of time prior to intervention, leading to worsened comorbidities, reduced health-span, and increased risk of mortality.

1.1c Classifying Metabolic Alterations

To better understand the pathophysiology of diabetes mellitus, it is pertinent to understand the metabolic alterations associated with disease development. Diabetes mellitus is classified and characterized by metabolic changes in insulin production and glucose management. Therefore, it becomes necessary to understand the basics of metabolism and how the body regulates the release of glucose and insulin in response to food intake or fasting conditions. In a healthy individual, food intake, and particularly carbohydrates, stimulates the pancreas to release the hormone insulin in a phase one response to the conversion of carbohydrates to glucose, and its presence in the blood (16, 17). The release of insulin stimulates cellular uptake and storage of glucose as fuel, as well as stimulates the muscles and the liver to store glucose as glycogen for later use (16, 17). Excess nutrients that are not utilized and cannot be stored as glycogen will be transformed into free fatty acids and stored in fat deposits (18). During this storage phase, blood glucose levels begin to fall and the pancreas moves into phase two insulin production, where it produces new insulin in preparation for the next meal. Conversely, during fasting conditions, low blood glucose levels stimulate the release of the hormone glucagon. Glucagon stimulates the conversion of glycogen stores in the liver into glucose through the process of gluconeogenesis, or the creation of new glucose, and releases steady levels of glucose into the blood stream to be used for fuel (16, 17).

T1DM and T2DM are characterized by distinct paradigms of metabolic changes that are ultimately based in disrupted insulin production or sensitivity, and glucose dysregulation. For the purposes of this dissertation, the metabolic changes associated with T2DM will be discussed. There is much debate about the role of hyperinsulinemia and insulin resistance in T2DM and metabolic syndrome, with some suggesting that insulin resistance is a root cause, or initiator, of disease development and metabolic unrest. Others, myself included, believe that hyperinsulinemia and insulin resistance begin as adaptive responses aimed at protecting the body from metabolic damage during situations of chronic nutrient overload (19-24). A metabolically flexible individual will shift between glucose and free fatty acids as primary sources of fuel during daily feeding and fasting windows (20). In situations of chronic nutrient overload, chronically high glucose and free fatty acid levels may be observable in the blood (20, 25, 26). This arguably dangerous dual availability of substrates caused by nutrient overload can cause cellular injury and tissue damage, also referred to as glucolipotoxicity (20, 23, 24).

While this adaptive process continues, blood glucose levels may temporarily remain steady even though the body is in a state of nutrient overload because they are being regulated by increased insulin secretion alone (15, 19). As the body continues to regulate blood glucose through the overproduction of insulin, it continues to require more and more to achieve proper glucose modulation (19). Tissues that are normally responsive to insulin stimulated glucose uptake, such as the heart and skeletal muscle, may become insulin resistant to protect themselves from metabolic damage and glucolipotoxicity (20, 23, 24). This cycle leads to a dependency on the phase 2 insulin response that if not properly managed may lead to beta cell dysfunction (16, 25, 26). Finally, when insulin hypersecretion alone cannot regulate blood glucose levels, the patient will present with clinically detectable hyperglycemia (14). At the time of diagnosis, the metabolic profile of a T2DM patient is centered around insulin resistance, hyperinsulinemia, and hyperglycemia, and often requires pharmacological intervention (15, 16). This substantial shift in substrate utilization and nutrient overload can be described as

a disruption of metabolic flexibility, resulting in hyperglycemia and excess free fatty acids that are not effectively utilized at the cellular level, and are consequently stored as fat deposits, within adipose tissue, muscle tissue, and organs (15, 16, 19).

1.1d Metabolic Inflexibility in the Type 2 Diabetic Heart

Metabolic flexibility describes to the ability to maintain homeostasis by responding and adapting to changes in metabolic demand. It is based on energy requirements, energy demand, caloric intake, and the availability of substrates (27-29). While the metabolic abnormalities observed in the T1DM phenotype may be normalized by proper management via insulin supplementation, the T2DM phenotype, regardless of management technique or intervention, is ultimately considered to be metabolically inflexible (30, 31).

In the T2DM condition a large percentage of energy is produced using fatty acids, or by fatty acid oxidation (31, 32). At the molecular level, metabolic inflexibility manifests as hyperlipidemia, or an increase in circulating free fatty acids, an increased dependency on fatty acids for energy production, and a decreased ability to use glucose as an energy substrate (18, 19, 31). This change in glucose and fatty acid utilization has been described extensively since its discovery in 1963 (31, 33). As an example, the heart is typically one of the most metabolically flexible organs in the body, but in T2DM, a reduced ability to fluctuate between glucose and fatty acids substrates for energy production occurs, and though there is plenty of glucose available it cannot be utilized effectively as a primary source of fuel (31, 34). This phenomenon has been described as "starved in the midst of plenty", and may be the most descriptive statement of the T2DM condition (31, 35). Further, metabolic inflexibility is currently thought to develop concomitantly with insulin resistance, but prior to the onset of hyperglycemia, indicating that metabolic rigidity may actually be an underlying cause of T2DM, rather than a consequence (31, 34, 36).

1.2 CVD

1.2a Mortality Risk in Diabetes Mellitus

CVD in the diabetic population, also known as diabetic cardiomyopathy (DCM), is the leading cause of death in the diabetic population (37, 38). Generally speaking, adults with diabetes mellitus are between 2 and 4 times more likely to die from CVD than their healthy counterparts, and at least 68% of people aged 65 and older with diabetes mellitus will succumb to CVD related complications (5, 9). The overwhelming prevalence of the T2DM condition means that CVD risk factors are well characterized. In persons with T2DM, CVD is the leading cause of mortality with death rates of 15.4% in those with no prior myocardial infarction (MI), and 42.0% in those having a history MI (1). Further, T2DM patients face a 2 to 4 times higher risk of experiencing a CVD related event (5, 39). Current CVD risk management in T2DM focuses on glycemic control in addition to exercise, blood pressure management, and other lifestyle factors (1, 40). Notably, CVD risk management may be de-emphasized in T2DM patients, as CVD may already be present at the time of diagnosis (1, 14). Because routine CVD screening is not currently recommended for diabetes mellitus, managing CVD risk in T2DM patients is comparable to management in the non-diabetic population (41).

1.2b Diabetic Cardiomyopathy

The term "diabetic cardiomyopathy" was coined by Rubler in 1972 and defined CVD in diabetes mellitus, which was thought to develop outside of the traditional factors responsible for CVD in the general population (i.e. hypertension, obesity, and coronary artery disease) (38, 42). This terminology is heavily debated as some suggest there is not enough evidence to determine whether there is a cardiomyopathy specifically tied to the diabetic condition, as many of the traditional factors, including hypertension and obesity, are relatively common among diabetic patients. Of the current reports addressing DCM, the majority appear to support a

distinct increase in the occurrence of CVD in the diabetic population (40, 43). Large population-based studies suggest that increased risk of atherosclerosis and other traditional risk factors inherent to diabetes mellitus cannot account for the prevalence of heart failure in the diabetic population, indicating the involvement of other factors (44). Even following adjustment for confounding factors, patients with diabetes mellitus are still subject to a 2 to 5 fold increase in risk for heart failure (44). Currently, the terminology is still used to describe CVD in the diabetic population, though it appears we may know less about its development than previously thought. At the time of writing, DCM is classified as a subtype of dilated cardiomyopathy within the non-ischemic heart failure phenotype, and describes the atypical development of CVD in the diabetic heart (37, 45, 46).

DCM is characterized by both structural and metabolic changes, requiring a multitude of tools to monitor its development and progression. While metabolic changes will be discussed at a later time, structural changes are a critical piece of the identification, diagnosis, and management scheme. Advancements in non-invasive imaging techniques continue to aid in the structural characterization of the diabetic heart (47, 48). Of note, changes in left ventricular structure, including both concentric and eccentric hypertrophy, lead to pathological increases in left ventricular mass (37). Increased left ventricular mass is not only a known predictor of cardiovascular morbidity and mortality, but has been shown to increase in the diabetic population independent of other risk factors (37, 47, 49). Additional assessments of left ventricular structural changes have shown that concentric remodeling has a higher association than eccentric remodeling with cardiovascular mortality based on echocardiographic and cardiac magnetic resonance studies (37, 50). Additionally, the observation of cardiac remodeling is an important characteristic of CVD in diabetic heart, and may provide increased certainty for diagnosis and future evaluations.

Many challenges surround the diagnosis and management of CVD in diabetes mellitus. It is not uncommon for diabetic patients to experience

asymptomatic development of CVD. Diastolic dysfunction is commonly cited as the first sign of disease in these patients, and may be the first sign of heart failure (37). Strong associations with systolic dysfunction in T2DM have not been identified, with exception in the "Strong Heart Study," where a correlation between ejection fraction (EF) and HbA1c levels was observed (37, 47). Because of these developmental patterns, traditional imaging modalities like M-mode echocardiography, which focus on major changes in systolic function as measures of diagnosing CVD, are often inadequate to assess subtle changes in functionality prior to diabetic patients becoming symptomatic (37). These challenges are emphasized by the current classification system of DCM. In the general population, classification begins as asymptomatic or at risk with no limitations, but stage 1 of DCM is considered by the New York Heart Association to already include the presence of diastolic dysfunction, but have normal EF (44).

Speckle tracking strain-based echocardiography (STE) is a more nuanced method of assessing cardiac function that focuses on cardiac deformation and motion, and is able to detect subtle changes in both diastolic and systolic function (51). STE allows for the observation of cardiac motion as global, regional, and segmental patterns of deformation, making it a useful tool in the diagnosis of clinical and sub-clinical CVD, and is currently utilized in humans and murine models (50-54). Global longitudinal strain is a widely accepted clinical marker of left ventricular dysfunction (52, 55). Numerous studies have demonstrated its use as a prognostic value, even in patients with no history of CVD, and it has been shown to be correlated with diabetic duration in T2DM patients (52, 55, 56). STE has seen applications in murine models of diabetes mellitus to identify cardiac strain abnormalities and regional affliction that may have otherwise been elusive (57, 58). Changes seen in global longitudinal strain as early as nine weeks post onset of streptozotocin-induced T1DM were associated with lessened myocardial contraction in the anterior and posterior regions (59). Li et al. demonstrated that STE could be used to evaluate early cardiac dysfunction in *Db/Db* mice, with significant reductions in radial and circumferential strains identified at 16 weeks

(58). The broad diagnostic capability of STE provides an opportunity to enhance current imaging modalities, and improve detection of CVD in the subclinical realm.

The pathophysiology of CVD is heavily related to the changes in metabolism discussed above, including altered glucose and fatty acid metabolism. To fully understand its development, the organelle primarily responsible for energy production and contractile ability, the mitochondrion, must be explored. Specifically, mitochondrial bioenergetic dysfunction is considered to be a central component of CVD development in diabetes mellitus (60-62).

1.3 Mitochondrial Dysfunction

1.3a Overview

The heart requires more energy than any other organ in the body due to maintain non-stop contractile activity. In situations of stress and high energy demand, such as physical activity, the heart can increase cardiac output by seven times (63). Increases in energy demand are met by enormous oxidative reserves, and can be maintained for long periods of time without activating anaerobic metabolism (63). The molecule responsible for this tremendous feat is ATP. ATP is primarily produced in the mitochondrion through oxidative phosphorylation and the electron transport chain (ETC). The ETC is comprised of five complexes; I, II, III, IV, and V (also referred to as ATP synthase), and functions by generating a proton gradient through the oxidation of NADH/NADPH (64, 65). Through a progressive cycle involving proton transfer, the release of intermediates that initiate the next step of the system, and eventually the production of ATP molecules, the ETC generates the energy needed for all aerobic functions, including cardiac contractility (65). The mitochondrion is responsible for upwards of 95% of the ATP production in the heart, and accounts for about one-third of the total volume of each cardiomyocyte (63, 66). Due to the heart's need for efficient ATP production, mitochondria are critical in both development and maintenance of cardiac function.

The importance of the mitochondrion is highlighted further in cardiac disease, where a commonly recurring feature is the dysfunction of mitochondrial bioenergetic and metabolic pathways (60, 61).

1.3b Mitochondrial Contribution to Cardiovascular Dysfunction in T2DM

Mitochondrial bioenergetic dysfunction is a critical entity in the development and the progression of DCM to heart failure, and is linked to pronounced left ventricular hypertrophy, overt systolic dysfunction, and cell death and fibrosis (30, 46). A healthy mitochondria is tremendously flexible, metabolically speaking, and can generate ATP using a variety of fuel substrates: triglycerides, non-esterified fatty acids, carbohydrates, ketone bodies, and amino acids (30, 67, 68). In T2DM, the inability to utilize glucose effectively leads to increased reliance on free fatty acids and mitochondrial strain. While the mitochondria are typically able to process free fatty acids, their fatty acid oxidative capacity is limited. Excess free fatty acids lead to accumulation of fatty acids, fatty acid intermediates, and eventually lipotoxicity (30). Lipotoxicity, or the accumulation of lipids in non-adipose tissues, is just one potential consequence of free fatty acid overload, and leads to a number of downstream consequences including increased cellular oxidative stress, impaired calcium homeostasis, and mitochondrial bioenergetic dysfunction (30, 34, 69).

Though lipotoxicity presents a major issue in the T2DM metabolism, the metabolic shift observed in the diabetic heart cannot be explained by lipotoxicity alone. Impaired oxidative phosphorylation by the ETC, the redox pathway located in the inner mitochondrial membrane that is fed through glycolysis and the citric acid cycle, is marked by numerous detriments (70, 71). Specifically, T2DM leads to increased proton leakage, oxidative stress and damage, decreased expression of mitochondrial genome encoded ETC components, and reduced ATP generating capacity (72-74). The uncoupling of oxidative phosphorylation, the induction of energy-wasting triglyceride fatty acids, and calcium cycling may also contribute to

11

elevated myocardial oxygen consumption and decreases in ATP generating efficiency (30). These changes manifest as an impaired cardiac energy reserve in patients with T2DM, and those with obesity and/or insulin resistance, as indicated by a lower phosphocreatine/ATP ratio (30, 50). Overall, reduced functionality of the ETC and oxidative phosphorylation process holds a critical role in DCM and the development of mitochondrial bioenergetic dysfunction (70, 73, 75).

Mitochondrial dysfunction is implicated in the development and progression of CVD. As we continue to study the pathophysiology of diabetes mellites and CVD, we continue to raise more questions about the role of the mitochondrion in cardiac contractile dysfunction and heart failure. It is still unknown if mitochondrial dysfunction is a cause or an effect of DCM, though current literature suggests that in T2DM mitochondrial dysfunction begins prior to even insulin resistance and hyperglycemia, contributing to the actual development of the pathology and not just its comorbidities (76, 77). It should be noted that mitochondrial dysfunction may appear concomitantly with metabolic inflexibility or insulin-deficiency, but it is also characterized by an array of unique genomic changes that were touched on briefly above. Altered transcriptional regulation of the proteins involved in cardiac energy metabolism pathways, and the regulatory network of the mitochondrial genome has been evaluated in diabetes mellitus (30, 66, 78, 79). Non-coding RNAs (ncRNA) are of particular interest to diabetes mellitus, because of their ability to regulate a wide array of transcriptional targets (79, 80).

1.4 NcRNA Regulation of the Mitochondria

1.4a MicroRNAs

Mitochondrial dysfunction is associated with a number of disturbances at the genome level, including altered DNA transcription, protein synthesis and import, and RNA regulation (66, 67, 73, 78, 81). MicroRNAs (miRs), a subtype of ncRNA, have gathered interest as a therapeutic target in diabetes mellitus due to

their diverse range of action, their localized distribution profiles, and evidence of their role in CVD and heart failure (80, 82). Mitochondrial dysfunction in the diabetic heart is well characterized, but to fully understand how mitochondrial dysfunction impacts cardiac function we need to delve into ncRNA regulation of the mitochondrial genome.

MiRs have been shown to have great implications in the regulation of mitochondrial function and the mitochondrial genome during diabetes mellitus. Mature miRs are roughly 18 – 22 nucleotides in length, and have the ability to bind and regulate target mRNA transcripts (83). Through complete or partial complementary of seed sequences on the 3' prime end of both transcripts, miRs can either completely or partially block the transcription of their mRNA targets into protein (83). MiRs are typically located in intronic regions or the untranslated region of a protein-coding gene in DNA, or those that were previously thought to be "junk" DNA (83, 84). The canonical pathway of miR transcription and processing is that miR genes are transcribed as large primary transcripts inside the nucleus, referred to as pri-microRNA, which are then processed in the nucleus by Drosha, an RNase III enzyme (83). The now ~70 nucleotide length precursor miR is then transported to the cytoplasm through an exportin system, and processed by a second RNase III enzyme, Dicer (83). After this double processing, the mature miR is approximately 22 nucleotides in length, and ready to be incorporated into the RNA-induced silencing complex (RISC), which mediates the silencing of target mRNAs (83). Argonaute 2, an endonuclease housed within the RISC, binds directly to the mature miR and assists in identifying target mRNAs that have complementarity to the miR's seed sequence. The "seed" region of miRs includes 2-7 nucleotides of the that assist in target association. If complementarity exists in the 9-11 nucleotide central region of the miR, then binding of the miR to the mRNA occurs, and the mRNA can be cleaved via argonaute 2 endonuclease activity (83). MiRs have a primary role in the regulation of gene expression and the transition from nucleotide to amino acid, making them critical regulators of all physiologic processes (66, 85).

1.3b Mitochondrial MiRs

MiRs have been implicated in numerous pathologies and diseases. Cardiac miRs are key regulators of gene expression in the heart and contribute to transcriptional and post-transcriptional regulation in DCM and the progression to heart failure (82, 85). Cardiac miRs target mitochondrial function through a number of pathways, including reactive oxygen species production, calcium handling perturbation, and initiation of apoptosis (43, 66). MiRs can further contribute to structural remodeling in the heart by influencing fibrosis or stiffening (86). In DCM, miRs travel throughout the body via the circulation to other cells, tissues, or organs, resulting in a redistribution of miRs in disease (80, 82). This redistribution of miRs can lead to a host of negative changes in gene regulation, which trickle down into every aspect of the biological system.

MiRs are involved in widespread transcriptional regulation, including nuclear and mitochondrial encoded genes. MiRs found inside the mitochondria have been termed mitomiRs, and can influence bioenergetic function of the mitochondrion through the regulation of mitochondrial genome encoded proteins (87, 88). MitomiRs influence all metabolic processes that take place in the mitochondrion, including the tri-carboxylic acid cycle, ETC and oxidative phosphorylation processes, and lipid and amino acid metabolism (78, 87). Further, previous reports have shown that the miR profile of the mitochondria is altered in diabetes mellitus (78). For the scope of this review, the impact of miRs on the ETC and oxidative phosphorylation will be covered.

MitomiRs are indirectly responsible for the breakdown of glucose, and the oxidation of substrates like carbohydrates, fats, and proteins (66, 88). While miR activity has been suggested to impact each of the five complexes of the ETC, those that impact complex V, ATP synthase, are the most intriguing. ATP synthase is required to produce ATP, and any disturbances to either the F_0 or F_1 complexes can severely reduce ATP production and lead to multiple mitochondrial diseases

(89-95). MiR-101-3p, miR-127-5p, miR-338-5p, and miR-378a have all been suggested to target specific components of the ATP synthase complex and regulate its expression (78, 87). MiR-378a, a miR identified by our laboratory to be increased within diabetic cardiac mitochondria, is able to bind and down-regulate mitochondrially encoded ATP synthase membrane subunit 6 (mt-ATP6), and is predicted to bind and regulate mt-ATP8 (78, 87). These two proteins, involved in the ATP synthase complex F_0 subunit, are the only two ATP synthase proteins that are encoded within the mitochondrial genome, indicating that miR-378a is acting as a regulator inside the mitochondria, and may contribute to decreases in ATP synthase activity and ATP generating capacity (78, 87).

1.4c MiR-378a

MiR-378a is the most highly expressed of the miR-378 sequences, and contains both leading and lagging strands (96). The miR-378a-3p, leading, and miR-378a-5p, lagging, strands are highly conserved between human and mice, with the miR-378a-5p mature strand matching exactly between species and the miR-378a-3p mature strand varying by only one nucleotide (96). This homology suggests that miR-378a focused research may be experimentally translatable between species.

MiR-378a is encoded on the first intron of the peroxisome proliferator-activated receptor gamma, coactivator 1 beta (*ppargc1b*) gene, who's exons encode peroxisome proliferator-activated receptor gamma (PPARγ) coactivator-1 (PGC-1) transcriptional coactivators, PGC-1α and PGC-1β (96). Together, PGC-1α and PGC-1β serve critical roles in regulating mitochondrial function and cellular energy metabolism, as were discussed above. Together, they stimulate transcription factors and nuclear receptor activity, and are enriched in highly oxidative tissues such as the heart (96). PGC-1β regulates mitochondrial energy metabolism, as well as glucose and fatty acid oxidation, making it a key player in diabetes mellitus (97, 98). Because miR-378a is co-expressed with PGC-1β, it is

suggested to have a critical regulatory role in fatty acid oxidation and mitochondrial energy homeostasis (96, 97, 99).

In 2012, miR-378a was shown to repress both carnitine O-acetyltransferase, a mitochondrial enzyme involved in fatty acid metabolism, and MED13, a component of the mediator complex that controls nuclear hormone receptor activity (97). It was identified as a regulatory unit that maintains energy homeostasis under metabolic stress, and the oxidative capacity of insulin-target tissues (97). MiR-378a knockout mice exhibited resistance to high-fat-diet-induced obesity, enhanced mitochondrial fatty acid metabolism, and increased oxidative capacity of insulin-target tissues (97). This data, gathered in the liver, provided the ground-work for the role of miR-378a in homeostasis of energy metabolism.

The role of miR-378a in the mitochondria has been further explored by our laboratory (78, 100, 101). In 2015, miR profiles were characterized in streptozotocin-induced T1DM cardiac mitochondrial subpopulations using microarray analysis (78). Results identified miR-378a as being overexpressed in interfibrillar mitochondria, which are most negatively impacted during T1DM (78, 102, 103). MiR-378a was identified as a miR of interest and predicted bioinformatically to bind and regulate both mt-ATP6 and mt-ATP8, the only proteins of the ATP synthase complex that are encoded by the mitochondrial genome (78). Luciferase assay confirmed the ability of miR-378a to bind mt-ATP6, and miR-378a overexpression in HL-1 cells was matched by significantly reduced levels of mt-ATP6 protein content and decreased ATP synthase activity (78). *In vivo* experimentation using LNA-linked antagomir delivery targeting miR-378a in streptozotocin-treated T1DM mice resulted in preservation of mt-ATP6 protein content and ATP synthase activity in interfibrillar mitochondria (78). Because of the relationship between mitochondrial dysfunction and cardiac contractile function, echocardiography was performed to assess ejection fraction (EF) and fractional shortening (FS) prior to and following treatment with the LNA-linked antagomir (78). Results demonstrated significantly higher EF and FS values in the treated

group when compared to controls (78). In summary, miR-378 overexpression led to reduced mt-ATP6 protein content and ATP synthase activity, ultimately reducing ATP generating capacity, while inhibition of miR-378 activity restored cardiac function in a murine model of T1DM (66, 78, 87).

1.4d Regulation of MiRs by Long Non-coding RNAs

Long non-coding RNAs (lncRNA) are a second class of ncRNA primarily transcribed in the nucleus which are much larger than miRs, ranging from 200 nucleotides into the thousands (104, 105). As relatively new players in the field, lncRNAs receive a lot of attention due to their ability to bind and regulate other ncRNAs, such as miRs (80). Mounting evidence suggests that the dysregulation of lncRNAs can result in aberrant expression of genetic targets that perpetuate the development of numerous diseases (66, 106). As recent as 2017, literature supported a potentially critical role for lncRNAs in diabetes mellitus, with miR-188-3p, miR-539, and miR-489 having been shown to be regulated in the cardiovascular and circulatory system by lncRNAs (66, 107-109). While it was understood that lncRNAs were somehow connected to the diabetic heart, no studies had yet implicated lncRNAs in miR regulation, CVD, or the mitochondrion in diabetes mellitus (66). Since then, there has been an explosion of lncRNA centered research (80, 105).

Differential expression analysis of lncRNAs in T2DM blood samples exposed 441 differentially regulated lncRNAs (366 upregulated and 75 downregulated), indicating aberrant dysregulation of the lncRNA network in T2DM (105). Less explored, analysis of the mitochondrial transcriptome shows lncRNAs residing within the mitochondrion, with speculation that RNA binding proteins, such as polynucleotide phosphorylase, may play a role in their transport into the mitochondria (106). LncRNAs are currently known to be important regulators of gene expression and therefore modulators of cellular function and disease (104,

106), but the biological significance of many lncRNAs, and particularly their influence on disease, have yet to be identified.

LncRNAs have been identified to inhibit miR function through a process described as sponging, where they act as endogenous competing RNAs and bind to complimentary miR response elements (66, 105). This unique function emphasizes why lncRNAs have been of such interest for researchers. A single lncRNA can bind multiple miRs at the same time, reducing their ability to bind and inhibit translation of their target mRNAs. In the same way, lncRNAs are naturally occurring and may provide another efficacious route for mitochondrial targeted reduction of miR activity. The balance of action between miRs and lncRNAs is delicate and easily disrupted by pathological conditions. In a healthy individual, a lncRNA would endogenously compete for miR binding within a balanced system, influenced by many external factors. In a system such as diabetes mellitus, many miRs are already in disarray, and it may be in part due to disruption of other ncRNA networks. For the purposes of this dissertation, we return to miR-378a as a target for lncRNA interactions. The mitochondrial ncRNA network may be disrupted to a greater extent than simply the miR profile, and act as a pervasive agent in the development of mitochondrial dysfunction (80, 106).

1.4e LncRNAs in Diabetes Mellitus and the Mitochondrion

The exploration of ncRNAs in disease has become a pervasive front, with dysregulation of the ncRNA network in numerous pathologies, including diabetes mellitus and CVD. NcRNAs, including miRs and lncRNAs, have been shown to be dynamic in disease, often operating in conjunction with one another (80, 105). In many cases, dynamic lncRNA expression appears to impact miRs and their downstream targets (80, 110-117). This association of lncRNAs and miRs is well established, with the discovery of each lncRNA paralleling the discovery of one or more lncRNA/miR regulatory axes (104, 105, 118).

18

An increasing number of studies suggest that nuclear-encoded lncRNAs, including those residing in the nucleus or cytoplasm, and mitochondrial genome encoded lncRNAs, play a role in mitochondrial genome regulation. In 2020, a review by Gusic and Prokisch summarized 18 lncRNAs known to impact the mitochondrial genome, including AK055347, shown to influence ATP synthase, indicating a delicate balance maintained by the import of lncRNAs into the mitochondria, the transcription of lncRNAs from the mitochondrial genome, and the dysregulation incurred by disease (80, 106, 119, 120). Importantly, lncRNA activity has been demonstrated to influence the mitochondrial genome primarily through the regulation of miRs and their downstream targets (119, 121-123). Though these interactions require further evaluation in diabetes mellitus and CVD, recent data from our laboratory suggests that lncRNAs, including lncRNA potassium voltage-gated channel subfamily Q member 1 overlapping transcript 1 (Kcnq1ot1), metastasis associated lung adenocarcinoma transcript 1 (Malat1), and Nuclear Enriched Abundant Transcript 1 (Neat1), are not only dysregulated in T2DM mitochondria, but have been predicted to interact with mitochondrially-located miRs and influence mitochondrial genome-encoded protein expression.

Of the many lncRNAs identified in diabetes mellitus, Kcnq1ot1 and Malat1 are among the most highly studied (119). Evidence suggests that alterations in Kcnq1ot1 and Malat1 may contribute to the development of diabetes mellitus and CVD (119). Specifically, both have been linked to pyroptosis, inflammation, apoptosis, and aberrant gene regulation, as part of altered miR regulatory axes (116, 124-127). Kcnq1ot1 has been found in several metabolically active tissues; skeletal muscle, liver, pancreas, and adipose (104), and has since been shown to have important roles within the heart (125, 128). Few studies exist which explore Kcnq1ot1 in diabetes mellitus and DCM. Kcnq1ot1 has consistently been shown to be increased in diabetes mellitus tissues, including the left ventricular tissue of *Db/Db* mice and T2DM patients (125, 129). In two separate reports, Yang et al. utilized a streptozotocin-induced model of T1DM and proposed that Kcnq1ot1 acts as a competing endogenous RNA which regulates the expression of caspase-1

through sponging of miR-214-3p, and further demonstrated that Kcnq1ot1 inhibition reduced pyroptosis and fibrosis (124). Shuo-Fang et al. reported that Kcnq1ot1 participates in the sponging of miR-181a-5p, leading to the overexpression of Programmed Cell Death 4 (PDCD4) protein (130). Further, Shuo-Fang found that Kcnq1ot1 knockdown reduced PDCD4 levels, myocardial inflammation, and cardiomyocyte apoptosis (130). Of note, these reports focused on Kcnq1ot1 at the tissue levels, rather than at the level of the mitochondrion. Kcnq1ot1 has yet to be identified in the mitochondrion, and its role in the development of mitochondrial dysfunction in T2DM remains elusive. Potential interactions with mitochondrial miRs are unexplored, but Kcnq1ot1 is predicted to bind and regulate miR-378a, containing 93 predicted binding sites specific to this miR. To this end, the focus of chapter 3 will be the exploration of this regulatory axis in a murine model of T2DM, and the cardioprotective effects of miR-378a genomic loss and inhibition.

1.6 Mitochondrial Transplantation

1.6a Overview

Mitochondrial transplantation is currently not utilized for the treatment of CVD in diabetes mellitus, but has the potential to be used as a non-invasive method to deliver healthy mitochondria to the diabetic heart. As discussed above, therapeutic interventions are often pharmacologic in nature, requiring dietary supplementation or consistent use of medication to manage diabetes mellitus, and in turn mitochondrial dysfunction and cardiac health.

Mitochondrial transplantation, a method that uses healthy mitochondria to replace or support dysfunctional mitochondria, has been extensively explored by Dr. James McCully, who dominates the field in relation to ischemia reperfusion injury, and its amelioration using mitochondrial transplantation techniques (131-135). His technique has been exclusively applied in the field of ischemia

reperfusion injury and shown great success by reaching clinical trials in pediatric patients (136). Fortunately, mitochondrial transplantation is easily performed during induced states of ischemia reperfusion because of the nature of the procedure. *In vivo* experimentation allows for the unique opportunity to provide therapeutic intervention at precisely the right moment, after ischemia but prior to reperfusion.

In 2009, McCully et al. performed mitochondrial transplantation in the ischemic heart during early reperfusion, and demonstrated protection of cardiac function and reduced damage following ischemia reperfusion (131). As with all therapeutic procedures, there is a chance of negative side effects. To determine if negative outcomes were associated with the mitochondrial transplantation procedure, an exhaustive list of outcomes were evaluated: the impact of mitochondrial transplantation on cardiac abnormalities, acute and chronic inflammation and apoptosis, variations between single or serial injection schemes, and the use of syngeneic or allogenic mitochondria, or mitochondria from self or a different individual of the same species (131, 134, 136, 137). Importantly, electrocardiographic recordings immediately following the transplantation of autologously derived, syngeneic, mitochondria showed no ventricular tachycardia, bradycardia, fibrillation, or conduction system defects or repolarization heterogeneity (137). In short, results determined that the procedure, regardless of injection scheme and source of donor mitochondria, does not incite any direct or indirect, acute or chronic side effects that indicated potential damage to the heart or lasting effects on cardiac function (134, 137). Not only did mitochondrial transplantation produce significant decreases in levels of cardiac energy markers myocardial creatine kinase and concentrative nucleoside transporter 1, following reperfusion, it also reduced apoptosis and apoptotic markers through decreases in tunnel staining, caspase 3 protein levels, infarct size, and area at risk (131).

In concurrent reports, these findings were recapitulated and heartily support mitochondrial transplantation for cardioprotection (134, 136, 137). Masuzawa et al.

utilized proteomic analysis following mitochondrial transplantation to show increased translation of differentially expressed proteins, and pathway induction of beneficial cytokine and proteomic pathways, suggesting that functional benefits may be stimulated through mitochondrial interactions and function within the tissue (137). Enhanced ATP content and oxygen consumption rate, as well as the replacement of depleted mitochondrial DNA was further identified as contributors to the mechanism of cardioprotection, suggesting that bioenergetic stimulation and support by transplanted mitochondria may play a critical role during ischemia reperfusion injury (132).

1.6b Mitochondrial Transplantation for Diabetic Cardiomyopathy

Until now, an extensive amount of functional support for mitochondrial transplantation in the heart was produced using a model of ischemia reperfusion. Though this pathological model differs in critical ways from DCM, the cardioprotective effects of mitochondrial transplantation are attractive and potentially applicable in a multitude of other pathologies. Critically, functional outcomes including improved ATP content, improved oxygen consumption rates, and the propagation of beneficial proteomic pathways is homologous to the functional improvements that would likely be beneficial in the context of a therapeutic for the treatment of DCM.

While traditional therapeutics for diabetes mellitus are centered heavily on medications for the management of cardiac contractile dysfunction, there are currently no reliable methods of management, and restoration of cardiac function is, at best, a far-off speculation. Mitochondrial transplantation is a terrific therapeutic opportunity for a number of reasons, one of which at its simplest is to provide support to an otherwise diseased mitochondrial population. In previous studies, the focus remained on the use, assessment, and perfection of the mitochondrial transplantation procedure for clinical translation (138). This focus left the mechanism of action arguably understudied, with limited insights available

regarding uptake and localization within tissues and cells (132, 133). To better understand the mechanism of action and the impact of mitochondria transplantation at the cellular level, more research is necessary. Overall, mitochondrial transplantation is not only readily available or a donor away, but if successfully applied in the diabetic population, could minimize the medical burden of diabetes mellitus and CVD dramatically. Further, emphasis on treatment of the mitochondrial network may reduce CVD related deaths, and improve quality of life in diabetes mellitus patients.

1.6c Overcoming Barriers to Application in Diabetes Mellitus

Adapting the procedure of mitochondrial transplantation to a diabetes mellitus model is no easy or quick feat. Critical changes in the methodology and experimental design will be necessary to overcome current barriers and test its efficacy as a prophylactic measure. Ultimately, the adaptation of mitochondrial transplantation as a prophylactic intervention opens a new range of possible applications for mitochondrial transplantation.

As discussed above, DCM is strongly associated with mitochondrial dysfunction and cardiac contractile function, making it a good candidate for mitochondrial transplantation, a procedure that has been shown to improve ATP content and oxygen consumption, and incite the activation of essential bioenergetic pathways (139). Though mitochondrial transplantation has been heavily studied, and reached clinical trial levels in pediatric patients, its applicability in diabetes mellitus is, at best, understudied. Mitochondrial transplantation use in diabetes mellitus provides a unique and novel opportunity to use a well-evaluated therapeutic that directly targets the mitochondrial network, and therefore cardiac contractile potential. That being said, multiple barriers exist that must be addressed.

Likely the most problematic barrier, DCM related cardiac events cannot be modeled in the same manner as ischemia reperfusion. Unlike ischemia reperfusion models, where both events are controlled and predetermined processes, a planned injection scheme for a CVD event in a diabetes mellitus model is unfeasible and not clinically translational. Additionally, because diabetes mellitus patients experience a diverse range of cardiac events, a design focused solely on MI is unrealistic. This means that during experimental procedures, there is no obvious area at risk or pre-determined location for mitochondrial transplantation as displayed in ischemia reperfusion models. Further, access to the heart is limited because the goal of reducing cardiac risk means that we are aiming to prevent a cardiac event, and do not perform transplantations in an open-heart scenario. Because of these factors, an alternative injection methodology and protocol becomes necessary. In order to be feasible and realistic, mitochondrial transplantation must be performed in a prophylactic manner aimed at both improving cardiac contractile function and reducing patient risk of a future cardiac event. The development of a procedure that maintains the ability to deliver mitochondria within the cardiac wall in a minimally invasive manner provides the greatest opportunity for positive results. Likely, ultrasound-guided echocardiography will provide a suitable injection mechanism that is both minimally invasive, and allows for quick recovery with limited side effects.

Further considerations are the internalization and localization of mitochondria within the left ventricular wall, and the mechanism of uptake into the cardiomyocytes. Evidence suggests that following injection, mitochondria remain in the tissue, are internalized by cardiomyocytes within two hours (137), and are viable for at least 28 days following transplantation (137). Current literature suggests that following transplantation, mitochondria are taken up by cardiomyocytes and localized within the intracellular space, and potentially within the host mitochondrial network (131-133), but further experimentation is necessary to determine if these behaviors will consistently be observed using alternative

injection schemes, in smaller animal models such as mice, and within normal non-ischemic cardiac tissue.

1.6d Improving Applicability in Diabetes Mellitus

CVD is typically managed by global or left ventricle methods regardless of the stage of dysfunction, and the identification of differentially impacted locales may provide a modality for pinpointed clinical care. This broad diagnostic capability provides the unique opportunity to assess localized patterns of dysfunction within the diabetic heart. Regional and segmental evaluations are a logical next step in determining localized impact of CVD on cardiovascular contractility. Currently, STE is utilized in CVD evaluations, but has yet to be earnestly applied to assess progressive regional and segmental dysfunction in the diabetic heart. Filling this gap in our understanding of cardiovascular diabetology may provide an opportunity to recognize and classify CVD in diabetes mellitus patients earlier and with greater specificity. It is noteworthy that the diagnosis of subclinical and overt CVD in diabetes mellitus is largely dependent on echocardiography. The usefulness of STE for DCM diagnosis and the visualization of subtle, potentially subclinical changes was discussed above. To go one step further, STE could be used to identify spatial and temporal changes in contractile ability and deformation of the heart, and may allow for better directed mitochondrial transplantation. Chapter 4 explores this possibility, and is focused on determining the most impacted regions and segments of the diabetic heart using a machine learning based approach.

References

1.   Einarson TR, Acs A, Ludwig C, Panton UH. Prevalence of Cardiovascular Disease in Type 2 Diabetes: A Systematic Literature Review of Scientific Evidence from across the World in 2007-2017. Cardiovascular diabetology. 2018;17(1):83. doi:10.1186/s12933-018-0728-6

2.   Organization WH. Diabetes World Health Organization website: World Health Organization; 2020. Available from: https://www.who.int/news-room/fact-sheets/detail/diabetes.

3.   Lin X, Xu Y, Pan X, Xu J, Ding Y, Sun X, et al. Global, Regional, and National Burden and Trend of Diabetes in 195 Countries and Territories: An Analysis from 1990 to 2025. Sci Rep. 2020;10(1):14790. doi:10.1038/s41598-020-71908-9

4.   Einarson TR, Acs A, Ludwig C, Panton UH. Economic Burden of Cardiovascular Disease in Type 2 Diabetes: A Systematic Review. Value Health. 2018;21(7):881-890. doi:10.1016/j.jval.2017.12.019

5.   Raghavan S, Vassy JL, Ho YL, Song RJ, Gagnon DR, Cho K, et al. Diabetes Mellitus-Related All-Cause and Cardiovascular Mortality in a National Cohort of Adults. J Am Heart Assoc. 2019;8(4):e011295. doi:10.1161/JAHA.118.011295

6.   Cheng WS, Wingard DL, Kritz-Silverstein D, Barrett-Connor E. Sensitivity and Specificity of Death Certificates for Diabetes: As Good as It Gets? Diabetes Care. 2008;31(2):279-284. doi:10.2337/dc07-1327

7.   McEwen LN, Karter AJ, Curb JD, Marrero DG, Crosson JC, Herman WH. Temporal Trends in Recording of Diabetes on Death Certificates: Results from Translating Research into Action for Diabetes (Triad). Diabetes Care. 2011;34(7):1529-1533. doi:10.2337/dc10-2312

8.   McEwen LN, Kim C, Haan M, Ghosh D, Lantz PM, Mangione CM, et al. Diabetes Reporting as a Cause of Death: Results from the Translating Research into Action for Diabetes (Triad) Study. Diabetes Care. 2006;29(2):247-253. doi:10.2337/diacare.29.02.06.dc05-0998

9.   Association AD. Statistics About Diabetes | Ada 2019. Available from: https://www.diabetes.org/resources/statistics/statistics-about-diabetes.

10.   Prevention CfDCa. Faststats - Deaths and Mortality 2019. Available from: https://www.cdc.gov/nchs/fastats/deaths.htm.

11.   Chen H, Chen G, Zheng X, Guo Y. Contribution of Specific Diseases and Injuries to Changes in Health Adjusted Life Expectancy in 187 Countries from 1990 to 2013: Retrospective Observational Study. BMJ. 2019;364:l969. doi:10.1136/bmj.l969

12.   Frank CJ, McNay EC. Breakdown of the Blood-Brain Barrier: A Mediator of Increased Alzheimer's Risk in Patients with Metabolic Disorders? J Neuroendocrinol. 2022;34(1):e13074. doi:10.1111/jne.13074

13.   Xu G, Liu B, Sun Y, Du Y, Snetselaar LG, Hu FB, et al. Prevalence of Diagnosed Type 1 and Type 2 Diabetes among Us Adults in 2016 and 2017: Population Based Study. BMJ. 2018;362:k1497. doi:10.1136/bmj.k1497

14.   Fonseca VA. Defining and Characterizing the Progression of Type 2 Diabetes. Diabetes Care. 2009;32 Suppl 2:S151-156. doi:10.2337/dc09-S301

15.   Galicia-Garcia U, Benito-Vicente A, Jebari S, Larrea-Sebal A, Siddiqi H, Uribe KB, et al. Pathophysiology of Type 2 Diabetes Mellitus. Int J Mol Sci. 2020;21(17). doi:10.3390/ijms21176275

16.   Exercise Fa. Diabetes and Metabolism: @Diabetescouk; 2019. Available from: https://www.diabetes.co.uk/diabetes-and-metabolism.html.

17.	Gerich JE. Is Reduced First-Phase Insulin Release the Earliest Detectable Abnormality in Individuals Destined to Develop Type 2 Diabetes? Diabetes. 2002;51 Suppl 1:S117-121. doi:10.2337/diabetes.51.2007.s117

18.	Sears B, Perry M. The Role of Fatty Acids in Insulin Resistance. Lipids Health Dis. 2015;14:121. doi:10.1186/s12944-015-0123-1

19.	Galgani JE, Moro C, Ravussin E. Metabolic Flexibility and Insulin Resistance. Am J Physiol Endocrinol Metab. 2008;295(5):E1009-1017. doi:10.1152/ajpendo.90558.2008

20.	Nolan CJ, Prentki M. Insulin Resistance and Insulin Hypersecretion in the Metabolic Syndrome and Type 2 Diabetes: Time for a Conceptual Framework Shift. Diab Vasc Dis Res. 2019;16(2):118-127. doi:10.1177/1479164119827611

21.	Connor T, Martin SD, Howlett KF, McGee SL. Metabolic Remodelling in Obesity and Type 2 Diabetes: Pathological or Protective Mechanisms in Response to Nutrient Excess? Clin Exp Pharmacol Physiol. 2015;42(1):109-115. doi:10.1111/1440-1681.12315

22.	Taegtmeyer H, Beauloye C, Harmancey R, Hue L. Insulin Resistance Protects the Heart from Fuel Overload in Dysregulated Metabolic States. Am J Physiol Heart Circ Physiol. 2013;305(12):H1693-1697. doi:10.1152/ajpheart.00854.2012

23.	Nolan CJ, Ruderman NB, Kahn SE, Pedersen O, Prentki M. Insulin Resistance as a Physiological Defense against Metabolic Stress: Implications for the Management of Subsets of Type 2 Diabetes. Diabetes. 2015;64(3):673-686. doi:10.2337/db14-0694

24.	Nolan CJ, Ruderman NB, Prentki M. Intensive Insulin for Type 2 Diabetes: The Risk of Causing Harm. Lancet Diabetes Endocrinol. 2013;1(1):9-10. doi:10.1016/S2213-8587(13)70027-5

25.   Eizirik DL, Pasquali L, Cnop M. Pancreatic Beta-Cells in Type 1 and Type 2 Diabetes Mellitus: Different Pathways to Failure. Nat Rev Endocrinol. 2020;16(7):349-362. doi:10.1038/s41574-020-0355-7

26.   Prentki M, Nolan CJ. Islet Beta Cell Failure in Type 2 Diabetes. J Clin Invest. 2006;116(7):1802-1812. doi:10.1172/JCI29103

27.   Smith RL, Soeters MR, Wüst RCI, Houtkooper RH. Metabolic Flexibility as an Adaptation to Energy Resources and Requirements in Health and Disease. Endocr Rev. 2018;39(4):489-517. doi:10.1210/er.2017-00211

28.   Rohm M, Savic D, Ball V, Curtis MK, Bonham S, Fischer R, et al. Cardiac Dysfunction and Metabolic Inflexibility in a Mouse Model of Diabetes without Dyslipidemia. Diabetes. 2018;67(6):1057-1067. doi:10.2337/db17-1195

29.   Goodpaster BH, Sparks LM. Metabolic Flexibility in Health and Disease. Cell Metab. 2017;25(5):1027-1036. doi:10.1016/j.cmet.2017.04.015

30.   Makrecka-Kuka M, Liepinsh E, Murray AJ, Lemieux H, Dambrova M, Tepp K, et al. Altered Mitochondrial Metabolism in the Insulin-Resistant Heart. Acta Physiol (Oxf). 2020;228(3):e13430. doi:10.1111/apha.13430

31.   Larsen TS, Aasum E. Metabolic (in)Flexibility of the Diabetic Heart. Cardiovasc Drugs Ther. 2008;22(2):91-95. doi:10.1007/s10557-008-6083-1

32.   Cortassa S, Caceres V, Tocchetti CG, Bernier M, de Cabo R, Paolocci N, et al. Metabolic Remodelling of Glucose, Fatty Acid and Redox Pathways in the Heart of Type 2 Diabetic Mice. The Journal of physiology. 2020;598(7):1393-1415. doi:10.1113/JP276824

33.   Randle PJ. Regulatory Interactions between Lipids and Carbohydrates: The Glucose Fatty Acid Cycle after 35 Years. Diabetes Metab Rev. 1998;14(4):263-283. doi:10.1002/(sici)1099-0895(199812)14:4<263::aid-dmr233>3.0.co;2-c

34. Corpeleijn E, Saris WH, Blaak EE. Metabolic Flexibility in the Development of Insulin Resistance and Type 2 Diabetes: Effects of Lifestyle. Obes Rev. 2009;10(2):178-193. doi:10.1111/j.1467-789X.2008.00544.x

35. Taegtmeyer H, Golfman L, Sharma S, Razeghi P, van Arsdall M. Linking Gene Expression to Function: Metabolic Flexibility in the Normal and Diseased Heart. Ann N Y Acad Sci. 2004;1015:202-213. doi:10.1196/annals.1302.017

36. Buchanan J, Mazumder PK, Hu P, Chakrabarti G, Roberts MW, Yun UJ, et al. Reduced Cardiac Efficiency and Altered Substrate Metabolism Precedes the Onset of Hyperglycemia and Contractile Dysfunction in Two Mouse Models of Insulin Resistance and Obesity. Endocrinology. 2005;146(12):5341-5349. doi:10.1210/en.2005-0938

37. Athithan L, Gulsin GS, McCann GP, Levelt E. Diabetic Cardiomyopathy: Pathophysiology, Theories and Evidence to Date. World J Diabetes. 2019;10(10):490-510. doi:10.4239/wjd.v10.i10.490

38. Bell DSH. Diabetic Cardiomyopathy. Diabetes Care. 2003;26(10):3. doi:10.2337/diacare.26.10.2949

39. Holscher ME, Bode C, Bugger H. Diabetic Cardiomyopathy: Does the Type of Diabetes Matter? Int J Mol Sci. 2016;17(12). doi:10.3390/ijms17122136

40. Parim B, Sathibabu Uddandrao VV, Saravanan G. Diabetic Cardiomyopathy: Molecular Mechanisms, Detrimental Effects of Conventional Treatment, and Beneficial Effects of Natural Therapy. Heart Fail Rev. 2019;24(2):279-299. doi:10.1007/s10741-018-9749-1

41. Lee SI, Patel M, Jones CM, Narendran P. Cardiovascular Disease and Type 1 Diabetes: Prevalence, Prediction and Management in an Ageing Population. Ther Adv Chronic Dis. 2015;6(6):347-374. doi:10.1177/2040622315598502

42.   Rubler S, Dlugash J, Yuceoglu YZ, Kumral T, Branwood AW, Grishman A. New Type of Cardiomyopathy Associated with Diabetic Glomerulosclerosis. Am J Cardiol. 1972;30(6):595-602. doi:10.1016/0002-9149(72)90595-4

43.   Jia G, Hill MA, Sowers JR. Diabetic Cardiomyopathy: An Update of Mechanisms Contributing to This Clinical Entity. Circ Res. 2018;122(4):624-638. doi:10.1161/CIRCRESAHA.117.311586

44.   Gulsin GS, Athithan L, McCann GP. Diabetic Cardiomyopathy: Prevalence, Determinants and Potential Treatments. Ther Adv Endocrinol Metab. 2019;10:2042018819834869. doi:10.1177/2042018819834869

45.   Jia G, Whaley-Connell A, Sowers JR. Diabetic Cardiomyopathy: A Hyperglycaemia- and Insulin-Resistance-Induced Heart Disease. Diabetologia. 2018;61(1):21-28. doi:10.1007/s00125-017-4390-4

46.   Jia G, DeMarco VG, Sowers JR. Insulin Resistance and Hyperinsulinaemia in Diabetic Cardiomyopathy. Nat Rev Endocrinol. 2016;12(3):144-153. doi:10.1038/nrendo.2015.216

47.   Devereux RB, Roman MJ, Paranicas M, O'Grady MJ, Lee ET, Welty TK, et al. Impact of Diabetes on Cardiac Structure and Function: The Strong Heart Study. Circulation. 2000;101(19):2271-2276. doi:10.1161/01.cir.101.19.2271

48.   Tadic M, Cuspidi C, Pencic B, Grassi G, Celic V. Myocardial Work in Hypertensive Patients with and without Diabetes: An Echocardiographic Study. J Clin Hypertens (Greenwich). 2020;22(11):2121-2127. doi:10.1111/jch.14053

49.   Savage DD, Levy D, Dannenberg AL, Garrison RJ, Castelli WP. Association of Echocardiographic Left Ventricular Mass with Body Size, Blood Pressure and Physical Activity (the Framingham Study). Am J Cardiol. 1990;65(5):371-376. doi:10.1016/0002-9149(90)90304-j

50.   Levelt E, Mahmod M, Piechnik SK, Ariga R, Francis JM, Rodgers CT, et al. Relationship between Left Ventricular Structural and Metabolic Remodeling in Type 2 Diabetes. Diabetes. 2016;65(1):44-52. doi:10.2337/db15-0627

51.   Lorenzo-Almoros A, Tunon J, Orejas M, Cortes M, Egido J, Lorenzo O. Diagnostic Approaches for Diabetic Cardiomyopathy. Cardiovascular diabetology. 2017;16(1):28. doi:10.1186/s12933-017-0506-x

52.   Liu JH, Chen Y, Yuen M, Zhen Z, Chan CW, Lam KS, et al. Incremental Prognostic Value of Global Longitudinal Strain in Patients with Type 2 Diabetes Mellitus. Cardiovascular diabetology. 2016;15(22):22. doi:10.1186/s12933-016-0333-5

53.   Hensel KO, Grimmer F, Roskopf M, Jenke AC, Wirth S, Heusch A. Subclinical Alterations of Cardiac Mechanics Present Early in the Course of Pediatric Type 1 Diabetes Mellitus: A Prospective Blinded Speckle Tracking Stress Echocardiography Study. J Diabetes Res. 2016;2016:2583747. doi:10.1155/2016/2583747

54.   Dandel M, Lehmkuhl H, Knosalla C, Suramelashvili N, Hetzer R. Strain and Strain Rate Imaging by Echocardiography - Basic Concepts and Clinical Applicability. Curr Cardiol Rev. 2009;5(2):133-148. doi:10.2174/157340309788166642

55.   Biering-Sorensen T, Biering-Sorensen SR, Olsen FJ, Sengelov M, Jorgensen PG, Mogelvang R, et al. Global Longitudinal Strain by Echocardiography Predicts Long-Term Risk of Cardiovascular Morbidity and Mortality in a Low-Risk General Population: The Copenhagen City Heart Study. Circ Cardiovasc Imaging. 2017;10(3). doi:10.1161/CIRCIMAGING.116.005521

56.   Elgohari A. Effect of Diabetic Duration on Left Ventricular Global Longitudinal Strain by Speckle Tracking Imaging. Atherosclerosis. 2019;287(125):E125-E125. doi:10.1016/j.atherosclerosis.2019.06.365

57.   Shepherd DL, Nichols CE, Croston TL, McLaughlin SL, Petrone AB, Lewis SE, et al. Early Detection of Cardiac Dysfunction in the Type 1 Diabetic Heart Using Speckle-Tracking Based Strain Imaging. J Mol Cell Cardiol. 2016;90:74-83. doi:10.1016/j.yjmcc.2015.12.001

58.   Li R, Yang J, Yang Y, Ma N, Jiang B, Sun Q, et al. Speckle Tracking Echocardiography in the Diagnosis of Early Left Ventricular Systolic Dysfunction in Type Ii Diabetic Mice. BMC Cardiovasc Disord. 2014;14. doi:10.1186/1471-2261-14-141

59.   Pappritz K, Grune J, Klein O, Hegemann N, Dong F, El-Shafeey M, et al. Speckle-Tracking Echocardiography Combined with Imaging Mass Spectrometry Assesses Region-Dependent Alterations. Sci Rep. 2020;10(1):3629. doi:10.1038/s41598-020-60594-2

60.   Verma SK, Garikipati VNS, Kishore R. Mitochondrial Dysfunction and Its Impact on Diabetic Heart. Biochim Biophys Acta Mol Basis Dis. 2017;1863(5):1098-1105. doi:10.1016/j.bbadis.2016.08.021

61.   Gerasimos Siasos VT, Marinos Kosmopoulos, Dimosthenis Theodosiadis, Spyridon Simantiris, Nikoletta Maria Tagkou, Athina Tsimpiktsioglou, Panagiota K. Stampouloglou, Evangelos Oikonomou, Konstantinos Mourouzis, Anastasios Philippou, Manolis Vavuranakis, Christodoulos Stefanadis, Dimitris Tousoulis, and Athanasios G. Papavassiliou. Mitochondria and Cardiovascular Diseases—from Pathophysiology to Treatment. Ann Trans Med. 2018;6(12). doi:10.21037/atm.2018.06.21

62.   Schilling JD. The Mitochondria in Diabetic Heart Failure: From Pathogenesis to Therapeutic Promise. Antioxidants & redox signaling. 2015;22(17):1515-1526. doi:10.1089/ars.2015.6294

63.   Pohjoismaki JL, Goffart S. The Role of Mitochondria in Cardiac Development and Protection. Free Radic Biol Med. 2017;106:345-354. doi:10.1016/j.freeradbiomed.2017.02.032

64.   Nolfi-Donegan D, Braganza A, Shiva S. Mitochondrial Electron Transport Chain: Oxidative Phosphorylation, Oxidant Production, and Methods of Measurement. Redox Biol. 2020;37:101674. doi:10.1016/j.redox.2020.101674

65.   Guo R, Gu J, Zong S, Wu M, Yang M. Structure and Mechanism of Mitochondrial Electron Transport Chain. Biomed J. 2018;41(1):9-20. doi:10.1016/j.bj.2017.12.001

66.   Hathaway QA, Pinti MV, Durr AJ, Waris S, Shepherd DL, Hollander JM. Regulating Microrna Expression: At the Heart of Diabetes Mellitus and the Mitochondrion. Am J Physiol Heart Circ Physiol. 2018;314(2):H293-H310. doi:10.1152/ajpheart.00520.2017

67.   Pinti MV, Fink GK, Hathaway QA, Durr AJ, Kunovac A, Hollander JM. Mitochondrial Dysfunction in Type 2 Diabetes Mellitus: An Organ-Based Analysis. Am J Physiol Endocrinol Metab. 2019;316(2):E268-E285. doi:10.1152/ajpendo.00314.2018

68.   Bertero E, Maack C. Metabolic Remodelling in Heart Failure. Nat Rev Cardiol. 2018;15(8):457-470. doi:10.1038/s41569-018-0044-6

69.   Ritchie RH, Zerenturk EJ, Prakoso D, Calkin AC. Lipid Metabolism and Its Implications for Type 1 Diabetes-Associated Cardiomyopathy. J Mol Endocrinol. 2017;58(4):R225-R240. doi:10.1530/JME-16-0249

70.   Croston TL, Thapa D, Holden AA, Tveter KJ, Lewis SE, Shepherd DL, et al. Functional Deficiencies of Subsarcolemmal Mitochondria in the Type 2 Diabetic Human Heart. Am J Physiol Heart Circ Physiol. 2014;307(1):H54-65. doi:10.1152/ajpheart.00845.2013

71.   Skuratovskaia D, Komar A, Vulf M, Litvinova L. Mitochondrial Destiny in Type 2 Diabetes: The Effects of Oxidative Stress on the Dynamics and Biogenesis of Mitochondria. PeerJ. 2020;8:e9741. doi:10.7717/peerj.9741

72.   Wende AR, Schell JC, Ha CM, Pepin ME, Khalimonchuk O, Schwertz H, et al. Maintaining Myocardial Glucose Utilization in Diabetic Cardiomyopathy Accelerates Mitochondrial Dysfunction. Diabetes. 2020;69(10):2094-2111. doi:10.2337/db19-1057

73.   Dabkowski ER, Baseler WA, Williamson CL, Powell M, Razunguzwa TT, Frisbee JC, et al. Mitochondrial Dysfunction in the Type 2 Diabetic Heart Is Associated with Alterations in Spatially Distinct Mitochondrial Proteomes. Am J Physiol Heart Circ Physiol. 2010;299(2):H529-540. doi:10.1152/ajpheart.00267.2010

74.   Kumar V, Santhosh Kumar TR, Kartha CC. Mitochondrial Membrane Transporters and Metabolic Switch in Heart Failure. Heart Fail Rev. 2019;24(2):255-267. doi:10.1007/s10741-018-9756-2

75.   Gollmer J, Zirlik A, Bugger H. Mitochondrial Mechanisms in Diabetic Cardiomyopathy. Diabetes Metab J. 2020;44(1):33-53. doi:10.4093/dmj.2019.0185

76.   Lin HY, Weng SW, Chang YH, Su YJ, Chang CM, Tsai CJ, et al. The Causal Role of Mitochondrial Dynamics in Regulating Insulin Resistance in Diabetes: Link through Mitochondrial Reactive Oxygen Species. Oxid Med Cell Longev. 2018;2018:7514383. doi:10.1155/2018/7514383

77.   Wang CH, Wei YH. Role of Mitochondrial Dysfunction and Dysregulation of Ca2+ Homeostasis in the Pathophysiology of Insulin Resistance and Type 2 Diabetes. J Biomed Sci. 242017.

78.   Jagannathan R, Thapa D, Nichols CE, Shepherd DL, Stricker JC, Croston TL, et al. Translational Regulation of the Mitochondrial Genome Following Redistribution of Mitochondrial Microrna in the Diabetic Heart. Circ Cardiovasc Genet. 2015;8(6):785-802. doi:10.1161/CIRCGENETICS.115.001067

79.   Vendramin R, Marine JC, Leucci E. Non-Coding Rnas: The Dark Side of Nuclear-Mitochondrial Communication. EMBO J. 2017;36(9):1123-1133. doi:10.15252/embj.201695546

80.   Jakubik D, Fitas A, Eyileten C, Jarosz-Popek J, Nowak A, Czajka P, et al. Micrornas and Long Non-Coding Rnas in the Pathophysiological Processes of Diabetic Cardiomyopathy: Emerging Biomarkers and Potential Therapeutics. Cardiovascular diabetology. 2021;20(1):55. doi:10.1186/s12933-021-01245-2

81.   Shepherd DL, Hathaway QA, Nichols CE, Durr AJ, Pinti MV, Hughes KM, et al. Mitochondrial Proteome Disruption in the Diabetic Heart through Targeted Epigenetic Regulation at the Mitochondrial Heat Shock Protein 70 (Mthsp70) Nuclear Locus. J Mol Cell Cardiol. 2018;119:104-115. doi:10.1016/j.yjmcc.2018.04.016

82.   Guo R, Nair S. Role of Microrna in Diabetic Cardiomyopathy: From Mechanism to Intervention. Biochim Biophys Acta Mol Basis Dis. 2017;1863(8):2070-2077. doi:10.1016/j.bbadis.2017.03.013

83.   Hammond SM. An Overview of Micrornas. Adv Drug Deliv Rev. 2015;87:3-14. doi:10.1016/j.addr.2015.05.001

84.   Fischer SEJ. Rna Interference and Microrna-Mediated Silencing. Curr Protoc Mol Biol. 2015;112:26 21 21-26 21 25. doi:10.1002/0471142727.mb2601s112

85.   Wojciechowska A, Braniewska A, Kozar-Kaminska K. Microrna in Cardiovascular Biology and Disease. Adv Clin Exp Med. 2017;26(5):865-874. doi:10.17219/acem/62915

86.   Wang H, Cai J. The Role of Micrornas in Heart Failure. Biochim Biophys Acta Mol Basis Dis. 2017;1863(8):2019-2030. doi:10.1016/j.bbadis.2016.11.034

87.   Baradan R, Hollander JM, Das S. Mitochondrial Mirnas in Diabetes: Just the Tip of the Iceberg. Can J Physiol Pharmacol. 2017;95(10):1156-1162. doi:10.1139/cjpp-2016-0580

88.   Geiger J, Dalgaard LT. Interplay of Mitochondrial Metabolism and Micrornas. Cell Mol Life Sci. 2017;74(4):631-646. doi:10.1007/s00018-016-2342-7

89.   Dautant A, Meier T, Hahn A, Tribouillard-Tanvier D, di Rago JP, Kucharczyk R. Atp Synthase Diseases of Mitochondrial Genetic Origin. Front Physiol. 2018;9:329. doi:10.3389/fphys.2018.00329

90.   Eipel C, Hildebrandt A, Scholz B, Schyschka L, Minor T, Kreikemeyer B, et al. Mutation of Mitochondrial Atp8 Gene Improves Hepatic Energy Status in a Murine Model of Acute Endotoxemic Liver Failure. Life Sci. 2011;88(7-8):343-349. doi:10.1016/j.lfs.2010.12.011

91.   Ng YS, Martikainen MH, Gorman GS, Blain A, Bugiardini E, Bunting A, et al. Pathogenic Variants in Mt-Atp6: A United Kingdom-Based Mitochondrial Disease Cohort Study. Ann Neurol. 2019;86(2):310-315. doi:10.1002/ana.25525

92.   Stendel C, Neuhofer C, Floride E, Yuqing S, Ganetzky RD, Park J, et al. Delineating Mt-Atp6-Associated Disease: From Isolated Neuropathy to Early Onset Neurodegeneration. Neurol Genet. 2020;6(1):e393. doi:10.1212/NXG.0000000000000393

93.   Nesci S, Trombetti F, Algieri C, Pagliarani A. A Therapeutic Role for the F1fo-Atp Synthase. SLAS Discov. 2019;24(9):893-903. doi:10.1177/2472555219860448

94.   Johnson JA, Ogbi M. Targeting the F1fo Atp Synthase: Modulation of the Body's Powerhouse and Its Implications for Human Disease. Curr Med Chem. 2011;18(30):4684-4714. doi:10.2174/092986711797379177

95.   Beck SJ, Guo L, Phensy A, Tian J, Wang L, Tandon N, et al. Deregulation of Mitochondrial F1fo-Atp Synthase Via Oscp in Alzheimer's Disease. Nature communications. 2016;7:11483. doi:10.1038/ncomms11483

96.   Krist B, Florczyk U, Pietraszek-Gremplewicz K, Jozkowicz A, Dulak J. The Role of Mir-378a in Metabolism, Angiogenesis, and Muscle Biology. Int J Endocrinol. 2015;2015:281756. doi:10.1155/2015/281756

97.   Carrer M, Liu N, Grueter CE, Williams AH, Frisard MI, Hulver MW, et al. Control of Mitochondrial Metabolism and Systemic Energy Homeostasis by Micrornas 378 and 378*. Proc Natl Acad Sci U S A. 2012;109(38):15330-15335. doi:10.1073/pnas.1207605109

98.   Gali Ramamoorthy T, Laverny G, Schlagowski AI, Zoll J, Messaddeq N, Bornert JM, et al. The Transcriptional Coregulator Pgc-1beta Controls Mitochondrial Function and Anti-Oxidant Defence in Skeletal Muscles. Nature communications. 2015;6:10210. doi:10.1038/ncomms10210

99.   Machado IF, Teodoro JS, Palmeira CM, Rolo AP. Mir-378a: A New Emerging Microrna in Metabolism. Cell Mol Life Sci. 2020;77(10):1947-1958. doi:10.1007/s00018-019-03375-z

100.   Shepherd DL, Hathaway QA, Pinti MV, Nichols CE, Durr AJ, Sreekumar S, et al. Exploring the Mitochondrial Microrna Import Pathway through Polynucleotide Phosphorylase (Pnpase). J Mol Cell Cardiol. 2017;110:15-25. doi:10.1016/j.yjmcc.2017.06.012

101.   Hathaway QA, Durr AJ, Shepherd DL, Pinti MV, Brandebura AN, Nichols CE, et al. Mirna-378a as a Key Regulator of Cardiovascular Health Following Engineered Nanomaterial Inhalation Exposure. Nanotoxicology. 2019;13(5):19. doi:10.1080/17435390.2019.1570372

102.   Hollander JM, Thapa D, Shepherd DL. Physiological and Structural Differences in Spatially Distinct Subpopulations of Cardiac Mitochondria:

Influence of Cardiac Pathologies. Am J Physiol Heart Circ Physiol. 2014;307(1):H1-14. doi:10.1152/ajpheart.00747.2013

103.   Dabkowski ER, Williamson CL, Bukowski VC, Chapman RS, Leonard SS, Peer CJ, et al. Diabetic Cardiomyopathy-Associated Dysfunction in Spatially Distinct Mitochondrial Subpopulations. Am J Physiol Heart Circ Physiol. 2009;296(2):H359-369. doi:10.1152/ajpheart.00467.2008

104.   Leung A, Natarajan R. Long Noncoding Rnas in Diabetes and Diabetic Complications. Antioxidants & redox signaling. 2018;29(11):1064-1073. doi:10.1089/ars.2017.7315

105.   Yang F, Chen Y, Xue Z, Lv Y, Shen L, Li K, et al. High-Throughput Sequencing and Exploration of the Lncrna-Circrna-Mirna-Mrna Network in Type 2 Diabetes Mellitus. Biomed Res Int. 2020;2020:8162524. doi:10.1155/2020/8162524

106.   Dong Y, Yoshitomi T, Hu JF, Cui J. Long Noncoding Rnas Coordinate Functions between Mitochondria and the Nucleus. Epigenetics Chromatin. 2017;10(1):41. doi:10.1186/s13072-017-0149-x

107.   Wang K, Liu CY, Zhou LY, Wang JX, Wang M, Zhao B, et al. Apf Lncrna Regulates Autophagy and Myocardial Infarction by Targeting Mir-188-3p. Nature communications. 2015;6:6779. doi:10.1038/ncomms7779

108.   Wang K, Long B, Zhou LY, Liu F, Zhou QY, Liu CY, et al. Carl Lncrna Inhibits Anoxia-Induced Mitochondrial Fission and Apoptosis in Cardiomyocytes by Impairing Mir-539-Dependent Phb2 Downregulation. Nature communications. 2014;5:3596. doi:10.1038/ncomms4596

109.   Wang K, Liu F, Zhou LY, Long B, Yuan SM, Wang Y, et al. The Long Noncoding Rna Chrf Regulates Cardiac Hypertrophy by Targeting Mir-489. Circ Res. 2014;114(9):1377-1388. doi:10.1161/CIRCRESAHA.114.302476

110.   Shao J, Pan X, Yin X, Fan G, Tan C, Yao Y, et al. Kcnq1ot1 Affects the Progression of Diabetic Retinopathy by Regulating Mir-1470 and Epidermal Growth Factor Receptor. J Cell Physiol. 2019;234(10):17269-17279. doi:10.1002/jcp.28344

111.   Li J, Li M, Bai L. Kcnq1ot1/Mir-18b/Hmga2 Axis Regulates High Glucose-Induced Proliferation, Oxidative Stress, and Extracellular Matrix Accumulation in Mesangial Cells. Molecular and cellular biochemistry. 2021;476(1):321-331. doi:10.1007/s11010-020-03909-1

112.   Zhang C, Gong Y, Li N, Liu X, Zhang Y, Ye F, et al. Long Noncoding Rna Kcnq1ot1 Promotes Sc5b-9-Induced Podocyte Pyroptosis by Inhibiting Mir-486a-3p and Upregulating Nlrp3. Am J Physiol Cell Physiol. 2021;320(3):C355-C364. doi:10.1152/ajpcell.00403.2020

113.   Yu L, Fu J, Yu N, Wu Y, Han N. Long Noncoding Rna Malat1 Participates in the Pathological Angiogenesis of Diabetic Retinopathy in an Oxygen-Induced Retinopathy Mouse Model by Sponging Mir-203a-3p. Can J Physiol Pharmacol. 2020;98(4):219-227. doi:10.1139/cjpp-2019-0489

114.   Shaker OG, Abdelaleem OO, Mahmoud RH, Abdelghaffar NK, Ahmed TI, Said OM, et al. Diagnostic and Prognostic Role of Serum Mir-20b, Mir-17-3p, Hotair, and Malat1 in Diabetic Retinopathy. IUBMB Life. 2019;71(3):310-320. doi:10.1002/iub.1970

115.   Zhang H, Yan Y, Hu Q, Zhang X. Lncrna Malat1/Microrna Let-7f/Klf5 Axis Regulates Podocyte Injury in Diabetic Nephropathy. Life Sci. 2021;266:118794. doi:10.1016/j.lfs.2020.118794

116.   Che H, Wang Y, Li H, Li Y, Sahil A, Lv J, et al. Melatonin Alleviates Cardiac Fibrosis Via Inhibiting Lncrna Malat1/Mir-141-Mediated Nlrp3 Inflammasome and Tgf-Beta1/Smads Signaling in Diabetic Cardiomyopathy. FASEB J. 2020;34(4):5282-5298. doi:10.1096/fj.201902692R

117.   Xia C, Liang S, He Z, Zhu X, Chen R, Chen J. Metformin, a First-Line Drug for Type 2 Diabetes Mellitus, Disrupts the Malat1/Mir-142-3p Sponge to Decrease Invasion and Migration in Cervical Cancer Cells. Eur J Pharmacol. 2018;830:59-67. doi:10.1016/j.ejphar.2018.04.027

118.   Chang W, Wang J. Exosomes and Their Noncoding Rna Cargo Are Emerging as New Modulators for Diabetes Mellitus. Cells. 2019;8(8). doi:10.3390/cells8080853

119.   Prokisch MGaH. Ncrnas: New Players in Mitochondrial Health and Disease? Front Genet. 2020;10.3389/fgene.2020.00095. doi:10.3389/fgene.2020.00095

120.   Chen G, Guo H, Song Y, Chang H, Wang S, Zhang M, et al. Long Noncoding Rna Ak055347 Is Upregulated in Patients with Atrial Fibrillation and Regulates Mitochondrial Energy Production in Myocardiocytes. Mol Med Rep. 2016;14(6):5311-5317. doi:10.3892/mmr.2016.5893

121.   Sirey TM, Roberts K, Haerty W, Bedoya-Reina O, Rogatti-Granados S, Tan JY, et al. Correction: The Long Non-Coding Rna Cerox1 Is a Post Transcriptional Regulator of Mitochondrial Complex I Catalytic Activity. eLife. 2019;8. doi:10.7554/eLife.50980

122.   Tian T, Lv X, Pan G, Lu Y, Chen W, He W, et al. Long Noncoding Rna Mprl Promotes Mitochondrial Fission and Cisplatin Chemosensitivity Via Disruption of Pre-Mirna Processing. Clin Cancer Res. 2019;25(12):3673-3688. doi:10.1158/1078-0432.CCR-18-2739

123.   Li HJ, Sun XM, Li ZK, Yin QW, Pang H, Pan JJ, et al. Lncrna Uca1 Promotes Mitochondrial Function of Bladder Cancer Via the Mir-195/Arl2 Signaling Pathway. Cell Physiol Biochem. 2017;43(6):2548-2561. doi:10.1159/000484507

124.   Yang F, Qin Y, Lv J, Wang Y, Che H, Chen X, et al. Silencing Long Non-Coding Rna Kcnq1ot1 Alleviates Pyroptosis and Fibrosis in Diabetic Cardiomyopathy. Cell Death Dis. 2018;9(10):1000. doi:10.1038/s41419-018-1029-4

125.   Yang F, Qin Y, Wang Y, Li A, Lv J, Sun X, et al. Lncrna Kcnq1ot1 Mediates Pyroptosis in Diabetic Cardiomyopathy. Cell Physiol Biochem. 2018;50(4):1230-1244. doi:10.1159/000494576

126.   Wu A, Sun W, Mou F. Lncrnamalat1 Promotes High Glucoseinduced H9c2 Cardiomyocyte Pyroptosis by Downregulating Mir1413p Expression. Mol Med Rep. 2021;23(4). doi:10.3892/mmr.2021.11898

127.   Wang C, Liu G, Yang H, Guo S, Wang H, Dong Z, et al. Malat1-Mediated Recruitment of the Histone Methyltransferase Ezh2 to the Microrna-22 Promoter Leads to Cardiomyocyte Apoptosis in Diabetic Cardiomyopathy. Sci Total Environ. 2021;766:142191. doi:10.1016/j.scitotenv.2020.142191

128.   Sun F, Yuan W, Wu H, Chen G, Sun Y, Yuan L, et al. Lncrna Kcnq1ot1 Attenuates Sepsis-Induced Myocardial Injury Via Regulating Mir-192-5p/Xiap Axis. Exp Biol Med (Maywood). 2020;245(7):620-630. doi:10.1177/1535370220908041

129.   Zhu B, Cheng X, Jiang Y, Cheng M, Chen L, Bao J, et al. Silencing of Kcnq1ot1 Decreases Oxidative Stress and Pyroptosis of Renal Tubular Epithelial Cells. Diabetes Metab Syndr Obes. 2020;13(13):365-375. doi:10.2147/DMSO.S225791

130.   Zhao SF, Ye YX, Xu JD, He Y, Zhang DW, Xia ZY, et al. Long Non-Coding Rna Kcnq1ot1 Increases the Expression of Pdcd4 by Targeting Mir-181a-5p, Contributing to Cardiomyocyte Apoptosis in Diabetic Cardiomyopathy. Acta Diabetol. 2021;58(9):1251-1267. doi:10.1007/s00592-021-01713-x

131.   McCully JD, Cowan DB, Pacak CA, Toumpoulis IK, Dayalan H, Levitsky S. Injection of Isolated Mitochondria During Early Reperfusion for Cardioprotection. Am J Physiol Heart Circ Physiol. 2009;296(1):H94-H105. doi:10.1152/ajpheart.00567.2008

132.   Pacak CA, Preble JM, Kondo H, Seibel P, Levitsky S, Del Nido PJ, et al. Actin-Dependent Mitochondrial Internalization in Cardiomyocytes: Evidence for Rescue of Mitochondrial Function. Biol Open. 2015;4(5):622-626. doi:10.1242/bio.201511478

133.   Cowan DB, Yao R, Thedsanamoorthy JK, Zurakowski D, Del Nido PJ, McCully JD. Transit and Integration of Extracellular Mitochondria in Human Heart Cells. Sci Rep. 2017;7(1):17450. doi:10.1038/s41598-017-17813-0

134.   Ramirez-Barbieri G, Moskowitzova K, Shin B, Blitzer D, Orfany A, Guariento A, et al. Alloreactivity and Allorecognition of Syngeneic and Allogeneic Mitochondria. Mitochondrion. 2019;46:103-115. doi:10.1016/j.mito.2018.03.002

135.   Blitzer D, Guariento A, Doulamis IP, Shin B, Moskowitzova K, Barbieri GR, et al. Delayed Transplantation of Autologous Mitochondria for Cardioprotection in a Porcine Model. Ann Thorac Surg. 2020;109(3):711-719. doi:10.1016/j.athoracsur.2019.06.075

136.   Emani SM, Piekarski BL, Harrild D, Del Nido PJ, McCully JD. Autologous Mitochondrial Transplantation for Dysfunction after Ischemia-Reperfusion Injury. J Thorac Cardiovasc Surg. 2017;154(1):286-289. doi:10.1016/j.jtcvs.2017.02.018

137.   Masuzawa A, Black KM, Pacak CA, Ericsson M, Barnett RJ, Drumm C, et al. Transplantation of Autologously Derived Mitochondria Protects the Heart from Ischemia-Reperfusion Injury. Am J Physiol Heart Circ Physiol. 2013;304(7):H966-982. doi:10.1152/ajpheart.00883.2012

138.   Emani SM, McCully JD. Mitochondrial Transplantation: Applications for Pediatric Patients with Congenital Heart Disease. Transl Pediatr. 2018;7(2):169-175. doi:10.21037/tp.2018.02.02

139.   Roushandeh AM, Kuwahara Y, Roudkenar MH. Mitochondrial Transplantation as a Potential and Novel Master Key for Treatment of Various Incurable Diseases. Cytotechnology. 2019;71(2):647-663. doi:10.1007/s10616-019-00302-9

CHAPTER 2: SPECIFIC AIM 1

Manipulation of the miR-378a/mt-ATP6 regulatory axis rescues ATP synthase in the diabetic heart and offers a novel role for lncRNA Kcnq1ot1

Andrya J. Durr[1,2], Quincy A. Hathaway[1,2,3], Amina Kunovac[1,2,3], Andrew D. Taylor[1,2], Mark V. Pinti[2,4,5], Saira Rizwan[1,2], Danielle L. Shepherd[1], Chris C. Cook[6], Garrett K. Fink[1], and John M. Hollander[1,2,3]

[1]Division of Exercise Physiology, West Virginia University School of Medicine, Morgantown, West Virginia. [2]Mitochondria, Metabolism & Bioenergetics Working Group, West Virginia University School of Medicine, Morgantown, West Virginia. [3]Center for Inhalation Toxicology, West Virginia University School of Medicine, Morgantown, West Virginia. [4]West Virginia University School of Pharmacy, Morgantown, West Virginia. [5]Department of Physiology and Pharmacology, Morgantown, West Virginia. [6]Cardiovascular and Thoracic Surgery, West Virginia University School of Medicine, Morgantown, West Virginia.

Corresponding Author:

John M. Hollander, PhD, FAHA

Professor and Graduate Director, Exercise Physiology

Sr. Asst. Dean for Research and Graduate Education, Human Performance

Director, Mitochondria, Metabolism & Bioenergetics

West Virginia University School of Medicine

1 Medical Center Drive

P.O. Box 9227

Morgantown, WV 26506

Ph: (304) 293-3683

Fax: (304) 293-7105

Email: jhollander@hsc.wvu.edu

Abstract

Diabetes mellitus has been linked to an increase in mitochondrial microRNA-378a (miR-378a) content. Enhanced miR-378a content has been associated with a reduction in mitochondrial genome-encoded mt-ATP6 abundance, supporting the hypothesis that miR-378a inhibition may be a therapeutic option for maintaining ATP synthase functionality during diabetes mellitus. Evidence also suggests that long noncoding RNAs (lncRNAs), including lncRNA potassium voltage-gated channel subfamily Q member 1 overlapping transcript 1 (Kcnq1ot1), participate in regulatory axes with microRNAs (miRs). Prediction analyses indicate that Kcnq1ot1 has the potential to bind miR-378a. This study aimed to determine if loss of miR-378a in a genetic mouse model could ameliorate cardiac dysfunction in type 2 diabetes mellitus (T2DM) and to ascertain whether Kcnq1ot1 interacts with miR-378a to impact ATP synthase functionality by preserving mt-ATP6 levels. MiR-378a was significantly higher in patients with T2DM and 25-week-old *Db/Db* mouse mitochondria, whereas mt-ATP6 and Kcnq1ot1 levels were significantly reduced when compared with controls. Twenty-five-week-old miR-378a knockout *Db/Db* mice displayed preserved mt-ATP6 and ATP synthase protein content, ATP synthase activity, and preserved cardiac function, implicating miR-378a as a potential therapeutic target in T2DM. Assessments following overexpression of the 500-bp Kcnq1ot1 fragment in established mouse cardiomyocyte cell line (HL-1) cardiomyocytes overexpressing miR-378a revealed that Kcnq1ot1 may bind and significantly reduce miR-378a levels, and rescue mt-ATP6 and ATP synthase protein content. Together, these data suggest that Kcnq1ot1 and miR-378a may act as constituents in an axis that regulates mt-ATP6 content, and that manipulation of this axis may provide benefit to ATP synthase functionality in type 2 diabetic heart.

Keywords: heart; lncRNA; microRNA; mitochondria; type 2 diabetes mellitus

Introduction

The frequency of type 2 diabetes mellitus (T2DM) has increased dramatically, with the World Health Organization and others documenting 422 million cases worldwide in 2014, and estimating a rise to 642 million by 2040 (1, 2). As T2DM prevalence rises, our understanding of the progression and comorbidities underlying its pathophysiological mechanisms become critical. Cardiovascular disease (CVD) is the leading cause of mortality in the diabetic population, occurring in approximately 32% of patients and leading to death in approximately 10% of those afflicted (1). The mechanisms contributing to the development of CVD in T2DM have not been fully elucidated, but mitochondrial dysfunction has been suggested to play a role in a number of key disease features, including the development of insulin resistance, the initial onset of disease, and the development of cardiac contractile dysfunction (3-5).

Non-coding RNAs (ncRNAs) have gained interest due to their ability to act both protectively and pathologically (6-8). MicroRNAs (miRs), a class of small ncRNAs that are approximately 22 nucleotides in length, can influence the development of CVD and T2DM due to their ability to regulate transcription both outside and inside the mitochondrion (6, 9, 10). Our laboratory and others have reported significant changes in the miR profile of diabetic cardiac mitochondria (6, 11-13). Following miR profiling, microRNA-378a (miR-378a), containing two strands, miR-378a-3p and miR-378a-5p, was shown to be significantly increased in cardiac mitochondria of streptozotocin-treated mice (11). Jagannathan et al. demonstrated the potential for miR-378a to bind and downregulate the expression of mitochondrial genome-encoded mt-ATP6, a component of the electron transport chain complex V (ATP synthase) F_0 complex (11). MiR-378a downregulation of mt-ATP6 led to a decrease in ATP synthase functionality (11, 14), and treatment with miR-378a-antagomir resulted in improved cardiac systolic function in streptozotocin-treated mice (11). These were complemented by *in vitro* cellular

models of miR-378a overexpression (11, 14). At current, the role of miR-378a remains unexplored in T2DM, the most prevalent form of diabetes mellitus.

Additional ncRNA species have been identified in the mitochondrion, including long non-coding RNAs (lncRNA) (15-17). Analysis of lncRNAs in T2DM blood samples revealed 441 differentially expressed lncRNAs, indicating that T2DM can influence the lncRNA network (17). Mitochondrial lncRNA presence has been observed, but data are limited (15). Undeniably, the role(s) played by lncRNAs in the mitochondrion are unclear. Evidence suggests that lncRNAs, including lncRNA potassium voltage-gated channel subfamily Q member 1 overlapping transcript 1 (Kcnq1ot1), may play a role in the regulatory activity of miRs through a process known as sponging, where they act as endogenous competing RNAs by binding to complimentary miR response elements, and influencing mRNA transcription (6, 17, 18). Kcnq1ot1 has been evaluated in a number of diabetic tissues, but its ultimate function and effect remains unclear (19-25). At current, the relationship between Kcnq1ot1 and miR-378a in the mitochondrion has not been elucidated. The objectives of this study were to determine if loss or inhibition of miR-378a could ameliorate cardiac dysfunction in T2DM, and to determine whether Kcnq1ot1 interacts with miR-378a in a sponging mechanism to influence mitochondrial genome-encoded mt-ATP6 and ATP synthase functionality.

Materials and Methods

Experimental animals

Animal experiments used in this study conformed to the National Institutes of Health Guidelines for the Care and Use of Laboratory Animals and were approved by the West Virginia University (WVU) Animal Care and Use Committee. Whole body miR-378a knockout (KO) mice were a kind gift from Dr. Eric Olson at the University of Texas Southwestern Medical Center (26). Experimental animals

included male and female FVB/NJ wild-type (WT) mice (RRID:IMSR_JAX:001800), FVB/NJ *Db/Db* mice (The Jackson Laboratory stock Cat. No. 006654) (27, 28), FVB/NJ miR-378a KO mice, and FVB/NJ miR-378a KO/*Db/Db* mice generated by our laboratory (Supplemental Figure S2.1). *Db/Db* mice develop severe hyperglycemia at 5 weeks of age (29). Animals were housed in the WVU Health Sciences Center animal facility on a 12-hour light/dark cycle in a temperature-controlled room. Animals were maintained on a standard chow diet and had access to both food and water *ad libitum*. Animals were euthanized at 25 weeks of age using cervical dislocation as a primary method, and critical organ removal as a secondary method of euthanasia. Cardiac ventricular tissues and serum were collected for biochemical analyses. Ideal samples sizes were determined using a 2-sided power analysis, with an alpha value of 0.05 and a desired power of 0.80, using previously collected echocardiography values (30). Initial evaluation of cardiac function in male and female animals presented no significant differences, therefore subsequent biochemical analyses utilized a combination of sexes. No animals were excluded from the study.

KO/Db/Db Model Characterization

Weight, fasting blood glucose, serum insulin, and miR-378a levels were evaluated at 25 weeks to verify diabetes mellitus progression in KO/*Db/Db* mice. Fasting blood glucose was measured using an Ascensia Contour blood glucose monitor (Bayer Healthcare LLC, Mishawaka IN) and corresponding blood glucose test strips (Ascensia, Cat. No. 7097C). Serum insulin levels were measured using a Mouse Insulin ELISA Kit (Thermo Fisher Scientific Cat. No. EMINS) according to manufacturer instructions. Briefly, mouse serum was collected from whole blood isolates after coagulation at room temperature for 30 minutes and centrifugation at 2,500 rcf for 10 min. Serum was diluted twofold, and processed according to manufacturer instructions. Measurements were acquired at 450 nm and 550 nm wavelengths. Values acquired at 550 nm were subtracted from values acquired at 450 nm to correct for optical imperfections in the microplate provided. MiR-378a-

3p and miR-378a-5p levels were assessed to verify miR-378a loss in KO and KO/*Db/Db* animals using qPCR. MiR-378a genomic deletion was verified in a previous study (26).

Study Approval and Patient Population

The WVU Institutional Review Board and Institutional Biosafety Committee approved the studies and data generated from this work, including all right atrial tissue and patient information acquired. When required by the Institutional Review Board, written informed consent was received from every participant or legal guardian by the WVU Heart and Vascular Institute, J.W. Ruby Memorial Hospital. Right atrial appendages were removed during open-heart and/or valvular surgery by a single co-operating physician, and all tissue and data were stored in a double de-identified process. Atrial tissue from patients who were either nondiabetic (ND) or with T2DM were used in the analyses. Patients' tissue was used irrespective of age, gender, and ethnicity/race. Patients with a history of smoking were excluded from the study.

Mitochondrial Isolation

Mitochondria were isolated from mouse and human cardiac tissues as previously described (31), with modifications by our laboratory (32-34). Briefly, mitochondria were isolated using a series of centrifugation steps to separate subsarcolemmal (SSM) and interfibrillar (IFM) subpopulations from nuclear and cytoplasmic portions. SSM and IFM subpopulations were combined to form a total mitochondrial population. Mitochondrial pellets were resuspended in 200 µl of KME buffer (100 mM KCl, 50 mM MOPS, and 0.5 mM EDTA; pH 7.4) to be assessed for mt-ATP6 protein and ATP synthase content, ATP synthase activity, and qPCR quantification. Nuclear portions remained once the cytoplasmic portion and mitochondria were removed and were saved for biochemical analysis.

Cross-linked Immunoprecipitation

Cross-linked immunoprecipitation (CLIP) was performed on mouse cardiac tissue as previously described (11), with modifications (35, 36). Briefly, tissues were finely minced in 1X PBS in a petri dish with a suspension depth of approximately 1 mm. Samples were irradiated 5 times with 400 mJ/cm2 on ice using a CL-1000 Ultraviolet Crosslinker (UVP, Upland, CA), and mixed between each irradiation. Two hundred and twenty-five micrograms of protein were diluted in NP-40 buffer (20mM Tris HCl; pH 8.0, 137mM NaCl, 10% Glycerol, 1% Triton X100, 2mM EDTA) up to 1 mL and the RNA digested by addition of 10 microliters of RNase I (Thermo Fisher Scientific Cat. No. EN0601, 1:500). Fifty microliters of Protein G magnetic beads (New England Biolabs Cat. No. S1430S) were washed 3 times with NP-40 buffer and then resuspended in 100 microliters of NP-40 buffer and 5 microliters of Recombinant Anti-Argonaute-2 antibody rabbit monoclonal (Abcam Cat. No. ab186733, RRID:AB_2713978). The antibody was allowed to bind to the beads by rotating the tubes overnight. Beads were washed three times with NP-40 buffer, and cross-linked tissue lysates added followed by tube rotation for 2 hours at 4°C. Beads were washed three times with NP-40 buffer. Thirty microliters of NP-40 was added to the beads and heated for 10 minutes at 70°C with shaking (1000 rpm). Supernatant was used for RNA isolation and qPCR analyses.

RT-qPCR

Total RNA was isolated from mouse and human mitochondria and cardiac tissue samples using the RNeasy Mini Kit (Qiagen Cat. No. 74104) according to manufacturer instructions. Total DNA was isolated from mouse cardiac tissue using the DNeasy Blood and Tissue Kit (Qiagen Cat. No. 69504) according to manufacturer instructions. Two step RT-qPCR analysis was performed, with miR amplification achieved using a high-capacity RNA to cDNA synthesis kit (Thermo

Fisher Scientific Cat. No. 4387406) and SYBR Green components in a total sample volume of 25 µl: 12.5 µl PowerUp SYBR Green Master Mix (Applied Biosystems Cat. No. A25742), 9.5 µl RNAse/Nuclease free water, 1 µl of primer pair for the control (U6/GAPDH) or experimental target, and 2 µl of sample cDNA. Samples were run in duplicate for target sequence and U6 or GAPDH control. Data represented as fold change are calculated as the $2^{\Delta\Delta Ct}$ of the target sequences, with all groups represented as change relative to control. MtDNA content was assessed as previously described (37), with modifications. To determine mtDNA content, delta threshold (Ct) values were acquired by subtracting nuclear DNA (nucDNA) from mtDNA. An Applied Biosystems 7500HT Fast Real-Time PCR System was used for analysis, with reaction conditions optimized to Origene's qSTAR miRNA qPCR Detection System instructions. Primer pair sequences are listed in Supplemental Table S2.1; see http://doi.org/10.6084/ m9.figshare.18940262.

Western Blotting

Mouse and human cardiac tissues were homogenized using a Polytron PowerGen 500 S1 tissue homogenizer (Fisher Scientific, Hampton, NH) in radioimmunoprecipitation assay (RIPA) buffer (Thermo Fisher Scientific Cat. No. 89901), then centrifuged at 10,000 rcf for 20 minutes to remove debris. The supernatant was kept for Western blot analysis, and the pellet was discarded. Samples were prepared as previously described (11, 38). Briefly, a Bradford assay was used to determine protein concentration (39), and 30-50 micrograms of protein were used per sample. NuPAGE™ LDS Sample Buffer (4x) (Thermo Fisher Scientific Cat. No. NP0007) was added to samples, and heated to 70° Celsius for 10 minutes to denature proteins. Samples were allowed to cool to room temperature before loading into the gel. NuPAGE™ 12% Bis-Tris Protein Gels, 1.0 mm, 15-well gels (Invitrogen Cat. No. NP0343BOX) and NuPAGE™ MES SDS Running Buffer (Thermo Fisher Scientific Cat. No. NP0002) were used as previously described (14, 32, 40, 41). Proteins were transferred to Nitrocellulose

Membrane (Thermo Fisher Scientific Cat. No. 88018), and blocked for 1 hour at room temperature in a 5% milk solution. Primary antibodies used in the study were: Anti-MT-ATP6 rabbit polyclonal (Thermo Fisher Scientific Cat. No. PA5-37129, RRID:AB_2553922, 1:1000), Anti-GAPDH mouse monoclonal (Abcam Cat. No. ab8245, RRID:AB_2107448, 1:1000), Anti-VDAC1 mouse monoclonal (Sigma-Aldrich Cat. No. SAB5201374-100UG, 1:1000), which was verified for specificity by Sigma-Aldrich during quality control testing, and Anti-β Actin mouse monoclonal (Sigma-Aldrich Cat. No. A5316, RRID:AB_476743, 1:1000). Secondary antibodies used in the study were: Rabbit Anti-Mouse IgG H&L (HRP) (Abcam Cat. No. ab6728, RRID:AB_955440, 1:2500) and Goat Anti-Rabbit IgG H&L (HRP) (Abcam Cat. No. ab6721, RRID:AB_955447, 1:2500). Radiance Plus Western blotting substrate (Azure Biosystems Cat. No. AC2103) was used to detect signal per manufacturer instructions. The G:Box Bioimaging system (Syngene, Frederick, MD) was used to detect luminescence, and data was captured using GeneSnap/GeneTools software. Densitometry was analyzed using Image J Software (ImageJ, RRID:SCR_003070) and all values were expressed as optical density with arbitrary units.

Blue Native-Page

ATP synthase content was assessed using blue native polyacrylamide gel electrophoresis (BN-PAGE) as previously described (42). Briefly, mitochondria were solubilized with 5% digitonin on ice. After addition of Coomassie G-250, samples were run on 4–16% NativePAGE 15-well gels (Thermo Fisher Scientific Cat. No. BN1004BOX) at 150 volts for 30 minutes, when dark buffer was replaced with light buffer and run at 250 volts for 1 hour, or until samples traveled the length of the gel. Following BN-PAGE, gels were removed from the cassette, rinsed with deionized water, and fixed in a solution containing 50% methanol and 8% acetic acid for 15 min. Gels were stained using a colloidal blue staining kit (Invitrogen Cat. No. LC6025) according to manufacturer instructions. Optical densities were measured using Image J Software as described in "Western Blotting."

Electron Transport Chain Complex Activities

The activity of complexes I, III, IV, and ATP synthase were measured spectrophotometrically on isolated mitochondria as previously described (31, 32, 43-45). Briefly, activities were measured for complexes I (reduction of decylubiquinone), III (reduction of cytochrome *c*), IV (oxidation of reduced cytochrome *c*), and ATP synthase (pyruvate kinase, phosphoenolpyruvate and ATP production). A Bradford assay was carried out on each sample to provide a basis for normalization to protein content. Values are expressed as nanomoles consumed per minute, per microgram of protein. For ATP synthase, this expression is equal to the nanomoles of NADH oxidized per minute, per microgram of protein.

Echocardiography

A single trained individual in the WVU Animal Models and Imaging Facility acquired ultrasound images in a blinded fashion in conscious mice to maintain normal left ventricle (LV) function and heart rate (46-49). Images were acquired using a 32–55 MHz linear array transducer on the Vevo2100 Imaging System (Visual Sonics, Toronto, Canada) as previously described (30, 32, 34, 41). Briefly, measurements including ejection fraction (EF), fractional shortening (FS), cardiac output, and stroke volume were obtained from LV images. Mouse identifiers were randomized prior to echocardiographic analysis to mask group, and were analyzed by a single individual. M-mode measurements were calculated over at least three consecutive cardiac cycles and averaged values were considered a single replicate. This was repeated for as many M-mode videos as provided up to 6 replicates.

Cell Culture

The established mouse cardiomyocyte cell line (HL-1) (Millipore Cat. No. SCC065, RRID:CVCL_0303) (Registered with the International Depositary Authority, American Type Culture Collection (ATCC); CRL-12197), which maintains a cardiac-specific phenotype following repeated passages, and a HL-1 miR-378a overexpressing cell line (HL-1-378a) generated by our laboratory, were used as previously described (11, 12, 14, 50). HL-1-378a cells demonstrate significant reductions in mt-ATP6 mRNA, mt-ATP6 protein content, and ATP synthase activity (11, 14). Cells were maintained at 5% CO_2/95% air and 37 °C in Claycomb medium (Sigma Aldrich Cat. No. 51800C-500ML) and prepared according to manufacturer instructions. The "n" presented in related results is representative of biological replicates. It should be noted that the advantage of this model is that it affords the opportunity to explore the mechanistic interaction between lncRNA Kcnq1ot1 and the miR-378a/mt-ATP6 axis in an artificial system of enhanced miR-378a presence.

Plasmid Construction

IntaRNA, lncBase, and DIANA software programs were utilized to determine Kcnq1ot1 binding sites for miR-378a (51-57). Of the two strands, miR-378a-5p was predicted to bind most strongly to Kcnq1ot1, and was utilized in plasmid production. Plasmids were generated using a pGL4.14_[luc2/Hygro] vector backbone containing a firefly luciferase reporter gene (Promega Cat. No. E6691). Three plasmids were designed and verified for sequence insertion between restriction enzymes BglII and HindIII prior to delivery; a Kcnq1ot1-miR-378a-5p fragment containing the sequence for a single binding site, a 500-bp Kcnq1ot1 fragment containing three miR-378a-5p binding sites, and Kcnq1ot1 scramble (Genscript, Piscataway, NJ). Plasmids were delivered at a 1mg/ml concentration in 1 mL of Tris-EDTA (TE) buffer. Kcnq1ot1 DNA sequences and

plasmid constructs can be found in Supplemental Table S2.2 and Supplemental Figure S2.2

Luciferase Assay

HL-1-378a cells were seeded in a 12 well plate and transfected at 60-70% confluency. Overexpression of Kcnq1ot1 fragments was established as previously described (14). Briefly, plasmid DNA was transfected at a concentration of 1.0 μg of DNA using Lipofectamine 3000 Transfection Reagent (Thermo Fisher Scientific Cat. No. L3000015) according to manufacturer instructions, and allowed to incubate for 48 h. The Dual-Luciferase Reporter Assay (Promega Cat. No. E1910) was used to measure firefly and renilla luciferase activity according to manufacturer instructions. Firefly luminescence indicating luciferase gene activation was normalized to renilla to account for background activity.

Overexpression of Kcnq1ot1 Fragment

HL-1-378a cells were seeded in a 150 mm plate and transfected at 60-70% confluency. Overexpression of Kcnq1ot1 fragments was established as described in "Luciferase Assay." Cells were transfected at a concentration of 10.5 – 21 μg of DNA using Lipofectamine 3000 Transfection Reagent according to manufacturer instructions. Forty-eight hours post transfection, cells were harvested for biochemical analysis.

Statistical Analysis

Statistical analyses were performed using GraphPad Prism version 8.02 (GraphPad Prism, RRID:SCR_002798). Mouse data were analyzed using a two-way ANOVA designed to compare the four experimental groups and their respective controls. Data were organized into two factors; miR-378a KO and control. The miR-378a KO factor included the miR-378a KO control group and the

miR-378a KO/*Db/Db* group. The control factor included the WT control group and the *Db/Db* group. Within the two-way ANOVA, multiple comparisons analysis was performed using a Fisher's least significance difference (LSD) test designed to allow for each comparison with standalone. A two-tailed Student's T-test was used for statistical analysis between ND and T2DM patients, and between HL-1 cell groups. Data are presented as mean ± standard error of the mean (SEM).

Results

Mitochondrial miR-378a/mt-ATP6 Regulatory Axis in T2DM

MiR-378a-3p and miR-378a-5p were significantly increased in mitochondria of patients with T2DM when compared with ND (Figure 2.1, A and B). Mt-ATP6 mRNA levels were significantly higher in mitochondria of patients with T2DM (Figure 2.1C), while mt-ATP6 protein content was significantly decreased in mitochondria of patients with T2DM patient mitochondria when compared with ND (Figure 2.1D). ATP synthase content was decreased in T2DM, averaging 58.61% of levels in ND patients, and corresponded to significantly lower ATP synthase activity (Figure 2.1, E and F).

Animal Model Characterization

Weight, fasting blood glucose, serum insulin, miR-378a-3p, and miR-378a-5p levels were measured at 25 weeks (Figure 2.2). Body weight was significantly increased in both *Db/Db* and KO/*Db/Db* groups when compared with control, indicating development of obesity (Figure 2.2A). Significant increases in fasting blood glucose in *Db/Db* and KO/*Db/Db* mice were observed when compared with control, confirming the development of hyperglycemia (Figure 2.2B). Concomitantly, significant increases in serum insulin levels were observed in *Db/Db* and KO/*Db/Db* mice when compared with controls, while KO/*Db/Db* mice also demonstrated insulin levels significantly higher than *Db/Db* mice, confirming

58

the presence of hyperinsulinemia (Figure 2.2C). MiR-378a-3p and miR-378a-5p levels were significantly lower in KO and KO/*Db/Db* animals when compared with controls, verifying significant loss of miR-378a (Figure 2.2D).

Impact of miR-378a Loss on ATP Synthase

To assess the impact of miR-378a genomic loss on ATP synthase, mt-ATP6 mRNA levels and protein content, ATP synthase content, and ATP synthase activity were assessed (Figure 2.3). MiR-378a-3p and miR-378a-5p were significantly increased in *Db/Db* mitochondria when compared with WT (Figure 2.3, A and B), whereas KO and KO/*Db/Db* mice contained negligible levels (Figure 2.2D). Mt-ATP6 mRNA content was not significantly altered between WT and Db/Db mice (Figure 2.3C), but was significantly increased in KO and KO/*Db/Db* mice when compared with controls (Figure 2.3D). To determine whether increased translational repression of mt-ATP6 mRNA by the RNA-induced silencing complex (RISC) occurs in T2DM, we performed a CLIP experiment with a key RISC component, argonaute 2 (Ago2). The level of mt-ATP6 cross linked with the RICS component Ago2 was significantly higher in *Db/Db* mice when compared with WT, whereas KO/*Db/Db* mice demonstrated significantly less mt-ATP6 cross linked with RISC component Ago2, when compared with *Db/Db* mice (Figure 2.3E). Mt-ATP6 protein content was significantly lower in *Db/Db* mice when compared with WT, but showed trending increases in KO/*Db/Db* animals when compared with *Db/Db* (P = 0.09) (Figure 2.3F). ATP synthase content was 62.0%, 89.6%, and 124.6% in *Db/Db*, KO, and KO/*Db/Db* respectively, when compared with WT (Figure 2.3G), suggesting that modest preservation of mt-ATP6 content may allow for the preservation of total ATP synthase content in KO/*Db/Db* animals. ATP synthase activity in total mitochondria was significantly lower in *Db/Db* mice as compared with WT, but was preserved in KO/*Db/Db* mice, which demonstrated significantly higher ATP synthase activity when compared with *Db/Db* (Figure 2.3H). To further assess the function of the mitochondrial electron transport chain, we assessed the activities of complexes I, III, and IV, as well as ATP content. No

significant differences were observed in the activity of complexes I (Supplemental Figure S2.3A) and IV (Supplemental Figure S2.3C). Complex III activity was significantly altered within the diabetic condition, showing modest reductions in *Db/Db* mice (P = 0.06), and significant reductions in KO/*Db/Db* mice when compared with WT (Supplemental Figure S2.3B). Finally, no significant differences were observed in mitochondrial ATP content (Supplemental Figure S2.3D).

In addition to mitochondrial bioenergetic function, we assessed whether changes in mt-ATP6 protein content and ATP synthase functionality could be due to alterations in total mt-DNA content in KO or KO/*Db/Db* mice. Delta Ct values for mt-16S rRNA were found to be significantly increased in *Db/Db* mice, and showed trending increases in KO/*Db/Db* mice (P = 0.09) when compared with WT controls (Supplemental Figure S2.4A). Delta Ct values for mt-ATP6 were significantly increased in *Db/Db* and KO/*Db/Db* mice when compared to controls (Supplemental Figure S2.4B). Mt-DNA content appeared unchanged for both mt-16s rRNA and mt-ATP6 in KO animals when compared with control, suggesting that miR-378a loss does not lead to alterations in mtDNA content (Supplemental Figure S2.4).

MiR-378a Loss Improves Cardiac Function in T2DM

M-mode echocardiography was used to assess the impact of miR-378a loss on systolic cardiac function (Table 2.1). *Db/Db* mice showed significant pathological changes in M-mode parameters, with notably decreased EF and FS, increased LV mass, and increased LV volume, LV diameter, and wall thicknesses when compared with WT (Table 2.1). Alternatively, KO/*Db/Db* mice exhibited significantly higher EF and FS when compared with *Db/Db* counterparts, indicating preserved systolic contractile function (Table 2.1).

Kcnq1ot1 Alterations in T2DM and Interactions with miR-378a-5p

Mitochondrial Kcnq1ot1 levels were significantly reduced in *Db/Db* mice cardiac mitochondria when compared with WT (Figure 2.4A), but were significantly increased in both nuclear and cardiac tissue (Figure 2.4, B and C). These results were recapitulated in patients with T2DM, where Kcnq1ot1 levels were significantly lower in mitochondria of patients with T2DM when compared with ND (Figure 2.4D), but were significantly higher in nuclear and cardiac tissue (Figure 2.4, E and F). Using the computational reference repository DIANA, we pictorially show Kcnq1ot1 sequence complementarity to miR-378a-5p, a match to the RNA utilized for assessment of luciferase activity (Figure 2.4G). Following transfection with both the Kcnq1ot1-miR-378a-5p fragment and the 500-bp Kcnq1ot1 fragment containing multiple miR-378a binding sites, luciferase activity was significantly reduced when compared with a scramble control (Figure 2.4H). These results indicate that Kcnq1ot1 has the potential to interact with miR-378a-5p.

Overexpression of a 500-bp Kcnq1ot1 Fragment Leads to miR-378a-5p Inhibition

To determine the effects of Kcnq1ot1 manipulation on the miR-378a/mt-ATP6 axis, a plasmid containing a 500-bp Kcnq1ot1 fragment containing three miR-378a-5p binding sites was used to overexpress Kcnq1ot1 *in vitro* in HL-1 and HL-1-378a cardiomyocytes (Supplemental Figure S2.5) (Figure 2.5). HL-1-378a cells demonstrated significantly higher levels of miR-378a when compared with HL-1 cells (Supplemental Figure S2.5A). Further, miR-378a cells exhibited significantly lower mt-ATP6 protein content (Supplemental Figure S2.5B). Significant increases in the 500-bp Kcnq1ot1 fragment, and significant decreases in miR-378a-5p levels, were confirmed following transfection when compared with HL-1 scramble cells (Supplemental Figure S2.5, C and D). No change was observed in mt-ATP6 mRNA levels in HL-1 cells overexpressing the 500-bp Kcnq1ot1 fragment when compared with HL-1 cells overexpressing a scrambled control (Supplemental Figure S2.5E). Overexpression of the 500-bp Kcnq1ot1

fragment was confirmed in HL-1-378a cells (Figure 2.5A). Significant decreases in miR-378a-5p levels were observed, indicating potential binding and a change in miR-378a-5p availability (Figure 2.5B). Overexpression of the 500-bp Kcnq1ot1 fragment resulted in significant increases of mt-ATP6 mRNA and protein content (Figure 2.5, C and D). Finally, rescue of ATP synthase content was confirmed (Figure 2.5E). These results indicate that Kcnq1ot1 may actively limit miR-378a availability and preserve ATP synthase content.

Discussion

T2DM associated morbidity and mortality continues to increase in prevalence, yet therapeutic interventions to ameliorate cardiac dysfunction remain limited. The mitochondrion has received a great deal of focus due to its role in generating ATP necessary for cardiac contractile function. Thus, mitochondrially-targeted therapeutics may present an opportunity for managing cardiac contractile dysfunction associated with diabetes mellitus (58, 59). The mitochondrial genome encodes 13 proteins which are constituents of the electron transport chain complexes, including complex V, which is part of the ATP generating complex, ATP synthase (60). Because they are capable of regulating protein expression, miRs, such as miR-378a, may provide a therapeutic option for limiting cardiac contractile dysfunction associated with the diabetic heart (11, 14). In the current study we determined that inhibition of miR-378a in the T2DM heart could provide benefit to ATP synthase content by preserving mt-ATP6 protein levels. In addition, our data suggest that miRs may not be the sole ncRNA regulators of mitochondrial genome-encoded proteins. Rather, other ncRNAs, such as lncRNAs, may be acting in concert with miRs to regulate mitochondrial genome-encoded protein expression. In the current study, we linked Kcnq1ot1 and miR-378a as constituents of a regulatory axis that can influence the expression of mitochondrial genome-encoded mt-ATP6, supporting the contention that the mitochondrial genome may be subject to a more complicated regulatory network.

The ncRNA network has been observed to be dysregulated in numerous pathologies, including diabetes mellitus and CVD (18, 61). NcRNAs, including miRs and lncRNAs, have been shown to be dynamic during disease states, often operating in conjunction with one another (17, 61, 62). In many cases, dynamic lncRNA expression appears to impact miRs and their downstream targets (19, 21, 25, 62-67). The association between lncRNAs and miRs has been observed in diabetes mellitus, with the discovery of each lncRNA paralleling the discovery of one or more lncRNA/miR regulatory axes (16, 17, 68). Of the many lncRNAs identified in diabetes mellitus, Kcnq1ot1 and Metastasis Associated Lung Adenocarcinoma Transcript 1 (MALAT1) are among the most highly studied (69). Evidence suggests that Kcnq1ot1 and MALAT1 may contribute to the development of diabetes mellitus and associated comorbidities (69). Specifically, both have been linked to pyroptosis, inflammation, apoptosis, and aberrant gene regulation, as part of altered miR regulatory axes in diabetes mellitus (23, 24, 66, 70, 71). Less clear are the roles of Kcnq1ot1 and MALAT1 in the diabetic heart, which have been minimally explored.

Though our data suggest a protective role for Kcnq1ot1 within the mitochondria, there is debate regarding the role of Kcnq1ot1 in the heart (23, 24, 72). Some studies suggest that Kcnq1ot1 may have deleterious effects and perpetuate dysfunction in the heart of streptozotocin-treated mice through miR-214-3p and caspase 1 repression (23, 24), while others have observed the opposite effects, and demonstrated that Kcnq1ot1 overexpression may be protective against sepsis-induced cardiac damage through sponging of miR-192-5p and downregulation of X-linked inhibitor of apoptosis (XIAP) protein content (72). The outcomes from the current study were more aligned with the later, and indicated a protective role for Kcnq1ot1 in the diabetic heart. The differences in these findings may be a function of the miRs being targeted by Kcnq1ot1 and their downstream effects on cardiac function (23, 24). In addition, lncRNAs may exhibit variable intracellular presence. Indeed, our data demonstrates significant increases in Kcnq1ot1 at the nuclear and tissue level, but demonstrates significant

reductions specific to the mitochondria. These findings suggest that subcellular location may be an important determinant for the mechanistic action of a given lncRNA. Taken together, these data suggest that altered expression of RNAs may not be ubiquitous across tissues type and organelles.

With mitochondrial dysfunction regarded as a crucial contributor to diabetes mellitus and CVD, we focused the current study on the ncRNA network of the mitochondrion. Our data and others suggest that the non-coding regulatory network of the mitochondrion is complex and includes numerous ncRNA species. An increasing number of studies suggest that nuclear genome-encoded lncRNAs, including those residing in the nucleus or cytoplasm, as well as mitochondrial genome-encoded lncRNAs, play a role in mitochondrial genome regulation. A review by Gusic and Prokisch summarized 18 lncRNAs known to impact the mitochondrial genome, including AK055347, which has been suggested to influence ATP synthase (69). Thus, a delicate balance needs to be maintained between the import of lncRNAs into the mitochondrion, the transcription of lncRNAs from the mitochondrial genome, and dysregulation of this balance may be incurred by disease (15, 62, 69, 73). Importantly, lncRNA activity has been demonstrated to influence the mitochondrial genome through the regulation of miRs and their downstream targets (69, 74-76). Though these interactions require further evaluation, we have also begun to explore additional lncRNAs, including MALAT1, and Nuclear Paraspeckle Assembly Transcript 1 (NEAT1), which may be impacted in T2DM mitochondria and are predicted to interact with mitochondrially-localized miRs.

Due to the role of the ncRNA network in the mitochondrion, we suggest that both miRs and lncRNAs may be efficacious targets for the amelioration of mitochondrial bioenergetic and cardiac dysfunction in T2DM (11, 14, 62). The use of human right atrial tissue presents a caveat to studying whole heart mechanisms of CVD. Previous studies from our laboratory evaluating mitochondrial function in right atrial tissue from T2DM patients reported alterations in mitochondrial

morphology and bioenergetics similar to that reported in ventricular tissue of *Db/Db* mice, suggesting comparable pathophysiology in the tissue types utilized (14, 44, 77). Still, target identification can be problematic, often with high specificity required to achieve desired outcomes. The overlap of the miR-378a/mt-ATP6 axis in both T1DM and T2DM human and mouse cardiac tissues implicate miR-378a as a potential therapeutic target. Though each condition manifests differently, diabetes mellitus types can impact similar key mitochondrial processes (11, 14, 78). The overlap of key processes, including those relating to the production of ATP, suggest that targeting miR-378a for therapeutic intervention could be beneficial for the treatment of both diabetic phenotypes (78). As of now, generalized miR inhibition in experimental settings can be achieved through silencing mechanisms or lncRNA alteration and sponging (11, 14, 23, 24, 66, 67, 79-81). Similarly, other reports show positive results using miR silencing for the amelioration of diabetes mellitus related ailments (14, 79, 82).

The current study demonstrates that miR-378a KO improves mt-ATP6 protein content, ATP synthase activity, and contractile function in T2DM. Other bioenergetic assessments, including that of complex III, indicate reduced complex III activity with the diabetic condition. Still, trending decreases in *Db/Db* mice may be a reflection of an increased need for cytochrome C production to fuel complex IV activity and the electron gradient, and/or notability higher variability in *Db/Db* samples, but no significant differences were observed between diabetic groups. An additional measure of mitochondrial bioenergetics, ATP content, was assessed. Total mitochondrial ATP control was found to be unchanged in all groups despite improved ATP synthase function and contractile ability, but changes in mitochondrial ATP content in the diabetic condition have been inconsistently reported, and may not be useful as a sole indicator of overall ATP generating ability (83-86). Additionally, while total mt-ATP6 mRNA levels were unchanged with the murine diabetic condition, miR-378a KO and miR-378a KO/*Db/Db* mice exhibited significant increases in mt-ATP6 mRNA compared to their respective controls, similar to the phenotype exhibited within T2DM patients.

Notably, we confirmed no significant differences in mt-DNA content in KO mice when compared to WT, or between diabetic groups, suggesting that changes in mt-ATP6 mRNA and protein content were not a result of miR-378a influencing total mt-DNA amount. To this point, apparent increases in mt-ATP6 mRNA, independent of changes in overall mt-DNA content, may be due to reduced interactions of mt-ATP6 mRNA with the RISC in KO/*Db/Db* mice. Concomitantly, *Db/Db* mice exhibit increased interaction of mt-ATP6 mRNA with the RISC, and reduced mt-ATP protein levels, despite unchanged levels of total mt-ATP6 mRNA. Together, these data suggest that miR-378a inhibition may provide benefit to ATP synthase through reduced interaction of mt-ATP6 mRNA with the RISC, and therefore reduced translational interference. The mechanism of translational interference, whether translational repression or mRNA degradation, is unclear. Current literature emphasizes the ambiguity in our understanding of miR mediated mRNA repression and degradation, with evidence to support the occurrence of both, but minimal evidence available to describe their mechanisms (87-91). Hence, further experimentation is necessary to fully elucidate the fate of mitochondrial mRNAs following RISC interaction.

In addition to miRs, lncRNAs may be utilized to target mitochondrially-located miRs and the mitochondrial genome (69). We suggest that downregulation of mitochondrial genome-encoded proteins may be rescued by reducing the availability of miRs known to target the mitochondrial genome (11, 14). This study is the first to identify mitochondrially-localized Kcnq1ot1, as well as identify reductions in Kcnq1ot1 levels in cardiac mitochondria. LncRNAs have been speculated to act in a sponging fashion by regulating and often inhibiting miR activity, but this is the first study to identify a role for Kcnq1ot1 as a potential regulator of mitochondrial genome-encoded proteins via the miR-378a-5p/mt-ATP6 axis. Notably, though overexpression of the 500-bp Kcnq1ot1 fragment in HL-1 cardiomyocytes exhibiting baseline levels of miR-378a, decreased detectable miR-378a-5p content, it did not result in changes in mt-ATP6 mRNA content. These results were logical, as one would suspect that healthy cells are

able to transcribe mt-ATP6 mRNA freely when miR-378a levels are not pathologically elevated. As a result, miR-378a inhibition ultimately, had no effect on mt-ATP6 content. Additionally, though the mechanism we postulate influences the mitochondrial genome, both RNAs are of nuclear origin, thus, we cannot disregard the possibility that Kcnq1ot1 may interact with miR-378a cytosolically, resulting in reduced miR-378a within the mitochondrion (11, 14). Nevertheless, the efficacy of lncRNAs as therapeutic targets for mitochondrial genome-encoded proteins requires more elucidation. The fate of miRs following lncRNA binding is variable and currently unclear, with some suggesting that miRs are sequestered by the lncRNA and later released, and others suggesting that lncRNA binding can initiate degradation (92-94).

Conclusions

In summary, Kcnq1ot1 and miR-378a may act as constituents of a regulatory axis that can influence the expression of mitochondrial genome-encoded mt-ATP6 in the T2DM heart. Further, overexpression of Kcnq1ot1 may reduce miR-378a levels and preserve mt-ATP6 protein content, suggesting that Kcnq1ot1 may participate in the regulation of the mitochondrial genome (Figure 2.6). Our data suggest that dysregulation of the ncRNA network may impact regulation of the mitochondrial genome, with evidence to suggest that lncRNA Kcnq1ot1 may act as a regulatory target in T2DM to rescue mitochondrially-encoded mt-ATP6 protein expression.

Data Availability

The data that supports this study are available upon request from the corresponding author

Supplemental Data

Supplemental Tables S1 and S2 and Supplemental Figures S1-S5. http://doi.org/10.6084/m9.figshare.18940262.

Acknowledgements

We acknowledge Dr. Eric Olson for his willingness to share miR-378a knockout mice, which were used for the studies.

Grants

Disclosures

No conflicts of interest, financial or otherwise, are declared by the authors.

Author Contributions

A.J.D., Q.A.H., A.D.T., D.L.S., and J.M.H. conceived and designed research; A.J.D., Q.A.H., A.K., A.D.T., M.V.P., S.R., D.L.S., C.C.C., and G.K.F. performed experiments; A.J.D. and Q.A.H. analyzed data; A.J.D., Q.A.H., A.K., A.D.T., M.V.P., and S.R. interpreted results of experiments; A.J.D. prepared figures; A.J.D. drafted manuscript; A.J.D., A.K., A.D.T., S.R., and J.M.H. edited and revised manuscript; A.J.D., Q.A.H., A.K., A.D.T., M.V.P., S.R., D.L.S., C.C.C., G.K.F., and J.M.H. approved final version of manuscript.

Supplemental Data Methods

MiR-378a KO/Db/Db Murine Model

MiR-378a KO mice were bred into a *Db/Db* background via breeding with heterozygous *Db/Db* mice through three consecutive breeding cycles that produced experimental KO/*Db/Db* (-/-) / (-/-) and KO (-/-) / (+/+) littermates (Supplemental Figure S2.1A). Agarose gel electrophoresis was used to genotype experimental animals, and verify miR-378a genomic loss in KO and KO/*Db/Db* animals (Supplemental Figure S2.1B). Experimental controls were housed under identical conditions and included WT and KO littermates from each consecutive breeding arrangement, heterozygous *Db/Db* breeding, and heterozygous miR-378a KO breeding.

ATP content

Following mitochondrial isolation, ATP content was quantified using the ATP determination kit (Thermo Fisher Scientific Cat. No. A22066). ATP content for experimental samples was quantified according to manufacturer instructions, and were calculated using the standard curve generated from the ATP standard solution.

References

1.   Einarson TR, Acs A, Ludwig C, Panton UH. Prevalence of Cardiovascular Disease in Type 2 Diabetes: A Systematic Literature Review of Scientific Evidence from across the World in 2007–2017. Cardiovascular diabetology. 2018;17. doi:10.1186/s12933-018-0728-6

2.   Organization WH. Diabetes World Health Organization website: World Health Organization; 2020. Available from: https://www.who.int/news-room/fact-sheets/detail/diabetes.

3.   Rindler PM, Crewe CL, Fernandes J, Kinter M, Szweda LI. Redox Regulation of Insulin Sensitivity Due to Enhanced Fatty Acid Utilization in the Mitochondria. Am J Physiol Heart Circ Physiol. 2013;305(5):H634-643. doi:10.1152/ajpheart.00799.2012

4.   Formentini L, Ryan AJ, Galvez-Santisteban M, Carter L, Taub P, Lapek JD, Jr., et al. Mitochondrial H(+)-Atp Synthase in Human Skeletal Muscle: Contribution to Dyslipidaemia and Insulin Resistance. Diabetologia. 2017;60(10):2052-2065. doi:10.1007/s00125-017-4379-z

5.   Fealy CE, Mulya A, Axelrod CL, Kirwan JP. Mitochondrial Dynamics in Skeletal Muscle Insulin Resistance and Type 2 Diabetes. Transl Res. 2018;202:69-82. doi:10.1016/j.trsl.2018.07.011

6.   Hathaway QA, Pinti MV, Durr AJ, Waris S, Shepherd DL, Hollander JM. Regulating Microrna Expression: At the Heart of Diabetes Mellitus and the Mitochondrion. Am J Physiol Heart Circ Physiol. 2018;314(2):H293-H310. doi:10.1152/ajpheart.00520.2017

7.   Joladarashi D, Thandavarayan RA, Babu SS, Krishnamurthy P. Small Engine, Big Power: Micrornas as Regulators of Cardiac Diseases and Regeneration. International Journal of Molecular Sciences. 2014;15(9):15891-15911. doi:10.3390/ijms150915891

8.   Nigi L, Grieco GE, Ventriglia G, Brusco N, Mancarella F, Formichi C, et al. Micrornas as Regulators of Insulin Signaling: Research Updates and Potential Therapeutic Perspectives in Type 2 Diabetes. Int J Mol Sci. 2018;19(12). doi:10.3390/ijms19123705

9.   Baradan R, Hollander JM, Das S. Mitochondrial Mirnas in Diabetes: Just the Tip of the Iceberg. Can J Physiol Pharmacol. 2017;95(10):1156-1162. doi:10.1139/cjpp-2016-0580

10.   Bartel DP. Micrornas: Genomics, Biogenesis, Mechanism, and Function. Cell. 2004;116(2):281-297. doi:10.1016/s0092-8674(04)00045-5

11.   Jagannathan R, Thapa D, Nichols CE, Shepherd DL, Stricker JC, Croston TL, et al. Translational Regulation of the Mitochondrial Genome Following Redistribution of Mitochondrial Microrna in the Diabetic Heart. Circ Cardiovasc Genet. 2015;8(6):785-802. doi:10.1161/CIRCGENETICS.115.001067

12.   Baseler WA, Thapa D, Jagannathan R, Dabkowski ER, Croston TL, Hollander JM. Mir-141 as a Regulator of the Mitochondrial Phosphate Carrier (Slc25a3) in the Type 1 Diabetic Heart. Am J Physiol Cell Physiol. 2012;303(12):C1244-1251. doi:10.1152/ajpcell.00137.2012

13.   Verma SK, Garikipati VNS, Kishore R. Mitochondrial Dysfunction and Its Impact on Diabetic Heart. Biochim Biophys Acta. 2017;1863(5):1098-1105. doi:10.1016/j.bbadis.2016.08.021

14.   Shepherd DL, Hathaway QA, Pinti MV, Nichols CE, Durr AJ, Sreekumar S, et al. Exploring the Mitochondrial Microrna Import Pathway through Polynucleotide Phosphorylase (Pnpase). J Mol Cell Cardiol. 2017;110:15-25. doi:10.1016/j.yjmcc.2017.06.012

15.   Dong Y, Yoshitomi T, Hu JF, Cui J. Long Noncoding Rnas Coordinate Functions between Mitochondria and the Nucleus. Epigenetics Chromatin. 2017;10(1):41. doi:10.1186/s13072-017-0149-x

16.   Leung A, Natarajan R. Long Noncoding Rnas in Diabetes and Diabetic Complications. Antioxidants & redox signaling. 2018;29(11):1064-1073. doi:10.1089/ars.2017.7315

17.   Yang F, Chen Y, Xue Z, Lv Y, Shen L, Li K, et al. High-Throughput Sequencing and Exploration of the Lncrna-Circrna-Mirna-Mrna Network in Type 2 Diabetes Mellitus. Biomed Res Int. 2020;2020:8162524. doi:10.1155/2020/8162524

18.   Moore JBt, Uchida S. Functional Characterization of Long Noncoding Rnas. Curr Opin Cardiol. 2020;35(3):199-206. doi:10.1097/HCO.0000000000000725

19.   Shao J, Pan X, Yin X, Fan G, Tan C, Yao Y, et al. Kcnq1ot1 Affects the Progression of Diabetic Retinopathy by Regulating Mir-1470 and Epidermal Growth Factor Receptor. J Cell Physiol. 2019;234(10):17269-17279. doi:10.1002/jcp.28344

20.   Liu J, Dong Y, Wen Y, Shi L, Zhu Z, Ke G, et al. Lncrna Kcnq1ot1 Knockdown Inhibits Viability, Migration and Epithelial-Mesenchymal Transition in Human Lens Epithelial Cells Via Mir-26a-5p/Itgav/Tgf-Beta/Smad3 Axis. Exp Eye Res. 2020;200:108251. doi:10.1016/j.exer.2020.108251

21.   Li J, Li M, Bai L. Kcnq1ot1/Mir-18b/Hmga2 Axis Regulates High Glucose-Induced Proliferation, Oxidative Stress, and Extracellular Matrix Accumulation in Mesangial Cells. Molecular and cellular biochemistry. 2021;476(1):321-331. doi:10.1007/s11010-020-03909-1

22.   Zhang Y, Song Z, Li X, Xu S, Zhou S, Jin X, et al. Long Noncoding Rna Kcnq1ot1 Induces Pyroptosis in Diabetic Corneal Endothelial Keratopathy. Am J Physiol Cell Physiol. 2020;318(2):C346-C359. doi:10.1152/ajpcell.00053.2019

23.   Yang F, Qin Y, Lv J, Wang Y, Che H, Chen X, et al. Silencing Long Non-Coding Rna Kcnq1ot1 Alleviates Pyroptosis and Fibrosis in Diabetic

Cardiomyopathy. Cell Death Dis. 2018;9(10):1000. doi:10.1038/s41419-018-1029-4

24.   Yang F, Qin Y, Wang Y, Li A, Lv J, Sun X, et al. Lncrna Kcnq1ot1 Mediates Pyroptosis in Diabetic Cardiomyopathy. Cell Physiol Biochem. 2018;50(4):1230-1244. doi:10.1159/000494576

25.   Zhang C, Gong Y, Li N, Liu X, Zhang Y, Ye F, et al. Long Noncoding Rna Kcnq1ot1 Promotes Sc5b-9-Induced Podocyte Pyroptosis by Inhibiting Mir-486a-3p and Upregulating Nlrp3. Am J Physiol Cell Physiol. 2021;320(3):C355-C364. doi:10.1152/ajpcell.00403.2020

26.   Carrer M, Liu N, Grueter CE, Williams AH, Frisard MI, Hulver MW, et al. Control of Mitochondrial Metabolism and Systemic Energy Homeostasis by Micrornas 378 and 378*. Proc Natl Acad Sci U S A. 2012;109(38):15330-15335. doi:10.1073/pnas.1207605109

27.   Chua S, Jr., Liu SM, Li Q, Yang L, Thassanapaff VT, Fisher P. Differential Beta Cell Responses to Hyperglycaemia and Insulin Resistance in Two Novel Congenic Strains of Diabetes (Fvb- Lepr (Db)) and Obese (Dba- Lep (Ob)) Mice. Diabetologia. 2002;45(7):976-990. doi:10.1007/s00125-002-0880-z

28.   Wang Z, Jiang T, Li J, Proctor G, McManaman JL, Lucia S, et al. Regulation of Renal Lipid Metabolism, Lipid Accumulation, and Glomerulosclerosis in Fvbdb/Db Mice with Type 2 Diabetes. Diabetes. 2005;54(8):2328-2335. doi:10.2337/diabetes.54.8.2328

29.   Laboratory TJ. 006654 - Fvb.Bks(D)-Lepr 2019. Available from: https://www.jax.org/strain/006654.

30.   Shepherd DL, Nichols CE, Croston TL, McLaughlin SL, Petrone AB, Lewis SE, et al. Early Detection of Cardiac Dysfunction in the Type 1 Diabetic Heart Using Speckle-Tracking Based Strain Imaging. J Mol Cell Cardiol. 2016;90:74-83. doi:10.1016/j.yjmcc.2015.12.001

31.   Dabkowski ER, Baseler WA, Williamson CL, Powell M, Razunguzwa TT, Frisbee JC, et al. Mitochondrial Dysfunction in the Type 2 Diabetic Heart Is Associated with Alterations in Spatially Distinct Mitochondrial Proteomes. Am J Physiol Heart Circ Physiol. 2010;299(2):H529-540. doi:10.1152/ajpheart.00267.2010

32.   Kunovac A, Hathaway QA, Pinti MV, Goldsmith WT, Durr AJ, Fink GK, et al. Ros Promote Epigenetic Remodeling and Cardiac Dysfunction in Offspring Following Maternal Engineered Nanomaterial (Enm) Exposure. Part Fibre Toxicol. 2019;16(1):24. doi:10.1186/s12989-019-0310-8

33.   Hathaway QA, Durr AJ, Shepherd DL, Pinti MV, Brandebura AN, Nichols CE, et al. Mirna-378a as a Key Regulator of Cardiovascular Health Following Engineered Nanomaterial Inhalation Exposure. Nanotoxicology. 2019;13(5):19. doi:10.1080/17435390.2019.1570372

34.   Kunovac A, Hathaway QA, Pinti MV, Durr AJ, Taylor AD, Goldsmith WT, et al. Enhanced Antioxidant Capacity Prevents Epitranscriptomic and Cardiac Alterations in Adult Offspring Gestationally-Exposed to Enm. Nanotoxicology. 2021;15(6):812-831. doi:10.1080/17435390.2021.1921299

35.   Tollervey JR, Curk T, Rogelj B, Briese M, Cereda M, Kayikci M, et al. Characterizing the Rna Targets and Position-Dependent Splicing Regulation by Tdp-43. Nat Neurosci. 2011;14(4):452-458. doi:10.1038/nn.2778

36.   O'Geen H, Echipare L, Farnham PJ. Using Chip-Seq Technology to Generate High-Resolution Profiles of Histone Modifications. Methods Mol Biol. 2011;791:265-286. doi:10.1007/978-1-61779-316-5_20

37.   Quiros PM, Goyal A, Jha P, Auwerx J. Analysis of Mtdna/Ndna Ratio in Mice. Curr Protoc Mouse Biol. 2017;7(1):47-54. doi:10.1002/cpmo.21

38.   Croston TL, Shepherd DL, Thapa D, Nichols CE, Lewis SE, Dabkowski ER, et al. Evaluation of the Cardiolipin Biosynthetic Pathway and Its Interactions in the Diabetic Heart. Life Sci. 2013;93(8):313-322. doi:10.1016/j.lfs.2013.07.005

39.   Bradford MM. A Rapid and Sensitive Method for the Quantitation of Microgram Quantities of Protein Utilizing the Principle of Protein-Dye Binding. Anal Biochem. 1976;72:248-254. doi:10.1006/abio.1976.9999

40.   Nichols CE, Shepherd DL, Knuckles TL, Thapa D, Stricker JC, Stapleton PA, et al. Cardiac and Mitochondrial Dysfunction Following Acute Pulmonary Exposure to Mountaintop Removal Mining Particulate Matter. Am J Physiol Heart Circ Physiol. 2015;309(12):H2017-2030. doi:10.1152/ajpheart.00353.2015

41.   Hathaway QA, Durr AJ, Shepherd DL, Pinti MV, Brandebura AN, Nichols CE, et al. Mirna-378a as a Key Regulator of Cardiovascular Health Following Engineered Nanomaterial Inhalation Exposure. Nanotoxicology. 2019;10.1080/17435390.2019.1570372:1-20. doi:10.1080/17435390.2019.1570372

42.   Jha P, Wang X, Auwerx J. Analysis of Mitochondrial Respiratory Chain Supercomplexes Using Blue Native Polyacrylamide Gel Electrophoresis (Bn-Page). Curr Protoc Mouse Biol. 2016;6(1):1-14. doi:10.1002/9780470942390.mo150182

43.   Dabkowski ER, Williamson CL, Bukowski VC, Chapman RS, Leonard SS, Peer CJ, et al. Diabetic Cardiomyopathy-Associated Dysfunction in Spatially Distinct Mitochondrial Subpopulations. Am J Physiol Heart Circ Physiol. 2009;296(2):H359-369. doi:10.1152/ajpheart.00467.2008

44.   Croston TL, Thapa D, Holden AA, Tveter KJ, Lewis SE, Shepherd DL, et al. Functional Deficiencies of Subsarcolemmal Mitochondria in the Type 2 Diabetic Human Heart. Am J Physiol Heart Circ Physiol. 2014;307(1):H54-65. doi:10.1152/ajpheart.00845.2013

45.   Trounce IA, Kim YL, Jun AS, Wallace DC. Assessment of Mitochondrial Oxidative Phosphorylation in Patient Muscle Biopsies, Lymphoblasts, and Transmitochondrial Cell Lines. Methods Enzymol. 1996;264:484-509. doi:10.1016/s0076-6879(96)64044-0

46.   Rottman JN, Ni G, Khoo M, Wang Z, Zhang W, Anderson ME, et al. Temporal Changes in Ventricular Function Assessed Echocardiographically in Conscious and Anesthetized Mice. J Am Soc Echocardiogr. 2003;16(11):1150-1157. doi:10.1067/S0894-7317(03)00471-1

47.   Pachon RE, Scharf BA, Vatner DE, Vatner SF. Best Anesthetics for Assessing Left Ventricular Systolic Function by Echocardiography in Mice. Am J Physiol Heart Circ Physiol. 2015;308(12):H1525-1529. doi:10.1152/ajpheart.00890.2014

48.   Roth DM, Swaney JS, Dalton ND, Gilpin EA, Ross J, Jr. Impact of Anesthesia on Cardiac Function During Echocardiography in Mice. Am J Physiol Heart Circ Physiol. 2002;282(6):H2134-2140. doi:10.1152/ajpheart.00845.2001

49.   Pan G, Munukutla S, Kar A, Gardinier J, Thandavarayan RA, Palaniyandi SS. Type-2 Diabetic Aldehyde Dehydrogenase 2 Mutant Mice (Aldh 2*2) Exhibiting Heart Failure with Preserved Ejection Fraction Phenotype Can Be Determined by Exercise Stress Echocardiography. PLoS One. 2018;13(4):e0195796. doi:10.1371/journal.pone.0195796

50.   Claycomb WC, Lanson NA, Jr., Stallworth BS, Egeland DB, Delcarpio JB, Bahinski A, et al. Hl-1 Cells: A Cardiac Muscle Cell Line That Contracts and Retains Phenotypic Characteristics of the Adult Cardiomyocyte. Proc Natl Acad Sci U S A. 1998;95(6):2979-2984. doi:10.1073/pnas.95.6.2979

51.   Karagkouni D, Paraskevopoulou MD, Tastsoglou S, Skoufos G, Karavangeli A, Pierros V, et al. Diana-Lncbase V3: Indexing Experimentally Supported Mirna Targets on Non-Coding Transcripts. Nucleic acids research. 2020;48(D1):D101-D110. doi:10.1093/nar/gkz1036

52.   Paraskevopoulou MD, Karagkouni D, Vlachos IS, Tastsoglou S, Hatzigeorgiou AG. Microclip Super Learning Framework Uncovers Functional Transcriptome-Wide Mirna Interactions. Nature communications. 2018;9(1):3601. doi:10.1038/s41467-018-06046-y

53.   Martin Mann PRW, and Rolf Backofen. Intarna 2.0: Enhanced and Customizable Prediction of Rna–Rna Interactions. Nucleic acids research. 2017;45(W1):435-439. doi:10.1093/nar/gkx279

54.   Patrick R. Wright JG, Martin Mann, Dragos A. Sorescu, Andreas S. Richter, Steffen Lott, Robert Kleinkauf, Wolfgang R. Hess, and Rolf Backofen. Coprarna and Intarna: Predicting Small Rna Targets, Networks and Interaction Domains. Nucleic acids research. 2014;42(1):119-123. doi:10.1093/nar/gku359

55.   Anke Busch ASR, and Rolf Backofen. Intarna: Efficient Prediction of Bacterial Srna Targets Incorporating Target Site Accessibility and Seed Regions. Bioinformatics. 2008;24(24):2849-2856. doi:10.1093/bioinformatics/btn544

56.   Martin Raden SMA, Omer S Alkhnbashi, Anke Busch, Fabrizio Costa, Jason A Davis, Florian Eggenhofer, Rick Gelhausen, Jens Georg, Steffen Heyne, Michael Hiller, Kousik Kundu, Robert Kleinkauf, Steffen C Lott, Mostafa M Mohamed, Alexander Mattheis, Milad Miladi, Andreas S Richter, Sebastian Will, Joachim Wolff, Patrick R Wright, and Rolf Backofen. Freiburg Rna Tools: A Central Online Resource for Rna-Focused Research and Teaching. Nucleic acids research. 2018;46(1):25-29. doi:10.1093/nar/gky329

57.   Paraskevopoulou MD, Georgakilas G, Kostoulas N, Reczko M, Maragkakis M, Dalamagas TM, et al. Diana-Lncbase: Experimentally Verified and Computationally Predicted Microrna Targets on Long Non-Coding Rnas. Nucleic acids research. 2013;41(Database issue):D239-245. doi:10.1093/nar/gks1246

58.   Uusitupa M, Khan TA, Viguiliouk E, Kahleova H, Rivellese AA, Hermansen K, et al. Prevention of Type 2 Diabetes by Lifestyle Changes: A Systematic Review and Meta-Analysis. Nutrients. 2019;11(11). doi:10.3390/nu11112611

59.   Brown DA, Perry JB, Allen ME, Sabbah HN, Stauffer BL, Shaikh SR, et al. Expert Consensus Document: Mitochondrial Function as a Therapeutic Target in Heart Failure. Nat Rev Cardiol. 2017;14(4):238-250. doi:10.1038/nrcardio.2016.203

60.   Taanman JW. The Mitochondrial Genome: Structure, Transcription, Translation and Replication. Biochim Biophys Acta. 1999;1410(2):103-123. doi:10.1016/s0005-2728(98)00161-3

61.   Bonnet S, Boucherat O, Paulin R, Wu D, Hindmarch CCT, Archer SL, et al. Clinical Value of Non-Coding Rnas in Cardiovascular, Pulmonary, and Muscle Diseases. Am J Physiol Cell Physiol. 2020;318(1):C1-C28. doi:10.1152/ajpcell.00078.2019

62.   Jakubik D, Fitas A, Eyileten C, Jarosz-Popek J, Nowak A, Czajka P, et al. Micrornas and Long Non-Coding Rnas in the Pathophysiological Processes of Diabetic Cardiomyopathy: Emerging Biomarkers and Potential Therapeutics. Cardiovascular diabetology. 2021;20(1):55. doi:10.1186/s12933-021-01245-2

63.   Yu L, Fu J, Yu N, Wu Y, Han N. Long Noncoding Rna Malat1 Participates in the Pathological Angiogenesis of Diabetic Retinopathy in an Oxygen-Induced Retinopathy Mouse Model by Sponging Mir-203a-3p. Can J Physiol Pharmacol. 2020;98(4):219-227. doi:10.1139/cjpp-2019-0489

64.   Shaker OG, Abdelaleem OO, Mahmoud RH, Abdelghaffar NK, Ahmed TI, Said OM, et al. Diagnostic and Prognostic Role of Serum Mir-20b, Mir-17-3p, Hotair, and Malat1 in Diabetic Retinopathy. IUBMB Life. 2019;71(3):310-320. doi:10.1002/iub.1970

65.   Zhang H, Yan Y, Hu Q, Zhang X. Lncrna Malat1/Microrna Let-7f/Klf5 Axis Regulates Podocyte Injury in Diabetic Nephropathy. Life Sci. 2021;266:118794. doi:10.1016/j.lfs.2020.118794

66.   Che H, Wang Y, Li H, Li Y, Sahil A, Lv J, et al. Melatonin Alleviates Cardiac Fibrosis Via Inhibiting Lncrna Malat1/Mir-141-Mediated Nlrp3 Inflammasome and Tgf-Beta1/Smads Signaling in Diabetic Cardiomyopathy. FASEB J. 2020;34(4):5282-5298. doi:10.1096/fj.201902692R

67.   Xia C, Liang S, He Z, Zhu X, Chen R, Chen J. Metformin, a First-Line Drug for Type 2 Diabetes Mellitus, Disrupts the Malat1/Mir-142-3p Sponge to Decrease Invasion and Migration in Cervical Cancer Cells. Eur J Pharmacol. 2018;830:59-67. doi:10.1016/j.ejphar.2018.04.027

68.   Chang W, Wang J. Exosomes and Their Noncoding Rna Cargo Are Emerging as New Modulators for Diabetes Mellitus. Cells. 2019;8(8). doi:10.3390/cells8080853

69.   Prokisch MGaH. Ncrnas: New Players in Mitochondrial Health and Disease? Front Genet. 2020;10.3389/fgene.2020.00095. doi:10.3389/fgene.2020.00095

70.   Wu A, Sun W, Mou F. Lncrnamalat1 Promotes High Glucoseinduced H9c2 Cardiomyocyte Pyroptosis by Downregulating Mir1413p Expression. Mol Med Rep. 2021;23(4). doi:10.3892/mmr.2021.11898

71.   Wang C, Liu G, Yang H, Guo S, Wang H, Dong Z, et al. Malat1-Mediated Recruitment of the Histone Methyltransferase Ezh2 to the Microrna-22 Promoter Leads to Cardiomyocyte Apoptosis in Diabetic Cardiomyopathy. Sci Total Environ. 2021;766:142191. doi:10.1016/j.scitotenv.2020.142191

72.   Sun F, Yuan W, Wu H, Chen G, Sun Y, Yuan L, et al. Lncrna Kcnq1ot1 Attenuates Sepsis-Induced Myocardial Injury Via Regulating Mir-192-5p/Xiap

Axis. Exp Biol Med (Maywood). 2020;245(7):620-630. doi:10.1177/1535370220908041

73.   Chen G, Guo H, Song Y, Chang H, Wang S, Zhang M, et al. Long Noncoding Rna Ak055347 Is Upregulated in Patients with Atrial Fibrillation and Regulates Mitochondrial Energy Production in Myocardiocytes. Mol Med Rep. 2016;14(6):5311-5317. doi:10.3892/mmr.2016.5893

74.   Sirey TM, Roberts K, Haerty W, Bedoya-Reina O, Rogatti-Granados S, Tan JY, et al. Correction: The Long Non-Coding Rna Cerox1 Is a Post Transcriptional Regulator of Mitochondrial Complex I Catalytic Activity. eLife. 2019;8. doi:10.7554/eLife.50980

75.   Tian T, Lv X, Pan G, Lu Y, Chen W, He W, et al. Long Noncoding Rna Mprl Promotes Mitochondrial Fission and Cisplatin Chemosensitivity Via Disruption of Pre-Mirna Processing. Clin Cancer Res. 2019;25(12):3673-3688. doi:10.1158/1078-0432.CCR-18-2739

76.   Li HJ, Sun XM, Li ZK, Yin QW, Pang H, Pan JJ, et al. Lncrna Uca1 Promotes Mitochondrial Function of Bladder Cancer Via the Mir-195/Arl2 Signaling Pathway. Cell Physiol Biochem. 2017;43(6):2548-2561. doi:10.1159/000484507

77.   Hathaway QA, Roth SM, Pinti MV, Sprando DC, Kunovac A, Durr AJ, et al. Machine-Learning to Stratify Diabetic Patients Using Novel Cardiac Biomarkers and Integrative Genomics. Cardiovascular diabetology. 2019;18(1):78. doi:10.1186/s12933-019-0879-0

78.   Hollander JM, Thapa D, Shepherd DL. Physiological and Structural Differences in Spatially Distinct Subpopulations of Cardiac Mitochondria: Influence of Cardiac Pathologies. Am J Physiol Heart Circ Physiol. 2014;307(1):H1-14. doi:10.1152/ajpheart.00747.2013

79.   Bijkerk R, Esguerra JLS, Ellenbroek JH, Au YW, Hanegraaf MAJ, de Koning EJ, et al. In Vivo Silencing of Microrna-132 Reduces Blood Glucose and Improves Insulin Secretion. Nucleic Acid Ther. 2019;29(2):67-72. doi:10.1089/nat.2018.0763

80.   Zhu L, Zhong Q, Yang T, Xiao X. Improved Therapeutic Effects on Diabetic Foot by Human Mesenchymal Stem Cells Expressing Malat1 as a Sponge for Microrna-205-5p. Aging (Albany NY). 2019;11(24):12236-12245. doi:10.18632/aging.102562

81.   Liu SX, Zheng F, Xie KL, Xie MR, Jiang LJ, Cai Y. Exercise Reduces Insulin Resistance in Type 2 Diabetes Mellitus Via Mediating the Lncrna Malat1/Microrna-382-3p/Resistin Axis. Molecular therapy Nucleic acids. 2019;18(18):34-44. doi:10.1016/j.omtn.2019.08.002

82.   Liang C, Gao L, Liu Y, Liu Y, Yao R, Li Y, et al. Mir-451 Antagonist Protects against Cardiac Fibrosis in Streptozotocin-Induced Diabetic Mouse Heart. Life Sci. 2019;224:12-22. doi:10.1016/j.lfs.2019.02.059

83.   Munusamy S, Saba H, Mitchell T, Megyesi JK, Brock RW, Macmillan-Crow LA. Alteration of Renal Respiratory Complex-Iii During Experimental Type-1 Diabetes. BMC Endocr Disord. 2009;9:2. doi:10.1186/1472-6823-9-2

84.   Wu J, Luo X, Thangthaeng N, Sumien N, Chen Z, Rutledge MA, et al. Pancreatic Mitochondrial Complex I Exhibits Aberrant Hyperactivity in Diabetes. Biochem Biophys Rep. 2017;11:119-129. doi:10.1016/j.bbrep.2017.07.007

85.   Guo X, Wu J, Du J, Ran J, Xu J. Platelets of Type 2 Diabetic Patients Are Characterized by High Atp Content and Low Mitochondrial Membrane Potential. Platelets. 2009;20(8):588-593. doi:10.3109/09537100903288422

86.   Szendroedi J, Schmid AI, Chmelik M, Toth C, Brehm A, Krssak M, et al. Muscle Mitochondrial Atp Synthesis and Glucose Transport/Phosphorylation in Type 2 Diabetes. PLoS Med. 2007;4(5):e154. doi:10.1371/journal.pmed.0040154

87.   Freimer JW, Hu TJ, Blelloch R. Decoupling the Impact of Micrornas on Translational Repression Versus Rna Degradation in Embryonic Stem Cells. eLife. 2018;7. doi:10.7554/eLife.38014

88.   Valencia-Sanchez MA, Liu J, Hannon GJ, Parker R. Control of Translation and Mrna Degradation by Mirnas and Sirnas. Genes Dev. 2006;20(5):515-524. doi:10.1101/gad.1399806

89.   Eisen TJ, Eichhorn SW, Subtelny AO, Bartel DP. Micrornas Cause Accelerated Decay of Short-Tailed Target Mrnas. Mol Cell. 2020;77(4):775-785 e778. doi:10.1016/j.molcel.2019.12.004

90.   O'Brien J, Hayder H, Zayed Y, Peng C. Overview of Microrna Biogenesis, Mechanisms of Actions, and Circulation. Front Endocrinol (Lausanne). 2018;9:402. doi:10.3389/fendo.2018.00402

91.   Gao K, Cheng M, Zuo X, Lin J, Hoogewijs K, Murphy MP, et al. Active Rna Interference in Mitochondria. Cell Res. 2021;31(2):219-228. doi:10.1038/s41422-020-00394-5

92.   Jan Krützfeldt NR, Ravi Braich, Kallanthottathil G. Rajeev, Thomas Tuschl, Muthiah Manoharan & Markus Stoffel. Silencing of Micrornas in Vivo with 'Antagomirs'. Nature. 2005;10.1038/nature04303. doi:10.1038/nature04303

93.   Li Feng, Huanqin Li, , Fan Li, Songhua Bei, Xiaohong Zhang. Lncrna Kcnq1ot1 Regulates Microrna-9-Lmx1a Expression and Inhibits Gastric Cancer Cell Progression. Aging. 2020;12(1). doi:10.18632/aging.102651

94.   Wang Y, Xu Z, Jiang J, Xu C, Kang J, Xiao L, et al. Endogenous Mirna Sponge Lincrna-Ror Regulates Oct4, Nanog, and Sox2 in Human Embryonic Stem Cell Self-Renewal. Dev Cell. 2013;25(1):69-80. doi:10.1016/j.devcel.2013.03.002
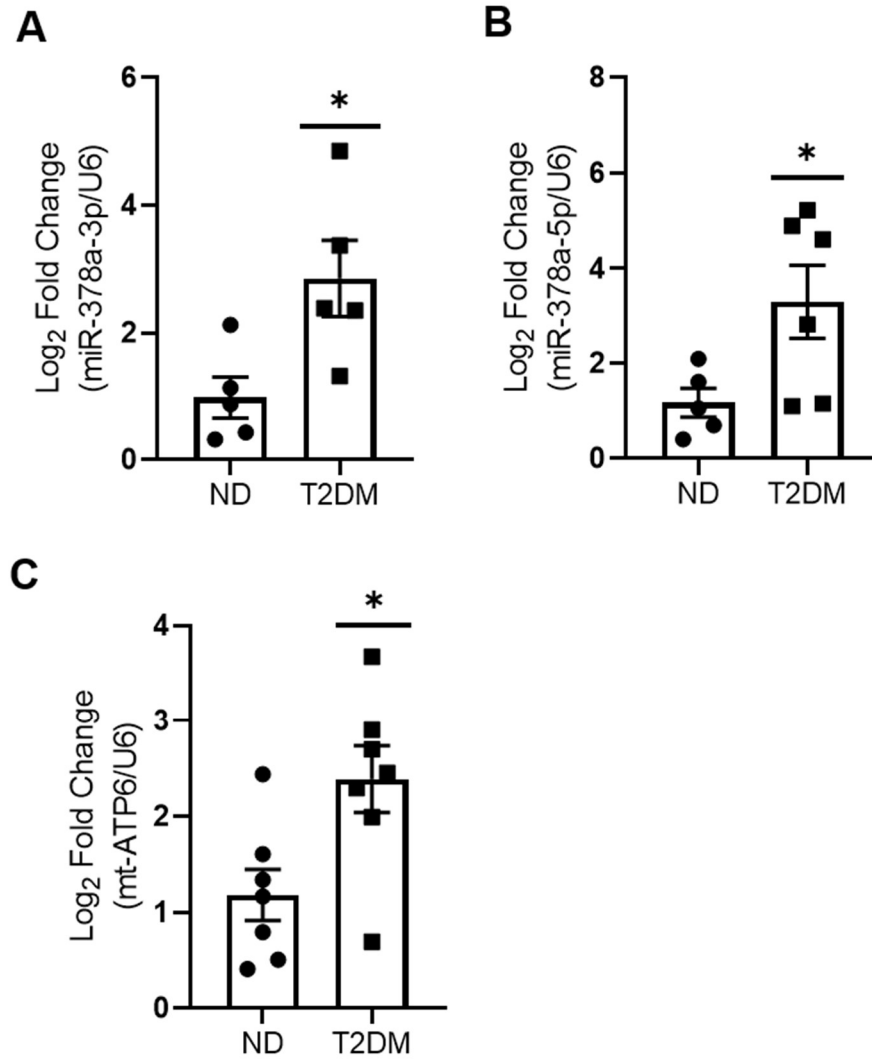
TABLES AND TABLE LEGENDS

Table 2.1: M-mode echocardiography assessments at 25 weeks

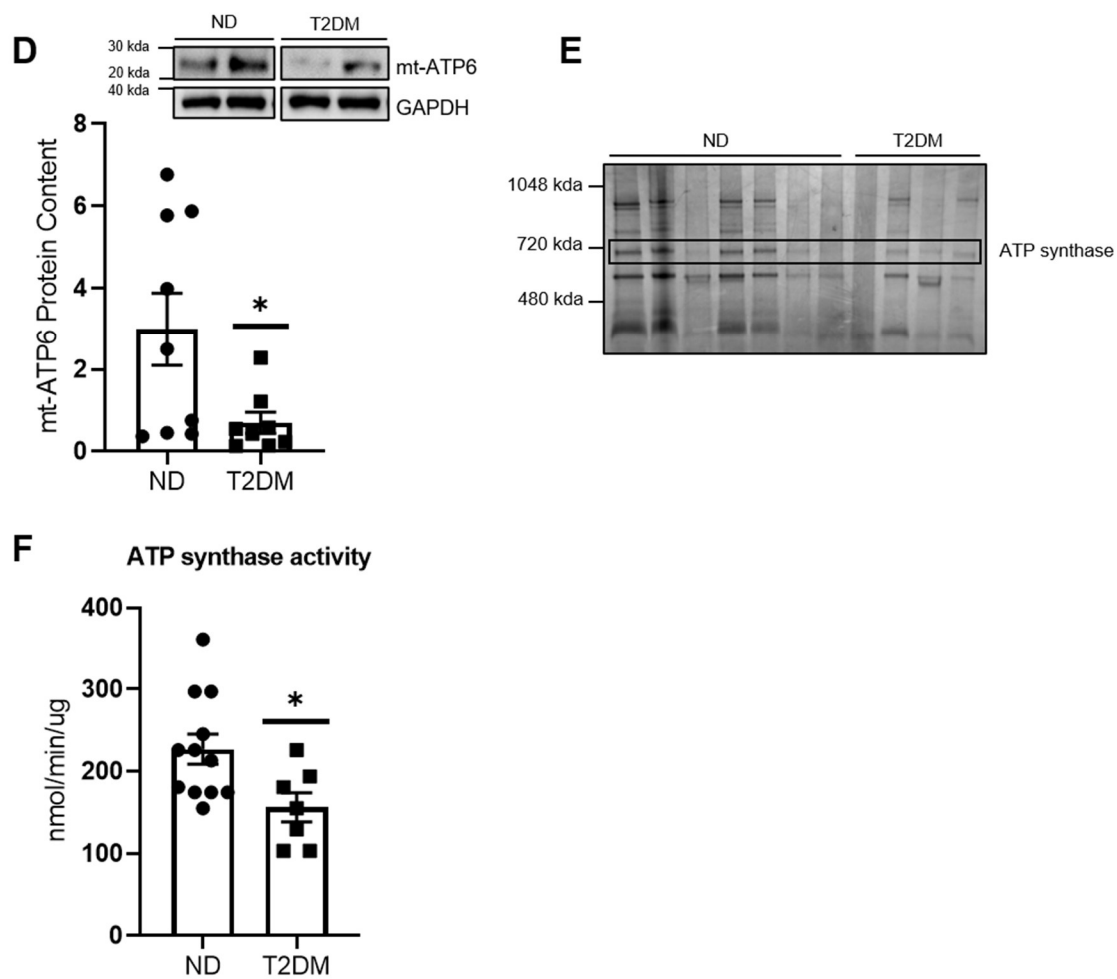| SAX M-mode	WT	*Db/Db*	KO	KO/*Db/Db*
Heart Rate	684.0 ± 14.7	634.7 ± 17.4	711.2 ± 9.0	532.3 ± 22.6*^
LVED;s (mm)	0.67 ± 0.04	0.90 ± 0.05*	0.49 ± 0.05	0.81 ± 0.07
LVED;d (mm)	2.1 ± 0.06	2.4 ± 0.1*	1.8 ± 0.05	2.3 ± 0.1
LVEV;s (µl)	0.7 ± 0.1	1.6 ± 0.2*	0.4 ± 0.1	1.3 ± 0.2*
LVEV;d (µl)	13.9 ± 0.9	19.5 ± 1.9*	10.6 ± 0.8	19.0 ± 1.6*
SV (µl)	13.5 ± 1.0	19.0 ± 2.0*	10.3 ± 0.7	17.4 ± 1.4*
EF (%)	95.0 ± 0.5	91.2 ± 0.7*	97.17 ± 0.5*	93.63 ± 0.8^
FS (%)	68.0 ± 1.4	60.0 ± 1.7*	74.8 ± 1.8*	65.8 ± 1.9^
CO (mL/min)	9.3 ± 0.8	11.1 ± 0.8	6.9 ± 0.2	9.0 ± 0.7^
LV Mass (mm)	100.1 ± 7.6	144.9 ± 6.3*	90.1 ± 4.8	139.2 ± 7.8*
LVAW;s (mm)	1.9 ± 0.05	2.1 ± 0.06*	1.8 ± 0.06	2.0 ± 0.05
LVAW;d (mm)	1.3 ± 0.04	1.5 ± 0.04*	1.3 ± 0.05	1.4 ± 0.04
LVPW;s (mm)	2.1 ± 0.08	2.3 ± 0.06*	2.1 ± 0.05	2.4 ± 0.04*
LVPW;d (mm)	1.6 ± 0.07	1.8 ± 0.07*	1.6 ± 0.05	2.0 ± 0.04*

Table 2.1: Averaged values for M-mode echocardiography. Cardiac contractile function was assessed at 25 weeks of age in WT (n = 13), *Db/Db* (n = 14), KO (n = 10), and KO/*Db/Db* (n = 18) mice. "n" is defined as biological replicates. Data were analyzed using a two-way ANOVA. WT (7 male, 6 female), *Db/Db* (5 male, 9 female), KO (4 male, 6 female), KO/*Db/Db* (8 male, 10 female) " * " Denotes P ≤ 0.05 vs. WT, " ^ " Denotes P ≤ 0.05 vs. *Db/Db*. Values are shown as mean ± SEM. WT; wild-type, KO; knockout, LV; left ventricle, LVED;s; LV end-systolic diameter, LVED;d; LV end-diastolic diameter, LVEV;s; LV end-systolic volume, LVEV;d; LV end-diastolic volume, LVAW;s; LV systolic anterior wall thickness, LVAW;d; LV diastolic anterior wall thickness, LVPW;s; LV systolic posterior wall thickness, LVPW;d; LV diastolic posterior wall thickness, SEM; standard error of the mean.

FIGURES AND FIGURE LEGENDS

Figure 2.1: Impact of T2DM on mitochondrial ATP synthase.
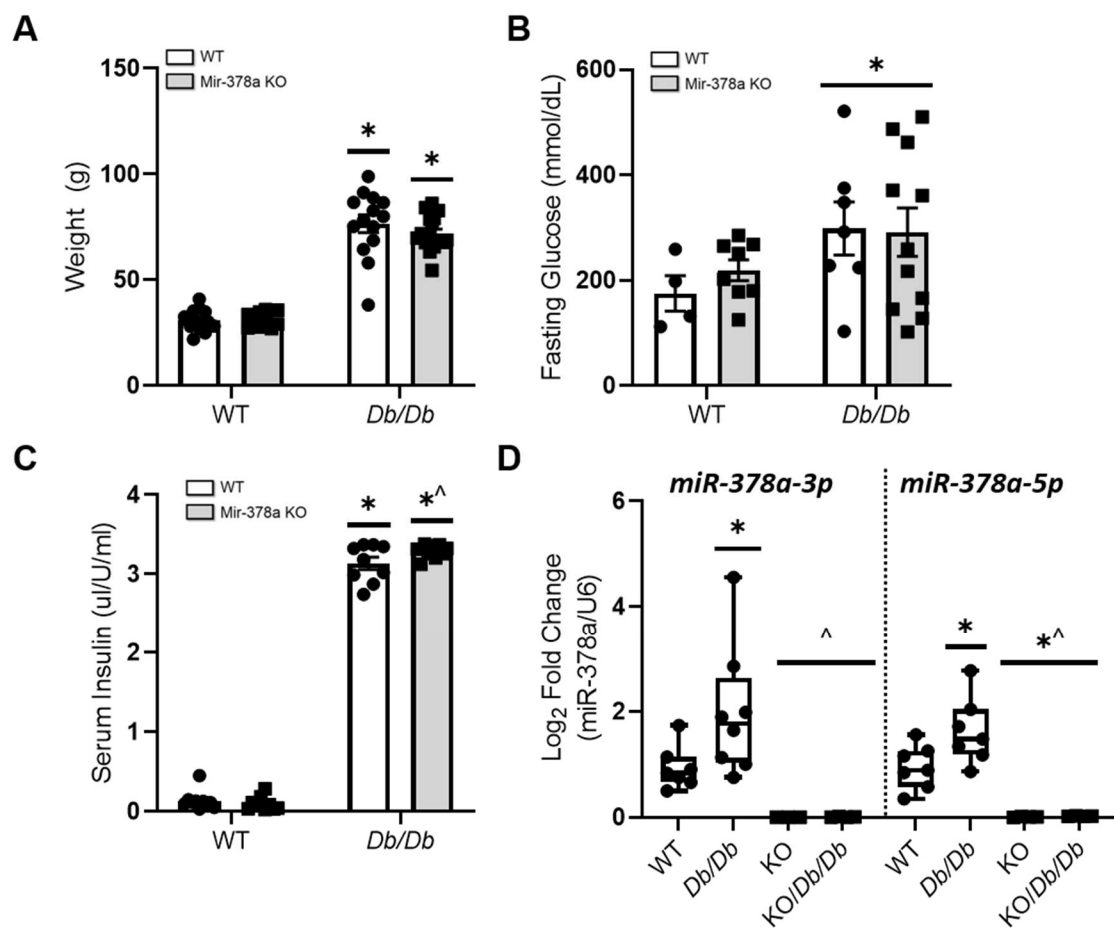
Figure 2.1:

D

30 kda
20 kda — mt-ATP6
40 kda — GAPDH

ND   T2DM

mt-ATP6 Protein Content

*

ND   T2DM

E

1048 kda
720 kda — ATP synthase
480 kda

ND   T2DM

F ATP synthase activity

nmol/min/ug

*

ND   T2DM

Figure 2.1: Impact of T2DM on mitochondrial ATP synthase. (A) MiR-378a-3p levels were assessed in cardiac tissue of ND (n = 5) and T2DM (n = 5) patients using qPCR. (B) MiR-378a-5p levels were assessed in cardiac tissue of ND (n = 5) and T2DM (n = 6) patients using qPCR. (C) Quantification of mt-ATP6 mRNA in ND (n = 7) and T2DM (n = 7) total cardiac mitochondria. (D) Representative Western blot of mt-ATP6 protein content and quantification in ND (n = 9) and T2DM (n = 8) total cardiac mitochondria. Two blots were required to achieve a suitable "n" for all groups; therefore, a representative sample was used for normalization between gels. The representative image was constructed by taking two samples for each group from a single Western blot. (E) Quantification of ATP synthase content in ND (n = 7) and T2DM (n = 4) total cardiac mitochondria. ATP synthase band is marked by "ATP Synthase". (F) Assessment of ATP synthase activity in ND (n = 12) and T2DM (n = 7) total cardiac mitochondria. "n" is defined as biological replicates. All experiments were performed with a minimum of two technical replicates. Figure panel D is based in 2 independent experiments. All other figure panels are based in 1 independent experiment. Data were analyzed using a Student's T-test. " * " Denotes $P \leq 0.05$ vs. ND. Values are shown as mean ± SEM. ND; non-diabetic, T2DM; type 2 diabetes mellitus, SEM; standard error of the mean. See Supplemental data.

**Figure 2.2:** Characterization of miR-378a KO/*Db/Db* animal model.

Figure 2.2: Characterization of miR-378a KO/*Db/Db* animal model. MiR-378a KO/*Db/Db* mice were characterized by (A) weight changes in WT (n = 13), *Db/Db* (n = 14), KO (n = 10), and KO/*Db/Db* (n = 17) mice, (B) fasting glucose in WT (n = 4), *Db/Db* (n = 7), KO (n = 8), and KO/*Db/Db* (n = 12) mice, (C) serum insulin levels in WT (n = 10), *Db/Db* (n = 9), KO (n = 10), and KO/*Db/Db* (n = 9) mice, and (D) mitochondrial miR-378a-3p and miR-378-5p quantification (n = 7 all groups). All experiments were performed with a minimum of two technical replicates. "n" is defined as biological replicates. Figure panels are based in 1 independent experiment. Data were analyzed using a two-way ANOVA. " * " Denotes $P \leq 0.05$ vs. WT, " ^ " Denotes $P \leq 0.05$ vs. *Db/Db*. Values are shown as mean ± SEM. WT; wild-type, KO; knockout, SEM; standard error of the mean. See Supplemental data

Figure 2.3: Mitochondrial impacts of miR-378a loss on ATP synthase ATP generating capacity.
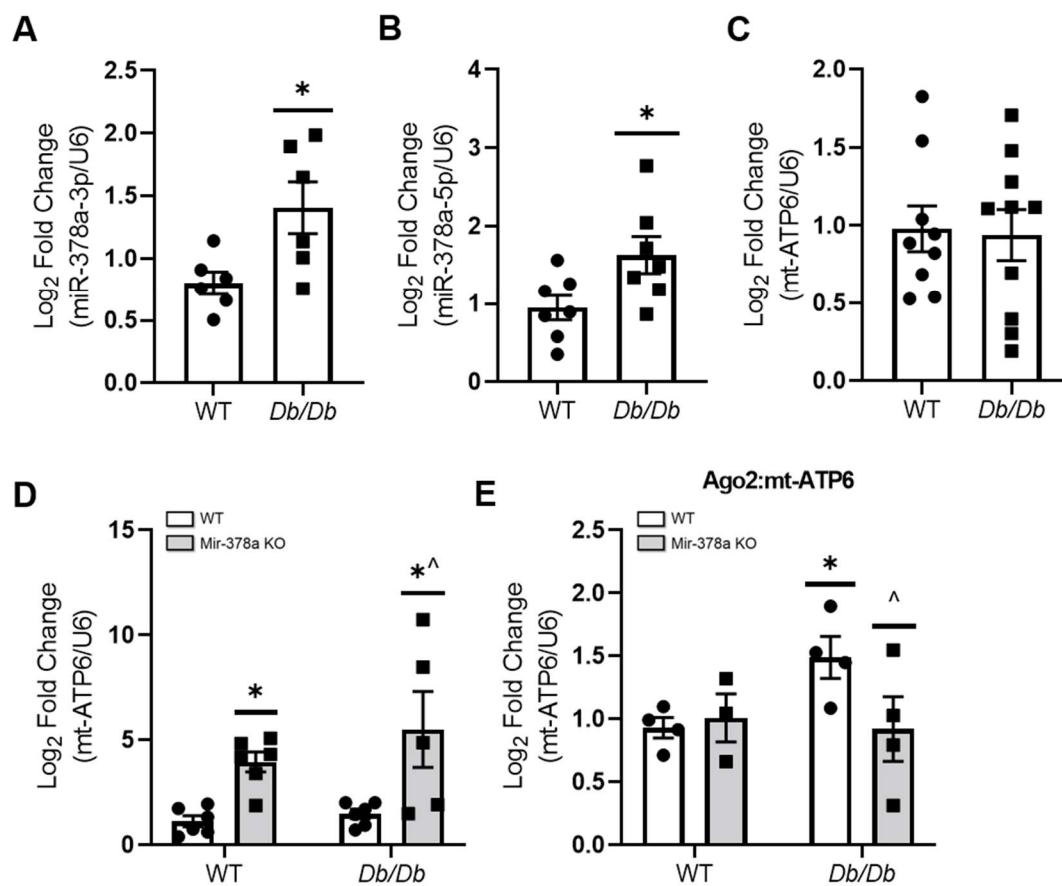
Figure 2.3:
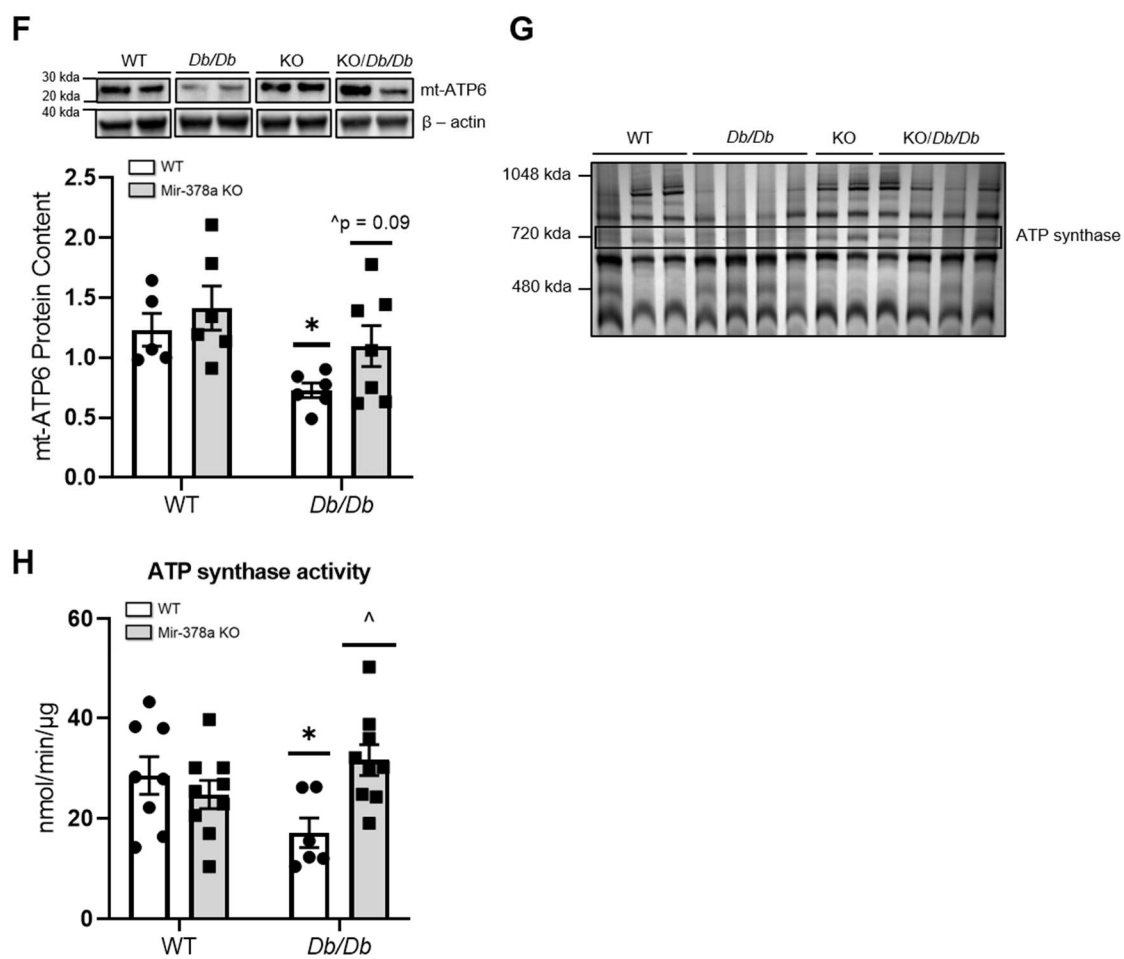
Figure 2.3: Mitochondrial impacts of miR-378a loss on ATP synthase ATP generating capacity. (A) Quantification of miR-378a-3p WT (n = 6) and *Db/Db* (n = 6) total cardiac mitochondria. (B) Quantification of miR-378a-5p WT (n = 7) and *Db/Db* (n = 7) total cardiac mitochondria. (C) Quantification of mt-ATP6 mRNA in WT (n = 9) and *Db/Db* (n = 10) total cardiac mitochondria. (D) Quantification of mt-ATP6 mRNA in WT (n = 6), *Db/Db* (n = 6), KO (n = 6), and KO/*Db/Db* (n = 5) mice. (E) Quantification of mt-ATP6 mRNA in mouse cardiac tissue following crosslinked immunoprecipitation of Ago2 in WT, *Db/Db*, KO, and KO/*Db/Db* mice (n = 5 all groups). (F) Representative Western blot of mt-ATP6 protein content and quantification in cardiac tissue of WT (n = 5), *Db/Db* (n = 6), KO (n = 6), and KO/*Db/Db* (n = 7) mice. Two blots were required to achieve a suitable "n" for all groups; therefore, a representative sample was used for normalization between gels. The representative image was constructed by taking two samples for each group from a single Western blot. (G) Quantification of ATP synthase content in WT (n = 3), *Db/Db* (n = 4), KO (n = 2), and KO/*Db/Db* (n = 4) mice. ATP synthase band is marked by "ATP Synthase". (H) Quantification of ATP synthase activity in WT (n = 8), *Db/Db* (n = 7), KO (n = 9), and KO/*Db/Db* (n = 9) mice. "n" is defined as biological replicates. All experiments were performed with a minimum of two technical replicates. Figure panel F is based in 2 independent experiments. All other figure panels are based in 1 independent experiment. Data were analyzed using a two-way ANOVA. " * " Denotes $P \leq 0.05$ vs. WT, " ^ " Denotes $P \leq 0.05$ vs. *Db/Db*. Values are shown as means ± SEM WT; wild-type, KO; knockout, SEM; standard error of the mean. See Supplemental data.

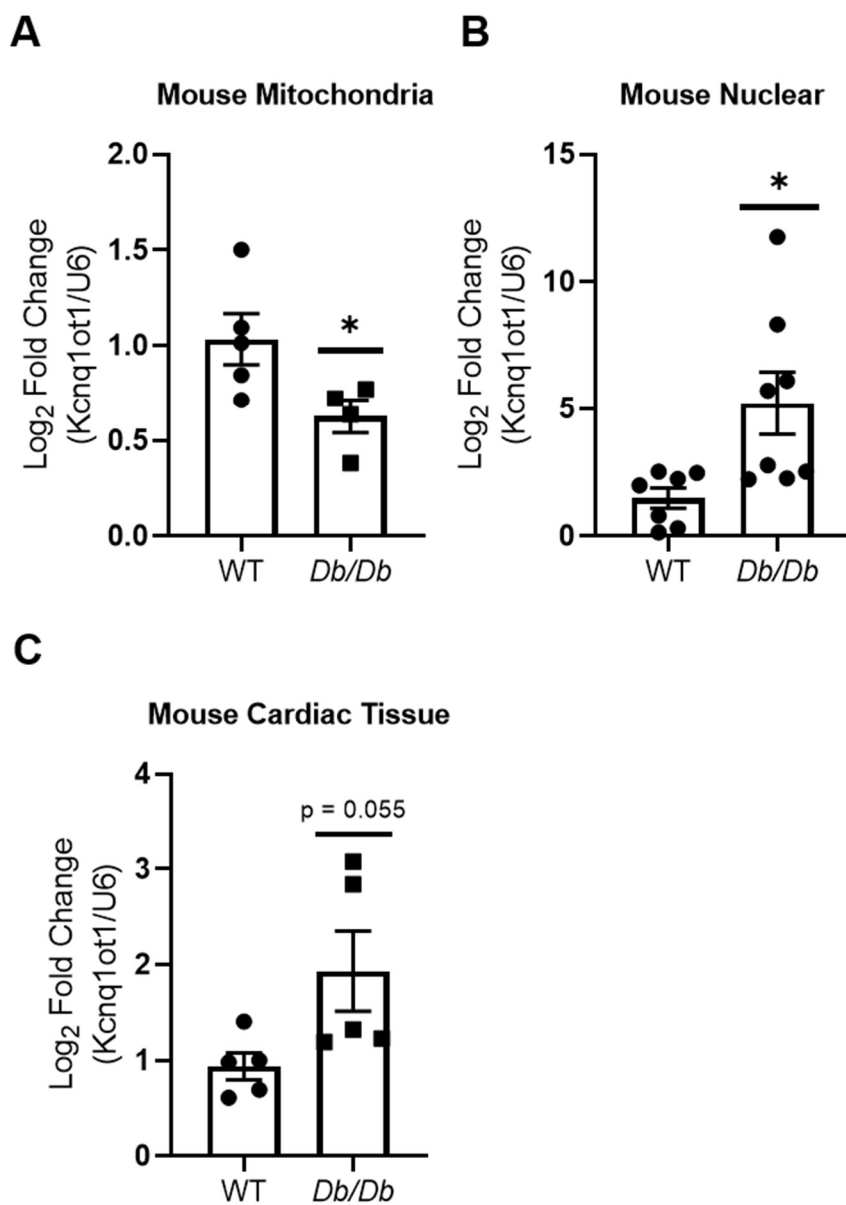**Figure 2.4:** Assessment of Kcnq1ot1 levels and binding of miR-378a-5p *in vitro*.

Figure 2.4

Figure 2.4

G

Kcnq1ot1 14   29

```
5'-UGG..UAUUG          A
              AGGACU      AGUCAGGAG
              ||||||      |||||||||
              UCCUGG      UCAGUCCUC
     3'-UGUG          ACC
```
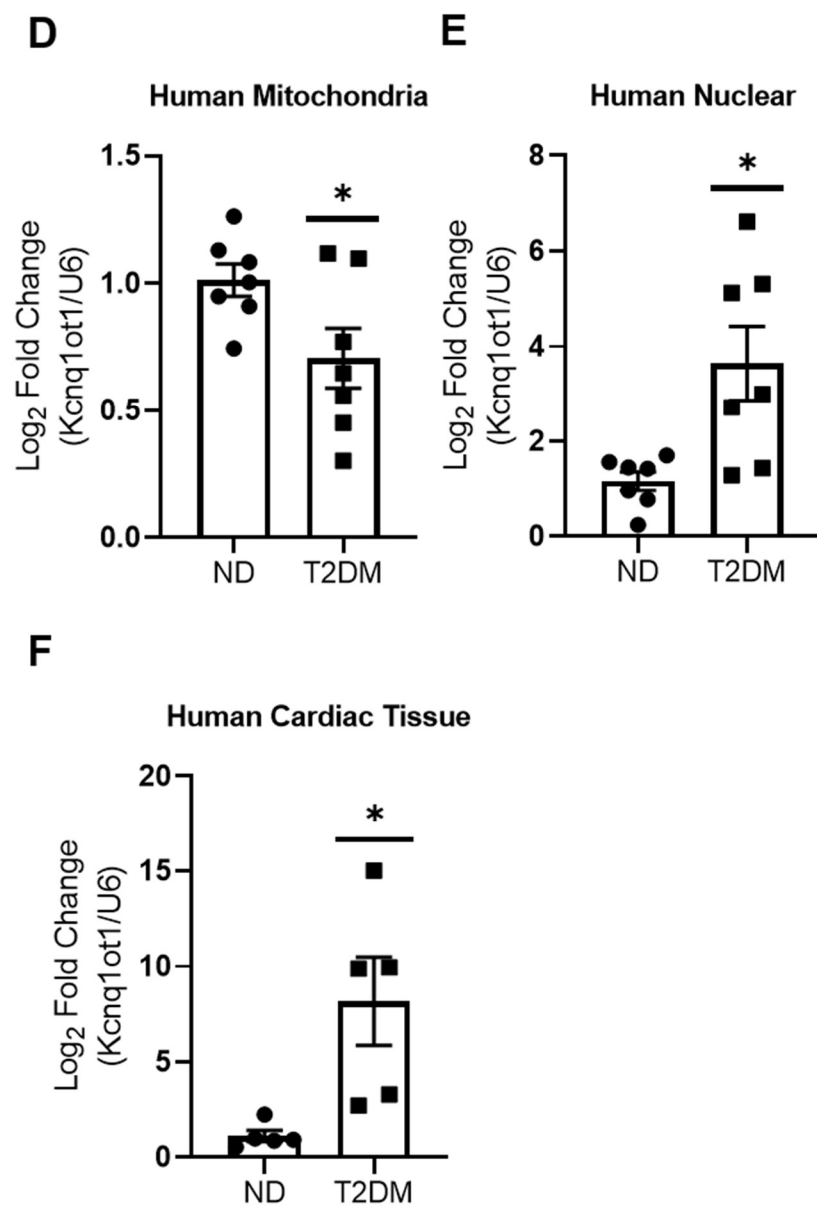
miR-378a-5p 18   1

H

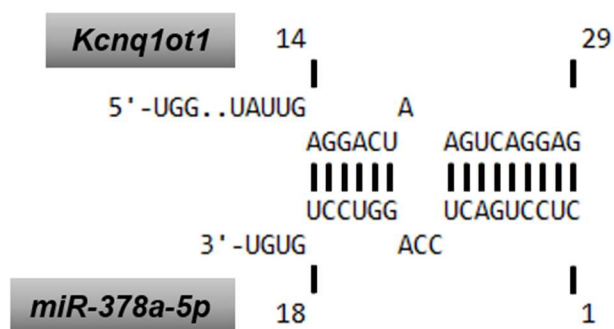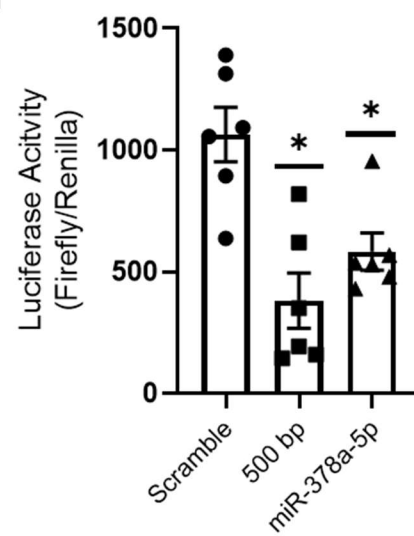**Figure 2.4:** Assessment of Kcnq1ot1 levels and binding of miR-378a-5p *in vitro*. (A-C) Quantification of Kcnq1ot1 in WT (n = 5) and *Db/Db* (n = 4) cardiac mitochondria, WT (n = 7) and *Db/Db* (n = 8) nuclear, and WT (n = 5) and *Db/Db* (n = 5) cardiac tissue, respectively. (D-F) Quantification of Kcnq1ot1 in ND (n = 7) and T2DM (n = 7) mitochondria, ND (n = 7) and T2DM (n = 7) nuclear (n = 6), ND (n = 5) and T2DM (n = 5) cardiac tissue, respectively. (G) Representative binding complementarity of Kcnq1ot1 to miR-378a-5p. (H) Kcnq1ot1 binding to miR-378a-5p was assessed using an *in vitro* luciferase assay system (n = 6 all groups). "n" is defined as biological replicates. All experiments were performed with a minimum of two technical replicates. Figure panels are based in 1 independent experiment. WT and *Db/Db* data were analyzed using a Student's T-test. Luciferase data were analyzed using a one-way ANOVA. " * " Denotes $P \leq 0.05$ vs. WT. Values are shown as means ± SEM. WT; wild-type, T2DM; type 2 diabetes mellitus. See Supplemental data.

Figure 2.5: Overexpression of 500-bp Kcnq1ot1 fragment in HL-1-378a cardiomyocytes.
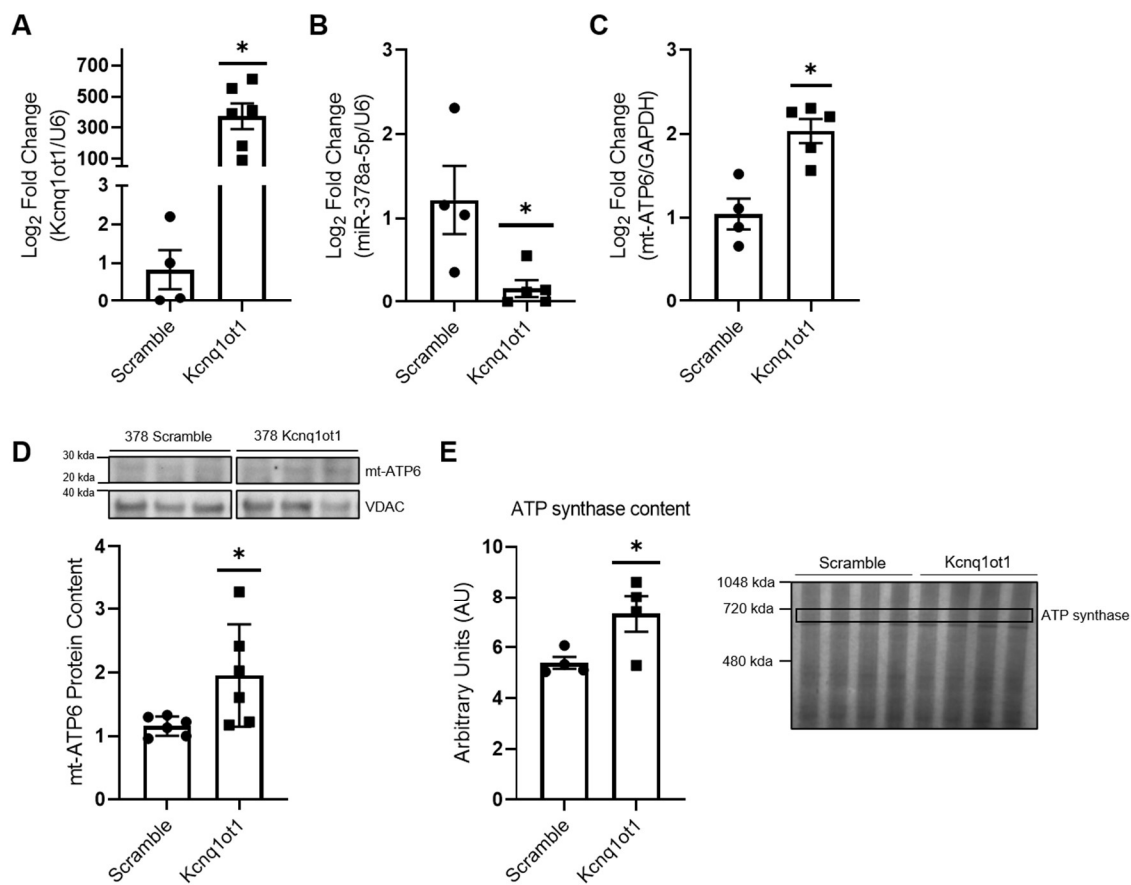
Figure 2.5: Overexpression of 500-bp Kcnq1ot1 fragment in HL-1-378a cardiomyocytes. (A) Verification of 500-bp Kcnq1ot1 fragment overexpression in HL-1-378a scramble (n = 4) and HL-1-378a Kcnq1ot1 (n = 6) groups. (B) MiR-378a-5p levels were assessed following 500-bp Kcnq1ot1 fragment overexpression in HL-1-378a scramble (n = 4) and HL-1-378a Kcnq1ot1 (n = 5) groups. (C) Quantification of mt-ATP6 mRNA in HL-1-378a scramble (n = 4) and HL-1-378a Kcnq1ot1 (n = 5) groups. (D) Quantification of mt-ATP6 protein content in HL-1-378a scramble (n = 6) and HL-1-378a Kcnq1ot1 (n = 6) groups, with representative Western blot. The representative image was constructed by taking three samples for each group from the same Western blot. (E) Quantification of ATP synthase content in HL-1-378a scramble (n = 4) and HL-1-378a Kcnq1ot1 (n = 4) groups as marked by "ATP synthase" with representative gel image. "n" is defined as biological replicates. All experiments were performed with a minimum of two technical replicates. Figure panels are based in 1 independent experiment. Data were analyzed using a Student's T-test. " * " Denotes $P \leq 0.05$ vs. WT. Values are shown as means ± SEM. See Supplemental data.

Figure 2.6: Summary overview of ncRNA network disruption in T2DM and rescue by miR-378a KO and inhibition.
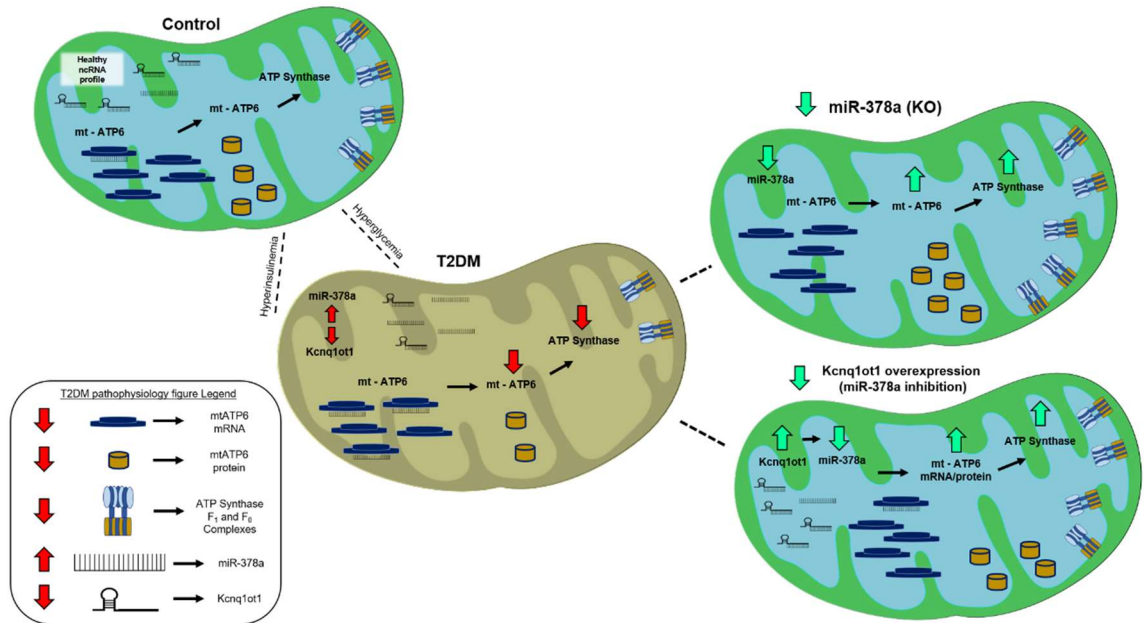
Figure 2.6: Summary overview of ncRNA network disruption in T2DM and rescue by miR-378a KO and inhibition. T2DM is characterized by increased mitochondrial miR-378a levels, decreased mt-ATP6 protein content, and decreased ATP synthase content and activity. MiR-378a KO/*Db/Db* mice lack miR-378a expression, and demonstrate significant improvements in mt-ATP6 protein content, ATP synthase content, and ATP synthase activity. These results are recapitulated in a cellular model when Kcnq1ot1, a lncRNA significantly reduced in T2DM mitochondria, is overexpressed, indicating the efficacy of Kcnq1ot1 as a therapeutic to benefit ATP synthase functionality. See Supplemental data.

SUPPLEMENTAL TABLES AND TABLE LEGENDS

Supplemental Table 2.1: Primer sequences for qPCR quantification

	Gene Name	Sequence	Orientation
Mouse	mt-ATP6	GCAGTCCGGCTTACAGCTAA	Forward
	mt-ATP6	AAGGAGGGCTGAAAAGGCTC	Reverse
	miR-378a-3p	CTGGACTTGGAGTCAGAA	Forward
	miR-378a-5p	CTGACTCCAGGTCCTGTG	Forward
	Standard Reverse	GAACATGTCTGCGTATCTC	Reverse
	Kcnq1ot1	GGCAGGCAGGATTAACCAGAT	Forward
	Kcnq1ot1	AGAACTATAATCAAGCAATCCAATC CTT	Reverse
	Kcnq1ot1 -miR-378a-5p site	AGAGTTGGACTTGGAATGCTCA	Forward
	Kcnq1ot1 -miR-378a-5p site	CCAACAGTACCGGAATGCCA	Reverse
	mt-16S rRNA	TGTAAAACGACGGCCAGTACCGTGC AAAG GTAGCATAAT	Forward
	mt-16S rRNA	CAGGAAACAGCTATGACCTCCGGTC TGAA CTCAGATCAC	Reverse
*Genotyping	miR-378a	GGCCAACTTGGGAAATGTA	Forward
*Genotyping	miR-378a	AGCTCACATGCAAACACAGG	Reverse
Human	mt-ATP6	TCCTAGAAATCGCTGTCGCC	Forward
	mt-ATP6	CTGTTAGGGGTCATGGGCTG	Reverse
	miR-378a-3p	CTGGACTTGGAGTCAGAA	Forward
	miR-378a-5p	CTGACTCCAGGTCCTGTG	Forward
	Standard Reverse	GAACATGTCTGCGTATCTC	Reverse
	Kcnq1ot1	GGAGTCTGGAACCTGACATCTG	Forward
	Kcnq1ot1	GTGTCAGGTGATGGAAGGACTC	Reverse

Cell	miR-378a-5p	CTGACTCCAGGTCCTGTG	Forward
	Standard Reverse	GAACATGTCTGCGTATCTC	Reverse
	Kcnq1ot1 500 bp plasmid	AGAGTTGGACTTGGAATGCTCA	Forward
	Kcnq1ot1 500 bp plasmid	CCAACAGTACCGGAATGCCA	Reverse
	Kcnq1ot1 Scramble plasmid	GATGCGCAATGTAGTAGAGGTCGTT AAGT	Forward
	Kcnq1ot1 Scramble plasmid	CTACGCGTTACATCATCTCCAGCAA TTCA	Reverse
Control Primers	U6	CTCGCTTCGGCAGCACAT	Forward
	U6	TTTGCGTGTCATCCTTGCG	Reverse
	GAPDH	CATCACTGCCACCCAGAAGACTG	Forward
	GAPDH	ATGCCAGTGAGCTTCCCGTTCAG	Reverse

Supplemental Table 2.1: Primer sequences for qPCR quantification. Mouse and human mt-ATP6 primers were designed using Primer-BLAST through NCBI. MiR-378a-3p and miR-378a-5p were matched to current sequences available in miRbase and designed according to Origene sequences. Kcnq1ot1 human primers were homogenous to Origene sequences, and Kcnq1ot1 mouse primers were acquired from Green et al, 2007. *Denotes sequences utilized for genotyping

Supplemental Table 2.2: DNA sequences for plasmid generation

Plasmid	Sequence
Kcnq1ot1-miR-378a-5p	TGGTTAGCTATTGAGGACTAAGTCAGGAG
Kcnq1ot1 miR-378a 500 bp	CAGGTGATAGAATTGAACAAAACCATCCAAGACCTAAAAACGGAAGTAGAAACAATAAAGAAAACCCAAAGTGGGACGACTCTGGAGGTAGAAACCCTAGGAAAGAAATCAGGAACCAAACATGTGAGCATCAGCAACAGAATACAAGAGATGGAAGAGAGAATCTCAGGTGCAGAAGATTCCATAGAGAACATGGGCACAACAATCAAAGAAAATGCGAAAGATTCTAACTCAAAACATCCAGGAATTCCAGGATACAATGAGTAGACAAACCTAGGGATAATAGGAGTAGAGGAGAATGAAGATTTTCAACTTAAAGGGTCAGCAAATATCTTCAACAAAATTATAGAAGAAAACTTCCCAAACCTAAAGTAAGAGATGCCCATGAACATACAAGAACCCTACAAAACTCCAAATAGACTGGACCAGAAAAGAAATTCCTCCCAACACATAATAATCAGAACAACAAATGCACTAAATATAGAATATTAAAAGTAGTAAGGGAAAAAGGTCAAGTGACATATAAAGG
Kcnq1ot1 Scramble	GATGCGCAATGTAGTAGAGGTCGTTAAGT

Supplemental Table 2.2: DNA sequences for plasmid generation. DNA sequences for plasmid generation. All plasmids were generated using a pGL4.14 (luc2/hygro) backbone with sequence insertion between BglII and HindIII restriction enzymes.

SUPPLEMENTAL FIGURES AND FIGURE LEGENDS

Supplemental Figure S2.1: Generation of miR-378a KO/*Db/Db* animal model.
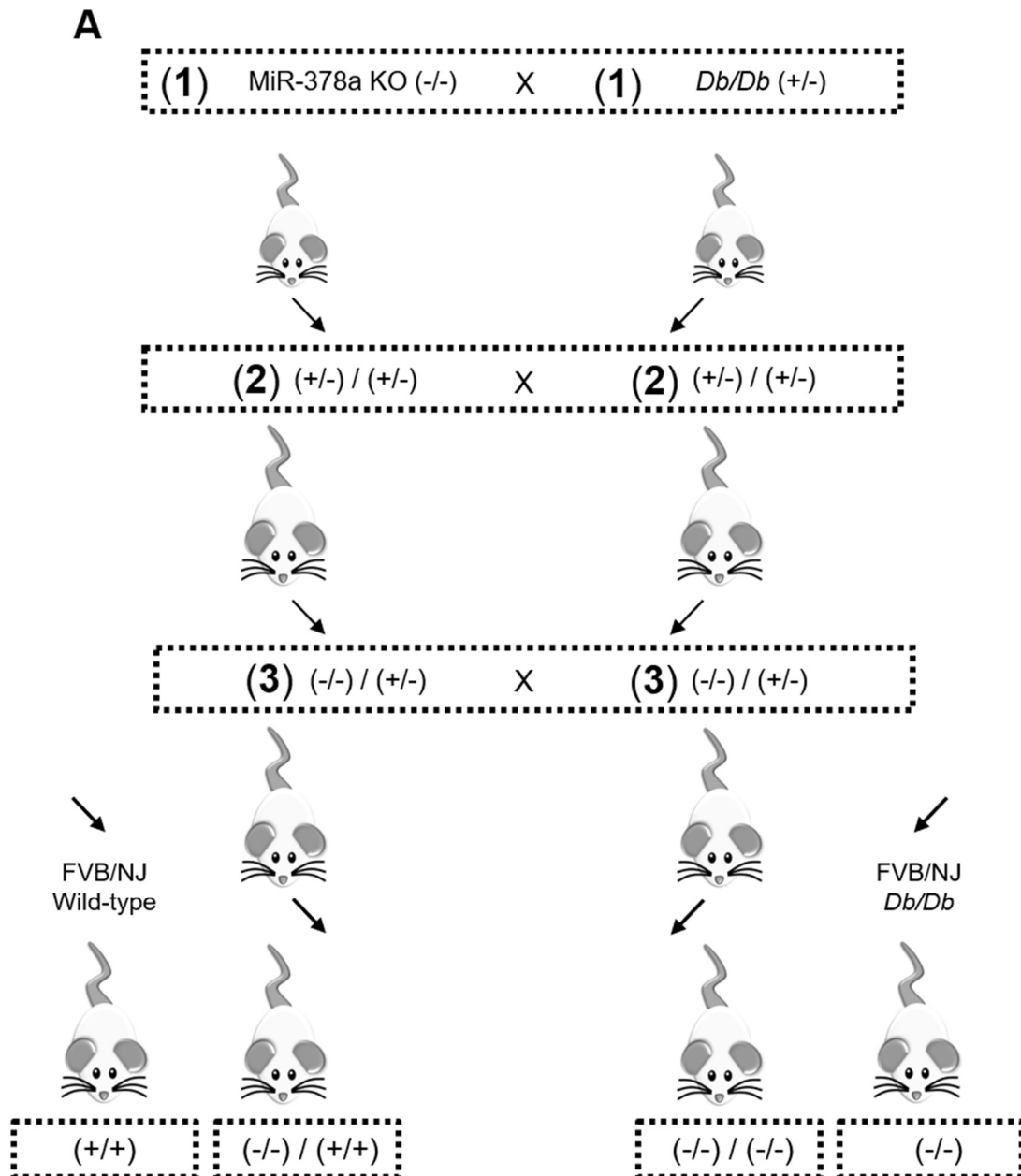
Supplemental Figure S2.1:
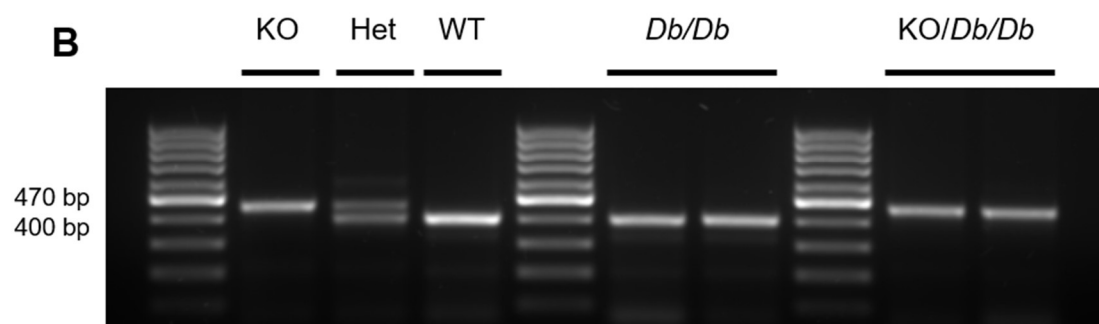
Supplemental Figure S2.1: Generation of miR-378a KO/*Db/Db* animal model. (A) KO/*Db/Db* animals were produced through a progressive breeding strategy, and (B) miR-378a KO was verified in KO/*Db/Db* mice using gel electrophoresis. Groups are designated (-/-) = KO, (+/-) = Het, (+/+) = WT. Agarose band of 470 bp = miR-378a KO, 400 bp = WT, 470 bp and 400 bp = heterozygous. KO; knockout, Het; heterozygous, WT; wild-type. See Supplemental data.

Supplemental Figure S2.2: Representative images of plasmids generated and certified by Genscript.
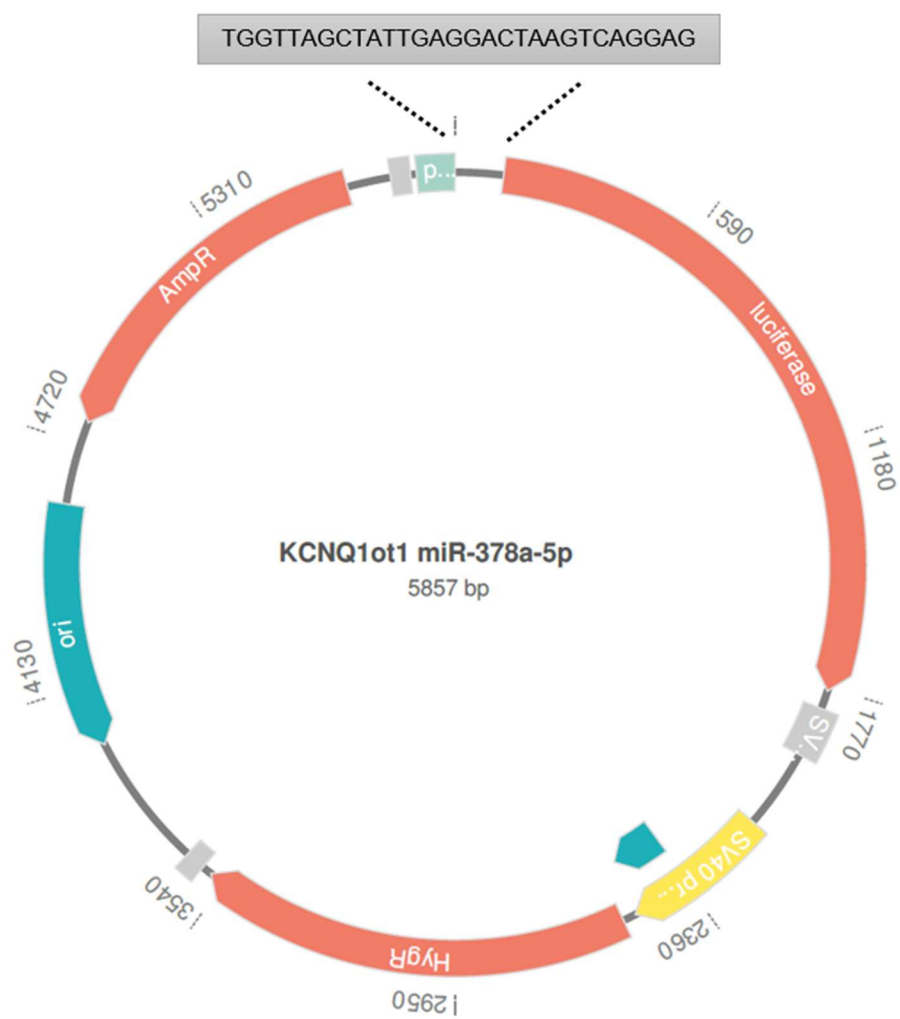
Supplemental Figure S2.2:

CAGGTGATAGAATTGAACAAAACCATCCAAGACCTAAAAACGGAAGTAGAAACAATAAAGAAA
ACCCAAAGTGGGACGACTCTGGAGGTAGAAACCCTAGGAAAGAAATCAGGAACCAAACATGT
GAGCATCAGCAACAGAATACAAGAGATGGAAGAGAGAATCTCAGGTGCAGAAGATTCCATAG
AGAACATGGGCACAACAATCAAAGAAAATGCGAAAAGATTCTAACTCAAAACATCCAGGAATTC
CAGGATACAATGAGTAGACAAAACCTAGGGATAATAGGAGTAGAGGAGAATGAAGATTTTCAA
CTTAAAGGGTCAGCAAATATCTTCAACAAAATTATAGAAGAAAACTTCCCAAACCTAAAGTAAG
AGATGCCCATGAACATACAAGAACCCTACAAAACTCCAAATAGACTGGACCAGAAAAGAAATT
CCTCCCAACACATAATAATCAGAACAACAAATGCACTAAATATAGAATATTAAAAGTAGTAAGG
GAAAAAGGTCAAGTGACATATAAAGG

KCNQ1ot1 500 bp
6359 bp

Supplemental Figure S2.2:

GATGCGCAATGTAGTAGAGGTCGTTAAGT

KCNQ1ot1 Scramble
5857 bp
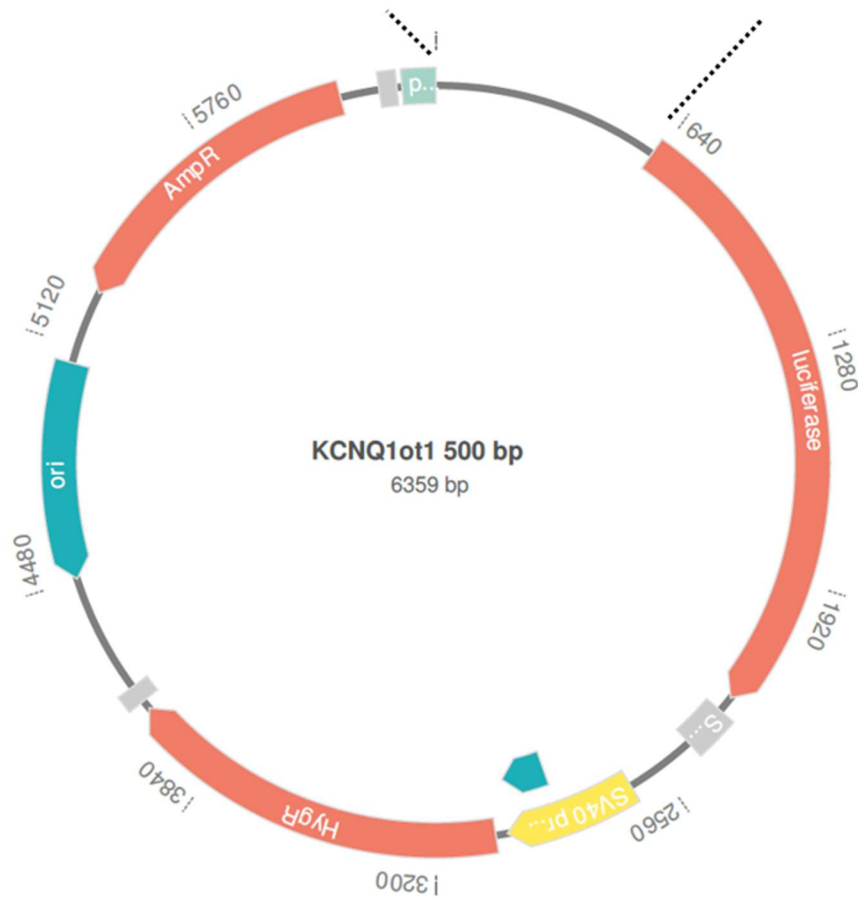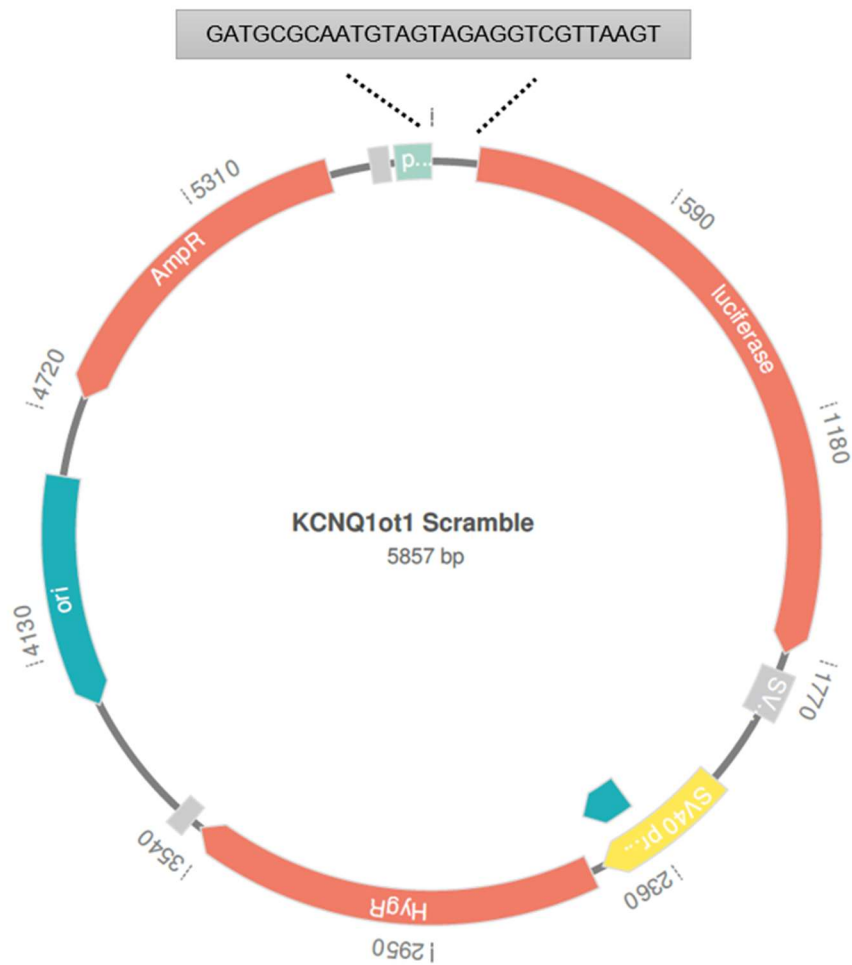
Supplemental Figure S2.2: Representative images of plasmids generated and certified by Genscript. Plasmids were generated using a pGL4.14[luc2/Hygro] plasmid construct, with sequences inserted between HindIII and BGIII restriction enzyme sites. See Supplemental data.

Supplemental Figure S2.3: Evaluation of mitochondrial electron transport chain complex activities and ATP content.
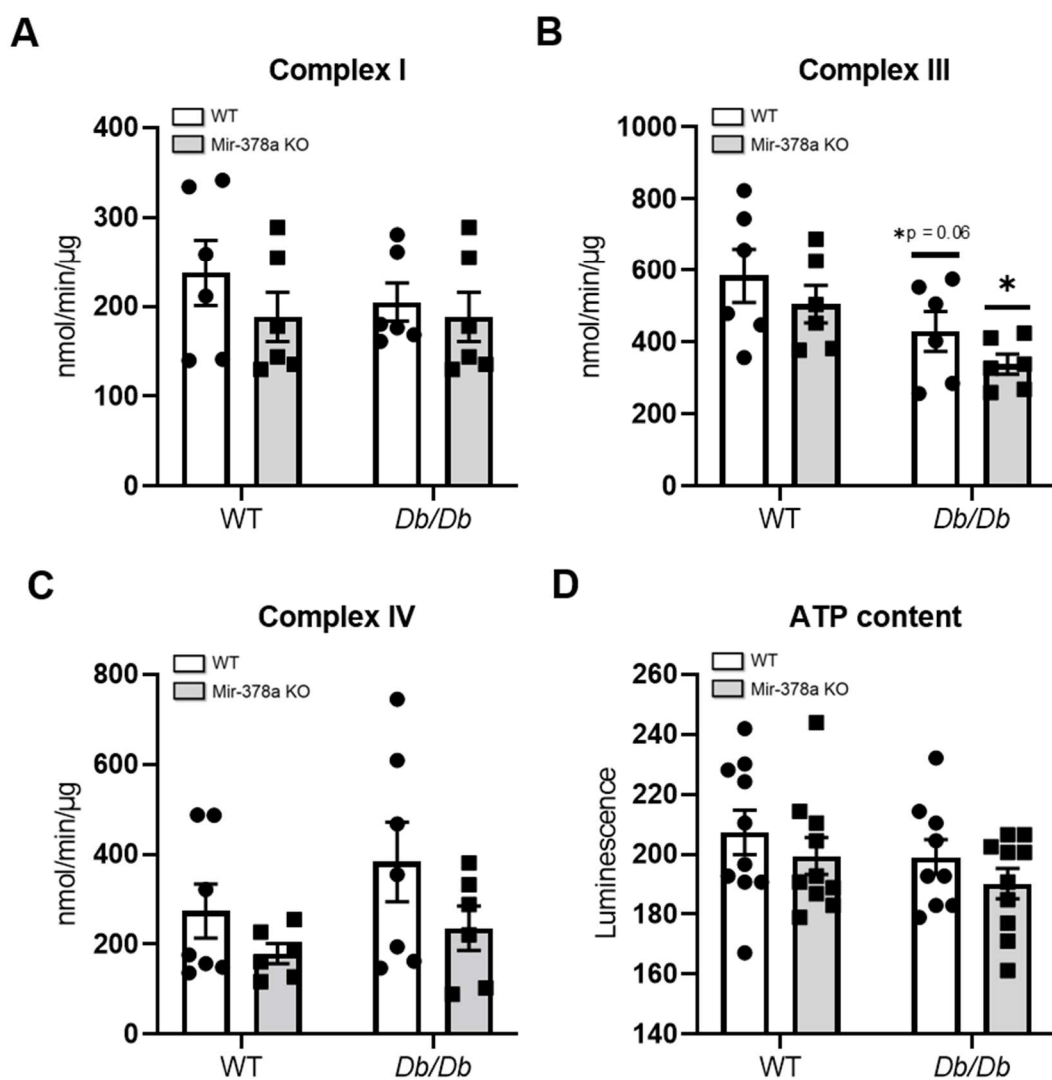
Supplemental Figure S2.3: Evaluation of mitochondrial electron transport chain complex activities and ATP content. (A) Complex I activity was assessed in WT (n = 6), *Db/Db* (n = 6), KO (n = 6), and KO/*Db/Db* (n = 6) mice. (B) Complex III activity was assessed in WT (n = 6), *Db/Db* (n = 6), KO (n = 6), and KO/*Db/Db* (n = 6) mice. (C) Complex IV activity was assessed in WT (n = 7), *Db/Db* (n = 7), KO (n = 6), and KO/*Db/Db* (n = 6) mice. (D) ATP content was assessed in WT (n = 10), *Db/Db* (n = 9), KO (n = 10), and KO/*Db/Db* (n = 10) mice. "n" is defined as biological replicates. Figure panels are based in 1 independent experiment. Data were analyzed using a two-way ANOVA. " * " Denotes $P \leq 0.05$ vs. WT, " ^ " Denotes $P \leq 0.05$ vs. *Db/Db*. Values are shown as means ± SEM WT; wild-type, KO; knockout, SEM; standard error of the mean. See Supplemental data.

Supplemental Figure S2.4: Evaluation of mtDNA content.
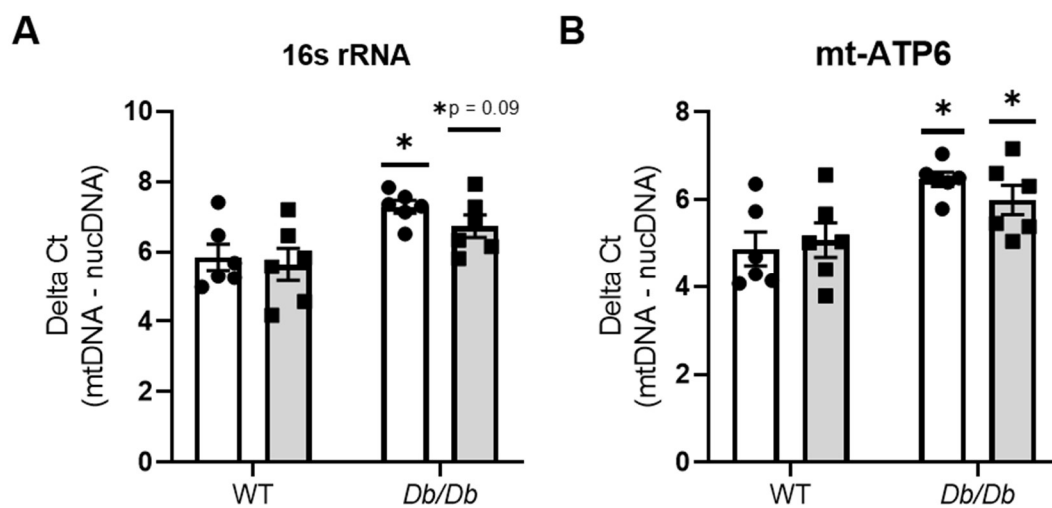
Supplemental Figure S2.4: Evaluation of mtDNA content. (A) MtDNA content was assessed using mt-16S rRNA in WT (n = 6), *Db/Db* (n = 6), KO (n = 6), and KO/*Db/Db* (n = 6) mice. (B) MtDNA content was assessed using mt-ATP6 in WT (n = 6), *Db/Db* (n = 6), KO (n = 6), and KO/*Db/Db* (n = 6) mice. "n" is defined as biological replicates. Figure panels are based in 1 independent experiment. Data were analyzed using a two-way ANOVA. " * " Denotes P ≤ 0.05 vs. WT, " ^ " Denotes P ≤ 0.05 vs. *Db/Db*. Values are shown as means ± SEM WT; wild-type, KO; knockout, SEM; standard error of the mean. See Supplemental data.

Supplemental Figure S2.5: Verification of HL-1-378a model, and the impact of 500-bp Kcnq1ot1 fragment overexpression in HL-1 cardiomyocytes.

Supplemental Figure S2.5: Verification of HL-1-378a model, and the impact of 500-bp Kcnq1ot1 fragment overexpression in HL-1 cardiomyocytes. (A) MiR-378a-5p levels were assessed in HL-1 scramble (n = 4) and HL-1-378a scramble (n = 3) cardiomyocytes. (B) Quantification of mt-ATP6 protein content in HL-1 scramble (n = 3) and HL-1-378a (n = 4) cardiomyocytes, with representative Western blot. (C) Verification of 500-bp Kcnq1ot1 fragment overexpression in HL-1 scramble (n = 3) and HL-1 Kcnq1ot1 (n = 6) groups. (D) MiR-378a-5p levels were assessed in HL-1 scramble (n = 3) and HL-1 Kcnq1ot1 (n = 3) cardiomyocytes. (E) Assessment of mt-ATP6 mRNA levels in HL-1 scramble (n = 6) and HL-1 Kcnq1ot1 (n = 6) cardiomyocytes. "n" is defined as biological replicates. All experiments were performed with a minimum of two technical replicates. Figure panels are based in 1 independent experiment. Data were analyzed using a Student's T-test. " * " Denotes $P \leq 0.05$ vs. WT. Values are shown as means ± SEM. See Supplemental data.

CHAPTER 3: SPECIFIC AIM IIa

Evaluation of Myocardial Mitochondrial Transplantation for Application in the Diabetic Heart

Andrya J. Durr[1,2], Sarah L. McLaughlin[3], Amina Kunovac[1,2,4], Andrew D. Taylor[1,2], Mark V. Pinti[5,6], Quincy A. Hathaway[1,2,4], Katelyn G. Pinti[1], and John M. Hollander[1,2,4]

[1]Division of Exercise Physiology, West Virginia University School of Medicine, Morgantown, WV, 26506, USA. [2]Mitochondria, Metabolism & Bioenergetics Working Group, West Virginia University School of Medicine, Morgantown, WV. [3]Animal Models and Imaging Facility, West Virginia University School of Medicine, Morgantown, WV, [4]Center for Inhalation Toxicology (iTOX), West Virginia University School of Medicine, Morgantown, WV. [5]West Virginia University School of Pharmacy, Morgantown, WV. [6]Department of Physiology, Pharmacology, Morgantown, WV.

Corresponding Author:

John M. Hollander, PhD, FAHA

Professor and Graduate Director, Exercise Physiology

Sr. Asst. Dean for Research and Graduate Education, Human Performance

Director, Mitochondria, Metabolism & Bioenergetics

West Virginia University School of Medicine

1 Medical Center Drive

P.O. Box 9227

Morgantown, WV 26506

Ph: (304) 293-3683

Fax: (304) 293-7105

Email: jhollander@hsc.wvu.edu

Abstract

As the prevalence of diabetes mellitus and cardiovascular comorbidities continue to rise, it is of critical importance to continue the exploration of novel therapeutic opportunities to improve patient morbidity and mortality outcomes. A wide range of cardiac pathologies are regularly characterized by bioenergetic dysfunction of the mitochondrion, which can perpetuate immediate or delayed harm to cardiac contractile function. Spontaneous cardiac events such as ischemia reperfusion, or MI, often occur without warning, and lead to tissue damage or death, and reduced mitochondrial bioenergetic capacity. Mitochondrial transplantation, a unique therapeutic approach involving the delivery of healthy mitochondria to the myocardium, has demonstrated positive impacts on tissue health following ischemia reperfusion events through the preservation of mitochondrial bioenergetic function. We surmised that mitochondrial transplantation may provide benefit to the ailing heart during diabetes mellitus, as dysfunctional mitochondria are a central component in the development and progression of cardiovascular disease (CVD). The efficacy of mitochondrial transplantation for CVD in diabetes mellitus is unexplored, and presents a number of challenges. Therefore, the aim of this project was to assess the efficacy of mitochondrial transplantation as a therapeutic approach in diabetes mellitus for the treatment of CVD. We hypothesized that mitochondria collected from a healthy donor of the same species could be deposited within the left ventricular myocardium using ultrasound-guided echocardiography. Further, we hypothesized that mitochondrial distribution, uptake, and localization following injection would mirror results obtained from mitochondrial transplantation during open heart surgery in a murine model. A transgenic mouse model containing mKate2 fluorescent mitochondria was used as a mitochondrial donor for all experimentation. Mitochondrial localization in HL-1 cardiomyocytes was assessed using a MIF Nikon A1R confocal microscope at 24- and 48-hours post transplantation. Of the estimated 7.1×10^8 mitochondria plated, 8.3×10^5 were attached to the cellular membrane (<1%) following media change at 24 hours. At

48 hours, mitochondrial host and mKate2 fluorescent signals overlapped, suggesting interaction of transplanted mitochondria with the host cell mitochondrial network. Mitochondrial transplantation was further assessed in a murine model using ultrasound-guided echocardiography. Following injection, mKate2 fluorescent signal was immediately verified in the heart using the IVIS SpectrumCT, and was further identified at 24 hours using immunohistochemistry and MIF Nikon A1R/SIM microscopy. Immunohistochemical analyses demonstrated synonymous detection of host and donor mitochondrial populations within and around sarcomeric α-actin signal. Mitochondrial counts and IMARIS 3D reconstruction indicated 1.08×10^6 and 8.6×10^3 mitochondria were identifiable in the left ventricular myocardium at 24 hours, >1% of those injected. Additionally, mitochondria were distributed over a calculated 30% of the left ventricular myocardium, but located primarily in and around the injection sites. In summary, these results are consistent with those presented in current literature and suggest that ultrasound-guided echocardiography is an efficacious, minimally invasive, method of mitochondrial transplantation that could be applied in diabetes mellitus.

Keywords: diabetes mellitus, mitochondrial transplantation, left ventricle, myocardium, ultrasound-guided echocardiography

Introduction

According to the World Health Organization, the prevalence of diabetes mellitus has risen exponentially, more than tripling from 108 to 422 million people diagnosed between 1980 and 2014 (1). The relationship between diabetes mellitus and cardiovascular disease (CVD) is well characterized, as CVD is the leading cause of mortality in the diabetic population (2). Adults with diabetes mellitus are up to four times more likely to die from heart disease than their healthy counterparts (2). This likelihood further increases with type 1 diabetes mellitus (T1DM), as CVD events are not only more common, but occur in higher frequencies than in the non-diabetic population. Additionally, those with T1DM often suffer for longer periods of time than those with type 2 diabetes mellitus (T2DM), increasing the likelihood of a cardiac event (3-5). While many mechanisms contribute to the pathophysiological development and progression of CVD in the diabetic heart, mitochondrial dysfunction is a critical component due to the mitochondrion's role as primary producer of ATP for contraction (6, 7). Altered bioenergetic function, alterations in mitochondrial structure and dynamics, and increased reactive oxygen species have been observed in diabetic mitochondria (8-10). Further, mitochondrial dysfunction has been suggested to play a role in a number of key disease features, including the development of insulin resistance, the initial onset of disease, and the development of cardiac contractile dysfunction (11-13). In totality, mitochondrial dysfunction has been determined as a major contributing factor for the progression of CVD to heart failure, making the mitochondria a widely studied and sought-after target for therapeutic intervention.

Mitochondrial targeted therapies are of great interest for disease management and have been utilized to treat and mitigate disease related comorbidities. Strategies have been developed to reduce mitochondrial dysfunction and stress, improve metabolic regulation, and limit the generation of reactive oxygen species (14-18). A unique therapeutic approach, mitochondrial transplantation, has demonstrated significant benefits to the heart during ischemia

124

reperfusion. Mitochondrial transplantation involves the transplantation of healthy mitochondria, isolated from either the same individual or a separate individual of the same species, into the myocardial wall, and is utilized in ischemia reperfusion to reduce cardiac dysfunction, area at risk, and tissue death (19-22). Exogenous healthy mitochondria assist the dysfunctional or damaged mitochondria by providing bioenergetic support including increased respiration and increased ATP production, thereby improving cardiac contractility (19-21, 23, 24).

Minimal data is available regarding the efficacy of mitochondrial transplantation to enhance post-ischemic myocardial functional recovery and reduce myocellular injury in the diabetic heart, and it has been unexplored as a prophylactic method. A number of barriers challenge the use of mitochondrial transplantation in diabetes mellitus. Specifically, a significant challenge is the delivery of mitochondria to the heart in a minimally invasive manner, in which mitochondria are adequately distributed within the myocardium and remain for a measurable period of time. Therefore, the purpose of this study was to assess the efficacy of mitochondrial transplantation as a therapeutic approach in diabetes mellitus for the treatment of CVD. We hypothesized that mitochondria collected from a healthy donor of the same species could be deposited within the left ventricular myocardium using ultrasound-guided echocardiography. Further, we aimed to determine the number of deposited mitochondria, and their range of distribution, to understand the efficiency of our procedure and identify further challenges to its application.

Materials and Methods

Experimental Animals

Animal experiments performed in this study conformed to the National Institutes of Health Guidelines for the Care and Use of Laboratory Animals and were approved by the West Virginia University (WVU) Care and Use Committee.

125

Experimental animals included male and female C57BL/6J/Tg(CAG-mKate2)1Poche/J mice (The Jackson Laboratory Cat. No. 032188) (25), FVB/NJ wild-type mice (RRID:IMSR_JAX:001800), and FVB/NJ *Db/Db* mice (The Jackson Laboratory stock Cat. No. 006654) (26, 27). Mice were housed in the WVU Health Sciences Center animal facility on a 12-hour light/dark cycle in a temperature-controlled room. Animals were maintained on a standard chow diet and had access to both food and water *ad libitum*. Animals were sacrificed at 25 weeks of age using cervical dislocation as a primary method, and critical organ removal as a secondary method of euthanasia. Animals were genotyped using the IVIS SpectrumCT *in vivo* spectrum imaging system (PerkinElmer, Waltham, MA) on excitation and emission peaks of 588 nm and 635 nm, respectively. The presence of fluorescent signal was considered a positive the presence of the transgenic mKate2 protein.

Estimating Total Mitochondrial Number in the Murine Heart

Because mitochondria are not viable for extended periods of time outside of a biological system, we aimed to estimate the number of mitochondria isolated from a whole murine heart to avoid the timely process of counting mitochondria using flow cytometry prior to injection. The number of myocytes isolated from a single adult mouse heart was estimated by extrapolating the number of mitochondria in a human heart, by weight and cellular volume, to mouse equivalents (Table 3.1) (28). The number of cardiomyocytes in the human heart averages 2.5 billion, accounting for about 30 percent of the total volume of cells (29). In the murine heart, cardiomyocytes account for a considerably higher volume of cells, with some estimates as high as 56 percent (28, 30). Based on these estimates, a 12-week-old adult C57BL/6J mouse averages a body weight of 23.8 grams, and contains 1.13×10^{10} mitochondria. Because this number is extrapolated from human sources, numbers vary based on individual weight. Additionally, estimates of mitochondrial number vary with sex due to differences in

body weight between male and female donors, and were taken into account during each isolation (28, 31).

Mitochondrial Isolation

Mitochondria were isolated from mouse ventricular tissue as previously described (32), with modifications by our laboratory (33-35). Briefly, mitochondrial subsarcolemmal and interfibrillar subpopulations were isolated using a series of centrifugation steps, and were combined to form a total mitochondrial population. Mitochondria were resuspended in 100 μl of respiration buffer (250 mmol/l sucrose, 2 mmol/l KH_2PO_4, 10 mmol/l $MgCl_2$, 20 mmol/l K+-HEPES buffer, pH 7.2, 0.5 mmol/l K+-EGTA, pH 8.0, 5 mmol/l glutamate, 5 mmol/l malate, 8 mmol/l succinate, and 1 mmol/l ADP) (21), and used immediately for mitochondrial transplantation or stored at -80 degrees for biochemical analysis.

Cell Culture

The established mouse cardiomyocyte cell line (HL-1) (Millipore Cat. No. SCC065, RRID:CVCL_0303) (Registered with the International Depositary Authority, American Type Culture Collection (ATCC); CRL-12197), which maintains a cardiac-specific phenotype following repeated passages, was used as previously described (10, 36, 37). Cells were maintained at 5% CO_2/95% air and 37 °C in Claycomb media (Sigma Aldrich Cat. No. 51800C-500ML) with supplementation according to manufacturer instruction (36). The "n" presented in related results is representative of biological replicates.

In Vitro Mitochondrial Transplantation

HL-1 cardiomyocytes were plated in two 35 mm glass bottom dishes (MatTek Cat # P35GCol-0-10-C). Once 80% confluence was reached, cells were either left untreated or were treated with MitoTracker Orange CMTMRos (Thermo

Fisher Scientific Cat # M7510) and CellTracker Green CMFDA (Thermo Fisher Scientific Cat. No. C7025) prior to mitochondrial transplantation to label host cell mitochondria and cellular membranes. For initial imaging of mitochondrial interactions, two groups were utilized; a control plate receiving an equal volume of cell culture media, without mKate2 mitochondria, and a second plate receiving 1.92 x 10^8 mKate2 mitochondria (1 x 10^7 per 50,000 cells) as previously described (38). For the first set of experiments, HL-1 cardiomyocytes were left untreated so that only mKate2 signal was present. Following transplantation, cells were imaged at 30-minute intervals for 24 hours to observe cellular behavior and interactions with mKate2 mitochondria. For a second set of experiments, HL-1 cardiomyocyte host mitochondria and cellular membranes were stained prior to mitochondrial transplantation, and were imaged at 24 and 48 hours to assess mitochondrial uptake and integration.

In Vivo Mitochondrial Transplantation

Animals were anesthetized using 2 to 3% isoflurane, and maintained under deep sedation to minimize discomfort and the potential for injury. All injections were performed using ultrasound-guided echocardiography and Clear Aquasonic Ultrasound Transmission Gel (Parker Laboratories Cat. No. BT-025-0037L) with 28-gauge insulin syringes (ADW Diabetes Cat. No. 329461PK4). It should be noted that the use of blue or colored ultrasound gel interferes with IVIS imaging and produces false fluorescent signal. Once in position, 30 microliters were deposited at each injection site, keeping the syringe in place for 5 seconds post injection to allow buffer and mitochondrial dispersion before the needle was removed (Supplemental Video S3.1 (https://figshare.com/s/48e1bcd943be9452c64c)). Removing the needle to soon following injection resulted in greater loss of mitochondrial volume, collection of mitochondria at the injection site, and reduced distribution. A minimum of two mice were used for mitochondrial transplantation trials; a mitochondrial transplant recipient and a respiration buffer control. MKate2 mitochondria recipients received

the equivalent of a single young (6-week-old) adult's total cardiac volume (1.13 x 10^{10}) of mitochondria or respiration buffer in three 30 microliter injections. Injections were staggered in the left ventricle myocardium beginning at the mid anterolateral wall and moved toward the apex. Notably, injections were placed far enough below to atria to be confident of no interference. During initial training sessions, injections placed too close to the atria posed a higher risk of cardiac arrythmias, and mortality.

Tissue Processing and Immunohistochemistry Preparation

Left ventricular tissues were processed by the WVU Electron Microscopy Histopathology and Tissue Bank to determine mitochondrial distribution and localization. Three mice were utilized for immunohistochemical analyses; one mKate2 mitochondrial transplant recipient, one respiration buffer control, and one control transgenic mKate2 positive mouse receiving no injection. A control transgenic mKate2 mouse was used to aid in microscopy training, and the initial identification of appropriate settings for visualizing mKate2 mitochondria. Following euthanasia, the left ventricle was extracted and oriented in a histochemistry tissue embedding cassette (Grayline Medical Cat. No. M516-3) with the endocardial wall facing down onto the embedding cassette sponge (Capitol Scientific Cat. No. DYN-230264-0001) so that the epicardial wall was the first to be sliced. This orientation allowed for complete slices of the left ventricular wall to be obtained. Left ventricle tissue was fixed by immersion in formaldehyde and paraffin embedded for processing. Because we were unsure what to expect following mitochondrial transplantation, mKate2 mitochondria recipient tissue was sliced in 10 μm sections, with no tissue discarded to allow for full exploration of the myocardium. In total, 24 slides with 3 tissue slices per slide were prepared, covering a total range of 720 μm, or the outer half of the left ventricular myocardium. The respiration buffer recipient and transgenic control mice were processed as described above, with modifications. Six slides with 3 tissue slices per slide were obtained by keeping a 10 μm section, then discarding 30 μm. In

totality, half of the left ventricles, or 720 μm, were sectioned but three of every four slices were discarded.

Immunohistochemistry Deparaffinization and Rehydration

Slides were deparaffinized and rehydrated according to the Abcam Immunohistochemistry (IHC) application guide prior to antigen retrieval and immunohistochemical staining. Slides were first incubated in Xylene 3 x 3-minute intervals. Next, slides were placed in 100% ethanol for three 2-minute intervals. Finally, slides were placed in 95%, 80%, and 70% ethanol for one interval of 2 minutes each in the order described. Lastly, slides were rinsed quickly in milliQ water and placed in 1x PBS until ready for heat-induced epitope retrieval, or antigen retrieval. Antigen retrieval was achieved by placing slides into a rice cooker containing citrate buffer tri-sodium citrate (dihydrate) 2.94 g, distilled water 1000 mL, adjust pH to 6.0 with HCl, add 0.5 mL Tween 20), pre-heated to 98 degrees C, but not boiling. Slides were completely submerged and incubated for 25 minutes. Slides were removed from the rice cooker and placed on ice for 20 minutes then rinsed in 1x PBST for 20 minutes, followed by two consecutive 5 minutes rinses in 1x PBST. Slides can be left in 1x PBST until ready for processing.

Immunohistochemistry Staining

Slides were placed in a blocking solution made with 5% normal goat serum (Vector Laboratories Cat. No. 2B0406) in 1x PBS for 1 hour. Primary antibodies solutions were diluted to 5 percent primary antibody in 1x PBS. Slides were incubated in 200 μl of antibody solution, enough to sufficiently cover each section, and contained using a hydrophobic pencil, for 1-2 hours at room temperature. Primary antibodies included: COX IV rabbit polyclonal (DyLight 550 conjugated) (Novus Biologicals Cat. No. NB110-39115R, 5% of total staining solution volume), verified for specificity by the manufacturer, and Alpha-Actinin-2 rabbit polyclonal (ALEXA FLUOR 488 conjugated) (Bioss Cat. No. bs-10367R-A488, 5% of total

staining solution volume), verified for specificity by the manufacturer. Following incubation, slides were rinsed in 1x PBST for 3 x 5-minute intervals. The secondary antibody used was Goat Anti-Rabbit IgG H&L goat polyclonal (HRP conjugated) (Abcam Cat. No. ab6721, RRID:AB_955447, 1:200 dilution in 1x PBST). Slides were incubated with secondary antibody for 1 hour in the dark, at room temperature. Slides were rinsed for 3 x 5-minute intervals in 1x PBST. Autofluorescence quenching was achieved using the Vector® TrueVIEW® Autofluorescence Quenching Kit with DAPI (Vector Laboratories Cat. No. SP-8500-15) according to manufacturer instructions. Slides were quickly rinsed in milliQ water prior to mounting with mounting media (Prolong gold Cat. No. P36931) and cover slips. Notably, enough mounting media should be used to completely cover the section with the addition of a cover slip, and air bubbles should be avoided. Cover slip edges were sealed using clear nail polish and allowed to dry for 24 hours at room temperature before imaging.

IVIS SpectrumCT

MKate2 Mitochondrial fluorescent signal was verified immediately following injection using the IVIS SpectrumCT *in vivo* spectrum imaging system (PerkinElmer, Waltham, MA). The mKate2 protein is visible under a DeepRed fluorescence, and therefore wavelengths were chosen within 588 nm (excitation) and 633 nm (emission). CT scans performed in conjunction with IVIS imaging illuminated the heart in a 3D orientation and provided further confirmation of mitochondrial presence within the heart.

Microscopy (Nikon A1R)

HL-1 cardiomyocytes and immunohistochemistry slides were imaged using the Nikon A1R microscope by a single trained individual in the WVU microscopy core. The 100x objective was used to obtain images of mKate2 mitochondria at the highest possible enlargement. Images were acquired for DAPI, COX IV, alpha-

actinin-2, and mKate2 protein using wavelengths 405 nm, 488 nm, 550 nm, and 640 nm, respectively. HL-1 cardiomyocytes were imaged every 30 minutes for 24 hours following mitochondrial transplantation, and once at 24 and 48 hours as described above.

Results

Mitochondrial Uptake and Localization

Following transplantation of mKate2 positive mitochondria, HL-1 cardiomyocytes were monitored for 24 hours. A time-lapse video following mitochondrial transplantation suggests that cells divide and move normally, without hinderance, while accumulating transplanted mitochondria along the outer edges of the cellular membrane (Supplemental Video S3.2 (https://figshare.com/s/48e1bcd943be9452c64c)). A breakdown of Supplemental Video S3.2 demonstrates the ability of HL-1 cardiomyocytes to move and interact with mKate2 positive mitochondria, appearing to accumulate mKate2 protein signal along the outer edges of the cell (Figure 3.1). Images of cell behavior at 0, 2, 4, and 6 hours demonstrate overall lower amounts of mKate2 protein signal, suggesting that transplanted mitochondria take 4 to 6 hours to completely settle out of solution onto the cell layer (Figure 3.1, A, B, C, and D). Beginning at 8 hours, mKate2 protein signal begins to accumulate along the edges of the cells, and appears to increase from 10 to 12 hours before remaining constant (Figure 3.1, E, F, and G). From 16 hours on, mKate2 protein signal remains consistent, and changes synonymously with cell movement (Figure 3.1, H and J).

Mitochondrial localization was assessed at 24 hours (Figure 3.2). At 24 hours, cell membranes (Figure 3.2A), host cell mitochondria (Figure 3.2B), and mKate2 positive mitochondria (Figure 3.2C) are visualized independently. Signal overlay demonstrates a clear separation between mKate2 (green) and host cell mitochondria (red) (Figure 3.2D). Further, while host cell mitochondria (red) are

visually identifiable as being within the bounds of the cellular membrane, mKate2 positive mitochondria appear attached to the surface of the cell (Figure 3.2D). Using Z-stack imagery, mitochondrial localization within the cell was further visualized. Cell membranes (Figure 3.2E), host cell mitochondria (Figure 3.2F), and mKate2 positive mitochondria (Figure 3.2G) are visualized following Z-stack imaging and movement of the visual plane to slice through the cell and visualize the internal components. We confirm that MKate2 positive mitochondrial signal is detectable solely on the outside of the cell, on the membrane surface, and is not present within the host cell (Figure 3.2H). These data indicate that at 24 hours post transfection, mKate2 positive mitochondria may attach themselves to the host cell membrane surface, but do not appear to interact with host cell mitochondrial populations.

At 48 hours, mitochondria were assessed a second time for localization and interactions with the host cell mitochondrial network (Figure 3.3). Cell membranes (Figure 3.3A), host cell mitochondria (Figure 3.3B), and mKate2 positive mitochondria (Figure 3.3C) are visualized independently. Signal overlay suggests that mKate2 positive mitochondria (green) overlap with the host cell mitochondrial signal (red) as determined by yellow/orange coloring, a combination of both MitoTracker orange (red) and mKate2 (green) fluorescent signals (Figure 3.3D). Using Z-stack imaging, cell membranes (Figure 3.3E), host cell mitochondria (Figure 3F), mKate2 positive mitochondria (Figure 3.3G) are visualized independently. MKate2 fluorescent signal (green) was confirmed to be co-localized with host mitochondrial MitoTracker orange signal (red) (Figure 3.3H). These data suggest that by 48 hours, transplanted mKate2 positive mitochondria are interacting with host cell mitochondria.

Because it was uncertain if mKate2 positive mitochondria were localized within the cellular membrane, or simply interacting with host cell mitochondria at the membrane level, HL-1 cardiomyocytes were further visualized using IMARIS 3D reconstruction (Figure 3.4). Mitochondrial signals were segregated into 4

categories, each marked by an independent color; host cell mitochondria outside of cell (red), host cell mitochondria inside of cell surface (purple), mKate2 positive mitochondria outside of cell (green), and mKate2 positive mitochondria inside of cell surface (blue). Visual assessments suggest that mKate2 positive mitochondria are primarily trapped within the cell membrane at both 24 (Figure 3.4A) and 48 (Figure 3.4B) hours. These data indicate that mKate2 positive mitochondria may not be fully integrated into HL-1 cardiomyocytes but instead be capable of sharing information across the cell membrane.

Ultrasound-guided Echocardiography

To determine the efficacy of mitochondrial transplantation for diabetes mellitus, we evaluated ultrasound-guided echocardiography as a minimally invasive method. A representative photo of experimental setup for echocardiography equipment and intracardiac injection is provided for reference (Figure 3.5A). Following injection of mKate2 positive mitochondria, the IVIS SpectrumCT was used to detect the immediate presence of mKate2 fluorescent signal (Figure 3.5B). Further, CT imaging confirmed the presence of mKate2 fluorescent signal within area of the heart (Figure 3.5C). Video footage of a single injection into the myocardial wall is provided in Supplemental Video S3.1 (https://figshare.com/s/48e1bcd943be9452c64c)

Calculating Mitochondrial Coverage and Distribution

Mitochondrial distribution and coverage area was calculated using two methods; IMARIS 3D image reconstruction and frame by frame calculations using individual fluorescent signals. The volume of a mitochondria was determined to be 0.75 μm in diameter, 2.0 μm in length, by 0.75 μm in thickness, resulting in a volume of 4.71 μm^3. To calculate the percentage of the left ventricle containing identifiable mitochondria, an ellipsoid model was used to calculate the total volume of the left ventricle myocardium (Figure 3.6A). Mitochondrial number was assessed

within a single injection site in a 1000 x 1000 um^2 square using Z-stack imaging and IMARIS analyses, and multiplied by three to include the two remaining injection sites. The depth of left ventricle sections containing mitochondria was a total of 250 μm, therefore the volume of the left ventricle was calculated as a length of 6,000 μm, a height of 5,000 μm, and a depth of 10 μm per section, or 250 μm for the total volume sectioned (Figure 3.6B). The total volume of a single section was calculated to be 125,600,000 μm^3, whereas the total volume of the left ventricle sectioned (ranging 250 μm in depth) was 31,400,000,000 μm^3. Because 34 frames were imaged at a 0.25 μm thickness and each section was only 10 μm thick, there was potential for frames to overlap images of the same mitochondrial signals. To accommodate this possibility, only frames 2, 5, 10, 15, 20, 25, 30, and 34 were analyzed to avoid duplication of mitochondria detected, and ranged from the first detected fluorescent signal to the last. The number of fluorescent signals were counted for each frame and used in the "frame by frame" method of analysis. Following immunohistochemical analyses, nuclei stained for DAPI (Figure 3.6C), host mitochondria stained for COX IV (Figure 3.6D), and mKate2 positive mitochondria (Figure 3.6E) are visualized independently. Images were merged for a representative overlay of signal, and mKate2 positive mitochondria are marked by yellow arrows (Figure 3.6F). Z-stack images demonstrate mitochondrial distribution within a 1000 x 1000 μm square. Nuclei stained with DAPI (Figure 3.6G), host mitochondria stained for COX IV (Figure 3.6H), and mKate2 positive mitochondria (Figure 3.6I) are visualized independently. Signal overlay confirm distribution of mKate2 positive mitochondria within a 1000 x 1000 μm volume, and are marked by yellow arrows (Figure 3.6J).

IMARIS analysis estimated 8.3 x 10^5 mitochondria present, in total, for all three injection sites based on volumetric analysis of fluorescent signal for mKate2 positive mitochondria. When normalized to mitochondrial volume, it was estimated that a total of 1.08 x 10^6 mitochondria were remained in the tissue at 24 hours. Based on the distribution of the 1000 x 1000 μm^2 surrounding a single injection site, the surface area considered to be substantially covered was estimated at

8,000,000 μm³. If consistent for all three injection sites, the total volume covered may be up to 24,000,000 μm³. Based on the total volume of the left ventricle, and the total volume of the injection sites containing at least one mitochondria, it was estimated that at least one mKate2 positive mitochondria is detectable within 30 percent of the left ventricle myocardium, but provides no indication of mitochondrial distribution or concentration within that 30 percent. Substantial coverage was translated to be only 0.076 percent, less than 1.0 percent, of the total volume of the left ventricle, but may reach as high as 47.75 percent coverage in high density areas, such as at or near injection sites. These data indicate that following transplantation, mKate2 positive mitochondria remain primarily near and within the sites of injection, though a minimal amount distribute farther into the myocardium.

Mitochondrial Distribution and Localization in Vivo

The left ventricular myocardium was assessed for localization of mKate2 positive mitochondria within the tissue at 24 hours post-injection (Figure 3.7). Following immunohistochemical analysis, nuclei stained for DAPI (Figure 3.7A), alpha actinin stained with alpha-actinin-2 (Figure 3.7B), host mitochondria stained for COX IV (Figure 3.7C), and mKate2 positive mitochondria (Figure 3.7D) are visualized independently. Merged signal, without DAPI, demonstrates overlay of mitochondrial COX IV (red) and mKate2 positive mitochondria (blue) signals, resulting in purple fluorescent signals identified by yellow arrows (Figure 3.7E), indicating mitochondrial presence within the cardiac tissue, appearing in and around alpha actinin proteins. Further, merged COX IV (red) and mKate2 (blue) mitochondria signals suggest the overlap of mKate2 positive mitochondrial signal within recipient mitochondrial populations, distinguished by purple signal and marked by yellow arrows (Figure 3.7F). Images suggest that mKate2 positive mitochondria are co-localized with recipient mitochondria. These data further suggest that ultrasound-guided intracardiac injection is a feasible method of mitochondrial transplantation in which mitochondria remain in the tissue for at least

24 hours post-injection, and demonstrate detectable interactions with recipient mitochondria.

Discussion

As diabetes mellitus continues to increase in prevalence, the need for improved therapeutic treatments becomes ever more critical. While mitochondrial transplantation provides a unique macroscale opportunity to ameliorate mitochondrial dysfunction through the replacement of unhealthy mitochondria with undamaged, bioenergetically competent mitochondria, many barriers impede the application of mitochondrial transplantation in diabetes mellitus. The most notable differences between treatment of CVD in diabetes mellitus versus ischemia reperfusion and other spontaneous cardiac events is the lack of timing and location. Therefore, the primary objective of this study was to determine the efficacy of mitochondrial transplantation as a prophylactic technique for diabetes mellitus. Prophylactic application appears to be the ideal course of action, as it is not being performed in response to a cardiac event. Further, there is no predetermined location for injection, such as with ischemia reperfusion studies. In order to perform the procedure prophylactically, and make it worthwhile clinically, the procedure must be performed in a minimally invasive manner. While many ischemia reperfusion studies provide direct, uninhibited, access to the heart through open-heart surgery, some alternative methods of mitochondrial delivery are available. Coronary artery cannulation, which provide widespread distribution of mitochondria rather than accumulation at an injection site, is one such method. Unfortunately, coronary artery cannulation provides a wide distribution of mitochondria, and may not provide enough localized assistance to the left ventricle (20). Therefore, it may be of benefit to identify a region of interest, such as the area of greatest dysfunction. These challenges must be met in order to adapt mitochondrial transplantation as a therapeutic approach in the diabetic heart.

Though previous studies suggest that mitochondria are incorporated into host cells, available data are limited. One such report by Masuzawa et al. demonstrated localization and uptake of transplanted mitochondria in the rabbit heart using immunohistochemistry and microscopy methodologies (21). While it appears that mitochondria may be incorporated into the myocardium following transplantation, we believed it was necessary to further assess the behavior of mitochondria following transplantation and the extent of their uptake and localization. We began with *in vitro* assessments of mitochondrial transplantation, which suggest that transplanted mitochondria may bind to the membrane surface of HL-1 cardiomyocytes, and interact with the host cell mitochondrial network, but are not incorporated into the cell by 48 hours. Interestingly, at 24 hours mitochondria appear connected to the cell membrane, but do not definitively interact with the host cell mitochondrial population. At 48 hours, mitochondria can be identified interacting with host cell mitochondria, but they do not appear to penetrate the cellular membrane and become fully localized. Indeed, microscopy imaging and IMARIS 3D reconstruction of the cardiomyocytes following transplantation suggest that transplanted mitochondria may interact with cardiomyocyte mitochondrial populations without complete incorporation into the cell. These conclusions oppose previous literature suggesting mitochondrial internalization *in vitro*, as it is seemingly unclear if mitochondria are within the cell, or simply attached to the surface (21). Importantly, these mitochondrial interactions have been suggested to occur through an actin-dependent or micropinocytosis related mechanisms that were not explored in this study (38-40).

In vivo transplantation of mitochondria using ultrasound-guided echocardiography appears effective for delivery of mitochondria to the left ventricle myocardium, and produced minimal side effects, suggesting it is feasible to use mitochondrial transplantation to deliver healthy mitochondria to the left ventricle myocardium using this method. Intracardiac injection in adult recipients (at least 8 weeks of age) did not lead to immediate cardiac arrhythmias or desynchrony, with a low risk of mortality. Mouse behavior remained normal and no immediate side

effects were observed. It is recommended that mice be at least 25 g in weight prior to injection, as mice under body weight may have hearts that are too small to safely receive injections. Heart size must be comparable to that of an adult mouse to receive mitochondrial transplantation in the volume described without significantly increasing risk of death. To inject leaner or younger mice, the volume of both respiration buffer and mitochondria would need to be adjusted to body weight in order to reduce risk of death. Further, adaptation for models involving changes to the heart size, weight, or structure may alter the injection protocol. Determining the precise volume and mitochondrial number necessary for each recipient would ameliorate increased risk of mortality. Specifically, the volume of respiration buffer and mitochondrial content may need to be adjusted to account for body weight and age in animal models. While these specific limitations may not apply to human patients, more research is necessary to determine these adjustments are necessary. Further, studies to determine the "effective amount" of mitochondria, or the number of mitochondria necessary to observe a beneficial effect, is unknown and would require further elucidation and customization. It should be noted that a limitation to this study is mitochondrial distribution within the myocardium, where mitochondria were located primarily in and around the sites of injection.

Subsequently, transplanted mitochondria were identified in the left ventricle myocardium 24 hours following injection, consistent with previously published literature (21). It should be noted that the accepted mitochondrial half-life is about 14 days (41, 42), and previous studies have demonstrated that transplanted mitochondria maintain viability and function for at least 28 days, therefore the sharing of information with recipient mitochondrial networks may provide an explanation for how transplanted mitochondria are acquiring both MitoTracker orange and COX IV signals following cellular interactions (23, 43). Overall, numerous studies demonstrate the ability of mitochondria to influence the host mitochondrial network and increase bioenergetic function through donation of healthy mitochondrial DNA, increased ATP production, and increased respiratory capacity (21, 23, 38, 40). Confocal microscopy images suggest that transplanted

mitochondria may not only integrate into recipient mitochondrial networks, but may be integrated is such a way that they are positioned precisely within both subsarcolemmal and interfibullar mitochondrial networks, rather than non-discriminately. These data coincide with a report by Cowan et al, in which they utilized microscopy to identify exogenous mitochondria within the myocardium following coronary artery cannulation, and suggested that transplanted mitochondria incorporate themselves within cardiac myocytes (20). To further elucidate the localization of transplanted mitochondria within the myocardium requires deeper exploration and perhaps more advanced methods of mitochondrial tracking and imaging. The microscopy techniques utilized in this paper allowed for mitochondrial tracking through fluorescent signals to identify overlap between host and donor mitochondria, but in turn reduced visual clarity. It should be noted that mitochondrial localization and integration require further elucidation, as overlap with mitochondrial host signal indicates overlap of signal, but does not confirm interactions. Further, while imaging suggests that mitochondria positioning align with mitochondrial networks, further studies segregating mitochondrial populations following injection may be beneficial in confirming the presence of donor mitochondria and these findings. In summary, this report suggests that mitochondrial transplantation can be performed using ultrasound-guided echocardiography efficiently enough to deposit mitochondrial within the LV wall, which can be identified, quantified, and visualized, suggesting that mitochondrial transplantation may be able to be utilized as a prophylactic measure in diabetes mellitus. To be beneficial for diabetes mellitus patients, mitochondrial transplantation must be applied in a minimally invasive prophylactic manner, with the intent of preventing future cardiac events and reducing overall risk of mortality.

References

1.   Organization WH. Diabetes World Health Organization website: World Health Organization; 2020. Available from: https://www.who.int/news-room/fact-sheets/detail/diabetes.

2.   Association AH. Cardiovascular Disease and Diabetes 2019. Available from: https://www.heart.org/en/health-topics/diabetes/why-diabetes-matters/cardiovascular-disease--diabetes.

3.   de Ferranti SD, de Boer IH, Fonseca V, Fox CS, Golden SH, Lavie CJ, et al. Type 1 Diabetes Mellitus and Cardiovascular Disease: A Scientific Statement from the American Heart Association and American Diabetes Association. Circulation. 2014;130(13):1110-1130. doi:10.1161/CIR.0000000000000034

4.   Shankar A, Klein R, Klein BE, Moss SE. Association between Glycosylated Hemoglobin Level and Cardiovascular and All-Cause Mortality in Type 1 Diabetes. Am J Epidemiol. 2007;166(4):393-402. doi:10.1093/aje/kwm096

5.   Soedamah-Muthu SS, Fuller JH, Mulnier HE, Raleigh VS, Lawrenson RA, Colhoun HM. High Risk of Cardiovascular Disease in Patients with Type 1 Diabetes in the U.K.: A Cohort Study Using the General Practice Research Database. Diabetes Care. 2006;29(4):798-804. doi:10.2337/diacare.29.04.06.dc05-1433

6.   Athithan L, Gulsin GS, McCann GP, Levelt E. Diabetic Cardiomyopathy: Pathophysiology, Theories and Evidence to Date. World J Diabetes. 2019;10(10):490-510. doi:10.4239/wjd.v10.i10.490

7.   Makrecka-Kuka M, Liepinsh E, Murray AJ, Lemieux H, Dambrova M, Tepp K, et al. Altered Mitochondrial Metabolism in the Insulin-Resistant Heart. Acta Physiol (Oxf). 2020;228(3):e13430. doi:10.1111/apha.13430

8.   El Hadi H, Vettor R, Rossato M. Cardiomyocyte Mitochondrial Dysfunction in Diabetes and Its Contribution in Cardiac Arrhythmogenesis. Mitochondrion. 2019;46:6-14. doi:10.1016/j.mito.2019.03.005

9.   Galloway CA, Yoon Y. Mitochondrial Morphology in Metabolic Diseases. Antioxidants & redox signaling. 2013;19(4):415-430. doi:10.1089/ars.2012.4779

10.   Jagannathan R, Thapa D, Nichols CE, Shepherd DL, Stricker JC, Croston TL, et al. Translational Regulation of the Mitochondrial Genome Following Redistribution of Mitochondrial Microrna in the Diabetic Heart. Circ Cardiovasc Genet. 2015;8(6):785-802. doi:10.1161/CIRCGENETICS.115.001067

11.   Rindler PM, Crewe CL, Fernandes J, Kinter M, Szweda LI. Redox Regulation of Insulin Sensitivity Due to Enhanced Fatty Acid Utilization in the Mitochondria. Am J Physiol Heart Circ Physiol. 2013;305(5):H634-643. doi:10.1152/ajpheart.00799.2012

12.   Formentini L, Ryan AJ, Galvez-Santisteban M, Carter L, Taub P, Lapek JD, Jr., et al. Mitochondrial H(+)-Atp Synthase in Human Skeletal Muscle: Contribution to Dyslipidaemia and Insulin Resistance. Diabetologia. 2017;60(10):2052-2065. doi:10.1007/s00125-017-4379-z

13.   Fealy CE, Mulya A, Axelrod CL, Kirwan JP. Mitochondrial Dynamics in Skeletal Muscle Insulin Resistance and Type 2 Diabetes. Transl Res. 2018;202:69-82. doi:10.1016/j.trsl.2018.07.011

14.   Lee TW, Bai KJ, Lee TI, Chao TF, Kao YH, Chen YJ. Ppars Modulate Cardiac Metabolism and Mitochondrial Function in Diabetes. J Biomed Sci. 2017;24(1):5. doi:10.1186/s12929-016-0309-5

15.   Turkmen K, Karagoz A, Kucuk A. Sirtuins as Novel Players in the Pathogenesis of Diabetes Mellitus. World J Diabetes. 2014;5(6):894-900. doi:10.4239/wjd.v5.i6.894

16.   Lagouge M, Argmann C, Gerhart-Hines Z, Meziane H, Lerin C, Daussin F, et al. Resveratrol Improves Mitochondrial Function and Protects against Metabolic Disease by Activating Sirt1 and Pgc-1alpha. Cell. 2006;127(6):1109-1122. doi:10.1016/j.cell.2006.11.013

17.   He Q, Harris N, Ren J, Han X. Mitochondria-Targeted Antioxidant Prevents Cardiac Dysfunction Induced by Tafazzin Gene Knockdown in Cardiac Myocytes. Oxid Med Cell Longev. 2014;2014:654198. doi:10.1155/2014/654198

18.   He J, Ford HC, Carroll J, Douglas C, Gonzales E, Ding S, et al. Assembly of the Membrane Domain of Atp Synthase in Human Mitochondria. Proc Natl Acad Sci U S A. 2018;115(12):2988-2993. doi:10.1073/pnas.1722086115

19.   Emani SM, Piekarski BL, Harrild D, Del Nido PJ, McCully JD. Autologous Mitochondrial Transplantation for Dysfunction after Ischemia-Reperfusion Injury. J Thorac Cardiovasc Surg. 2017;154(1):286-289. doi:10.1016/j.jtcvs.2017.02.018

20.   Cowan DB, Yao R, Akurathi V, Snay ER, Thedsanamoorthy JK, Zurakowski D, et al. Intracoronary Delivery of Mitochondria to the Ischemic Heart for Cardioprotection. PLoS One. 2016;11(8):e0160889. doi:10.1371/journal.pone.0160889

21.   Masuzawa A, Black KM, Pacak CA, Ericsson M, Barnett RJ, Drumm C, et al. Transplantation of Autologously Derived Mitochondria Protects the Heart from Ischemia-Reperfusion Injury. Am J Physiol Heart Circ Physiol. 2013;304(7):H966-982. doi:10.1152/ajpheart.00883.2012

22.   Emani SM, McCully JD. Mitochondrial Transplantation: Applications for Pediatric Patients with Congenital Heart Disease. Transl Pediatr. 2018;7(2):169-175. doi:10.21037/tp.2018.02.02

23.   Cowan DB, Yao R, Thedsanamoorthy JK, Zurakowski D, Del Nido PJ, McCully JD. Transit and Integration of Extracellular Mitochondria in Human Heart Cells. Sci Rep. 2017;7(1):17450. doi:10.1038/s41598-017-17813-0

24.   McCully JD, Levitsky S, Del Nido PJ, Cowan DB. Mitochondrial Transplantation for Therapeutic Use. Clin Transl Med. 2016;5(1):16. doi:10.1186/s40169-016-0095-4

25.   Barrasso AP, Tong X, Poche RA. The Mito::Mkate2 Mouse: A Far-Red Fluorescent Reporter Mouse Line for Tracking Mitochondrial Dynamics in Vivo. Genesis. 2018;56(2). doi:10.1002/dvg.23087

26.   Chua S, Jr., Liu SM, Li Q, Yang L, Thassanapaff VT, Fisher P. Differential Beta Cell Responses to Hyperglycaemia and Insulin Resistance in Two Novel Congenic Strains of Diabetes (Fvb- Lepr (Db)) and Obese (Dba- Lep (Ob)) Mice. Diabetologia. 2002;45(7):976-990. doi:10.1007/s00125-002-0880-z

27.   Wang Z, Jiang T, Li J, Proctor G, McManaman JL, Lucia S, et al. Regulation of Renal Lipid Metabolism, Lipid Accumulation, and Glomerulosclerosis in Fvbdb/Db Mice with Type 2 Diabetes. Diabetes. 2005;54(8):2328-2335. doi:10.2337/diabetes.54.8.2328

28.   Mariko Omatsu-Kanbe NN, Yuka Nishino, Ken-ichi Mukaisho, Hiroyuki Sugihara, Hiroshi Matsuura Identification of Cardiac Progenitors That Survive in the Ischemic Human Heart after Ventricular Myocyte Death. Nature. 2017;10.1038/srep41318. doi:10.1038/srep41318

29.   Tirziu D, Giordano FJ, Simons M. Cell Communications in the Heart. Circulation. 2010;122(9):928-937. doi:10.1161/CIRCULATIONAHA.108.847731

30.   Banerjee I, Fuseler JW, Price RL, Borg TK, Baudino TA. Determination of Cell Types and Numbers During Cardiac Development in the Neonatal and Adult Rat and Mouse. Am J Physiol Heart Circ Physiol. 2007;293(3):H1883-1891. doi:10.1152/ajpheart.00514.2007

31.   Laboratory TJ. Body Weight Information for C57bl/6j (000664) The Jackson Laboratory website: The Jackson Laboratory; Available from:

https://www.jax.org/jax-mice-and-services/strain-data-sheet-pages/body-weight-chart-000664.

32.   Dabkowski ER, Baseler WA, Williamson CL, Powell M, Razunguzwa TT, Frisbee JC, et al. Mitochondrial Dysfunction in the Type 2 Diabetic Heart Is Associated with Alterations in Spatially Distinct Mitochondrial Proteomes. Am J Physiol Heart Circ Physiol. 2010;299(2):H529-540. doi:10.1152/ajpheart.00267.2010

33.   Kunovac A, Hathaway QA, Pinti MV, Goldsmith WT, Durr AJ, Fink GK, et al. Ros Promote Epigenetic Remodeling and Cardiac Dysfunction in Offspring Following Maternal Engineered Nanomaterial (Enm) Exposure. Part Fibre Toxicol. 2019;16(1):24. doi:10.1186/s12989-019-0310-8

34.   Hathaway QA, Durr AJ, Shepherd DL, Pinti MV, Brandebura AN, Nichols CE, et al. Mirna-378a as a Key Regulator of Cardiovascular Health Following Engineered Nanomaterial Inhalation Exposure. Nanotoxicology. 2019;13(5):19. doi:10.1080/17435390.2019.1570372

35.   Kunovac A, Hathaway QA, Pinti MV, Durr AJ, Taylor AD, Goldsmith WT, et al. Enhanced Antioxidant Capacity Prevents Epitranscriptomic and Cardiac Alterations in Adult Offspring Gestationally-Exposed to Enm. Nanotoxicology. 2021;15(6):812-831. doi:10.1080/17435390.2021.1921299

36.   Baseler WA, Thapa D, Jagannathan R, Dabkowski ER, Croston TL, Hollander JM. Mir-141 as a Regulator of the Mitochondrial Phosphate Carrier (Slc25a3) in the Type 1 Diabetic Heart. Am J Physiol Cell Physiol. 2012;303(12):C1244-1251. doi:10.1152/ajpcell.00137.2012

37.   Claycomb WC, Lanson NA, Jr., Stallworth BS, Egeland DB, Delcarpio JB, Bahinski A, et al. Hl-1 Cells: A Cardiac Muscle Cell Line That Contracts and Retains Phenotypic Characteristics of the Adult Cardiomyocyte. Proc Natl Acad Sci U S A. 1998;95(6):2979-2984. doi:10.1073/pnas.95.6.2979

38.   Pacak CA, Preble JM, Kondo H, Seibel P, Levitsky S, Del Nido PJ, et al. Actin-Dependent Mitochondrial Internalization in Cardiomyocytes: Evidence for Rescue of Mitochondrial Function. Biol Open. 2015;4(5):622-626. doi:10.1242/bio.201511478

39.   Kesner EE, Saada-Reich A, Lorberboum-Galski H. Characteristics of Mitochondrial Transformation into Human Cells. Sci Rep. 2016;6:26057. doi:10.1038/srep26057

40.   Kitani T, Kami D, Matoba S, Gojo S. Internalization of Isolated Functional Mitochondria: Involvement of Macropinocytosis. J Cell Mol Med. 2014;18(8):1694-1703. doi:10.1111/jcmm.12316

41.   R A Menzies PHG. The Turnover of Mitochondria in a Variety of Tissues of Young Adult and Aged Rats. J Biol Chem. 1971;246(8):6. doi,

42.   Gottlieb RA, Stotland A. Mitotimer: A Novel Protein for Monitoring Mitochondrial Turnover in the Heart. J Mol Med (Berl). 2015;93(3):271-278. doi:10.1007/s00109-014-1230-6

43.   Katrangi E, D'Souza G, Boddapati SV, Kulawiec M, Singh KK, Bigger B, et al. Xenogenic Transfer of Isolated Murine Mitochondria into Human Rho0 Cells Can Improve Respiratory Function. Rejuvenation Res. 2007;10(4):561-570. doi:10.1089/rej.2007.0575

TABLES AND TABLE LEGENDS

Table 3.1: Number of Mitochondria Isolated from an Adult Mouse Heart

Extrapolation Category	Calculated Numerical Value
Cardiomyocytes (%)	50
Other cell types (%)	50
Est. Number of cardiomyocytes	2,700,000
Est. Number of other cell types	2,700,000
Total number of Cells	5,400,000
Mito per cardiomyocyte	5000
Mito per all other cell types	1500
Number of mitochondria from myocytes	13,500,000,000
Number of mitochondria from other	4,000,000,000
Est. heart weight – C57BL/6J female	0.113 g
Est. heart weight - C57BL/6J male	0.15 g
Total mitochondria isolated from heart	13,000,000,000

Table 3.1: Number of Mitochondria Isolated from an Adult Mouse Heart. The number of myocytes isolated from a single adult mouse heart was estimated by extrapolating the number of mitochondria in a human heart.

FIGURES AND FIGURE LEGENDS

Figure 3.1: Accumulation of mKate2 positive mitochondria with HL-1 cardiomyocytes.
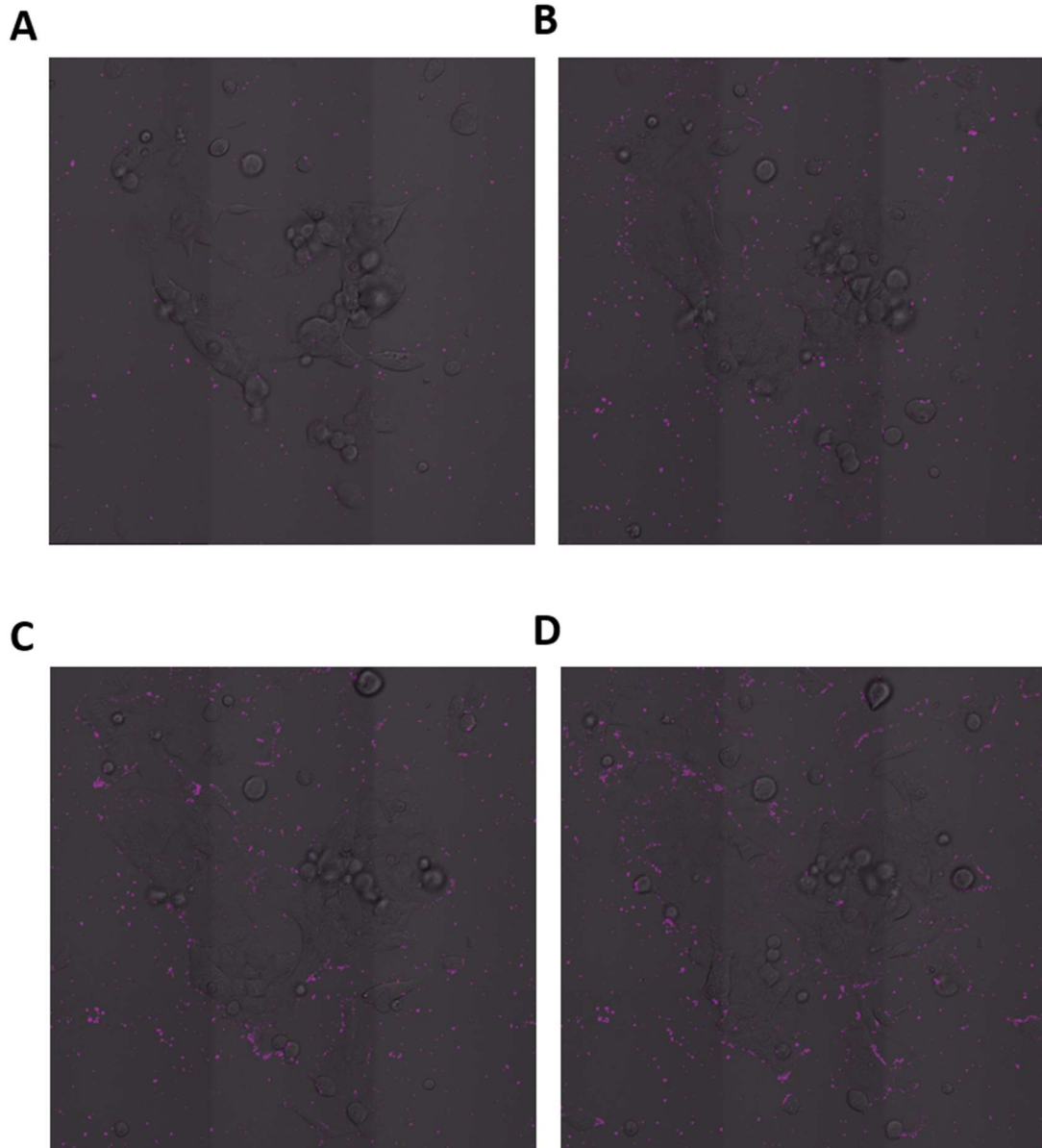
Figure 3.1

E
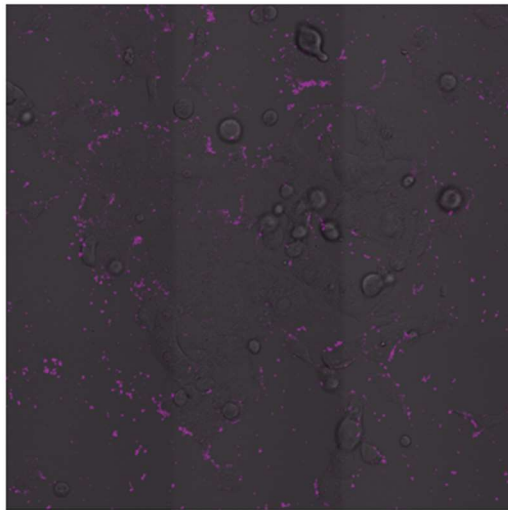
F
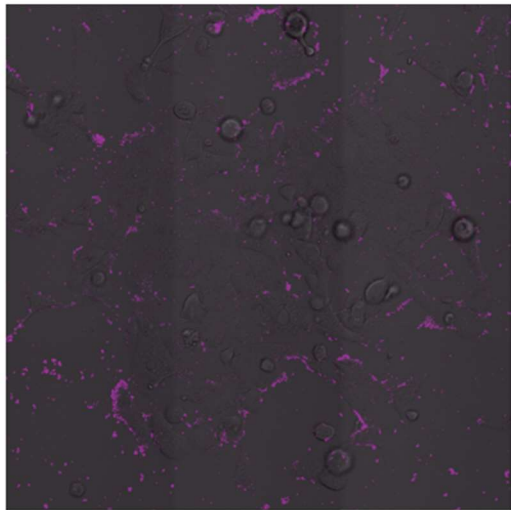
G
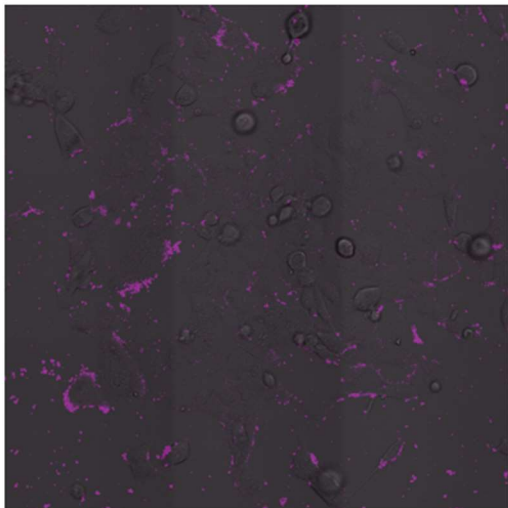
H
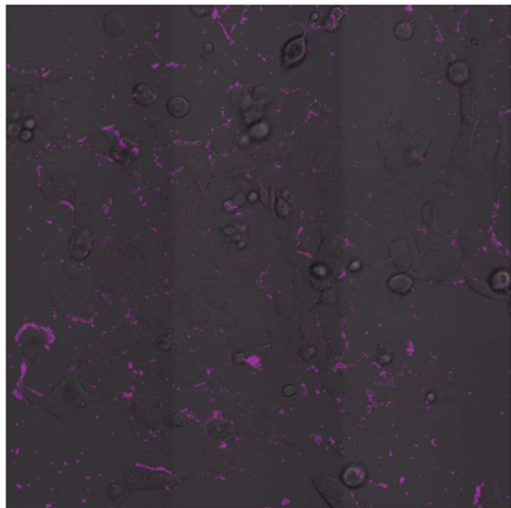
Figure 3.1

I
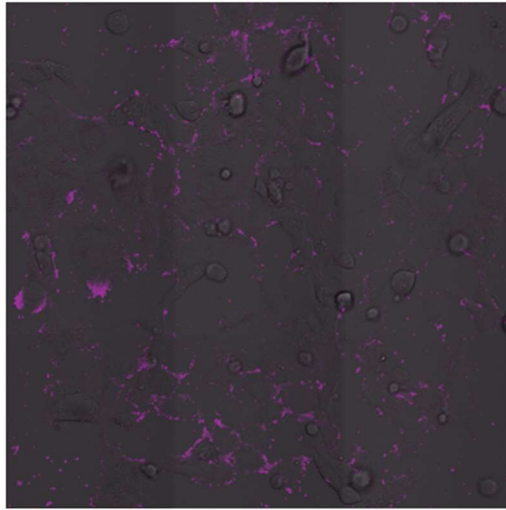
J
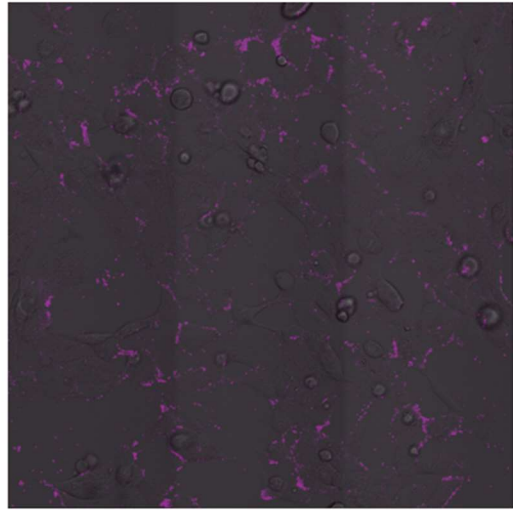
Figure 3.1: Accumulation of mKate2 positive mitochondria with HL-1 cardiomyocytes. Figure demonstrates representative co-localization of mKate2 signal with cellular membranes. (A) 0 hours, (B) 2 hours, (C) 4 hours, (D) 6 hours, (E) 8 hours, (F) 10 hours, (G) 12 hours, (H) 16 hours, (I) 20 hours, and (J) 24 hours. Purple signal indicates mKate2 positive mitochondria.

Figure 3.2: Accumulation of mKate2 positive mitochondria on cell membrane surface at 24 hours.

Figure 3.2
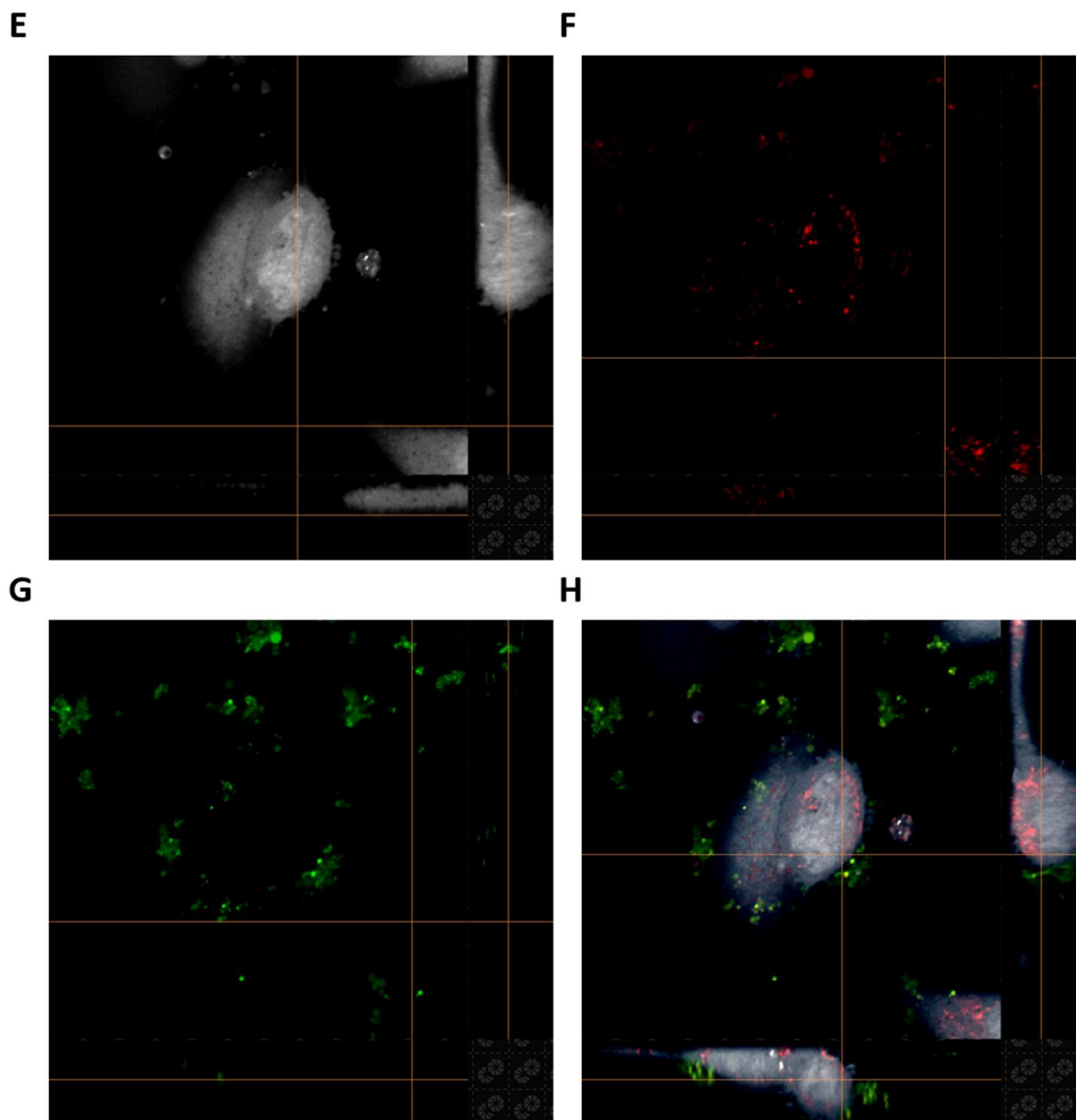
E

F

G

H

Figure 3.2: Accumulation of mKate2 positive mitochondria on cell membrane surface at 24 hours. Following transplantation, HL-1 cardiomyocytes transplanted with mKate2 mitochondria were stained for (A) alpha actin (white; *upper left*), (B) host mitochondria were stained for COX IV (red; *upper left middle*), (C) and mKate2 mitochondria (purple; *upper right middle*) were acquired. (D) Images were merged for a representative overlay of signal (*upper right*). Z-stack imaging of HL-1 cardiomyocytes stained for (E) alpha actin (white; *lower left*), show distinct separation between (F) host mitochondria stained for COX IV (red; *lower left middle*), and (G) mKate2 mitochondria (purple; *lower right middle*) were acquired distribution in and on the cell. (H) Images were merged for a representative overlay of signal (*lower right*).

Figure 3.3: Accumulation of mKate2 positive mitochondria on cell membrane surface at 48 hours.
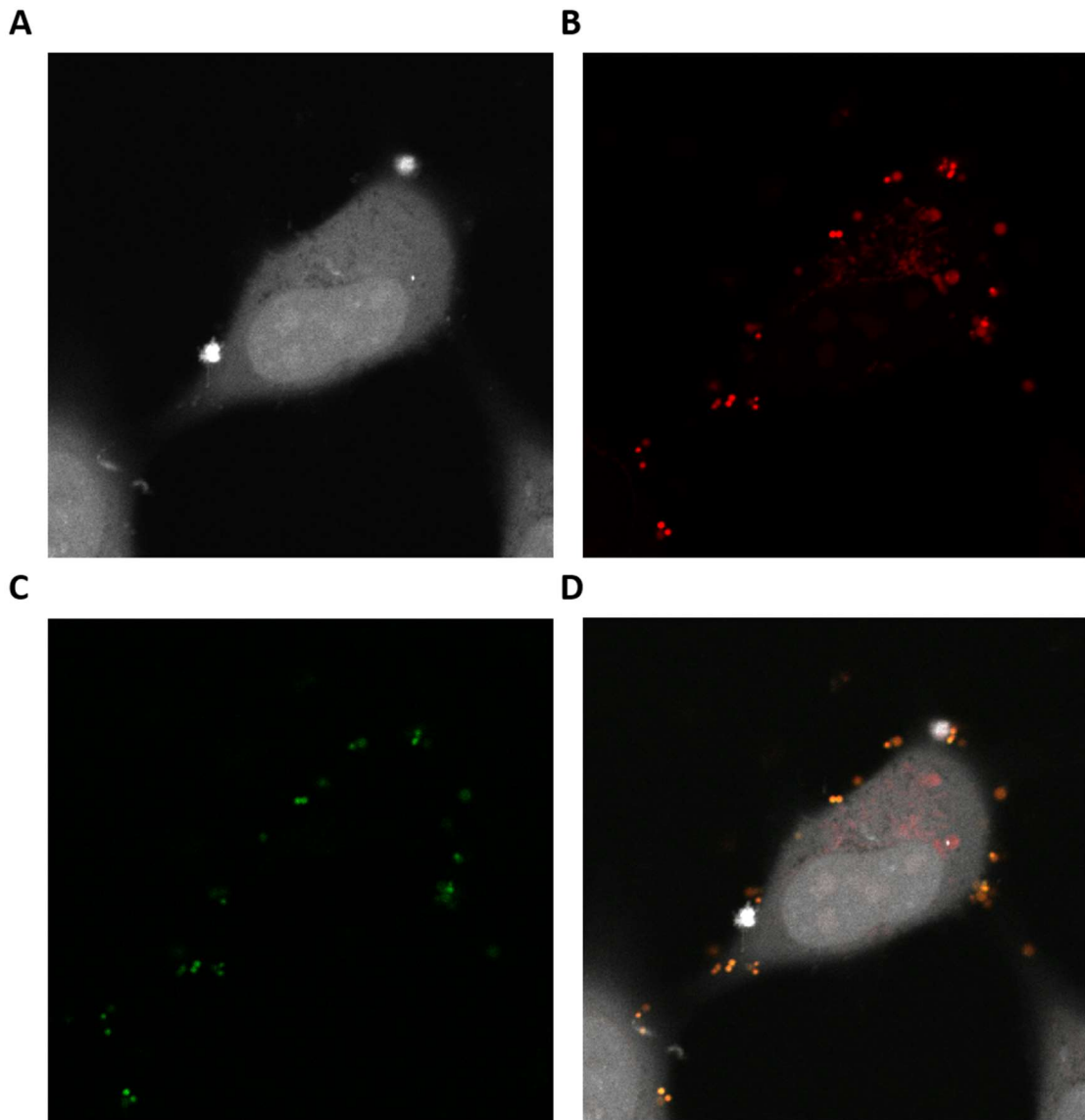
Figure 3.3

E
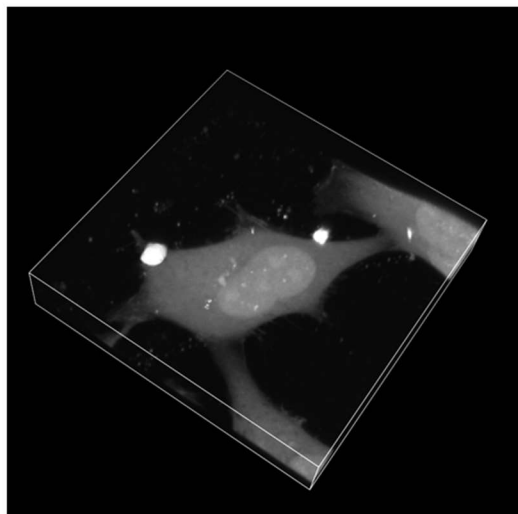
F
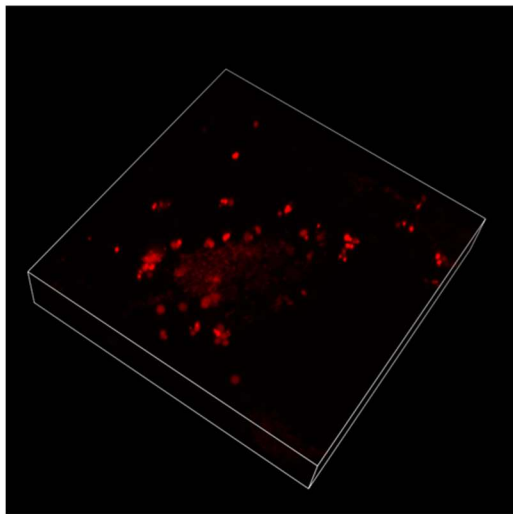
G
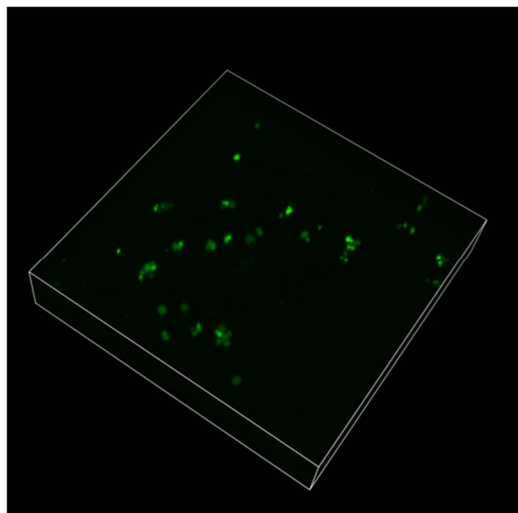
H
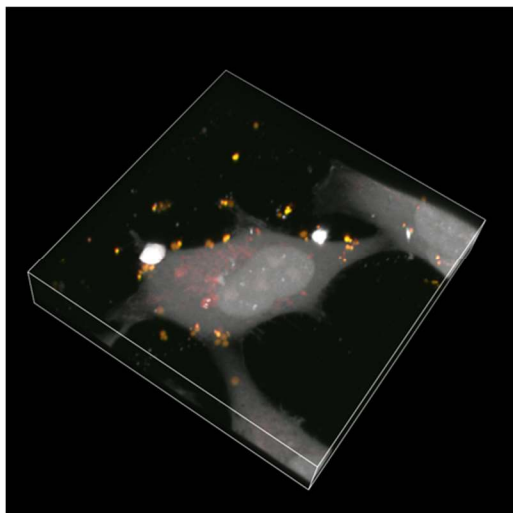
Figure 3.3: Accumulation of mKate2 positive mitochondria on cell membrane surface at 48 hours. Following transplantation, HL-1 cardiomyocytes transplanted with mKate2 mitochondria were stained for (A) alpha actin (white; *upper left*), (B) host mitochondria were stained for COX IV (red; *upper left middle*), (C) and mKate2 mitochondria (purple; *upper right middle*) were acquired. (D) Images were merged for a representative overlay of signal (*upper right*). Z-stack imaging of HL-1 cardiomyocytes stained for (E) alpha actin (white; *lower left*), show distinct separation between (F) host mitochondria stained for COX IV (red; *lower left middle*), and (G) mKate2 mitochondria (purple; *lower right middle*) were acquired distribution in and on the cell. (H) Exogenous mitochondria overlayed with host mitochondrial signal appear yellow/orange (*lower right*).

Figure 3.4: Visual representation of host and mKate2 mitochondrial integration in HL-1 cardiomyocytes.
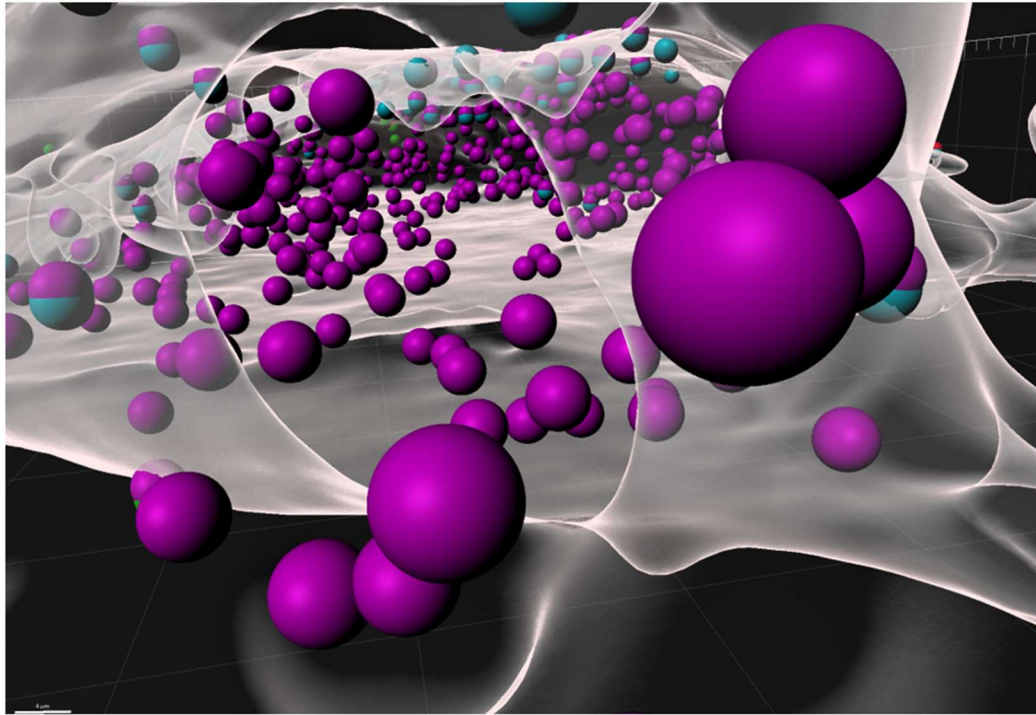
Figure 3.4

B
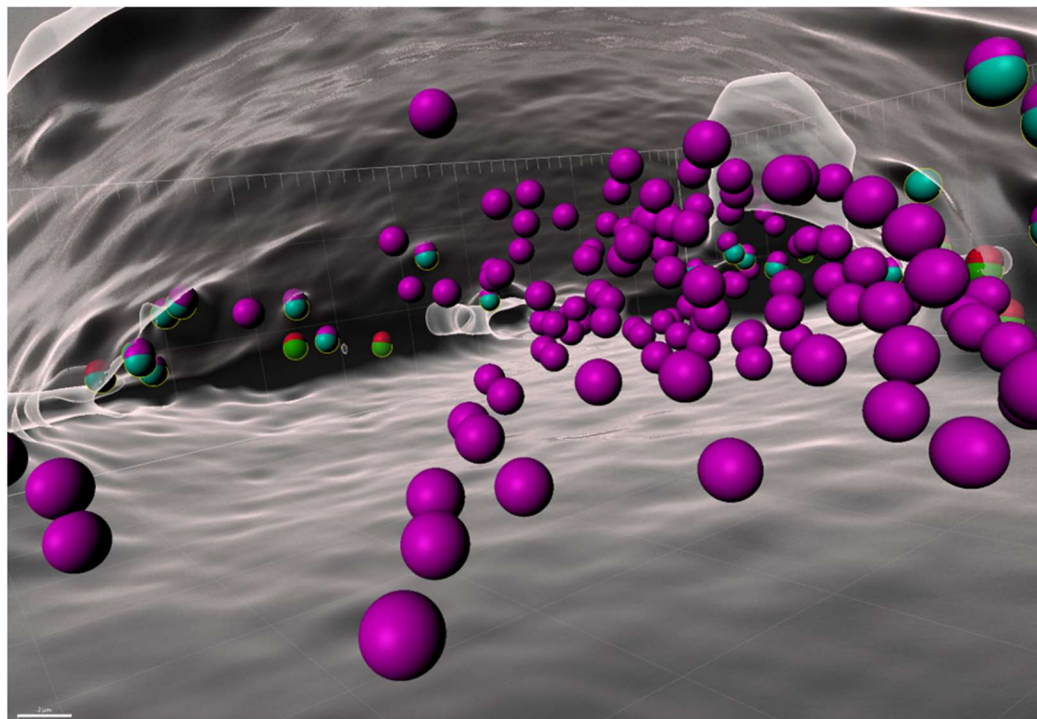
Figure 3.4: Visual representation of host and mKate2 mitochondrial integration in HL-1 cardiomyocytes. (A) 24 hours, and (B) 48 hours. Red; host mitochondria outside, Green; mKate2 mitochondria outside, Purple; host mitochondria inside the cell surface, Blue; mKate2 mitochondria inside the cell surface

Figure 3.5: Experimental outline and mitochondrial detection.
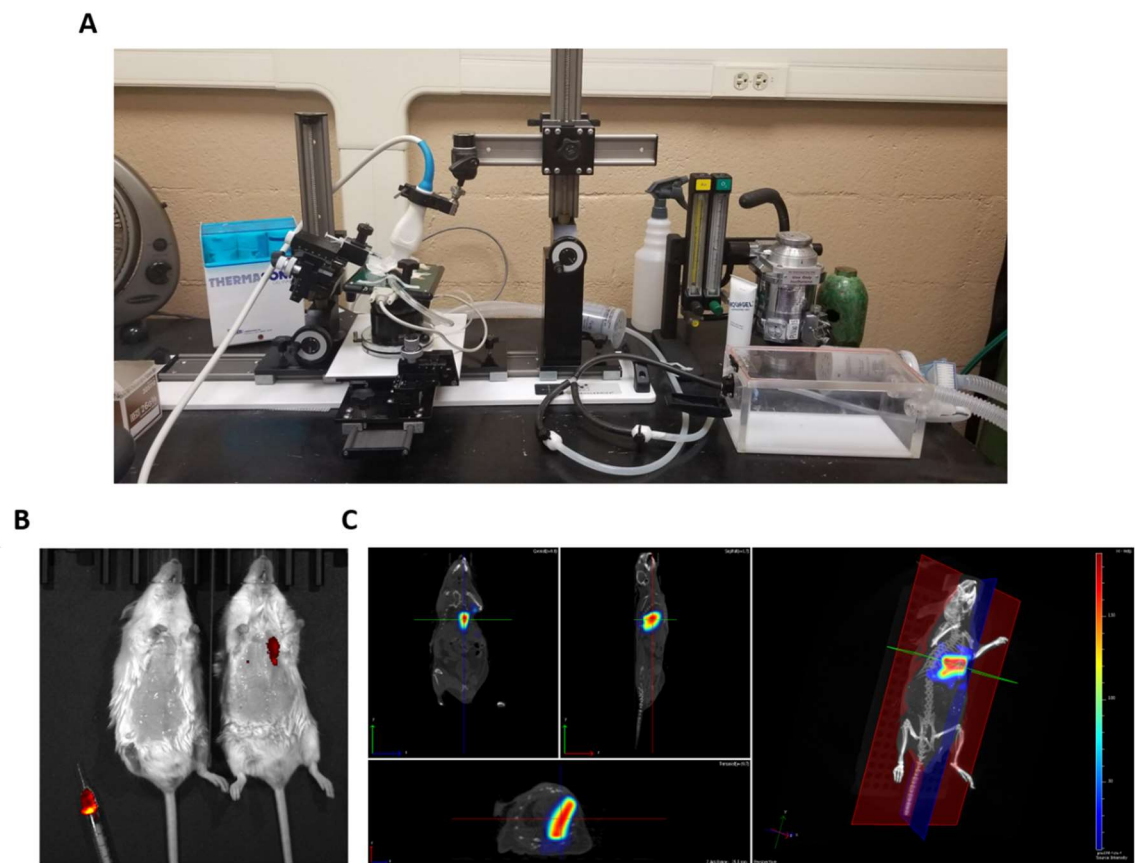
Figure 3.5: Experimental outline and mitochondrial detection. (A) A representative image of equipment setup and orientation is provided for reference. (B-C) Verification of mitochondrial presence using IVIS SpectumCT imaging shows detection of fluorescent signal in both 2D and 3D imaging planes immediately following injection.

Figure 3.6: Distribution of mKate2 positive mitochondria following transplantation *in vitro*.
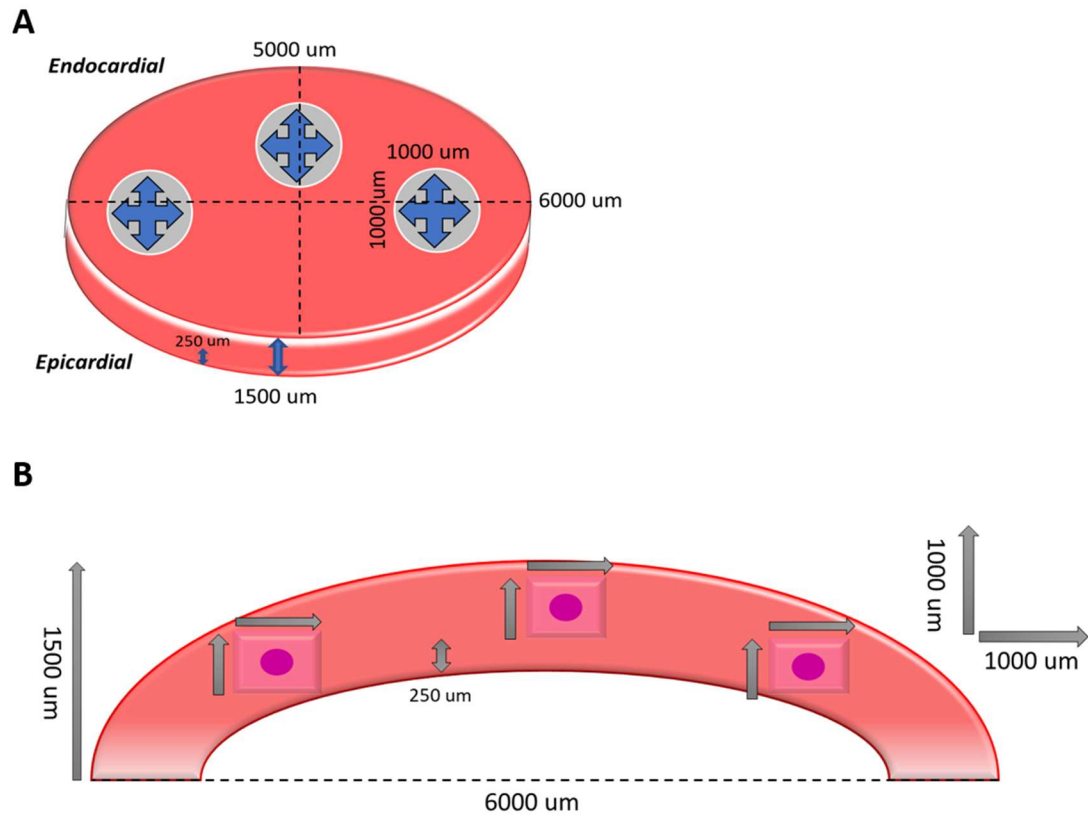
Figure 3.6
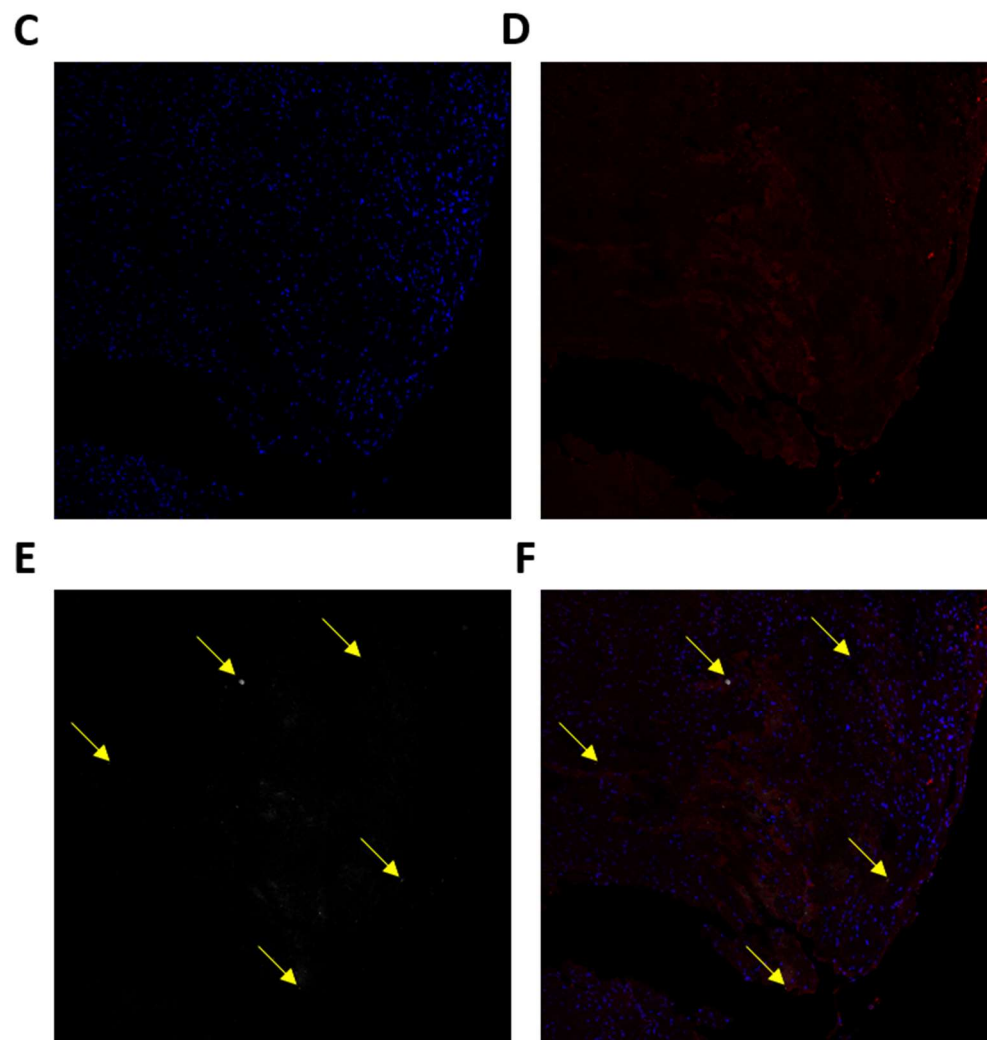
Figure 3.6
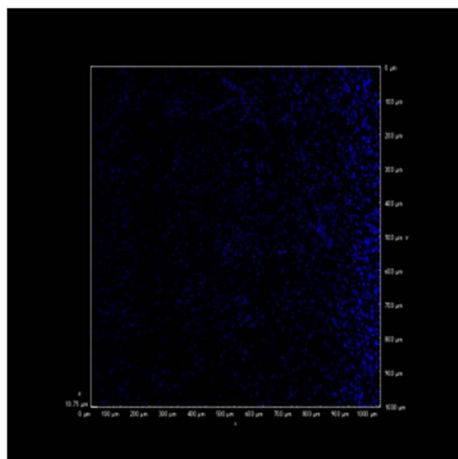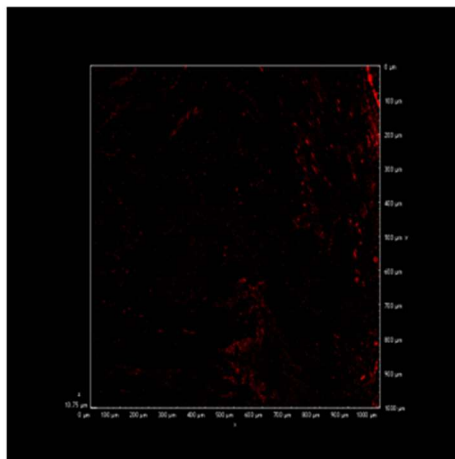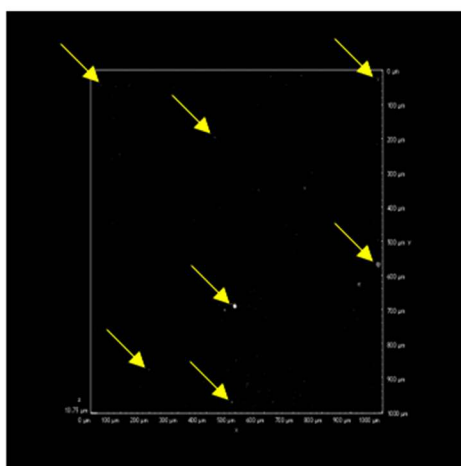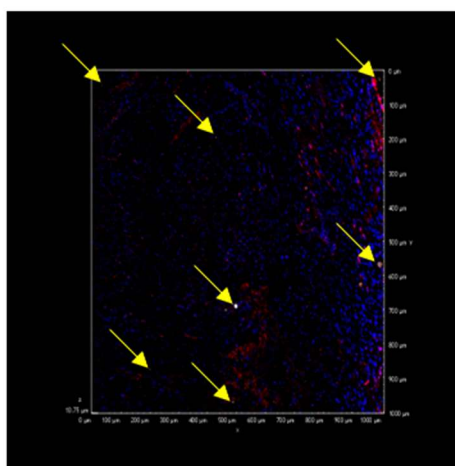
Figure 3.6: Distribution of mKate2 positive mitochondria following transplantation *in vitro*. Representative images of (A) ellipsoid model and (B) left ventricle mitochondrial distribution calculations. Images of mouse left ventricular tissue stained for (C) nuclei are stained for DAPI (blue; *upper left*), (D) host mitochondria stained for COX IV (red; *upper left middle*), (E) and mKate mitochondria (white; *upper right middle*) were acquired. (F) Images were merged for a representative overlay of signal (*upper right*). Z-stack images show mitochondrial distribution within a 1000 x 1000 μm square (G) nuclei are stained with DAPI (blue; *lower left*), (H) host mitochondria are stained for COX IV (red; *lower left middle*), and (I) mKate mitochondria (white; *lower right middle*) were acquired distribution in and on the cell. (J) Signal overlay show distribution of mKate mitochondria in a 1000 x 1000 μm volume (*lower right*). Transplanted mKate2 positive mitochondria are indicated by yellow arrows.

Figure 3.7: Localization of mKate2 positive mitochondria following transplantation.
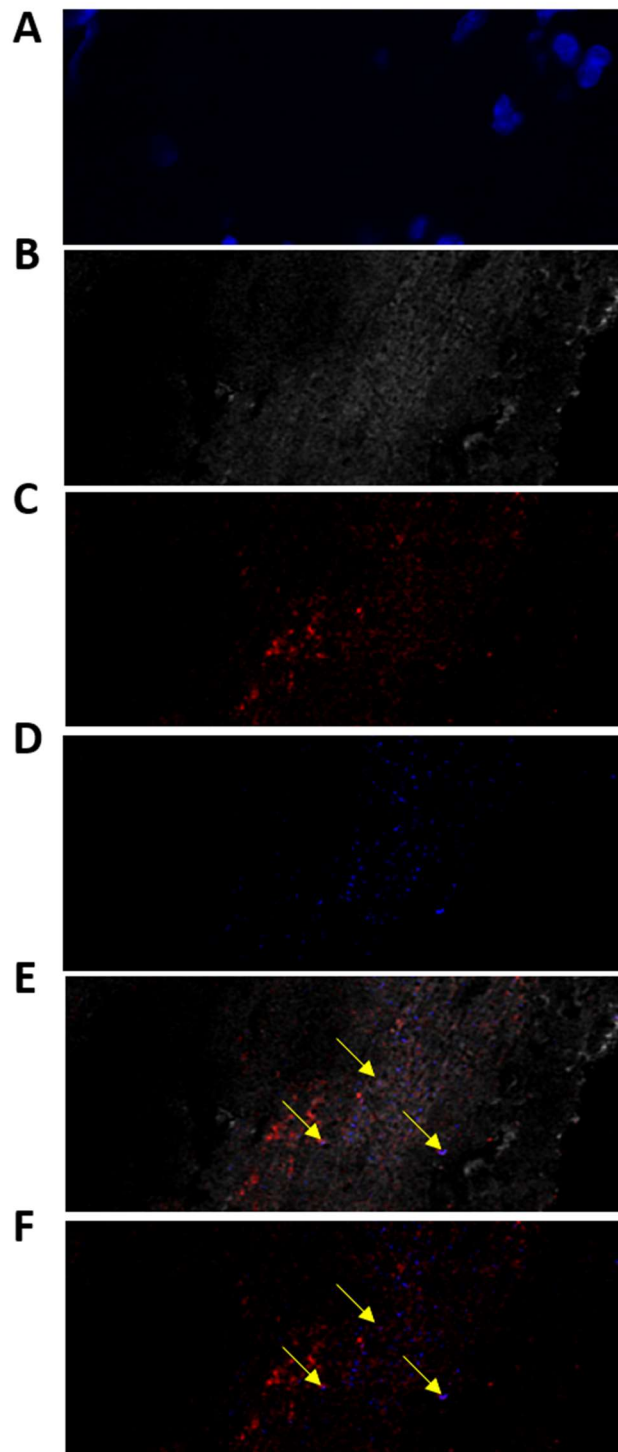
Figure 3.7: Localization of mKate2 positive mitochondria following transplantation. Images of mouse left ventricular tissue including, (A) nuclei stained for DAPI (blue), (B) alpha-actinin-2 (white), (C) host mitochondria stained for COX IV (red), and (D) mKate mitochondria (blue) were acquired. (E) Merged signal, without DAPI, for a representative overlay of signal to show mitochondrial localization in cardiac tissue with alpha-actinin-2 and COX IV. (F) Merged mitochondria signals to show co-localization of mKate2 mitochondria with COX IV signal. Purple signals indicating shared COX IV and mKate2 fluorescent signal are indicated by yellow arrows.

CHAPTER 4: SPECIFIC AIM IIb

Machine Learning for Spatial Stratification of Progressive Cardiovascular Dysfunction in a Murine Model of Type 2 Diabetes Mellitus

Andrya J. Durr, BS[1,2], Anna S. Korol, BS[3], Quincy A. Hathaway, PhD[1,2,4], Amina Kunovac, PhD[1,2,4], Andrew D. Taylor, BS[1,2], Saira Rizwan, MS[1,2], Mark V. Pinti, BS[2,5,6], and John M. Hollander, PhD[1,2]

[1]Division of Exercise Physiology, West Virginia University School of Medicine, PO Box 9227, 1 Medical Center Drive, Morgantown, WV, 26505, USA. [2]Mitochondria, Metabolism & Bioenergetics Working Group, West Virginia University School of Medicine, Morgantown, WV, 26505, USA. [3]Rockefeller Neuroscience Institute, Department of Neuroscience, West Virginia University School of Medicine, 33 Medical Center Drive, Morgantown, WV, 26505, USA. [4]Center for Inhalation Toxicology (iTOX), West Virginia University School of Medicine, Morgantown, WV, 26505, USA. [5]West Virginia University School of Pharmacy, Morgantown, WV, USA. [6]West Virginia University School of Pharmacy, Morgantown, WV, 26505, USA.

Corresponding Author:

John M. Hollander, PhD, FAHA

Professor and Graduate Director, Exercise Physiology

Sr. Asst. Dean for Research and Graduate Education, Human Performance

Director, Mitochondria, Metabolism & Bioenergetics

West Virginia University School of Medicine

1 Medical Center Drive

P.O. Box 9227

Morgantown, WV 26506

Ph: (304) 293-3683

Fax: (304) 293-7105

Email: jhollander@hsc.wvu.edu

Abstract

Speckle tracking echocardiography (STE) has been utilized to evaluate spatial and progressive alterations in the diabetic heart independently, but the spatial and temporal manifestation of cardiac dysfunction remains elusive. The objectives of this study were to elucidate if cardiac dysfunction associated with type 2 diabetes mellitus (T2DM) occurs spatially, and if patterns of regional or segmental dysfunction manifest in a temporal fashion. Non-invasive echocardiography (i.e., conventional M-mode and pulse-wave Doppler) and STE datasets were utilized to segregate mice into two pre-determined groups, wild-type and *Db/Db*, at 5, 12, 20, and 25 weeks. Support vector machine and ReliefF algorithms were used to identify and rank cardiac regions, segments, and features by their ability to identify cardiac dysfunction. STE features more accurately segregated animals as diabetic or non-diabetic when compared with conventional echocardiography, and the ReliefF algorithm efficiently ranked STE features by their ability to identify cardiac dysfunction. The Septal region, and the AntSeptum segment, best identified cardiac dysfunction at 5, 20, and 25 weeks, with the AntSeptum also containing the greatest number of features which differed between diabetic and non-diabetic mice. Cardiac dysfunction manifests in a spatial and temporal fashion, and is defined by patterns of regional and segmental dysfunction in the diabetic heart. The Septal region, and AntSeptum segment, may provide a locale of interest for therapeutic interventions aimed at ameliorating cardiac dysfunction in T2DM. Machine learning may provide a more thorough approach to managing contractile data with the intention of identifying experimental, clinical, and therapeutic targets.

Introduction

Cardiovascular dysfunction is the leading cause of mortality in the diabetic population, with the risk of developing cardiovascular disease at 2-to-4 times greater than that of the general population (1-3). As many as 65% of people with diabetes mellitus will die from cardiovascular complications or stroke (1, 4). The identification and diagnosis of cardiac contractile dysfunction, whether sub-clinical or overt, is largely dependent on cardiac imaging modalities such as echocardiography, myocardial perfusion imaging, magnetic resonance imaging, and computed tomography (5). Conventional echocardiography, including M-mode and pulse wave Doppler (PWD), is the first-line choice for non-invasive diagnosis of cardiac contractile dysfunction, but relies on the detection of overt systolic dysfunction (5-7).

Speckle tracking echocardiography (STE) can detect sub-clinical changes in cardiac function (8, 9), and allows for the observation of cardiac motion as global, regional, or segmental patterns of deformation, making it a useful tool in the diagnosis of sub-clinical cardiac contractile dysfunction. Cardiac remodeling, defined as a change in size, shape, structure, and/or function, is a critical feature of cardiac contractile dysfunction in T2DM and often precedes contractile dysfunction (10-13). Moreover, left ventricular (LV) wall motion abnormalities, a common consequence of cardiac remodeling, have been linked to 2.4-to-3.4-fold higher risks of cardiovascular dysfunction related mortality (14-16). STE has the ability to detect these subtle shifts in cardiac function, and is currently utilized clinically in humans and murine models (8, 17-20).

Numerous studies have demonstrated the prognostic value of STE, even in patients with no history of cardiac contractile dysfunction. Global longitudinal strain is a widely accepted clinical marker of LV dysfunction, and has been shown to be correlated with diabetic duration in T2DM patients (17, 21, 22). Further, STE has been utilized to identify cardiac strain abnormalities and regional afflictions in

murine models that may have otherwise been elusive (9, 23, 24). Li et al. demonstrated significant reductions in radial and circumferential strains at 16 weeks in *Db/Db* mice, and suggested that strain metrics may be useful for the detection of early LV contractile dysfunction (23, 24). Subsequently, STE may be used to assess localized patterns of dysfunction within the diabetic heart.

Cardiac contractile dysfunction is currently treated via global or LV focused methods regardless of the stage of dysfunction, and the identification of differentially impacted locales in the T2DM heart may provide a modality for pinpointed clinical care. At current, spatial (i.e., regional and segmental) and progressive alterations have been evaluated in T2DM independently (9, 23-26). but we have yet to elucidate if cardiac contractile dysfunction manifests spatially, and if spatial changes in function correlate to the temporal progression of the T2DM pathophysiology. Therefore, the objectives of this study were to elucidate if cardiac contractile dysfunction associated with T2DM occurs spatially, and if patterns of regional or segmental dysfunction manifest in a temporal fashion. We further aimed to utilize machine learning to identity cardiac regions, segments, and features that best describe cardiac contractile dysfunction at each timepoint.

Materials and Methods

All datasets used for machine learning analyses and related code have been made publicly available at github.com and can be accessed at https://doi.org/10.5281/zenodo.6391011. We attest that one author had full access to all the data in the study and takes responsibility for its integrity and the data analysis.

Experimental Animals

Animal experiments used in this study conformed to the National Institutes of Health Guidelines for the Care and Use of Laboratory Animals and were

approved by the West Virginia University (WVU) Care and Use Committee. Experimental animals included male and female FVB/NJ wild-type (WT) mice (RRID:IMSR_JAX:001800) and FVB/NJ *Db/Db* mice (The Jackson Laboratory stock Cat. No. 006654) (27, 28). *Db/Db* mice develop severe hyperglycemia and obesity between 5 and 6 weeks of age (29). Mice were housed in the WVU Health Sciences Center animal facility on a 12-hour light/dark cycle in a temperature-controlled room. Animals were maintained on a standard chow diet and had access to both food and water *ad libitum*. Animals were euthanized at 25 weeks of age following, and no animals were excluded from the study. Initial evaluation of cardiac function in male and female animals presented no significant differences, therefore both sexes were utilized for machine learning analyses.

Echocardiography

Animals were imaged at 5, 12, 20, and 25 weeks of age. Twelve weeks was chosen to represent a central timepoint between 5 weeks, where initial onset of disease occurs, and 25 weeks, where the diabetic condition is at its most severe. Twenty weeks was chosen as a secondary endpoint due to the potential of animals perishing prior to 25 weeks of age due to the severity of untreated diabetes mellitus and the deterioration caused by the diabetic condition. Therefore, animals were imaged at both 20 and 25 weeks to ensure that all animals received an echo during the most severe stage of cardiovascular dysfunction. A single trained individual in the WVU Animal Models and Imaging Facility acquired ultrasound images in a blinded fashion in conscious mice to maintain normal left ventricle (LV) function and heart rate (30-33). Images were acquired using a 32–55 MHz linear array transducer on the Vevo2100 Imaging System (Visual Sonics, Toronto, Canada) as previously described (9, 34-36), and were acquired at the highest frame rate (233-401 frames/second) as determined by image resolution. M-mode images were acquired by placing a gate through the center of the short-axis B-mode images to obtain recordings of the internal features of the myocardium. Long-axis B-mode images and short-axis B-mode images were acquired for STE analysis.

M-mode Analysis and Pulse-wave Doppler

Conventional echocardiography analysis was completed on grayscale M-mode parasternal short-axis images acquired at the mid-papillary level of the LV as previously described (9, 34, 36). Data were analyzed by a single trained individual in a blinded fashion. M-mode measurements were calculated over at least three consecutive cardiac cycles and averaged values were considered a single replicate. This was repeated for as many M-mode videos as provided up to 6 replicates. PWD measurements were acquired by taking at least 3 replicates of consistent cardiac cycles, and calculated in the same manner described above to acquire the best representative measurements. The reliability of conventional measurements was assessed previously (9).

Speckle Tracking Strain-based Imaging Analysis

Velocity, displacement, strain, and strain rate were acquired for all dimensions using the Visual Sonics VevoStrain software (Toronto, Canada). B-mode videos were selected based on the quality of the image and the ability to visualize the endocardial and epicardial wall borders. The borders of the endocardial wall were traced and checked through three consecutive cycles to ensure sufficient tracking. Tracing lines were considered sufficient if they moved faultlessly with both the endocardial and epicardial walls during the three cardiac cycles, ensuring proper measurements. Both the endocardial and epicardial borders were tracked through the image in a frame-by-frame manner. Parameters were calculated in the radial, circumferential, and longitudinal dimensions using the parasternal short and long-axis B-mode videos as previously described (9, 23, 34, 36). Analysis was performed for both systolic and diastolic values. Velocity, displacement, and strain-based values were initially collected as either positive or negative depending on the direction of motion (i.e., shortening, lengthening, thickening, or thinning). Therefore, values were evaluated as absolute, with both

177

positive and negative values farther from zero indicating faster velocities, increased displacement, increased strain, and increased strain rate. Absolute values were normalized to LV mass.

Data Cleaning and Feature Generation

The experimental design and outline used for the data collection and the machine learning pipeline are provided in Figure 4.1. Echocardiography features including conventional echocardiography (i.e., M-mode and PWD), and STE were collected in WT (n = 14) and *Db/Db* (n = 13) mice (Figure 4.1A). Echocardiography features were documented for 5, 12, 20, and 25 weeks, which included 379 features per timepoint (Figure 4.1B). Segmental LV features included the following: anterior free segment (AntFree); lateral segment (LatWall); posterior segment (PostWall); inferior free segment (InfFreeWall); posterior septal segment (PostSeptal); and anterior septal segment (AntSeptum). Additional features including the Anterior, Posterior, Septal, Free, Anterior Free, and Posterior Free regions were generated from segmental STE values and included the following: Anterior (AntSeptum, AntFree, and LatWall), Posterior (PostSeptal, InfFreeWall, and PostWall), Septal (AntSeptum and PostSeptal), Free (AntFree, LatWall, PostWall, and InfFreeWall), Anterior Free (AntFree and LatWall), and Posterior Free (InfFreeWall and PostWall). The regional features described above were represented by the calculated average of the included segments.

Once all additional features were established, prior to input into MATLAB, the "Complete" datasets, including a total of 379 features per timepoint, were assessed for missing values and outliers. The "Complete" dataset is comprised of all cardiac features, including M-mode, PWD, and STE values. Missing values occurred when specific features were unattainable for a single animal. Outliers were determined as specified in the "*Statistical Analysis*" section of the methods. The number of outliers or missing values within a given feature at a given timepoint typically included two or less values, with rare instances of 3 or more per class

178

(i.e., WT or *Db/Db*). Prior to input for machine learning, outliers and missing values were replaced with the mean value of the feature to negate the loss of animals, maintain model accuracy, and determine features. Missing values and outliers were excluded from statistical analysis using GraphPad Prism version 8.02 (GraphPad Prism, RRID:SCR_002798). Each "Complete" dataset was further partitioned into 16 subsets of data containing distinct feature groups: PWD (12 features), M-mode (17 features), Global (36 features), Segmental (195 features), Anterior Free (67 features), Posterior Free (67 features), Anterior (99 features), Posterior (99 features), Septal (67 features), Free (features), AntFree (35 features), LatWall (35 features), PostWall (35 features), InfFreeWall (35 features), PostSeptal (35 features), and AntSeptum (35 features) (Figure 4.1B). Initial evaluation of normality indicated that data were not consistently normally distributed. Therefore, to account for variability within datasets, non-parametric assessments were performed. Data were normalized using the MATLAB function '*normalize*' to rescale the range of the data to between 0 and 1 to mimic a Gaussian distribution for machine learning applications (37). Statistical analyses were performed on raw data values without supplemented means for missing data or outliers.

Feature Selection and Ranking

In order to estimate feature importance and relevance to binary classification (i.e. WT or *Db/Db*), six feature selection algorithms were assessed for feature ranking capability including: maximum relevancy minimum redundancy, neighborhood component analysis, out-of-bag importance, predictor importance, ReliefF, and chi-square using the MATLAB built-in functions '*fscmrmr*', '*fscnca/featureWeights*', '*fitcencemble/oobPermutedPredictorImportance*', '*fitcencemble/predictorImportance*', '*relieff*', and '*fscchi2*', respectively. The ReliefF MATLAB algorithm, and subsequently the '*relieff*' function, was chosen because it is a method of gaining mutual information about datapoints that is noise-tolerant and able to recognize feature interactions without removing redundant features,

thus providing an ideal method to rank features by their importance to binary classification at all timepoints (5, 12, 20, and 25 weeks) (38). The ReliefF algorithm ranks predictors based on the Euclidean distance, or the length of a distance between two points, for each class. A near-hit was defined as the samples that had a shorter distance from the same class, where a near-miss is represented as a closer sample from another class (38). The threshold values of near-hit and near-miss were set as the mean values. Finally, the features selected by the ReliefF algorithm were used to assess the effect of feature reduction on testing accuracy in two conditions: 1) above zero score values (i.e., all "relevant" features) and 2) top 50 features most descriptive of cardiac contractile dysfunction. Importantly, the goal of feature selection was not to remove redundant features, but to rank features by their importance for classification in order to manually reduce feature dimensionality for future applications.

Classification and Model Performance

Supervised machine learning and data processing was conducted in MATLAB (MathWorks Inc., R2020a, LN: 556683) using the Statistics and Machine Learning Toolbox. Data was partitioned to training and testing datasets at a 65% training/35% testing ratio using the MATLAB function '*cvpartition'*. The 65% of data used for training included, at minimum, 9 WT and 8 *Db/Db* mice. For each of the 5 testing iterations, animals were randomly selected and the model was trained using five-fold cross validation. Six classification models were initially assessed for training and testing accuracies: classification trees, discriminant analysis, naive bayes, nearest neighbors, support vector machine (SVM), and classification ensembles using MATLAB in-built functions: '*fitctree'*, '*fitcdiscr'*, '*fitcnb'*, '*fitcknn'*, '*fitcsvm'*, and '*fitcensemble'*, respectively. Classification algorithms used echocardiography features to predict the class of the animals based on cardiac function data, placing them into 1 of 2 categories; WT or *Db/Db*. For each dataset, testing was performed for 5 iterations and the average accuracies were obtained for model comparison.

The SVM model, on average, scored the highest accuracy and F-score values between datasets and was chosen as the highest performing model. Training and testing using the SVM model was performed for 5 iterations before the results were averaged for reporting (Supplemental Table S4.1). Model performance was evaluated using testing accuracies before and after feature reduction. Due to the large size of the "Complete" dataset, we assessed two approaches of reducing dataset dimensionality. The first approach was to reduce feature number to a ReliefF score of greater than zero, where a higher positive score indicated the strength of the feature as an identifier of class, and determines features considered relevant to the classification model. This approach removes irrelevant and redundant features, making it a traditional method of dataset dimensionality reduction. Machine learning was used as the statistical tool to compare the ability of conventional and STE features to identify animals as being within the non-diabetic (WT) or diabetic (*Db/Db*) conditions. Related code is provided on GitHub (https://doi.org/10.5281/zenodo.6391011).

Most Prevalent vs. Strongest Identifier

Regional and segmental prevalence was determined using the most descriptive of cardiac contractile dysfunction features from each "Segmental" dataset. Each cardiac segment (i.e., AntSeptum, AntFree, LatWall, PostWall, InfFreeWall, and PostSeptal) is represented by a total of 16 features relating to cardiac orientation (i.e., short/systolic, short/diastolic, long/systolic, and long/diastolic) and STE deformation features (i.e., velocity, displacement, strain, and strain rate). Each cardiac region (i.e., Anterior, Posterior, Septal, Free, Anterior Free, Posterior Free) is represented by the number of included segments, multiplied by a factor of 16, to acquire the number of features per segment. "Most prevalent" is used to describe the segment or region with the greatest percentage of features within the top 50 features most descriptive of cardiac contractile dysfunction ranked by their importance for the identification of the diabetic

condition. For example, to calculate the prevalence of the anterior region, each instance of a feature belonging to the segments constructing the Anterior region (AntSeptum, AntFree, and LatWall) were summed and divided by the total number of features selected by the ReliefF algorithm (i.e., 50). Because the number of segments that makes up each region differs, each region was normalized to the number of total contributing segments. The same calculation was applied for segmental prevalence.

"Strongest Identifier" refers to the regions and segments that produced the highest testing accuracies when tested with the machine learning SVM model. The SVM machine learning model was applied to the segmental (i.e., AntSeptum, AntFree, LatWall, PostWall, InfFreeWall, and PostSeptal) and regional (i.e., Anterior, Posterior, Free, Septal, Anterior Free, Posterior Free) datasets in order to the determine which segments and/or regions possessed the strongest ability to categorize an animal with cardiac contractile dysfunction as diabetic.

Statistical Analysis

Statistical analyses on raw data values were performed using GraphPad Prism version 8.02 (GraphPad Prism, RRID:SCR_002798). Data are presented as mean ± standard error of the mean (SEM). Data were analyzed using a two-tailed Students T-test. A p-value of $p \leq 0.05$ was considered statistically significant.

Results

Conventional M-mode echocardiography was utilized to verify progressive cardiac contractile dysfunction in *Db/Db* mice when compared to WT controls. At 5 weeks of age, no significant differences in contractile features or LV structural measures were observed in *Db/Db* mice when compared to WT controls (Table 4.1). At 12 weeks of age, *Db/Db* mice began exhibiting structural changes, including significantly increased LV mass, systolic LV anterior wall thickness

(LVAW;s), systolic LV posterior wall thickness (LVPW;s), diastolic LV posterior wall thickness (LVPW;d), and LV end diastolic volume (LVEV;d) and diameter (LVED;d) (Table 4.1). Additionally, stroke volume (SV) was significantly increased in *Db/Db* mice when compared to WT (Table 4.1). Together, the 12-week data reveals the development of well-known structural alterations in the diabetic heart. At 20 weeks of age, *Db/Db* mice demonstrated sustained increases in SV, but were further characterized by overt contractile dysfunction marked by significant decreases in ejection fraction (EF) and fractional shortening (FS) when compared to WT controls (Table 4.1). A similar structural profile was maintained, with the addition of significant increases in diastolic LV anterior wall thickness (LVAW;d) and LV end-systolic volume (LVEV;s), though alterations in posterior wall thicknesses were no longer significant. Cardiac contractile dysfunction and structural changes were maintained at 25 weeks in *Db/Db* mice when compared to WT (Table 4.1).

To confirm the ability of the ReliefF feature selection algorithm to identify and rank M-mode features by their ability to identify cardiac contractile dysfunction, each of the M-mode data subsets were ranked by their ability to identify cardiac contractile dysfunction at each timepoint (Supplemental Figure S4.1). The 5 echocardiography features identified to be the strongest identifiers of cardiac contractile dysfunction at each timepoint, were tested for statistical significance, and compared against Table 4.1. Week 5 showed no changes in the 5 best identifiers; heart rate, LVPW;d, LVEV's, EF, or FS (Supplemental Figure S4.1, A, B, C, D, and E). At Week 12, the 5 strongest identifiers paralleled significantly altered structural features in Table 4.1 (Supplemental Figure S4.1, F, G, H, I and J). Four of the 5 features including LV mass, LVPW;s, LVPW;d, and LVAW;s were significantly increased in *Db/Db* mice when compared to WT (Supplemental Figure S4.1, F, G, H, I, and J). A single parameter, LVAW;d, was unchanged at 12 weeks (Supplemental Figure S4.1J). At week 20, the 5 strongest identifiers included significantly higher LV mass, LVED;s, LVAW;d, and LVEV;s, with significantly lower EF, in *Db/Db* mice when compared to WT (Supplemental Figure S4.1, K, L, M, N, and O). At week 25, the 5 strongest identifiers included significantly higher

LV mass, LVAW;d, LVEV;s, and LVAW;s, with significantly lower EF, in *Db/Db* mice when compared to WT (Supplemental Figure S4.1, P, Q, R, S, and T). Together, the 5 strongest identifiers of cardiac contractile dysfunction paralleled the progressive structural changes and decreases in cardiac contractile function observed in Table 4.1. These data suggest that the ReliefF algorithm was able to adequately rank features based on their importance to the identification of cardiac contractile dysfunction associated with the diabetic condition.

Next, we aimed to determine if conventional echocardiography or STE could more accurately segregate animals into their pre-determined category of diabetic or non-diabetic. An SVM machine learning model was used to compare conventional echocardiography and STE features as identifiers of cardiac contractile dysfunction associated with the diabetic condition. SVM model performance, including training accuracy, standard deviation, testing accuracy, and F-score, were reported for each timepoint in Supplemental Table S4.1. SVM model testing accuracies demonstrated that STE datasets were better able to segregate animals into the correct category of diabetic vs. non-diabetic when compared to conventional echocardiography subsets (M-mode and PWD), at all timepoints (Figure 4.2). At week 5, when no overt systolic dysfunction was detectable, STE datasets including the Septal, Anterior, and Segmental were the strongest identifiers of cardiac dysfunction, while M-mode features were a weak identifier of cardiac dysfunction, and segregated mice with the poorest accuracy (Figure 4.2). At week 12, the Complete, Segmental, and Anterior datasets were able to identify cardiac dysfunction with the greatest accuracy (Figure 4.2). By week 20, overt contractile dysfunction was detectable using conventional M-mode echocardiography and PWD, yet the Posterior and Anterior datasets were the strongest identifiers of cardiac dysfunction (Figure 4.2). At week 25, the STE Free and Global datasets were able to best identify cardiac contractile dysfunction associated with the diabetic condition despite significant decreases in nearly all M-mode features (Figure 4.2) (Table 4.1), suggesting that STE echocardiography, which provides strain-based outcomes, may be more capable of distinguishing a

state of cardiac contractile dysfunction as compared to changes in systolic function parameters (i.e., EF and FS).

We next aimed to use the ReliefF algorithm to rank features in the "Complete" datasets by their ability to identify a state of cardiac dysfunction. We began with the testing accuracies for the "Complete" dataset, containing 376 features, at all timepoints, and reduced the number of features to only those that were considered to be important for the classification of the diabetic condition. At week 5, the "Complete", unedited, dataset was able to correctly categorize mice as diabetic or non-diabetic 82% of the time (Figure 4.3A). Further, the 5 strongest identifiers of cardiac dysfunction were MPI, SD PostSeptalWall RD, SD Septal RD, SS AntFree RSR, and SD InfFreeWall, which were determined to be significantly different between WT and *Db/Db* mice (Figure 4.3B) (Supplemental Figure S4.2, A, B, C, D, and E). Reducing the number of features to those considered "relevant" to the identification of cardiac dysfunction, or having a score above zero, failed to sufficiently reduce dataset size, with the week 5 dataset retaining 158 features (Supplemental Table S4.2). Rather, reducing the complete dataset to only the top 50 strongest identifiers of cardiac contractile dysfunction increased testing accuracy by 0.14 percent as designated by a red arrow (Figure 4.3C) (Supplemental Table S4.3).

At week 12, the "Complete", unedited, dataset was able to correctly categorize mice as diabetic or non-diabetic 96% of the time (Figure 4.3A). Further, the 5 strongest identifiers of cardiac dysfunction were LS AntSeptum RV, LS AntSeptum RSR, SS LatWall CV, LS Septal RSR, and LS Anterior RSR, which were determined to be significantly decreased in *Db/Db* mice when compared to WT (Figure 4.3B) (Supplemental Figure S4.2, F, G, H, I, and J). Reducing the number of features to those considered relevant failed to sufficiently reduce dataset size, with the dataset at 12 weeks retaining 319 features (Supplemental Table S4.2). Rather, reducing the complete dataset to only the top 50 strongest identifiers of cardiac contractile dysfunction

increased testing accuracy by 0.02 percent as designated by a red arrow (Figure 4.3C) (Supplemental Table S4.3).

At week 20, the "Complete", unedited, dataset was able to correctly categorize mice as diabetic or non-diabetic 91% of the time (Figure 4.3A). Further, the 5 strongest identifiers of cardiac contractile dysfunction were LS PostSeptalWall RSR, LS Anterior RSR, LS Septal RSR, SS AntSeptum RSR, and LS Posterior RSR, which were determined to be significantly decreased in *Db/Db* mice when compared to WT (Figure 4.3B) (Supplemental Figure S4.2, K, L, M, N, and O). Reducing the number of features to those considered relevant failed to sufficiently reduce dataset size, with the dataset at 20 weeks retaining 330 features (Supplemental Table S4.2). Rather, reducing the complete dataset to only the top 50 features most descriptive of cardiac contractile dysfunction increased testing accuracy by 0.02 percent as designated by a red arrow (Figure 4.3C) (Supplemental Table S4.2). Reducing the complete dataset to only the top strongest identifiers of cardiac contractile dysfunction significantly reduced dataset size, and did not change testing accuracy as designated by a red arrow (Figure 4.3C) (Supplemental Table S4.3).

At week 25, the "Complete", unedited, dataset was able to correctly categorize mice as diabetic or non-diabetic 89% of the time (Figure 4.3A). Further, the 5 strongest identifiers of cardiac dysfunction were SSG Radial Strain, SS Anterior RS, SS Free RS, SS Anterior RV, and SS AntFree RS, which were determined to be significantly decreased in *Db/Db* mice when compared to WT (Figure 4.3B) (Supplemental Figure S4.2, P, Q, R, S, and T). Reducing the number of features to those considered relevant failed to sufficiently reduce dataset size, with the dataset at 20 weeks retaining 288 features (Supplemental Table S4.2). Rather, reducing the complete dataset to only the top 50 strongest identifiers of cardiac contractile dysfunction increased testing accuracy by 0.09 percent as designated by a red arrow (Figure 4.3C) (Supplemental Table S4.3).

Because STE features appeared to identify cardiac dysfunction with the greatest accuracy, the ability of regional and segmental features to identify cardiac contractile dysfunction were assessed using the Segmental, Anterior, Posterior, Septal, Free, Anterior Free, Posterior Free, AntFree, AntSeptum, InfFreeWall, LatWall, PostSeptal, and PostWall datasets. SVM model performance, including training accuracy, standard deviation, testing accuracy, and F-score, were reported for each dataset at each timepoint in Supplemental Table S4.4 and were visually represented in Supplemental Figure S4.3. These analyses suggest that changes in regional and segmental features are able to accurately segregate cardiac contractile function associated with the diabetic and non-diabetic conditions.

We next assessed the ability of STE regional and segmental features to identify spatial cardiac dysfunction using two analytical methods. To determine the spatial impact of regional and segmental features on cardiac contractile function, we utilized the Segmental, Anterior, Posterior, Septal, Free, Anterior Free, Posterior Free, AntFree, AntSeptum, InfFreeWall, LatWall, PostSeptal, and PostWall datasets. First, the heart was segregated into regions, which represented locales of the heart that could be evaluated independently from the LV as a whole. Regions were ranked by their ability to identify cardiac contractile dysfunction, based on their ability to segregate animals into the diabetic and non-diabetic conditions at each timepoint (Table 4.2). At week 5, the Septal region, containing both the AntSeptum and PostSeptal segments, was the strongest identifier of cardiac dysfunction when compared to other cardiac regions, and segregated animals as diabetic or non-diabetic with an 84% testing accuracy (Table 4.2). At week 12, the Anterior Free region, comprised of the AntFree and LatWall segments, rather than the Septal region (91% accuracy), was the strongest identifier of cardiac contractile dysfunction, with a 98% testing accuracy (Table 4.2). At week 20, the Septal region returned as the strongest identifier of cardiac contractile dysfunction, with a 98% testing accuracy (Table 4.2). At week 25, the Septal region remained the strongest identifier of cardiac contractile dysfunction

187

when compared to other cardiac regions, with a 98% testing accuracy (Table 4.2). These data suggest that the Septal region is the strongest identifier of cardiac dysfunction, and may be identifiable as early as 5 weeks.

Secondly, cardiac segments representing the smallest possible locales for evaluation of cardiac function, were ranked by their ability to identify cardiac contractile dysfunction at each timepoint (Table 4.3). At week 5, the InfFreeWall segment was the strongest identifier of cardiac contractile dysfunction when compared to other cardiac segments, and segregated animals as diabetic or non-diabetic with a 76% testing accuracy (Table 4.3). At week 12, the LatWall segment was the strongest identifier of cardiac contractile dysfunction, with a 98% testing accuracy (Table 4.3). At week 20, the AntSeptum segment was the strongest identifier of cardiac contractile dysfunction, with a 96% testing accuracy (Table 4.3). At week 25, the AntFree segment was the strongest identifier of cardiac contractile dysfunction, with a 96% testing accuracy (Table 4.3).

Finally, to determine if the regions and segments defined as being the strongest identifiers of cardiac contractile dysfunction contained the largest number of noteworthy and altered features, we assessed the prevalence of each region and segment. The calculations used to determine the "most prevalent" regions and segments is described in the methods section "*Most Prevalent vs. Strongest Identifier*". At week 5, each region appeared to contribute a similar percentage of features, but the Anterior and Septal regions contributed the largest number of features most descriptive of cardiac contractile dysfunction, representing 19% and 18% of the features, respectively (Figure 4.4A). Inspection of the prevalence of the individual segments at week 5 revealed that the AntSeptum and InfFreeWall segments were of equal prevalence, with each accounting for 22% of features (Figure 4.4B). Moreover, the AntSeptum segment was the largest contributor to the prevalence of the Anterior and Septal regions, accounting for the largest percentage of features in both the Anterior and Septal regions at 39% and 61%, respectively (Figure 4.4C). Accordingly, the InfFreeWall

segment also drove the prevalence of the Posterior, Free, and Posterior Free regions (Figure 4.4C). Based on the number of features contributed by each region and segment, the AntSeptum segment, and the Anterior and Septal regions contained the largest number of noteworthy metrics, which may indicate locales containing the largest number of features contributing to cardiac contractile dysfunction at week 5 (Figure 4.4D).

At week 12, the Septal region contributed the largest number of features most descriptive of cardiac contractile dysfunction, representing 24% of the features (Figure 4.5A). Inspection of the prevalence of the individual segments at week 12 further revealed that the AntSeptum segment was of the greatest prevalence, accounting for 28% of the features (Figure 4.5B). Additionally, the AntSeptum segment was the largest contributor to the prevalence of both the Septal and Anterior regions, accounting for the largest percentage of features at 58% and 56%, respectively (Figure 4.5C). Based on the number of features contributed by each region and segment, the AntSeptum segment, and co-concomitantly, the Septal region contained the largest number of noteworthy metrics, and represent the locales containing the largest number of features contributing to cardiac contractile dysfunction at week 12 (Figure 4.5D).

At week 20, each region contributed a similar percentage of features, but the Anterior and Anterior Free regions contributed the largest number of features most descriptive of cardiac contractile dysfunction, representing 19.3% and 19% of the features, respectively (Figure 4.6A). Inspection of the prevalence of the individual segments at week 20 demonstrated that the AntFree segment was the most prevalent, accounting for 22% of features (Figure 4.6B). The AntFree segment was the largest contributor to the prevalence of the Anterior and Anterior Free regions, accounting for the largest percentage of features in both the Anterior and Anterior Free regions at 38% and 58%, respectively (Figure 4.6C). Based on the number of features contributed by each region and segment, the AntFree segment, and the Anterior and Anterior Free regions contained the largest number

of noteworthy metrics, which may indicate locales containing the largest number of features contributing to cardiac contractile dysfunction at week 20 (Figure 4.6D).

At week 25, the Anterior and Anterior Free regions contributed the largest number of features most descriptive of cardiac contractile dysfunction, representing 22% and 20% of the features, respectively (Figure 4.7A). Inspection of the prevalence of the individual segments at week 25 demonstrated that the AntSeptum and AntFree segments were the most prevalent, accounting for 26% and 22% of features, respectively (Figure 4.7B). The AntSeptum segment was the largest contributor to the prevalence of the Anterior and Septal regions, accounting for the largest percentage of features in both the Anterior and Septal regions at 39% and 76%, respectively (Figure 4.7C). Based on the number of features contributed by each region and segment, the AntSeptum and AntFree segments, and the Anterior and Anterior Free regions contained the largest number of noteworthy metrics, which may indicate locales containing the largest number of features contributing to cardiac contractile dysfunction at week 25 (Figure 4.7D).

Discussion

The etiology of cardiovascular contractile dysfunction in T2DM remains unknown, and as morbidity and mortality continue to rise, our understanding of its pathophysiology will be critical to produce new and improved diagnostic and treatment opportunities. STE is an invaluable tool for the evaluation of cardiac function, and has been utilized to evaluate changes in contractility and deformation in both murine models of T1DM (9, 24), T2DM (23), and human subjects (17, 18, 22, 39). At current, STE has not been utilized to evaluate progressive changes in regional and segmental function as a method of identifying patterns of cardiac contractile dysfunction in the type 2 diabetic heart. Elucidating changes in cardiac function, to the fullest extent possible, may aid in filling this gap in our knowledge, and may provide an alternative method to identify cardiovascular dysfunction in diabetes mellitus patients earlier and with greater specificity than current methods.

In this study, we aimed to elucidate if cardiac contractile dysfunction associated with the T2DM condition occurs spatially, and if patterns of regional or segmental dysfunction manifest in a temporal fashion. We further aimed to utilize machine learning to identity the cardiac regions, segments, and features that best described a state of cardiac contractile dysfunction using solely non-invasive echocardiography features. A summary of study results and potential applications can be seen in Figure 4.8.

The use of machine learning enhanced our ability to predict what regions and segments of the heart were most impacted during disease progression, and to further explore those that were best able to identify cardiac contractile dysfunction. Traditional data analyses use descriptive and exploratory methods to provide results and discover patterns in current or past data, but do not make predictions about the future. We aimed to compare traditional data analyses with machine learning methodologies to determine if the regions and segments that were best able to identify cardiac contractile dysfunction also contained the largest number of dysfunctional parameters. By determining the prevalence of a region or segment, we gained insight into the cardiac locales that were likely impacted by T2DM to the greatest extent, and exhibited the largest number of noteworthy changes.

We were able to identify the regions and segments which best identified a state of cardiac contractile dysfunction, and the features which best defined it. The Septal region, and primarily the AntSeptum segment, were determined to be the strongest identifiers of cardiac dysfunction at 5, 20, and 25 weeks. Moreover, the Septal region was identified as a region of interest early in T2DM development, and was maintained into the late stages of disease. These data suggest that the Septal region, and the segments contained within, may provide a new metric for the identification of subclinical cardiac dysfunction. The importance of the Septal region may be explained, in part, by the role of the septum in conduction of the heart. The electrical sequence in the heart follows a pre-defined order in healthy

191

individuals, but may be disrupted in individuals with cardiovascular contractile dysfunction (40). For example, the healthy septum transfers energy between the ventricles, acting as a third pump. Diseases that increase septal elastance, such as diabetes mellitus, can resemble left ventricular diastolic dysfunction (41). Myocardial work, or the contribution by each region to contraction, has been found to be significantly affected by both hypertension and diabetes, with diabetic patients having lower strain values in the septal and lateral segments (42). Further, the observation of early Septal region dysfunction has been utilized as a method of identifying and monitoring diabetes mellitus (42-44). These reports suggest that alterations in the Septal region may be observable early in the pathophysiology of T2DM, prior to the onset of clinically recognizable symptoms of cardiac dysfunction. The data presented in this study suggest that the Septal region may benefit most from therapeutic interventions aimed at preventing the progression of cardiac contractile dysfunction in T2DM when initiated early in disease.

Interestingly, the Septal region was the second-best classifier of the diabetic condition at week 12, where the Anterior Free region, and the LatWall segment, were able to identify cardiac contractile dysfunction with the greatest accuracy. This shift from the Septal wall to the AntFree region and LatWall segment at 12 weeks, and back to the Septal region again at 20 weeks, may be the result of the cardiac structural and metabolic remodeling preceding, and ultimately leading to the development of overt contractile dysfunction (45-49). Metabolic inflexibility and substrate overload initiate several metabolic and structural changes that manifest during the subclinical stages of cardiac contractile dysfunction as an adaptive mechanism to protect the heart (12, 46, 50, 51). In healthy individuals, the LV primarily performs contractile or shortening work, but in patients with cardiomyopathies, the ability of the septum to provide energy for contraction may be decreased, with a greater amount energy being wasted (52). This means that even though the Septal region begins the contractile process, the Free and Anterior regions may overcompensate for the Septal regions lack of energy contribution by contributing additional energy for contraction (53). Metabolically,

segments contributing the greatest level of contractile energy also exhibit the highest levels of glucose metabolism, and show a disruption of glucose metabolism, and therefore an ability to produce energy for contraction, with disease (54). This metabolic shift suggests that regions displaying this pattern of energy waste may experience larger amounts of mitochondrial dysfunction, including impaired glucose metabolism, increased reliance on fatty acid oxidation, and changes in mitochondrial DNA (54-57). With this in mind, structural and metabolic alterations may manifest in the Anterior Free region, prior to the onset of overt contractile dysfunction that temporarily improve its ability to identify animals as diabetic or non-diabetic. As a result, we believe that future directions should include the biochemical analysis of regional and segmental metabolism.

Analysis of our data using traditional methods produced results similar to those observed using machine learning. Subsequently, determining the most prevalent regions and segments, or those containing the largest number of noteworthy, and likely dysfunctional metrics were reflective of the most impacted cardiac locale at each timepoint. We observed that the prevalence of regions and segments overlapped, with the most prevalent region containing the most prevalent segment. Overall, these results suggest the AntSeptum segment may contain the greatest number of features contributing to cardiac contractile dysfunction, and may be a metric to identify and monitor throughout the T2DM pathology. Taken together, these data support assessments of regional and segmental function using feature ranking algorithms as a feasible alternative to traditional data analysis to determine regions or locales of interest for experimental, therapeutic, or clinical purposes.

The healthcare community has largely benefited from the implementation of STE, which has provided a great deal of insight into cardiac contractile dysfunction, and the incorporation of machine learning in the evaluation of echocardiography represents a new and powerful tool for the study (58-60). Further, machine learning and features ranking methodologies with the intention

of identifying regions and segments of interest for experimental, clinical, and therapeutic purposes. Combining these techniques may provide a more descriptive and thorough approach to managing large amounts of contractile data, as well as improve the process of analyzing and interpreting cardiovascular contractile data (39, 61, 62). These applications in echocardiography are increasing exponentially, particularly for their ability to develop innovative models of diagnosis and care (39, 63-65). The initial collection and analysis of data can be difficult, leading to the interpretation of a small subset of data collected, rather than the data as a whole (62). In clinical settings, the ability to automate data acquisition, processing, and interpretation may help to improve methods of evaluating cardiac dysfunction in the T2DM heart (61, 66, 67). The data presented in this study support that machine learning can be used as a tool to identify cardiac contractile dysfunction by using solely non-invasive echocardiography features in a murine model of T2DM. We demonstrate that feature ranking algorithms can be used to identify regional and segmental patterns of cardiovascular contractile dysfunction in T2DM, suggesting that cardiovascular contractile dysfunction occurs not only in a temporal fashion, but progresses spatially.

Interestingly, despite significant changes in M-mode parameters, STE outperformed conventional echocardiography at all timepoints, and was consistently better at identifying cardiac contractile dysfunction. Prior to the development of overt systolic dysfunction, as at 5 and 12 weeks, the ability of STE to outperform conventional M-mode echocardiography was expected due to its ability to detect subclinical changes in cardiac function. Alternatively, M-mode echocardiography demonstrated significant decreases in EF and FS features at 20 and 25 weeks of age, but was not as strong of an identifier of cardiac contractile dysfunction as STE features. This discrepancy may be due, in part, to the methodology used by machine learning classification. Specifically, M-mode may contain a large number of significantly altered features, but if the STE regions and segments discussed above contain an overall larger number of altered features, it could indirectly increase the ability of STE features to identify cardiac contractile

dysfunction. In terms of clinical applicability, numerous altered STE features may be necessary to outperform the ability of EF to identify contractile dysfunction. Moreover, M-mode echocardiography parameters, including EF and FS, may be a stronger indicator of contractile dysfunction once overt dysfunction is present, but M-mode echocardiography remains unable to detect clinical and subclinical measures of dysfunction. Hence, the focus of STE should remain the assessment and diagnosis of subclinical cardiac dysfunction. As discussed above, the Septal region may provide a metric for clinicians to identify subclinical changes in cardiac deformation, aid in the diagnosis and staging of cardiac contractile dysfunction prior to the presence of overt systolic dysfunction, and monitor, in addition to EF, during late stages of disease. Further evaluation is necessary to determine if the spatial and temporal patterns of STE observed in *Db/Db* mice also occur in T2DM human subjects.

In summary, cardiac contractile dysfunction associated with the T2DM condition manifests spatially, and patterns of regional and segmental dysfunction appear early in the T2DM pathology while progressing in a temporal fashion. Further, the Septal region may provide a metric for the identification of subclinical dysfunction, the diagnosis and staging of cardiac contractile dysfunction prior to the presence of overt systolic dysfunction, and a target for therapeutic interventions aimed at preventing the progression of cardiac contractile dysfunction in T2DM when initiated early in the disease. Additionally, these data support that assessments of regional and segmental function using machine learning and feature ranking algorithms may be a feasible alternative to traditional data analysis and may provide a more descriptive and thorough approach to managing large amounts of contractile data with the intention of identifying regions and segments of interest for experimental, clinical, and therapeutic purposes.

Disclosures

None

References

1.   Raghavan S, Vassy JL, Ho YL, Song RJ, Gagnon DR, Cho K, et al. Diabetes Mellitus-Related All-Cause and Cardiovascular Mortality in a National Cohort of Adults. J Am Heart Assoc. 2019;8(4):e011295. doi:10.1161/JAHA.118.011295

2.   Dal Canto E, Ceriello A, Ryden L, Ferrini M, Hansen TB, Schnell O, et al. Diabetes as a Cardiovascular Risk Factor: An Overview of Global Trends of Macro and Micro Vascular Complications. Eur J Prev Cardiol. 2019;26(2_suppl):25-32. doi:10.1177/2047487319878371

3.   Einarson TR, Acs A, Ludwig C, Panton UH. Economic Burden of Cardiovascular Disease in Type 2 Diabetes: A Systematic Review. Value Health. 2018;21(7):881-890. doi:10.1016/j.jval.2017.12.019

4.   Association AH. Cardiovascular Disease and Diabetes 2019. Available from: https://www.heart.org/en/health-topics/diabetes/why-diabetes-matters/cardiovascular-disease--diabetes.

5.   Makaryus RRVSYAN. 2022. Treasure Island, FL: StatPearls Publishing.

6.   Sachdeva S, Gupta SK. Imaging Modalities in Congenital Heart Disease. Indian J Pediatr. 2020;87(5):385-397. doi:10.1007/s12098-020-03209-y

7.   Sasikumar IAN. 2021. StatPearls.

8.   Lorenzo-Almoros A, Tunon J, Orejas M, Cortes M, Egido J, Lorenzo O. Diagnostic Approaches for Diabetic Cardiomyopathy. Cardiovascular diabetology. 2017;16(1):28. doi:10.1186/s12933-017-0506-x

9.   Shepherd DL, Nichols CE, Croston TL, McLaughlin SL, Petrone AB, Lewis SE, et al. Early Detection of Cardiac Dysfunction in the Type 1 Diabetic Heart Using Speckle-Tracking Based Strain Imaging. J Mol Cell Cardiol. 2016;90:74-83. doi:10.1016/j.yjmcc.2015.12.001

10.   Azevedo PS, Polegato BF, Minicucci MF, Paiva SA, Zornoff LA. Cardiac Remodeling: Concepts, Clinical Impact, Pathophysiological Mechanisms and Pharmacologic Treatment. Arq Bras Cardiol. 2016;106(1):62-69. doi:10.5935/abc.20160005

11.   Gulsin GS, Swarbrick DJ, Hunt WH, Levelt E, Graham-Brown MPM, Parke KS, et al. Relation of Aortic Stiffness to Left Ventricular Remodeling in Younger Adults with Type 2 Diabetes. Diabetes. 2018;67(7):1395-1400. doi:10.2337/db18-0112

12.   Yap J, Tay WT, Teng TK, Anand I, Richards AM, Ling LH, et al. Association of Diabetes Mellitus on Cardiac Remodeling, Quality of Life, and Clinical Outcomes in Heart Failure with Reduced and Preserved Ejection Fraction. J Am Heart Assoc. 2019;8(17):e013114. doi:10.1161/JAHA.119.013114

13.   Shah AM, Hung CL, Shin SH, Skali H, Verma A, Ghali JK, et al. Cardiac Structure and Function, Remodeling, and Clinical Outcomes among Patients with Diabetes after Myocardial Infarction Complicated by Left Ventricular Systolic Dysfunction, Heart Failure, or Both. American heart journal. 2011;162(4):685-691. doi:10.1016/j.ahj.2011.07.015

14.   Cicala S, de Simone G, Roman MJ, Best LG, Lee ET, Wang W, et al. Prevalence and Prognostic Significance of Wall-Motion Abnormalities in Adults without Clinically Recognized Cardiovascular Disease: The Strong Heart Study. Circulation. 2007;116(2):143-150. doi:10.1161/CIRCULATIONAHA.106.652149

15.   Opthof T, Sutton P, Coronel R, Wright S, Kallis P, Taggart P. The Association of Abnormal Ventricular Wall Motion and Increased Dispersion of Repolarization in Humans Is Independent of the Presence of Myocardial Infarction. Front Physiol. 2012;3:235. doi:10.3389/fphys.2012.00235

16.   Kamran S, Akhtar N, Singh R, Imam Y, Haroon KH, Amir N, et al. Association of Major Adverse Cardiovascular Events in Patients with Stroke and

Cardiac Wall Motion Abnormalities. J Am Heart Assoc. 2021;10(14):e020888. doi:10.1161/JAHA.121.020888

17.   Liu JH, Chen Y, Yuen M, Zhen Z, Chan CW, Lam KS, et al. Incremental Prognostic Value of Global Longitudinal Strain in Patients with Type 2 Diabetes Mellitus. Cardiovascular diabetology. 2016;15(22):22. doi:10.1186/s12933-016-0333-5

18.   Hensel KO, Grimmer F, Roskopf M, Jenke AC, Wirth S, Heusch A. Subclinical Alterations of Cardiac Mechanics Present Early in the Course of Pediatric Type 1 Diabetes Mellitus: A Prospective Blinded Speckle Tracking Stress Echocardiography Study. J Diabetes Res. 2016;2016:2583747. doi:10.1155/2016/2583747

19.   Levelt E, Mahmod M, Piechnik SK, Ariga R, Francis JM, Rodgers CT, et al. Relationship between Left Ventricular Structural and Metabolic Remodeling in Type 2 Diabetes. Diabetes. 2016;65(1):44-52. doi:10.2337/db15-0627

20.   Dandel M, Lehmkuhl H, Knosalla C, Suramelashvili N, Hetzer R. Strain and Strain Rate Imaging by Echocardiography - Basic Concepts and Clinical Applicability. Curr Cardiol Rev. 2009;5(2):133-148. doi:10.2174/157340309788166642

21.   Elgohari A. Effect of Diabetic Duration on Left Ventricular Global Longitudinal Strain by Speckle Tracking Imaging. Atherosclerosis. 2019;287(125):E125-E125. doi:10.1016/j.atherosclerosis.2019.06.365

22.   Biering-Sorensen T, Biering-Sorensen SR, Olsen FJ, Sengelov M, Jorgensen PG, Mogelvang R, et al. Global Longitudinal Strain by Echocardiography Predicts Long-Term Risk of Cardiovascular Morbidity and Mortality in a Low-Risk General Population: The Copenhagen City Heart Study. Circ Cardiovasc Imaging. 2017;10(3). doi:10.1161/CIRCIMAGING.116.005521

23.   Li R, Yang J, Yang Y, Ma N, Jiang B, Sun Q, et al. Speckle Tracking Echocardiography in the Diagnosis of Early Left Ventricular Systolic Dysfunction in Type Ii Diabetic Mice. BMC Cardiovasc Disord. 2014;14. doi:10.1186/1471-2261-14-141

24.   Pappritz K, Grune J, Klein O, Hegemann N, Dong F, El-Shafeey M, et al. Speckle-Tracking Echocardiography Combined with Imaging Mass Spectrometry Assesses Region-Dependent Alterations. Sci Rep. 2020;10(1):3629. doi:10.1038/s41598-020-60594-2

25.   Gehan Magdy YG, Eman Yousef , Mohamed Zaiton and Dina Ismail. Assessment of Subclinical Left Ventricular Dysfunction in Asymptomatic Type Ii Diabetic Patients Using Strain Echocardiography. J Cardiol & Cardiovasc Ther. 2017;7(1). doi:10.19080/JOCCT.2017.06.555708

26.   Lange T, Schuster A. Quantification of Myocardial Deformation Applying Cmr-Feature-Tracking-All About the Left Ventricle? Curr Heart Fail Rep. 2021;18(4):225-239. doi:10.1007/s11897-021-00515-0

27.   Chua S, Jr., Liu SM, Li Q, Yang L, Thassanapaff VT, Fisher P. Differential Beta Cell Responses to Hyperglycaemia and Insulin Resistance in Two Novel Congenic Strains of Diabetes (Fvb- Lepr (Db)) and Obese (Dba- Lep (Ob)) Mice. Diabetologia. 2002;45(7):976-990. doi:10.1007/s00125-002-0880-z

28.   Wang Z, Jiang T, Li J, Proctor G, McManaman JL, Lucia S, et al. Regulation of Renal Lipid Metabolism, Lipid Accumulation, and Glomerulosclerosis in Fvbdb/Db Mice with Type 2 Diabetes. Diabetes. 2005;54(8):2328-2335. doi:10.2337/diabetes.54.8.2328

29.   Laboratory TJ. 006654 - Fvb.Bks(D)-Lepr 2019. Available from: https://www.jax.org/strain/006654.

30.   Rottman JN, Ni G, Khoo M, Wang Z, Zhang W, Anderson ME, et al. Temporal Changes in Ventricular Function Assessed Echocardiographically in

Conscious and Anesthetized Mice. J Am Soc Echocardiogr. 2003;16(11):1150-1157. doi:10.1067/S0894-7317(03)00471-1

31.   Pachon RE, Scharf BA, Vatner DE, Vatner SF. Best Anesthetics for Assessing Left Ventricular Systolic Function by Echocardiography in Mice. Am J Physiol Heart Circ Physiol. 2015;308(12):H1525-1529. doi:10.1152/ajpheart.00890.2014

32.   Roth DM, Swaney JS, Dalton ND, Gilpin EA, Ross J, Jr. Impact of Anesthesia on Cardiac Function During Echocardiography in Mice. Am J Physiol Heart Circ Physiol. 2002;282(6):H2134-2140. doi:10.1152/ajpheart.00845.2001

33.   Pan G, Munukutla S, Kar A, Gardinier J, Thandavarayan RA, Palaniyandi SS. Type-2 Diabetic Aldehyde Dehydrogenase 2 Mutant Mice (Aldh 2*2) Exhibiting Heart Failure with Preserved Ejection Fraction Phenotype Can Be Determined by Exercise Stress Echocardiography. PLoS One. 2018;13(4):e0195796. doi:10.1371/journal.pone.0195796

34.   Kunovac A, Hathaway QA, Pinti MV, Goldsmith WT, Durr AJ, Fink GK, et al. Ros Promote Epigenetic Remodeling and Cardiac Dysfunction in Offspring Following Maternal Engineered Nanomaterial (Enm) Exposure. Part Fibre Toxicol. 2019;16(1):24. doi:10.1186/s12989-019-0310-8

35.   Hathaway QA, Durr AJ, Shepherd DL, Pinti MV, Brandebura AN, Nichols CE, et al. Mirna-378a as a Key Regulator of Cardiovascular Health Following Engineered Nanomaterial Inhalation Exposure. Nanotoxicology. 2019;10.1080/17435390.2019.1570372:1-20. doi:10.1080/17435390.2019.1570372

36.   Kunovac A, Hathaway QA, Pinti MV, Durr AJ, Taylor AD, Goldsmith WT, et al. Enhanced Antioxidant Capacity Prevents Epitranscriptomic and Cardiac Alterations in Adult Offspring Gestationally-Exposed to Enm. Nanotoxicology. 2021;15(6):812-831. doi:10.1080/17435390.2021.1921299

37.   Roy B. All About Feature Scaling tawardsdatascience website2020. Available from: https://towardsdatascience.com/all-about-feature-scaling-bcc0ad75cb35.

38.   Urbanowicz RJ, Meeker M, La Cava W, Olson RS, Moore JH. Relief-Based Feature Selection: Introduction and Review. J Biomed Inform. 2018;85:189-203. doi:10.1016/j.jbi.2018.07.014

39.   František Sabovčik NC, Celine Vens, Tatiana Kuznetsova. Erratum. European Heart Journal - Digital Health. 2022;3(1):115-116. doi:10.1093/ehjdh/ztab098

40.   Sengupta PP, Korinek J, Belohlavek M, Narula J, Vannan MA, Jahangir A, et al. Left Ventricular Structure and Function: Basic Science for Cardiac Imaging. J Am Coll Cardiol. 2006;48(10):1988-2001. doi:10.1016/j.jacc.2006.08.030

41.   Luo C, Ware DL, Zwischenberger JB, Clark JW, Jr. A Mechanical Model of the Human Heart Relating Septal Function to Myocardial Work and Energy. Cardiovasc Eng. 2008;8(3):174-184. doi:10.1007/s10558-008-9054-z

42.   Kaushik A, Kapoor A, Dabadghao P, Khanna R, Kumar S, Garg N, et al. Use of Strain, Strain Rate, Tissue Velocity Imaging, and Endothelial Function for Early Detection of Cardiovascular Involvement in Young Diabetics. Ann Pediatr Cardiol. 2021;14(1):1-9. doi:10.4103/apc.APC_158_19

43.   Lindner O, Vogt J, Kammeier A, Wielepp P, Holzinger J, Baller D, et al. Effect of Cardiac Resynchronization Therapy on Global and Regional Oxygen Consumption and Myocardial Blood Flow in Patients with Non-Ischaemic and Ischaemic Cardiomyopathy. Eur Heart J. 2005;26(1):70-76. doi:10.1093/eurheartj/ehi046

44.   Iozzo P, Chareonthaitawee P, Rimoldi O, Betteridge DJ, Camici PG, Ferrannini E. Mismatch between Insulin-Mediated Glucose Uptake and Blood

Flow in the Heart of Patients with Type Ii Diabetes. Diabetologia. 2002;45(10):1404-1409. doi:10.1007/s00125-002-0917-3

45.   Borghetti G, von Lewinski D, Eaton DM, Sourij H, Houser SR, Wallner M. Diabetic Cardiomyopathy: Current and Future Therapies. Beyond Glycemic Control. Front Physiol. 2018;9:1514. doi:10.3389/fphys.2018.01514

46.   Salvatore T, Pafundi PC, Galiero R, Albanese G, Di Martino A, Caturano A, et al. The Diabetic Cardiomyopathy: The Contributing Pathophysiological Mechanisms. Front Med (Lausanne). 2021;8:695792. doi:10.3389/fmed.2021.695792

47.   Tran DH, Wang ZV. Glucose Metabolism in Cardiac Hypertrophy and Heart Failure. J Am Heart Assoc. 2019;8(12):e012673. doi:10.1161/JAHA.119.012673

48.   Gibb AA, Hill BG. Metabolic Coordination of Physiological and Pathological Cardiac Remodeling. Circ Res. 2018;123(1):107-128. doi:10.1161/CIRCRESAHA.118.312017

49.   Wende AR, Brahma MK, McGinnis GR, Young ME. Metabolic Origins of Heart Failure. JACC Basic Transl Sci. 2017;2(3):297-310. doi:10.1016/j.jacbts.2016.11.009

50.   Chong CR, Clarke K, Levelt E. Metabolic Remodeling in Diabetic Cardiomyopathy. Cardiovasc Res. 2017;113(4):422-430. doi:10.1093/cvr/cvx018

51.   Connor T, Martin SD, Howlett KF, McGee SL. Metabolic Remodelling in Obesity and Type 2 Diabetes: Pathological or Protective Mechanisms in Response to Nutrient Excess? Clin Exp Pharmacol Physiol. 2015;42(1):109-115. doi:10.1111/1440-1681.12315

52.   Russell K, Eriksen M, Aaberge L, Wilhelmsen N, Skulstad H, Gjesdal O, et al. Assessment of Wasted Myocardial Work: A Novel Method to Quantify Energy

Loss Due to Uncoordinated Left Ventricular Contractions. Am J Physiol Heart Circ Physiol. 2013;305(7):H996-1003. doi:10.1152/ajpheart.00191.2013

53.   Samset E. Evaluation of Segmental Myocardial Work in the Left Ventricle ge healthcare website: GE Healthcare; 2017. Available from: https://www.gehealthcare.com/-/media/8cab29682ace4ed7841505f813001e33.pdf.

54.   Lionetti V, Guiducci L, Simioniuc A, Aquaro GD, Simi C, De Marchi D, et al. Mismatch between Uniform Increase in Cardiac Glucose Uptake and Regional Contractile Dysfunction in Pacing-Induced Heart Failure. Am J Physiol Heart Circ Physiol. 2007;293(5):H2747-2756. doi:10.1152/ajpheart.00592.2007

55.   Larsen CK, Aalen JM, Stokke C, Fjeld JG, Kongsgaard E, Duchenne J, et al. Regional Myocardial Work by Cardiac Magnetic Resonance and Non-Invasive Left Ventricular Pressure: A Feasibility Study in Left Bundle Branch Block. Eur Heart J Cardiovasc Imaging. 2020;21(2):143-153. doi:10.1093/ehjci/jez231

56.   Hicks S, Labinskyy N, Piteo B, Laurent D, Mathew JE, Gupte SA, et al. Type Ii Diabetes Increases Mitochondrial DNA Mutations in the Left Ventricle of the Goto-Kakizaki Diabetic Rat. Am J Physiol Heart Circ Physiol. 2013;304(7):H903-915. doi:10.1152/ajpheart.00567.2012

57.   Wende AR, Schell JC, Ha CM, Pepin ME, Khalimonchuk O, Schwertz H, et al. Maintaining Myocardial Glucose Utilization in Diabetic Cardiomyopathy Accelerates Mitochondrial Dysfunction. Diabetes. 2020;69(10):2094-2111. doi:10.2337/db19-1057

58.   Dinh A, Miertschin S, Young A, Mohanty SD. A Data-Driven Approach to Predicting Diabetes and Cardiovascular Disease with Machine Learning. BMC Med Inform Decis Mak. 2019;19(1):211. doi:10.1186/s12911-019-0918-5

59.   Kusunose K, Haga A, Abe T, Sata M. Utilization of Artificial Intelligence in Echocardiography. Circ J. 2019;83(8):1623-1629. doi:10.1253/circj.CJ-19-0420

60.   Yasmin F, Shah SMI, Naeem A, Shujauddin SM, Jabeen A, Kazmi S, et al. Artificial Intelligence in the Diagnosis and Detection of Heart Failure: The Past, Present, and Future. Rev Cardiovasc Med. 2021;22(4):1095-1113. doi:10.31083/j.rcm2204121

61.   Chang A, Cadaret LM, Liu K. Machine Learning in Electrocardiography and Echocardiography: Technological Advances in Clinical Cardiology. Curr Cardiol Rep. 2020;22(12):161. doi:10.1007/s11886-020-01416-9

62.   Seetharam K, Raina S, Sengupta PP. The Role of Artificial Intelligence in Echocardiography. Curr Cardiol Rep. 2020;22(9):99. doi:10.1007/s11886-020-01329-7

63.   Smole T, Zunkovic B, Piculin M, Kokalj E, Robnik-Sikonja M, Kukar M, et al. A Machine Learning-Based Risk Stratification Model for Ventricular Tachycardia and Heart Failure in Hypertrophic Cardiomyopathy. Comput Biol Med. 2021;135:104648. doi:10.1016/j.compbiomed.2021.104648

64.   Butt UM, Letchmunan S, Ali M, Hassan FH, Baqir A, Sherazi HHR. Machine Learning Based Diabetes Classification and Prediction for Healthcare Applications. J Healthc Eng. 2021;2021:9930985. doi:10.1155/2021/9930985

65.   Hathaway QA, Roth SM, Pinti MV, Sprando DC, Kunovac A, Durr AJ, et al. Machine-Learning to Stratify Diabetic Patients Using Novel Cardiac Biomarkers and Integrative Genomics. Cardiovascular diabetology. 2019;18(1):78. doi:10.1186/s12933-019-0879-0

66.   Seetharam K, Shrestha S, Sengupta PP. Artificial Intelligence in Cardiovascular Medicine. Curr Treat Options Cardiovasc Med. 2019;21(6):25. doi:10.1007/s11936-019-0728-1

67.   Seetharam K, Kagiyama N, Sengupta PP. Application of Mobile Health, Telemedicine and Artificial Intelligence to Echocardiography. Echo Res Pract. 2019;6(2):R41-R52. doi:10.1530/ERP-18-0081

TABLES AND TABLE LEGENDS

Table 4.1: Conventional M-Mode Echocardiography

M-mode	5 weeks		12 weeks		20 weeks		25 weeks	
	WT	*Db/Db*	WT	*Db/Db*	WT	*Db/Db*	WT	*Db/Db*
HR	698.4 ± 5	665.3 ± 9*	696.4 ± 11	667.0 ± 14	701.8 ± 6	598.4 ± 27*	684.0 ± 14	634.7 ± 17*
EF	95.8 ± 0.7	94.0 ± 0.9	92.9 ± 1.0	92.6 ± 1.0	93.9 ± 0.7	88.2 ± 1.5*	95.0 ± 0.5	91.2 ± 0.7*
FS	71.2 ± 1.7	67.6 ± 2.0	65.2 ± 2.1	64.3 ± 1.7	66.8 ± 1.4	58.5 ± 2.1*	68.0 ± 1.4	60.0 ± 1.7*
CO	10.2 ± 1.2	10.1 ± 1.0	10.0 ± 0.7	11.3 ± 1.1	10.3 ± 0.9	12.2 ± 0.8	9.3 ± 0.8	11.1 ± 0.8
SV	14.9 ± 1.7	15.2 ± 1.5	14.3 ± 1.0	18.6 ± 1.5*	14.8 ± 1.3	21.1 ± 1.5*	13.5 ± 1.0	19.0 ± 2.0*
LV Mass	69.4 ± 4.1	73.7 ± 3.1	79.4 ± 4.2	117.7 ± 4.1*	92.0 ± 5.4	134.2 ± 6.9*	100.1 ± 7.6	144.9 ± 6.3*
LVAW;s	1.8 ± 0.03	1.8 ± 0.04	1.7 ± 0.07	2.0 ± 0.05*	1.9 ± 0.05	2.0 ± 0.04*	1.9 ± 0.05	2.1 ± 0.06*
LVAW;d	1.1 ± 0.04	1.1 ± 0.04	1.2 ± 0.04	1.3 ± 0.04	1.3 ± 0.04	1.5 ± 0.04*	1.3 ± 0.04	1.5 ± 0.04*
LVPW;s	1.8 ± 0.07	1.9 ± 0.05	1.9 ± 0.05	2.2 ± 0.06*	2.0 ± 0.06	2.1 ± 0.09	2.1 ± 0.08	2.3 ± 0.06
LVPW;d	1.3 ± 0.05	1.3 ± 0.07	1.3 ± 0.09	1.7 ± 0.07*	1.5 ± 0.06	1.6 ± 0.09	1.6 ± 0.07	1.8 ± 0.07
LVED;s	0.6 ± 0.04	0.7 ± 0.06	0.8 ± 0.04	0.9 ± 0.06	0.7 ± 0.05	1.1 ± 0.08*	0.7 ± 0.04	0.9 ± 0.05*
LVED;d	2.1 ± 0.1	2.2 ± 0.09	2.1 ± 0.06	2.4 ± 0.08*	2.1 ± 0.08	2.6 ± 0.09*	2.1 ± 0.06	2.4 ± 0.1*
LVEV;s	0.6 ± 0.1	1.1 ± 0.3	1.2 ± 0.2	1.6 ± 0.3	1.1 ± 0.2	3.3 ± 0.6*	0.7 ± 0.09	1.6 ± 0.2*
LVEV;d	15.7 ± 1.9	16.3 ± 1.7	15.6 ± 1.2	20.1 ± 1.7*	15.8 ± 1.5	24.4 ± 2.0*	13.9 ± 0.9	19.5 ± 1.9*

Table 4.1: Conventional m-Mode echocardiography. Progressive cardiac dysfunction is observable in *Db/Db* mice at 12, 20, and 25 weeks of age. "*" denotes significantly different from WT. Data are presented as mean ± standard error of the mean (SEM). HR; heart rate, EF; ejection fraction, FS; fractional shortening, CO; cardiac output, SV; stroke volume, LV; left ventricle, LVAW;s; LV anterior wall systolic thickness, LVAW;d; LV anterior wall diastolic thickness, LVPW;s; LV posterior wall systolic thickness, LVPW;d; LV posterior wall diastolic thickness, LVED;s; LV end-systolic diameter, LVED; d; LV end-diastolic diameter, LVEV;s; LV end-systolic volume, LVEV;d; LV end-diastolic volume.

Table 4.2: Ranking of Regions most representative of overt cardiac contractile dysfunction at 5, 12, 20, and 25 weeks of age.

Timepoint (weeks)	Region	Test Accuracy
5	Septal	84
	Anterior	82
	Posterior Free	76
	Posterior	71
	Anterior Free	71
	Free	67
	Septal	84
	Anterior	82
	Posterior Free	76
12	Anterior Free	98
	Septal	91
	Anterior	89
	Posterior Free	84
	Posterior	78
	Free	78
	Anterior Free	98
	Septal	91
	Anterior	89
20	Septal	93
	Anterior	93
	Posterior	89
	Anterior Free	87
	Free	84
	Posterior Free	78
	Septal	93
	Anterior	93
	Posterior	89
25	Septal	98
	Anterior Free	95
	Anterior	91
	Posterior Free	91
	Posterior	78
	Free	76
	Septal	98
	Anterior Free	95
	Anterior	0.91

Table 4.2: Ranking of Regions most representative of overt cardiac contractile dysfunction at 5, 12, 20, and 25 weeks of age. Testing accuracies of each region ranked by its ability to identify cardiac contractile dysfunction associated with diabetes mellitus.

Table 4.3: Ranking of segments most representative of overt cardiac contractile dysfunction at 5, 12, 20, and 25 weeks of age.

Timepoint (weeks)	Region	Test Accuracy
5	InfFreeWall	76
	PostSeptal	73
	AntFree	71
	LatWall	71
	AntSeptum	67
	PostWall	49
	InfFreeWall	76
	PostSeptal	73
	AntFree	71
12	LatWall	98
	AntSeptum	96
	PostWall	93
	AntFree	84
	InfFreeWall	82
	PostSeptal	76
	LatWall	98
	AntSeptum	96
	PostWall	93
20	AntSeptum	96
	LatWall	93
	PostSeptal	89
	PostWall	89
	AntFree	71
	InfFreeWall	71
	AntSeptum	96
	LatWall	93
	PostSeptal	89
25	AntFree	96
	AntSeptum	93
	LatWall	93
	InfFreeWall	78
	PostSeptal	60
	PostWall	60
	AntFree	96
	AntSeptum	93
	LatWall	93

Table 4.3: Ranking of segments most representative of overt cardiac contractile dysfunction at 5, 12, 20, and 25 weeks of age. Testing accuracies of each segment ranked by its ability to identify cardiac contractile dysfunction associated with diabetes mellitus.

FIGURES AND FIGURE LEGENDS

Figure 4.1: Schematic of experimental design and the machine learning pipeline.

A.
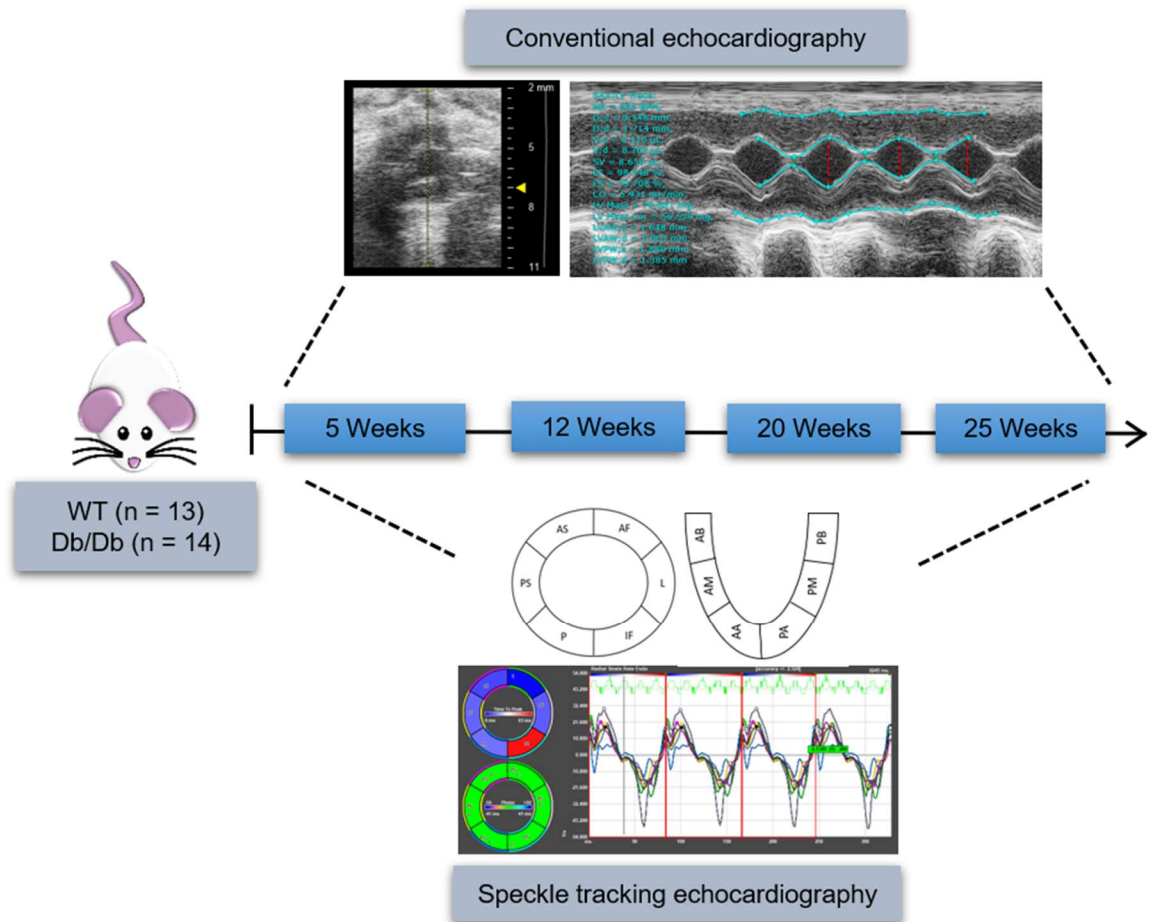
Figure 4.1
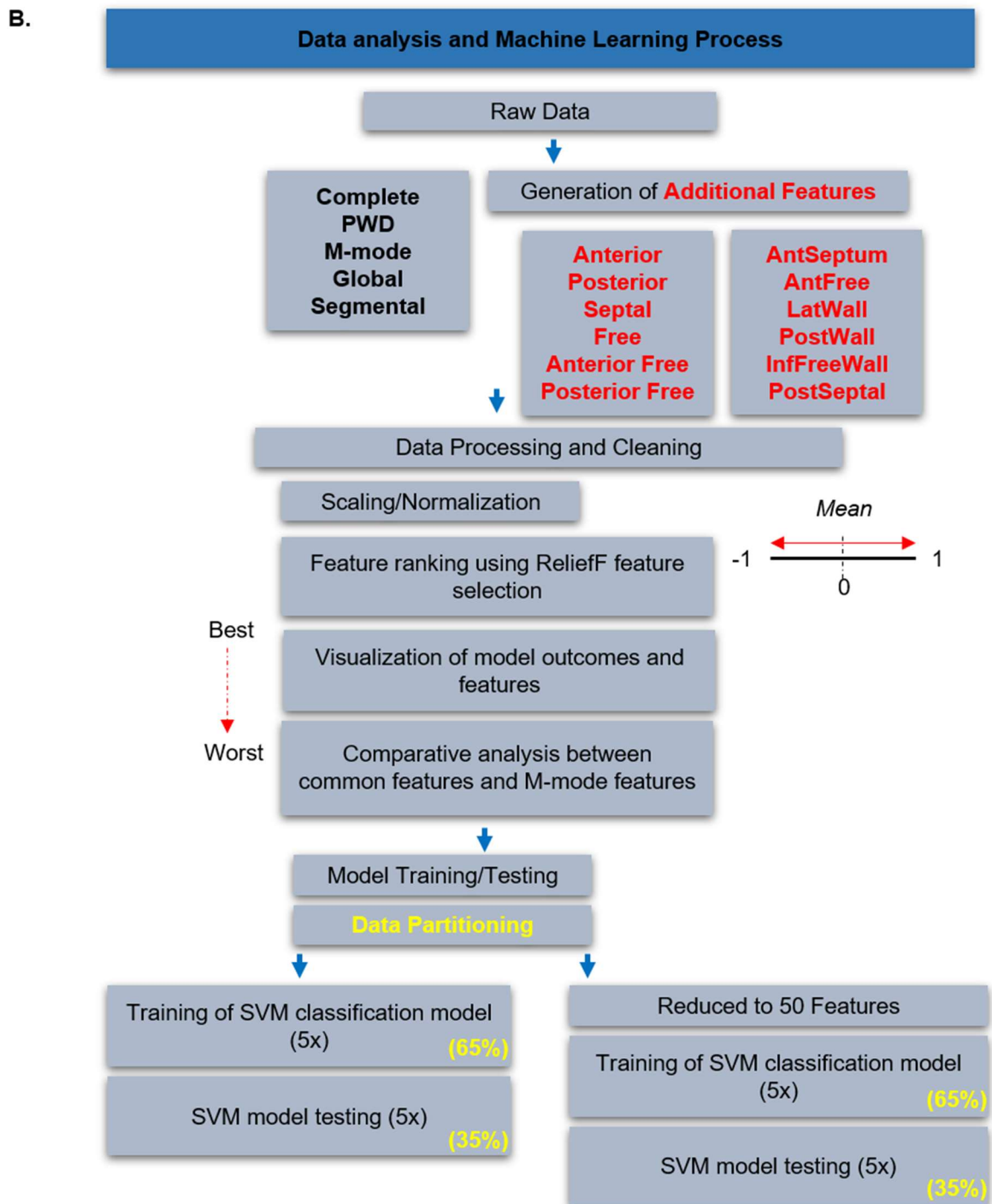
Figure 4.1: Schematic of experimental design and the machine learning pipeline. (A) WT (n = 13) and *Db/Db* mice (n = 14) underwent conventional M-mode and speckle tracking strain-based echocardiography assessments at 5, 12, 20, and 25 weeks of age. (B) Data was segregated into 5 raw data sets including both M-mode and stress-strain assessments, as well as 12 datasets generated using stress-strain segmental values. Feature selection and machine learning using a ReliefF algorithm and SVM model were used to determine the reliability of conventional echocardiography as a predictor of T2DM, and further assess the spatial and temporal progression of cardiovascular dysfunction. WT; Wild-type, PWD; pulse-wave doppler, SVM; support vector machine, T2DM; type 2 diabetes mellitus.

Figure 4.2: SVM Model Testing Accuracies
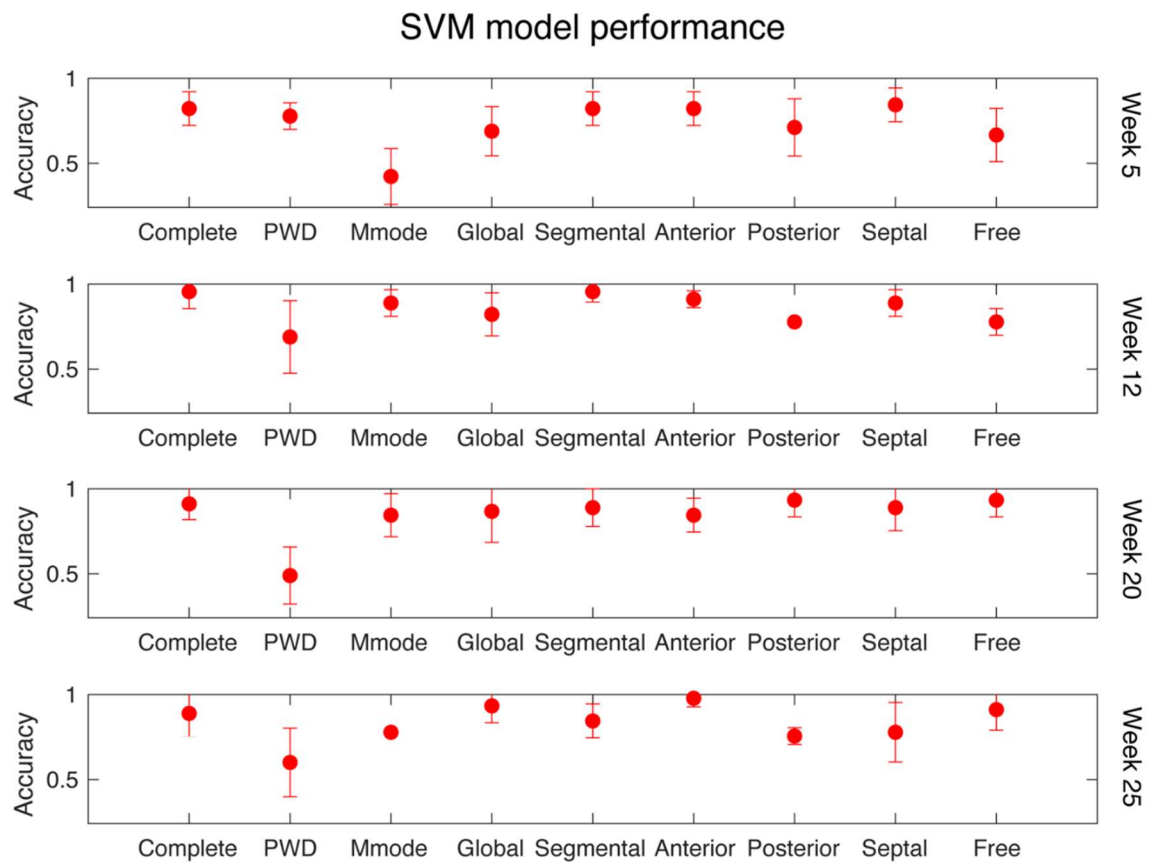
Figure 4.2: SVM model testing accuracies were demonstrated for the complete, PWD, M-mode, Global, Segmental, Anterior, Posterior, Septal, and Free datasets at 5, 12, 20, and 25 weeks of age. SVM; support vector machine, PWD; pulse-wave doppler. Values are shown as means ± SEM.

Figure 4.3: Machine Learning and Feature Reduction
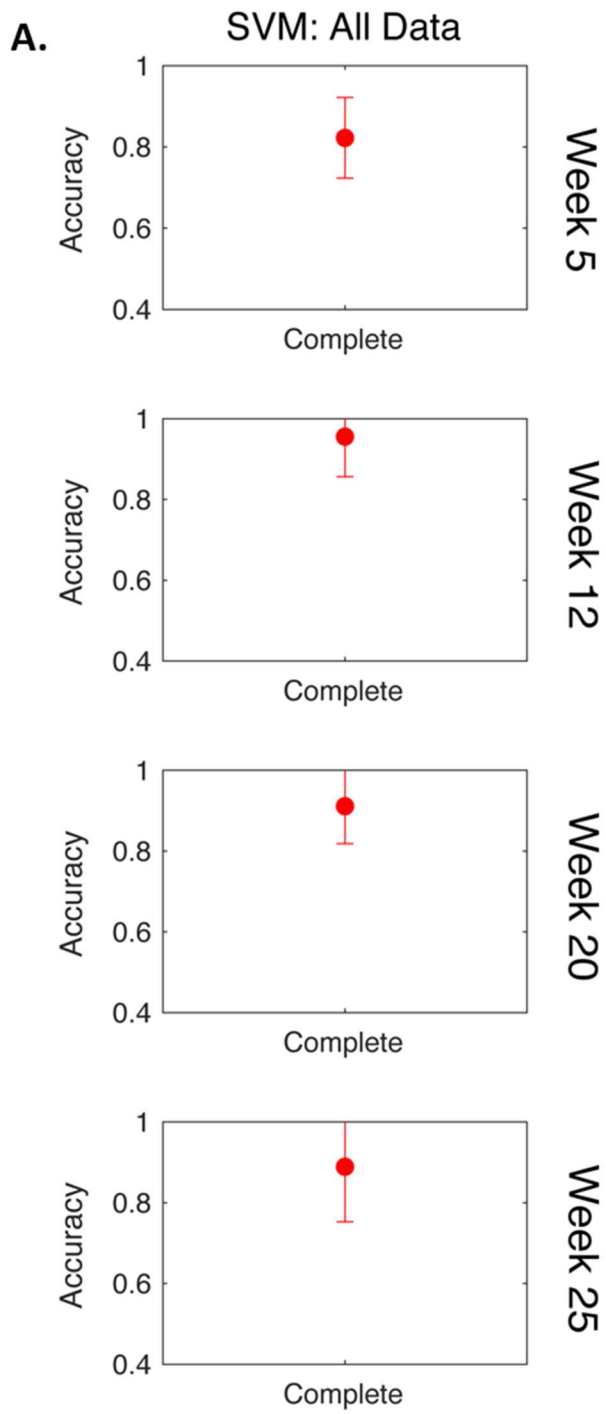
Figure 4.3:
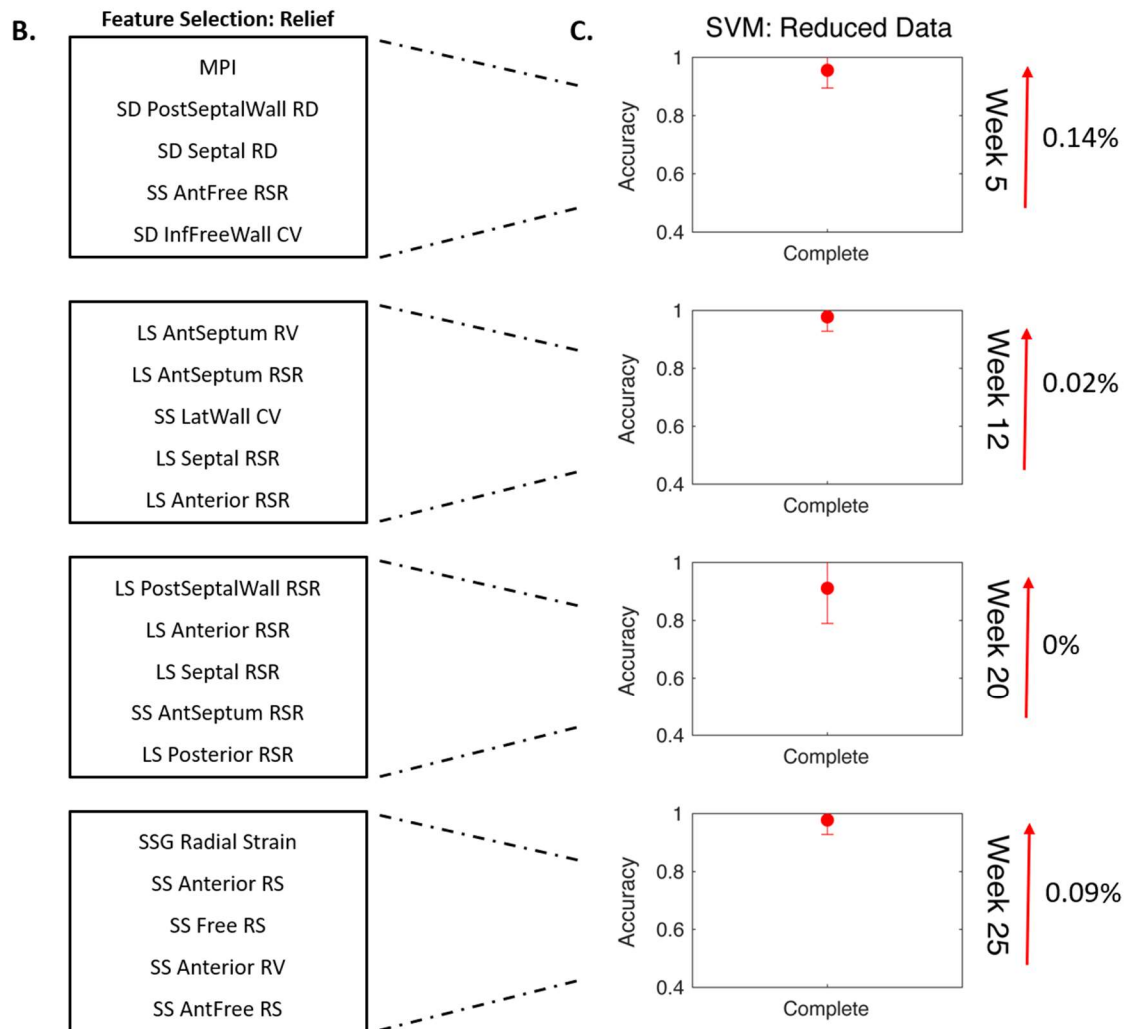
Figure 4.3: Machine learning and feature reduction. (A) Testing accuracies for the complete dataset at 5, 12, 20, and 25 weeks. (B) Feature selection using the ReliefF algorithm ranked all available features by importance to the classification model. (C) Testing accuracy for the top 50 features most descriptive of cardiac contractile dysfunction for the complete dataset, and resulting change in testing accuracy for the reduced dimensionality dataset (B). Values are shown as means ± SEM.

Figure 4.4: Spatial and temporal progression of cardiovascular dysfunction at 5 weeks.
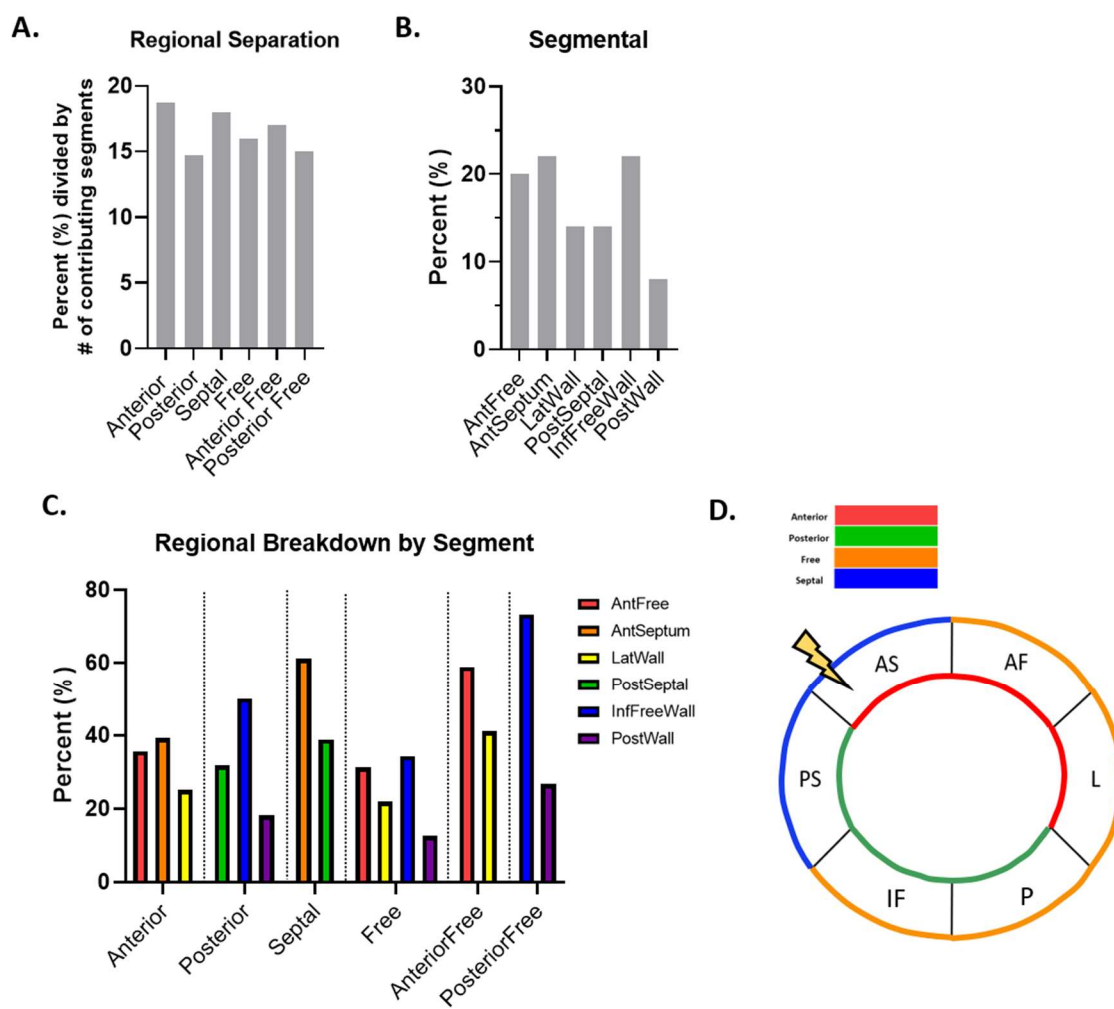
Figure 4.4: Spatial and temporal progression of cardiovascular dysfunction at 5 weeks. (A) Regional separation as calculated with segmental values demonstrates the percent each region is represented in the top 50 features most descriptive of cardiac contractile dysfunction, listed with the regions ranked in order of testing accuracy. (B) The 6 segments were represented as a percentage of all segmental values in the top 50 features most descriptive of cardiac contractile dysfunction, and were ranked in order of testing accuracy. (C) Each region was broken down into its contributing segments relative to the percent contributed by the region. (D) The locale of greatest impact.

Figure 4.5: Spatial and temporal progression of cardiovascular dysfunction at 12 weeks.
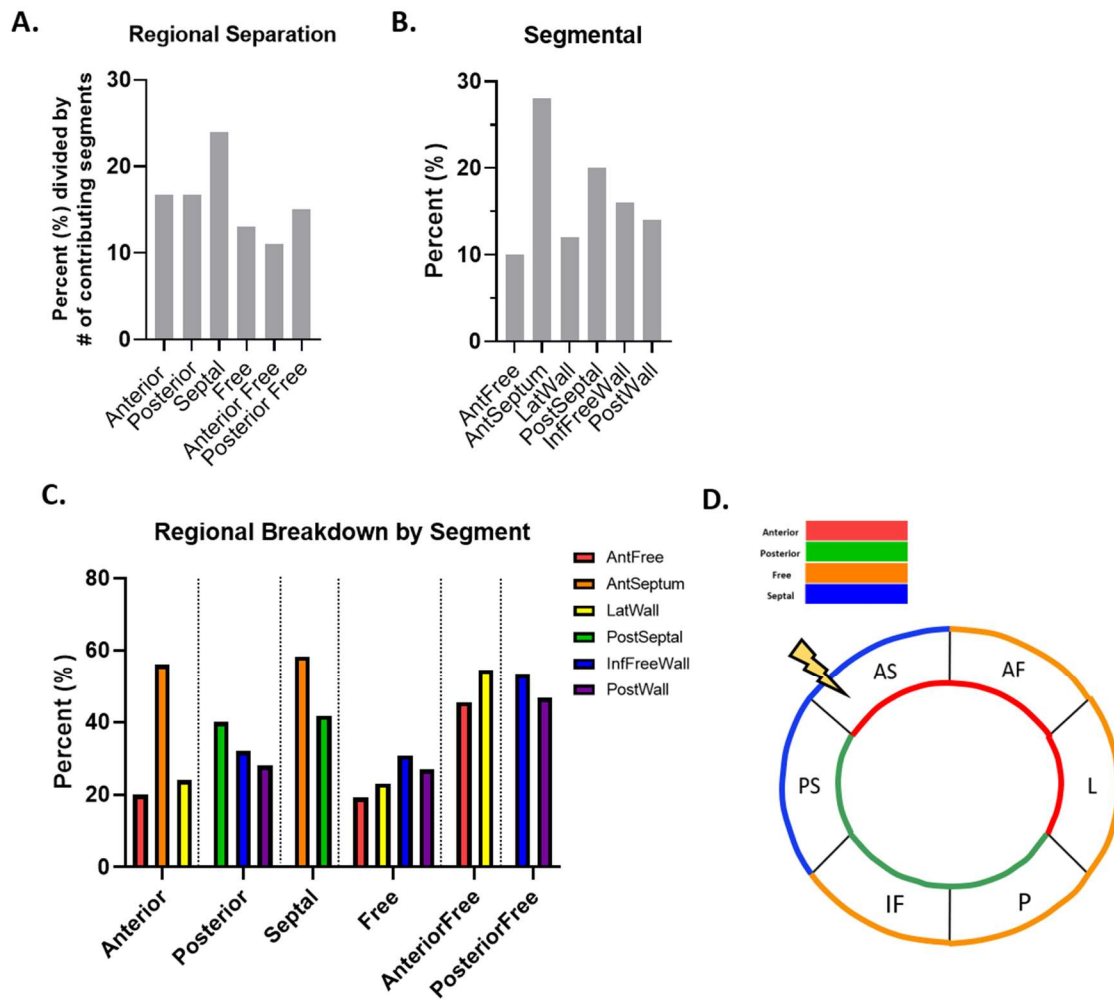
Figure 4.5: Spatial and temporal progression of cardiovascular dysfunction at 12 weeks. (A) Regional representation as calculated with segmental values demonstrates the percent each region is represented in the top 50 features most descriptive of cardiac contractile dysfunction, listed with the regions ranked in order of testing accuracy. (B) The 6 segments were represented as a percentage of all segmental values in the top 50 features most descriptive of cardiac contractile dysfunction, and were ranked in order of testing accuracy. (C) Each region was broken down into its contributing segments relative to the percent contributed by the region. (D) The locale of greatest impact.

Figure 4.6: Spatial and temporal progression of cardiovascular dysfunction at 20 weeks.
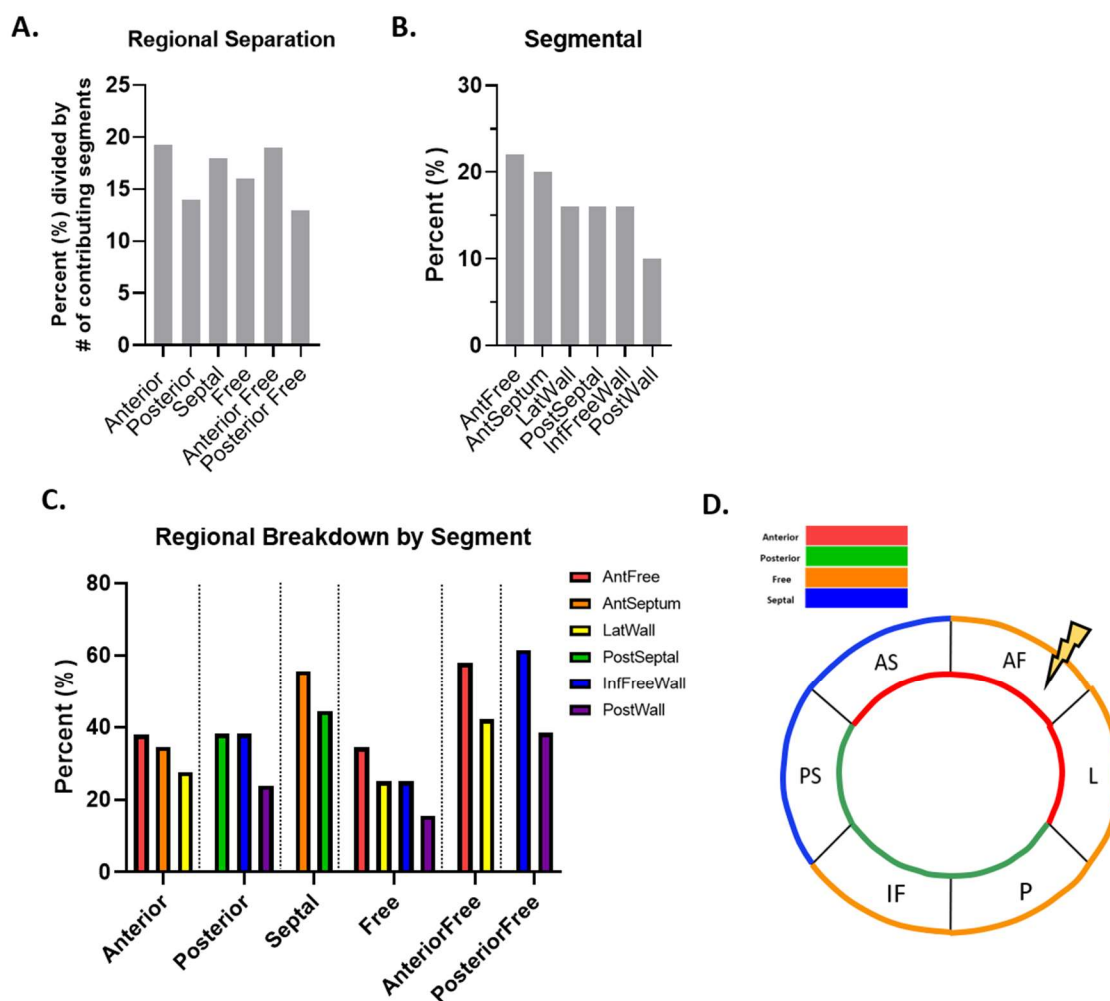
Figure 4.6: Spatial and temporal progression of cardiovascular dysfunction at 20 weeks. (A) Regional representation as calculated with segmental values demonstrates the percent each region was represented in the top 50 features most descriptive of cardiac contractile dysfunction, listed with the regions ranked in order of testing accuracy. (B) The 6 segments were represented as a percentage of all segmental values in the top 50 features most descriptive of cardiac contractile dysfunction, and were ranked in order of testing accuracy. (C) Each region was broken down into its contributing segments relative to the percent contributed by the region. (E) The locale of greatest impact.

Figure 4.7: Spatial and temporal progression of cardiovascular dysfunction at 25 weeks.
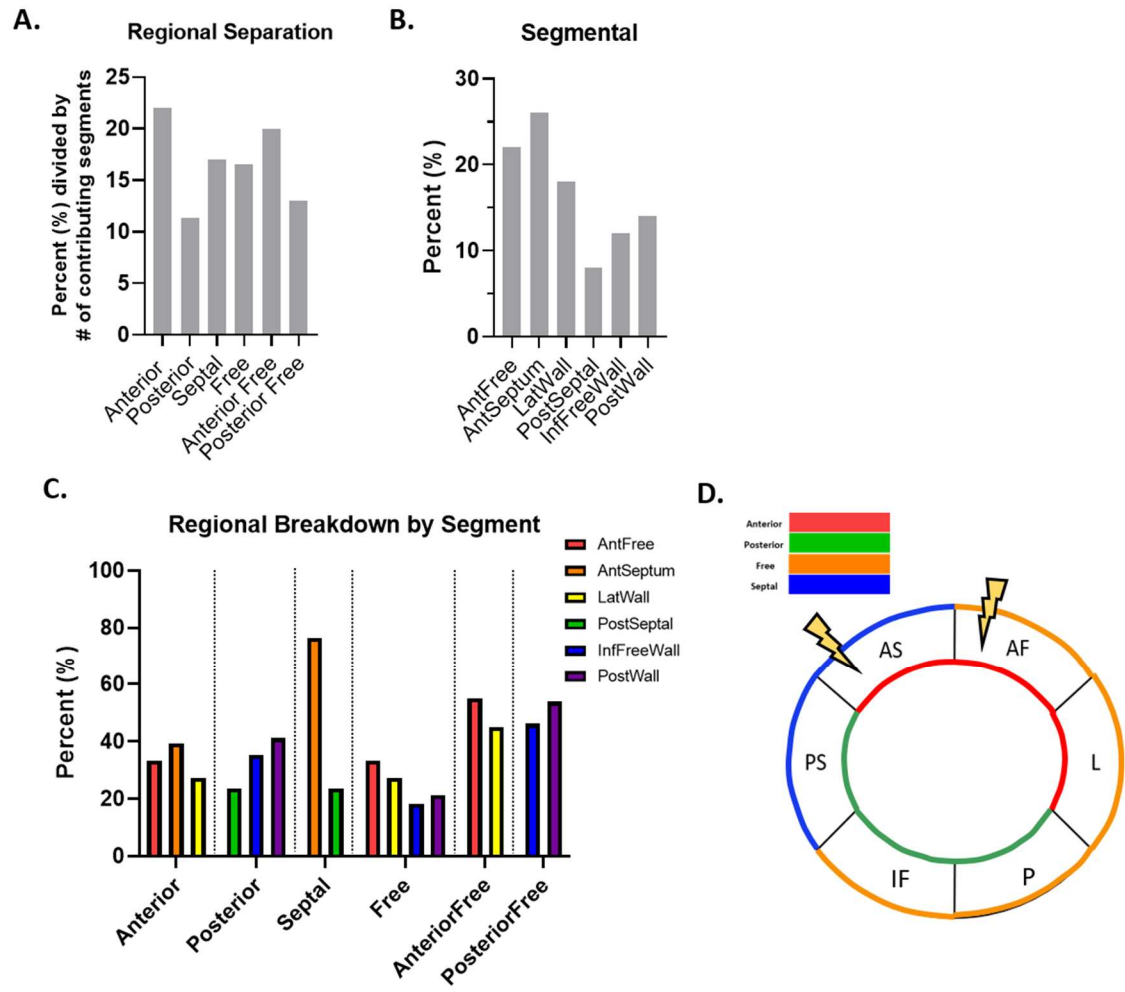
Figure 4.7: Spatial and temporal progression of cardiovascular dysfunction at 25 weeks. (A) Regional representation as calculated with segmental values demonstrates the percent each region was represented in the top 50 features most descriptive of cardiac contractile dysfunction, listed with the regions ranked in order of testing accuracy. (B) The 6 segments were represented as a percentage of all segmental values in the top 50 features most descriptive of cardiac contractile dysfunction, and were ranked in order of testing accuracy. (C) Each region was broken down into its contributing segments relative to the percent contributed by the region. (E) The locale of greatest impact.

Figure 4.8: Summary of contributions and future directions.
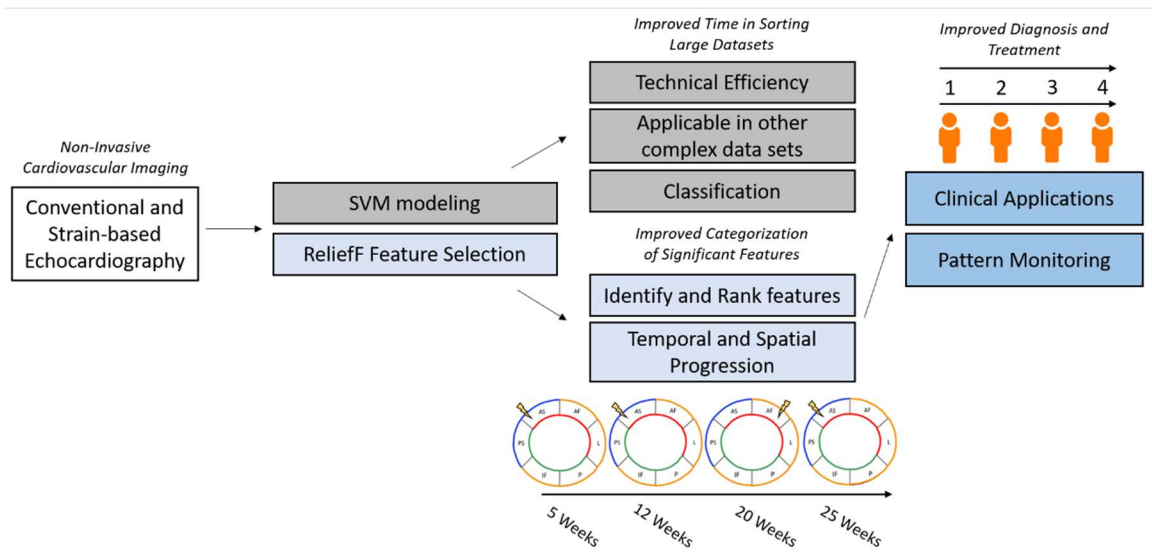
Figure 4.8: Summary of contributions and future directions. Conventional and strain-based echocardiography can be analyzed using machine learning and ReliefF-based feature selection algorithms. Supervised modeling allows for increased technical efficiency and unbiased ranking of features by importance to class prediction, and can be applied in multiple situations concerning large datasets. The ReliefF feature selection algorithm provides an unbiased approach to identify and rank features in order of how important they were for classification and provide insight into the temporal and spatial progression of T2DM, through segmental analysis. The identification of patterns of spatial and temporal features critical to disease progression and development could improve current diagnostic capabilities of cardiovascular contractile dysfunction in T2DM.

SUPPLEMENTAL TABLES AND TABLE LEGENDS

Supplemental Table S4.1: Performance of supervised machine learning SVM models for all datasets at 5, 12, 20, and 25 weeks of age.

Timepoint (weeks)	Data Subset	Training Accuracy	Std. Deviation	Test Accuracy	F-score
5	Complete	0.93	0.02	0.82	0.76
	PWD	0.84	0.06	0.78	0.78
	M-mode	0.60	0.07	0.42	0.36
	Global	0.77	0.07	0.69	0.72
	Segmental	0.86	0.12	0.82	0.79
	Anterior	0.69	0.09	0.82	0.79
	Posterior	0.73	0.14	0.71	0.68
	Septal	0.83	0.10	0.84	0.83
	Free	0.68	0.09	0.67	0.64
12	Complete	0.91	0.03	0.96	0.95
	PWD	0.78	0.12	0.69	0.68
	M-mode	0.96	0.05	0.89	0.86
	Global	0.82	0.09	0.82	0.80
	Segmental	0.94	0.04	0.96	0.93
	Anterior	0.92	0.06	0.91	0.91
	Posterior	0.84	0.02	0.78	0.73
	Septal	0.93	0.05	0.89	0.87
	Free	0.82	0.10	0.78	0.70
20	Complete	0.91	0.06	0.91	0.91
	PWD	0.59	0.07	0.49	0.37
	M-mode	0.77	0.05	0.84	0.83
	Global	0.86	0.05	0.87	0.85
	Segmental	0.88	0.02	0.89	0.90
	Anterior	0.91	0.05	0.84	0.81
	Posterior	0.84	0.07	0.93	0.94
	Septal	0.88	0.05	0.89	0.89
	Free	0.81	0.05	0.93	0.93
25	Complete	0.97	0.03	0.89	0.86
	PWD	0.66	0.09	0.60	0.59
	M-mode	0.82	0.09	0.78	0.75
	Global	0.88	0.07	0.93	0.95
	Segmental	0.93	0.05	0.84	.83
	Anterior	0.98	0.03	0.98	0.97
	Posterior	0.76	0.11	0.76	0.63
	Septal	0.80	0.09	0.78	.77
	Free	0.83	0.09	0.91	.87

Supplemental Table S4.1: Performance of supervised machine learning SVM models for all datasets at 5, 12, 20, and 25 weeks of age. Training accuracies and the associated standard deviations, test accuracies, and F-scores are reported. SVM; support vector machine, PWD; pulse-wave doppler.

Supplemental Table S4.2: SVM Model Performance "Relevant" Features.

Timepoint (weeks)	Data Subset	Training Accuracy	Testing Accuracy	Number of Features	Training Accuracy	Std. Deviation	Testing Accuracy	F-score
5	Complete	0.93	0.82	158	0.96	0.02	1	1
12	Complete	0.91	0.96	319	0.93	0.02	0.91	0.90
20	Complete	0.91	0.91	330	0.87	0.06	0.93	0.93
25	Complete	0.97	0.89	288	0.94	0	1	1

Supplemental Table S4.2: SVM Model Performance "Relevant" Features. A ReliefF score of above zero was used to select relevant features and reduce dataset dimensionality. Training and testing accuracies are reported for both the full and reduced datasets.

Supplemental Table S4.3: SVM Model Performance of Reduced Dimensional Dataset Containing Top 50 Features.

Timepoint (weeks)	Data Subset	Training Accuracy	Testing Accuracy	Number of Features	Training Accuracy	Std. Deviation	Testing Accuracy	F-score
5	Complete	0.93	0.82	50	1	0	0.96	0.94
12	Complete	0.91	0.96	50	0.92	0.05	0.98	0.97
20	Complete	0.91	0.91	50	0.96	0.05	0.91	0.90
25	Complete	0.97	0.89	50	0.97	0.03	0.98	0.97

Supplemental Table S4.3: SVM Model Performance of Reduced Dimensional Dataset Containing Top 50 Features. The top 50 features were taken and tested as an independent dataset for each timepoint. Training and testing accuracies are reported for both the full and reduced datasets.

Supplemental Table S4.4: Performance of supervised machine learning SVM models for segmental datasets at 5, 12, 20, and 25 weeks of age.

Timepoint (weeks)	Data Subset	Training Accuracy	Std. Deviation	Test Accuracy	F-score
5	AntFree	0.80	0.06	0.71	0.68
	AntSeptum	0.64	0.16	0.67	0.69
	InfFreeWall	0.69	0.08	0.76	0.60
	LatWall	0.63	0.09	0.71	0.68
	PostSeptal	0.68	0.12	0.73	0.71
	PostWall	0.54	0.07	0.49	0.48
	Anterior Free	0.80	0.12	0.71	0.68
	Posterior Free	0.91	0.09	0.76	0.75
12	AntFree	0.83	0.11	0.84	0.83
	AntSeptum	0.92	0.03	0.96	0.96
	InfFreeWall	0.70	0.05	0.82	0.80
	LatWall	0.93	0.12	0.98	0.98
	PostSeptal	0.87	0.09	0.76	0.71
	PostWall	0.83	0.09	0.93	0.93
	Anterior Free	0.93	0.02	0.98	0.98
	Posterior Free	0.90	0.08	0.84	0.84
20	AntFree	0.80	0.07	0.71	0.68
	AntSeptum	0.80	0.08	0.96	0.96
	InfFreeWall	0.87	0.03	0.71	0.64
	LatWall	0.88	0.07	0.93	0.93
	PostSeptal	0.90	0.06	0.89	0.90
	PostWall	0.79	0.10	0.89	0.85
	Anterior Free	0.86	0.03	0.87	0.81
	Posterior Free	0.77	0.11	0.78	0.79
25	AntFree	0.90	0.05	0.96	0.94
	AntSeptum	0.83	0.04	0.93	0.91
	InfFreeWall	0.76	0.10	0.78	0.68
	LatWall	0.90	0.06	0.93	0.95
	PostSeptal	0.82	0.06	0.60	0.59
	PostWall	0.73	0.07	0.60	0.51
	Anterior Free	0.92	0.05	0.95	0.95
	Posterior Free	0.80	0.09	0.91	0.89

Supplemental Table S4.4: Performance of supervised machine learning SVM models for segmental datasets at 5, 12, 20, and 25 weeks of age. Training accuracies and the associated standard deviations, test accuracies, and F-scores are reported. SVM; support vector machine.

SUPPLEMENTAL FIGURES AND FIGURE LEGENDS

Supplemental Figure S4.1: Top five M-mode features identified by the ReliefF algorithm for each timepoint confirm progression of disease as strong indicators of class.

Supplemental Figure S4.1

Week 12

Supplemental Figure S4.1

K.

L.

M.

N.

O.

Week 20

242
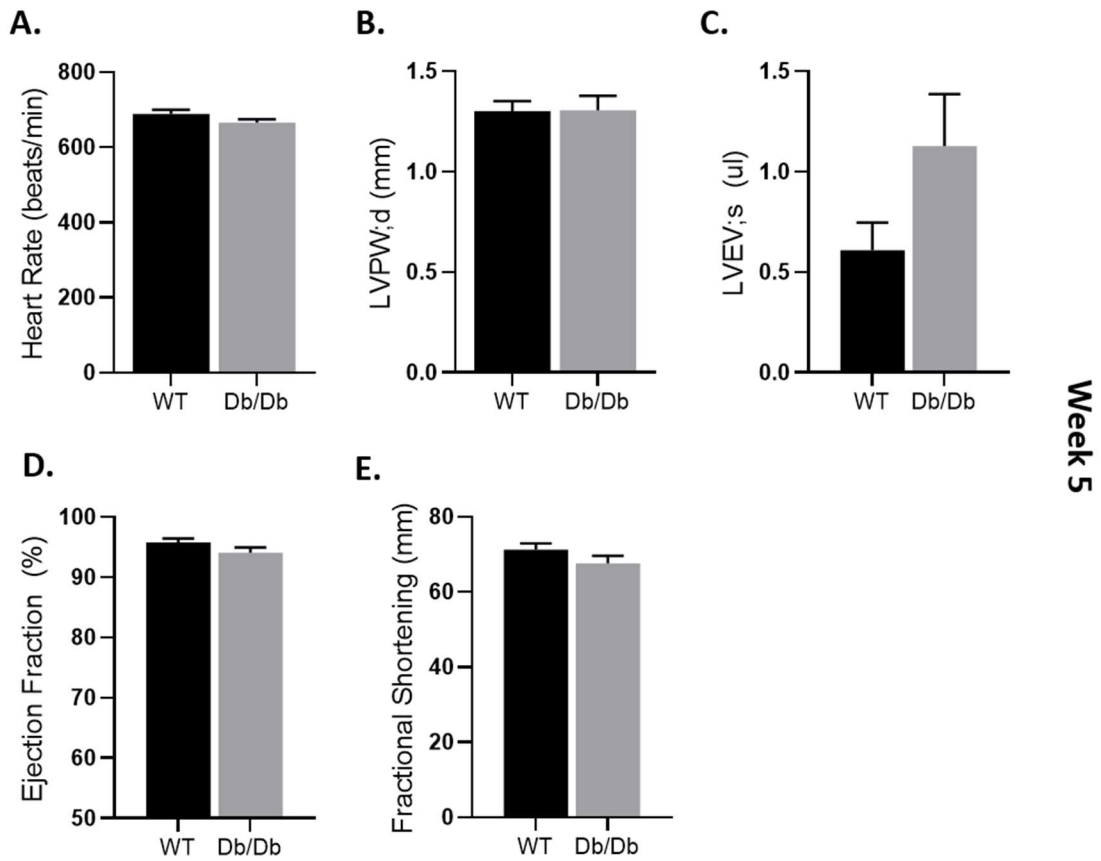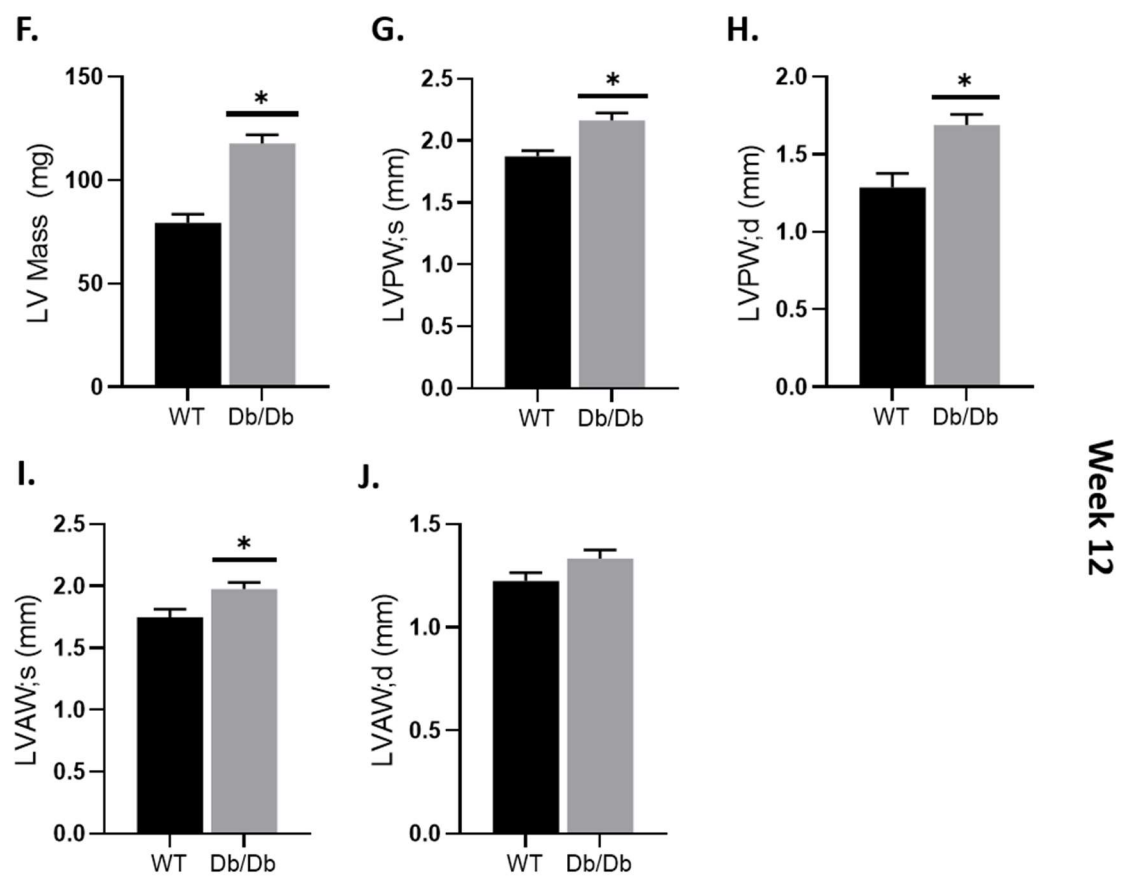
Supplemental Figure S4.1
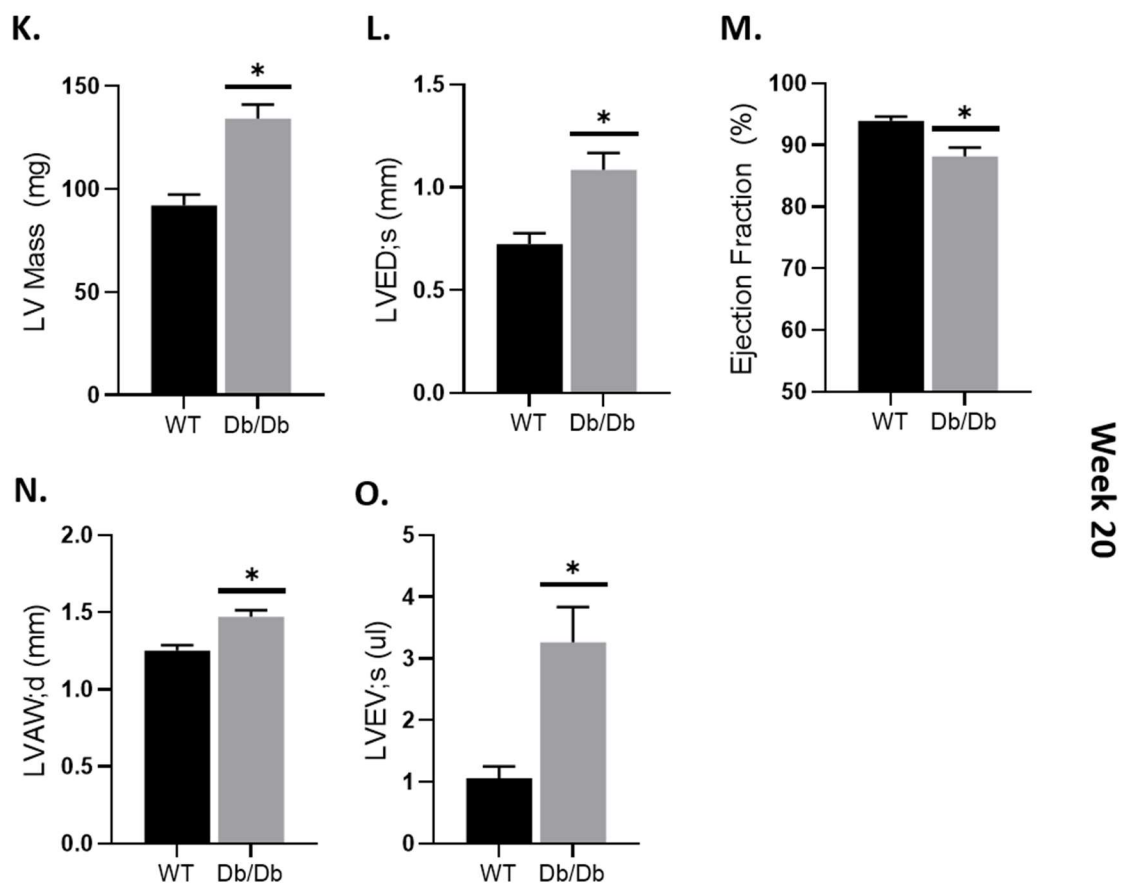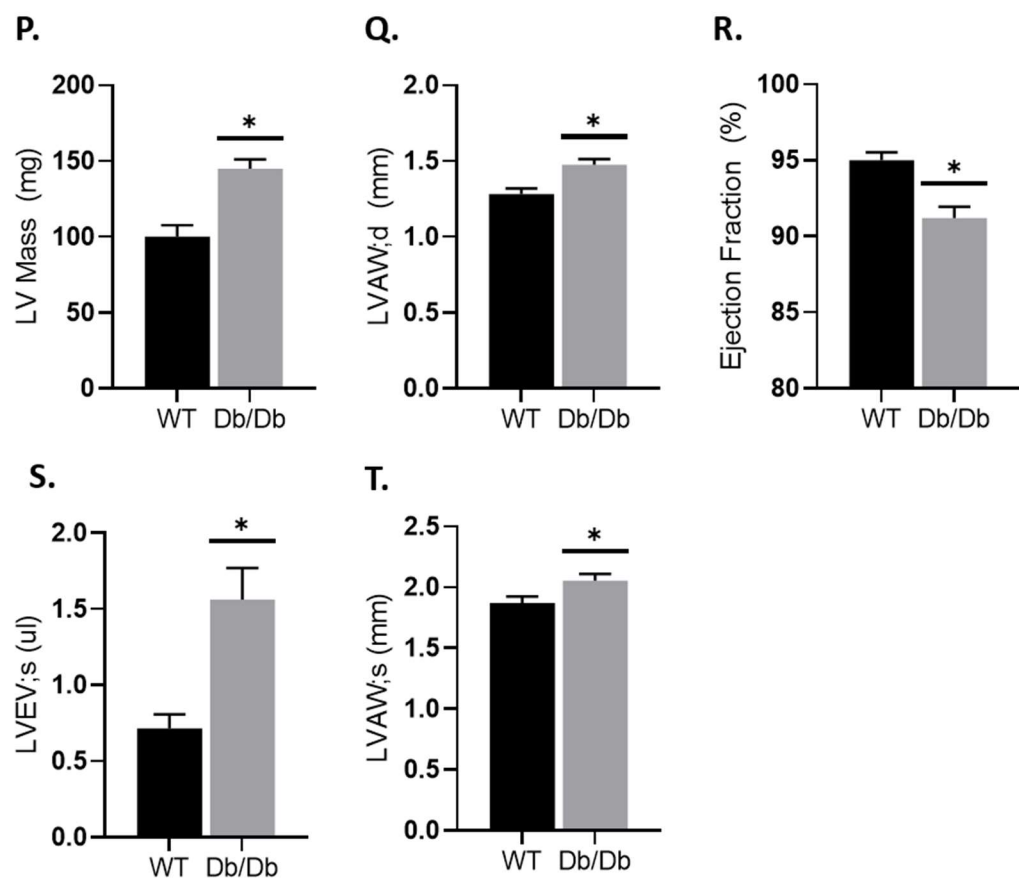
Supplemental Figure S4.1*:* Top five M-mode features identified by the ReliefF algorithm for each timepoint confirm progression of disease as strong indicators of class. The 5 echocardiography features identified to be most descriptive of cardiac contractile dysfunction selected for 5 weeks; HR, LVPW;d, LVEV;s, EF, FS (A-E), 12 weeks; LV Mass, LVPW;s, LVPW;d, LVAW;s, LVAW;d (F-J), 20 weeks; LV Mass, LVED;s, EF, LVAW;d, LVEV;s (F-G), and 25 weeks; LV Mass, LVAW;d, EF, LVEV;s, LVAW; s (K-O). HR; heart rate, LV; left ventricle, LVPW;d; LV posterior wall diastolic thickness, LVEV;s; LV end-systolic volume, EF; ejection fraction, FS; fractional shortening, LVPW;s; LV posterior wall systolic thickness, LVED;s; LV end-systolic diameter, LVAW;d; LV anterior wall diastolic thickness. "n" is defined as biological replicates. Figure panels are based in 1 independent experiment. WT and *Db/Db* data were analyzed using a Student's T-test. " * " Denotes P ≤ 0.05 vs. WT. Values are shown as means ± SEM.

Supplemental Figure S4.2: Analysis in Graphpad of the 5 echocardiography features identified to be most descriptive of cardiac contractile dysfunction for the complete dataset at each timepoint.
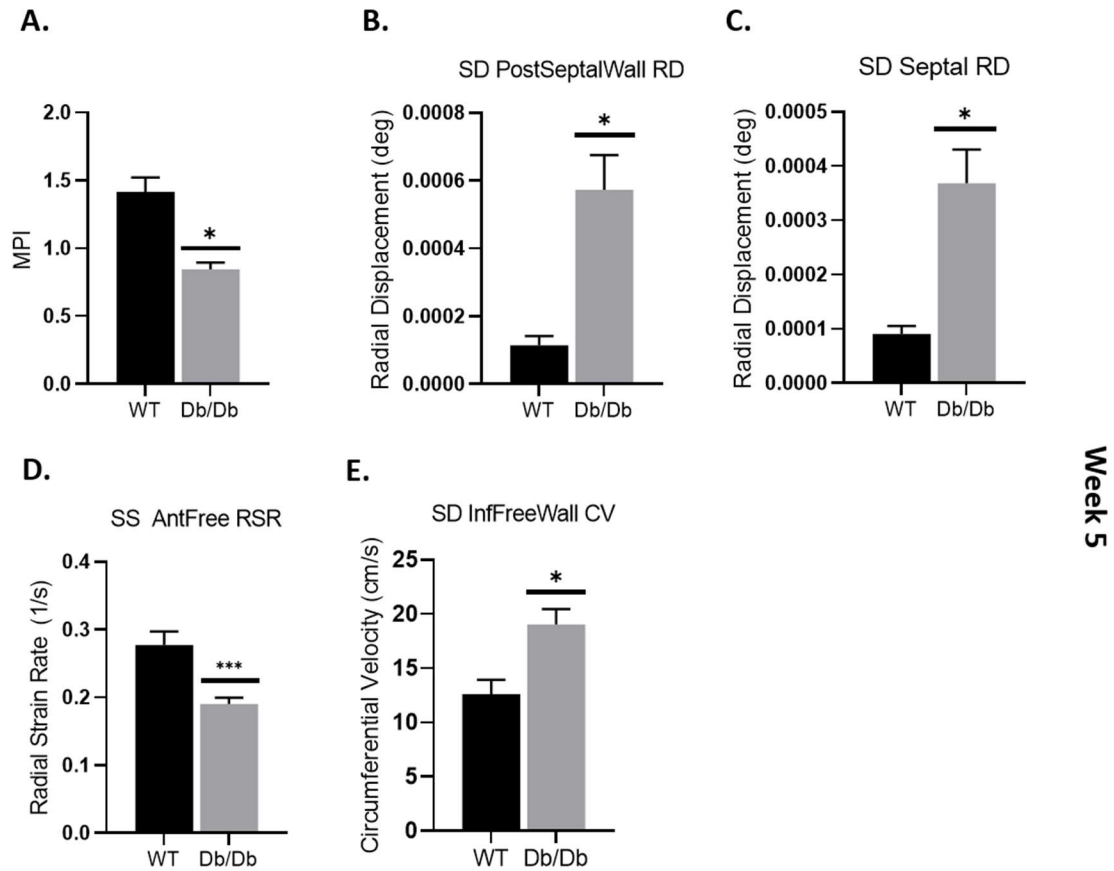
Supplemental Figure S4.2:

Week 12

Supplemental Figure S4.2:
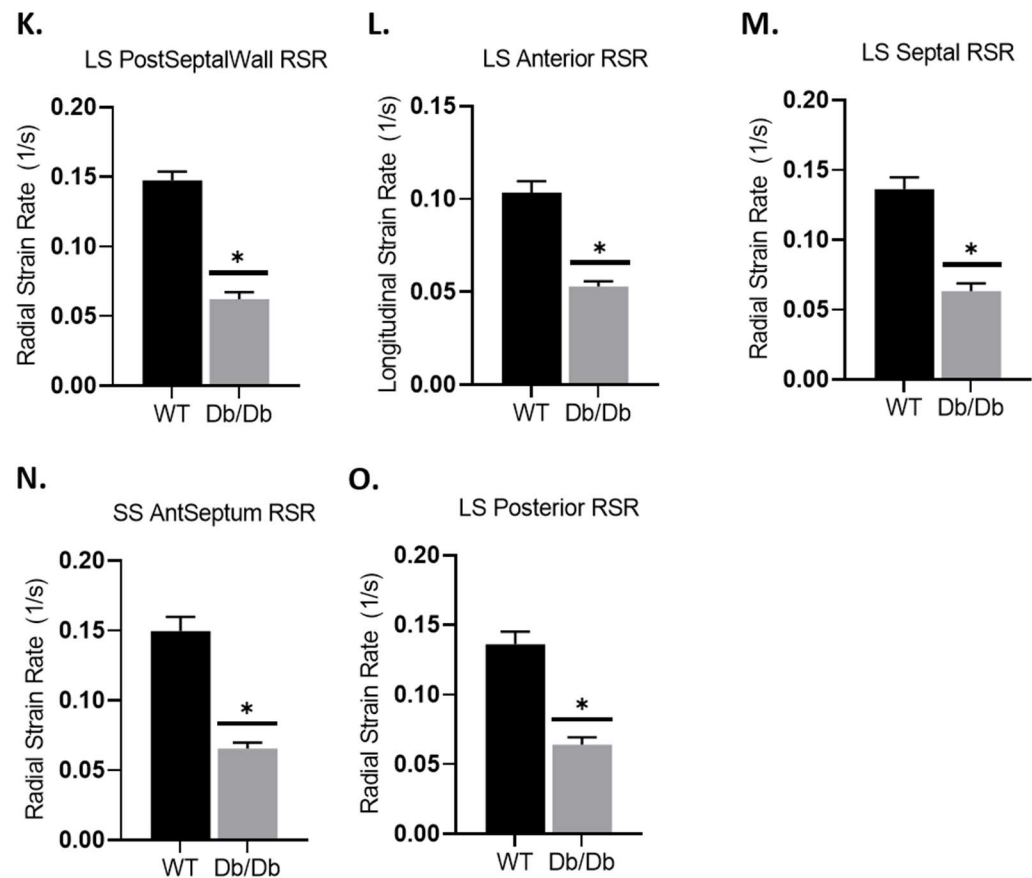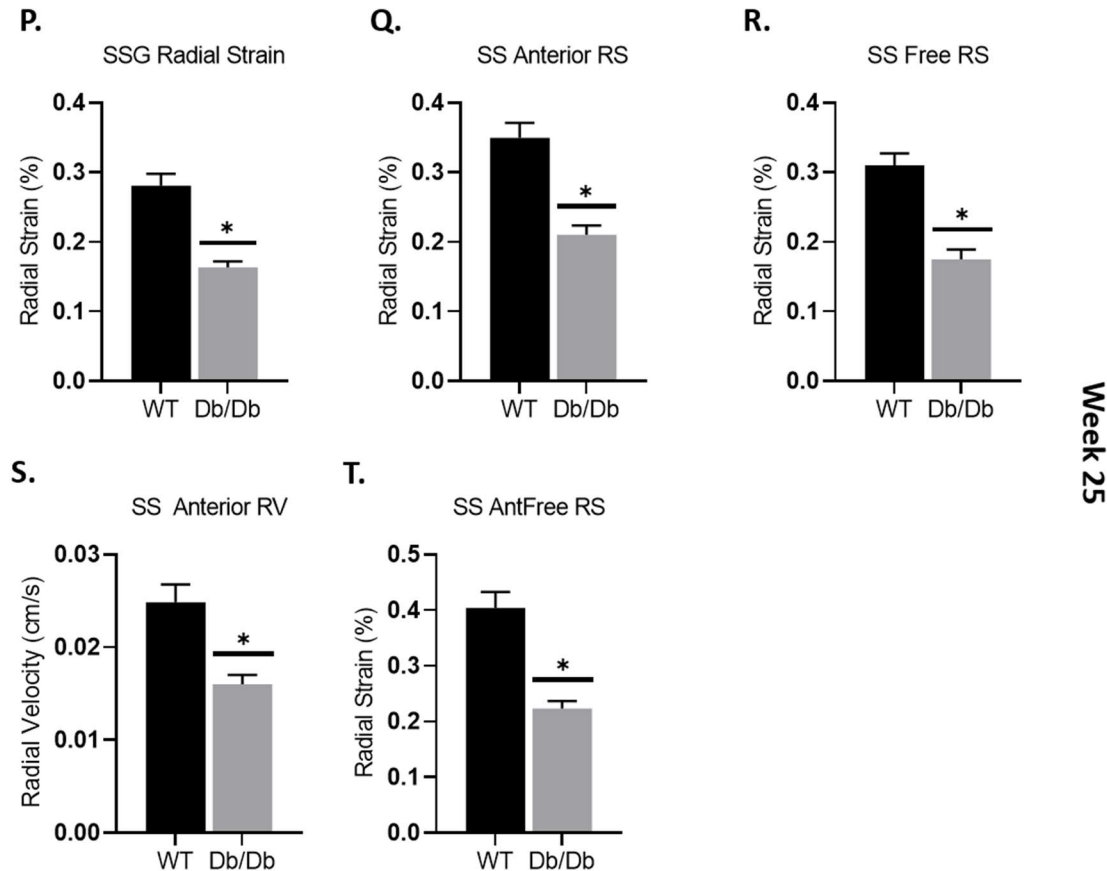
K. LS PostSeptalWall RSR

L. LS Anterior RSR

M. LS Septal RSR

N. SS AntSeptum RSR

O. LS Posterior RSR

Week 20

Supplemental Figure S4.2:

P. SSG Radial Strain

Q. SS Anterior RS

R. SS Free RS

S. SS Anterior RV

T. SS AntFree RS

Week 25

248

Supplemental Figure S4.2: Analysis in Graphpad of the 5 echocardiography features identified to be most descriptive of cardiac contractile dysfunction for the complete dataset at each timepoint. (A-E) The 5 echocardiography features identified to be most descriptive of cardiac contractile dysfunction for 5 weeks, (F-J) 12 weeks, (K-O) 20 weeks, and (P-T) 25 weeks. "n" is defined as biological replicates. Figure panels are based in 1 independent experiment. WT and *Db/Db* data were analyzed using a Student's T-test. " * " Denotes P ≤ 0.05 vs. WT. Values are shown as means ± SEM.

Supplemental Figure S4.3: SVM Model Testing Accuracies

SVM model performance
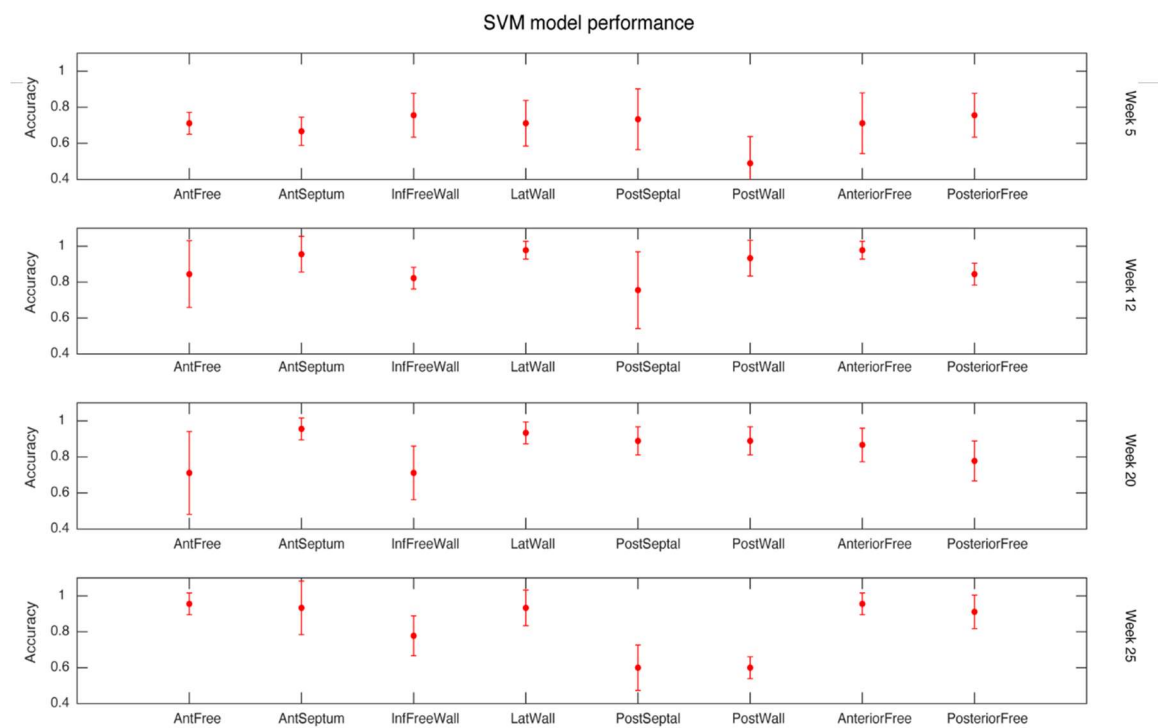
Supplemental Figure S4.3: SVM model testing accuracies were demonstrated for AntFree, AntSeptum, InfFreeWall, LatWall, PostSeptal, PostWall, Anterior Free, and Posterior Free datasets at 5, 12, 20, and 25 weeks of age. SVM; support vector machine, PWD; pulse-wave doppler. Values are shown as means ± SEM.

Chapter 5: GENERAL DISCUSSION

The primary objectives of this dissertation were to evaluate two therapeutic approaches to preserve and restore mitochondrial ATP synthase functionality and cardiac contractile dysfunction in diabetes mellitus. **Chapter 2** aimed to determine: (1) if loss or inhibition of miRNA-378a could improve mitochondrial ATP synthase functionality and ameliorate cardiac contractile dysfunction in T2DM, and (2) if Kcnq1ot1 and miR-378a act as constituents of a regulatory axis that influences the translation of mitochondrial genome encoded ATP6. **Chapter 3** aimed to: (1) evaluate the efficacy of mitochondrial transplantation as a prophylactic measure to ameliorate cardiac contractile dysfunction in the diabetic heart through the replacement of dysfunctional mitochondria with healthy mitochondria obtained from a different individual of the same species using minimally invasive ultrasound-guided echocardiography. **Chapter 4** aimed to: (1) identify if patterns of spatial and temporal dysfunction exist in the T2DM murine heart, which could be identified during the pathophysiological progression of cardiac contractile dysfunction, and (2) identify regions, segment, and locales of interest for more specific, pinpointed mitochondrial transplantation, (3) determine if machine learning may provide a more descriptive and thorough approach to managing large amounts of contractile data with the intention of identifying locales of interest for experimental, clinical, and therapeutic purposes. Our **long-term goal** was to advance our knowledge of mitochondrially-targeted therapeutics through the evaluation of ncRNA targets and mitochondrial transplantation for the amelioration of mitochondrial bioenergetic and cardiovascular contractile dysfunction in diabetes mellitus. The **central hypothesis** of this dissertation was that both the inhibition of miR-378a and mitochondrial transplantation may be two very different, yet conceivable methods of ameliorating mitochondrial bioenergetic dysfunction and cardiovascular contractile dysfunction in the diabetic heart. The **rationale** for the undertaken research was based upon the belief that the development and identification of therapeutic opportunities and targets may aid in the development of innovative and novel ways to alleviate mitochondrial and cardiovascular contractile dysfunction

during diabetes mellitus, and reduce overall morbidity and mortality of the diabetic population.

As diabetes mellitus associated morbidity and mortality continues to rise, our understanding of the pathophysiology of cardiac contractile dysfunction will be essential to produce new and improved diagnostic and treatment opportunities aimed at the amelioration of mitochondrial and cardiac contractile dysfunction. Beginning at the microscale level, the mitochondrion has received a great deal of focus due to its critical role in ATP production, yet therapeutic interventions aimed at the rescue of ATP generating capacity, and the amelioration of cardiac dysfunction, remain limited. The mitochondrial genome provides an array of potential therapeutic targets. The mitochondrial genome encodes 13 protein constituents which make up the electron transport chain respiratory complexes, including ATP synthase (1). These 13 proteins provide mitochondrial specific targets, but they are not the only genes, RNAs, and proteins of interest. NcRNAs have gained interest from those studying mitochondrial function due to their ability to act protectively and pathologically (2-5), as they have been observed interacting with and regulating nuclear and mitochondrially genome encoded proteins (3, 4, 6-8). Further, ncRNAs are capable of regulating protein expression, and miRs, such as miR-378a, may provide a therapeutic option for limiting cardiac contractile dysfunction associated with the diabetic heart (9, 10). In chapter 2, we determined that inhibition of miR-378a in the T2DM heart could provide benefit to ATP synthase functionality by preserving mt-ATP6 protein levels and ATP synthase content. We further linked Kcnq1ot1 and miR-378a as constituents of a regulatory axis that can influence the expression of mitochondrial genome-encoded mt-ATP6, supporting the contention that the mitochondrial genome may be subject to a more complicated regulatory network. Overall, our results suggest that miRs may not be the sole ncRNA regulators of mitochondrial genome-encoded proteins. Rather, lncRNAs may be acting in concert with miRs to regulate mitochondrial genome-encoded protein expression.

The ncRNA network has been observed to be dysregulated in numerous pathologies, including diabetes mellitus and CVD (5, 11). NcRNAs, including miRs and lncRNAs, have been shown to be dynamic during disease states, often operating in conjunction with one another (5, 7, 12). In many cases, dynamic lncRNA expression appears to impact miRs and their downstream targets (7, 13-20). The association between lncRNAs and miRs has been observed in diabetes mellitus, with the discovery of each lncRNA paralleling the discovery of one or more lncRNA/miR regulatory axes (12, 21, 22). Of the many lncRNAs identified in diabetes mellitus, Kcnq1ot1 and Metastasis Associated Lung Adenocarcinoma Transcript 1 (MALAT1) are among the most highly studied (23). Evidence suggests that Kcnq1ot1 and MALAT1 may contribute to the development of diabetes mellitus and associated comorbidities (23). Specifically, both have been linked to pyroptosis, inflammation, apoptosis, and aberrant gene regulation, as part of altered miR regulatory axes in diabetes mellitus (19, 24-27). Less clear are the roles of Kcnq1ot1 and MALAT1 in the diabetic heart, which have been minimally explored.

The data presented in chapter 2 suggest a protective role for Kcnq1ot1 within the mitochondria, but there is still debate regarding the role of Kcnq1ot1 in the heart (24, 25, 28). Studies focused at the tissue specific level suggest that Kcnq1ot1 may perpetuate dysfunction in the heart of streptozotocin-treated mice through miR-214-3p and caspase 1 repression (24, 25), while others have observed the opposite effects, and demonstrated that Kcnq1ot1 overexpression may be protective against sepsis-induced cardiac damage through sponging of miR-192-5p and downregulation of XIAP protein content (28). The outcomes from the current study were more aligned with the later, and indicated a protective role for Kcnq1ot1 in the diabetic heart. The differences in these findings may be a function of the miRs being targeted by Kcnq1ot1 and their downstream effects on cardiac function (24, 25). In addition, lncRNAs may exhibit variable intracellular presence. Indeed, our data demonstrates significant increases in Kcnq1ot1 at the

nuclear and tissue level, but demonstrates significant reductions specific to the mitochondria. These findings suggest that subcellular location may be an important determinant for the mechanistic action of a given lncRNA. Taken together, these data suggest that altered expression of RNAs may not be ubiquitous across tissues type and organelles.

With mitochondrial dysfunction regarded as a crucial contributor to diabetes mellitus and CVD, we focused the current study on the ncRNA network of the mitochondrion. Our data and others suggest that the non-coding regulatory network of the mitochondrion is complex and includes numerous ncRNA species. An increasing number of studies suggest that nuclear genome-encoded lncRNAs, including those residing in the nucleus and/or cytoplasm, as well as mitochondrial genome-encoded lncRNAs, play a role in mitochondrial genome regulation. A review by Gusic and Prokisch summarized 18 lncRNAs known to impact the mitochondrial genome, including AK055347, which has been suggested to influence ATP synthase (23). Thus, a delicate balance needs to be maintained between the import of ncRNAs, including lncRNAs, into the mitochondrion and the transcription of lncRNAs from the mitochondrial genome (7, 23, 29, 30). Importantly, lncRNA activity has been demonstrated to influence the mitochondrial genome through the regulation of miRs and their downstream targets (23, 31-33). Though these interactions require further evaluation, we have also begun to explore additional lncRNAs, including MALAT1, and Nuclear Paraspeckle Assembly Transcript 1 (NEAT1), which may be impacted in T2DM mitochondria and are predicted to interact with mitochondrially-localized miRs. Indeed, a complex regulatory network may exist within the mitochondria, in which miRs are regulated by a host of lncRNAs, both of which are altered in diabetes mellitus.

Due to the role of the ncRNA network in the mitochondrion, we suggest that both miRs and lncRNAs may be efficacious targets for the amelioration of mitochondrial bioenergetic and cardiac dysfunction in T2DM (7, 9, 10). The use of human right atrial tissue presents a caveat to studying whole heart mechanisms of

CVD. Previous studies from our laboratory evaluating mitochondrial function in right atrial tissue from T2DM patients reported alterations in mitochondrial morphology and bioenergetics similar to that reported in ventricular tissue of *Db/Db* mice, suggesting comparable pathophysiology in the tissue types utilized (9, 34, 35). Still, target identification can be problematic, often with high specificity required to achieve desired outcomes. The overlap of the miR-378a/mt-ATP6 axis in both T1DM and T2DM human and mouse cardiac tissues implicate miR-378a as a potential therapeutic target. Though each condition manifests differently, diabetes mellitus types can impact similar key mitochondrial processes (9, 10, 36). The overlap of key processes, including those relating to the production of ATP, suggest that targeting miR-378a for therapeutic intervention could be beneficial for the treatment of both diabetic phenotypes (36). As of now, generalized miR inhibition in experimental settings can be achieved through silencing mechanisms or lncRNA alteration and sponging (9, 10, 19, 20, 24, 25, 37-39). Similarly, other reports show positive results using miR silencing for the amelioration of diabetes mellitus related ailments (9, 37, 40). Current methods of miR inhibition may prove problematic in the case of mitochondrially localized ncRNAs, particularly in the case of Kcnq1ot1, where subcellular changes in expression may exist.

The current study demonstrates that miR-378a KO preserved mt-ATP6 protein content, ATP synthase activity, and contractile function in T2DM. Other bioenergetic assessments, including that of complex III, indicate reduced complex III activity with the diabetic condition. Still, trending decreases in *Db/Db* mice may be a reflection of an increased need for cytochrome C production to fuel complex IV activity and the electron gradient, and/or notability higher variability in *Db/Db* samples, but no significant differences were observed between diabetic groups. An additional measure of mitochondrial bioenergetics, ATP content, was assessed. Total mitochondrial ATP content was found to be unchanged in all groups despite improved ATP synthase function and contractile ability, but changes in mitochondrial ATP content in the diabetic condition have been inconsistently reported, and may not be useful as a sole indicator of overall ATP

generating ability (41-44). It appears that miR-378a loss may not benefit the ETC as a whole, and may only provide benefit to the ATP synthase complex. Further, ETC complex activities serve as a surrogate for respiratory function, but do not provide the same insight as respiratory analyses such as the Seahorse assay and the Oxytherm Electrode System, which provide a more comprehensive view of mitochondrial respiration (45, 46).

Additionally, while total mt-ATP6 mRNA levels were unchanged with the murine diabetic condition, miR-378a KO and miR-378a KO/*Db/Db* mice exhibited significant increases in mt-ATP6 mRNA compared to their respective controls, similar to the phenotype exhibited within T2DM patients. Notably, we confirmed no significant differences in mt-DNA content in KO mice when compared to WT, or between diabetic groups, suggesting that changes in mt-ATP6 mRNA and protein content were not a result of miR-378a influencing total mt-DNA amount. To this point, apparent increases in mt-ATP6 mRNA, independent of changes in overall mt-DNA content, may be due to reduced interactions of mt-ATP6 mRNA with the RISC in KO/*Db/Db* mice. Concomitantly, *Db/Db* mice exhibit increased interaction of mt-ATP6 mRNA with the RISC, and reduced mt-ATP protein levels, despite unchanged levels of total mt-ATP6 mRNA. Together, these data suggest that miR-378a inhibition may provide benefit to ATP synthase through reduced interaction of mt-ATP6 mRNA with the RISC, and therefore reduced translational interference. The mechanism of translational interference, whether translational repression or mRNA degradation, is unclear. The question of translational repression versus mRNA degradation was not emphasized in the study, but indicates an area of interest for future experimentation. Current literature emphasizes the ambiguity in our understanding of miR mediated mRNA repression and degradation, with evidence to support the occurrence of both, but minimal evidence available to describe their mechanisms (47-51). Hence, further experimentation is necessary to fully elucidate the fate of mitochondrial mRNAs following RISC interaction.

In addition to miRs, lncRNAs may be utilized to target mitochondrially-located miRs and the mitochondrial genome (23). We suggest that downregulation of mitochondrial genome-encoded proteins may be rescued by reducing the availability of miRs known to target the mitochondrial genome (9, 10). This study is the first to identify mitochondrially-localized Kcnq1ot1, as well as identify reductions in Kcnq1ot1 levels in cardiac mitochondria. LncRNAs have been speculated to act in a sponging fashion by regulating and often inhibiting miR activity, but this is the first study to identify a role for Kcnq1ot1 as a potential regulator of mitochondrial genome-encoded proteins via the miR-378a-5p/mt-ATP6 axis. Notably, though overexpression of the 500-bp Kcnq1ot1 fragment in HL-1 cardiomyocytes exhibiting baseline levels of miR-378a, decreased detectable miR-378a-5p content, it did not result in changes in mt-ATP6 mRNA content. These results were logical, as one would suspect that healthy cells are able to transcribe mt-ATP6 mRNA freely when miR-378a levels are not pathologically elevated. As a result, miR-378a inhibition ultimately, had no effect on mt-ATP6 content. Additionally, though the mechanism we postulate influences the mitochondrial genome, both RNAs are of nuclear origin, thus, we cannot disregard the possibility that Kcnq1ot1 may interact with miR-378a cytosolically, resulting in reduced miR-378a within the mitochondrion (9, 10). More specifically, the experiments centered around Kcnq1ot1 fragment overexpression were performed in an *in vitro* model which did not allow for the evaluation of mitochondrial specific changes in miR-378a and Kcnq1ot1, which present a limitation to the study. The changes observed in the study were likely the result of cytosolic interactions, and further experimentation is necessary to evaluate mitochondrial specific changes. As a whole, the efficacy of lncRNAs as therapeutic targets for mitochondrial genome-encoded proteins requires more elucidation.

While we understand the basic of lncRNA-miR interactions, the fate of miRs following lncRNA binding is variable and currently unclear, with some suggesting that miRs are sequestered by the lncRNA and later released, and others suggesting that lncRNA binding can initiate degradation (52-54). The mechanism

of action regarding sponging of miRs represents a momentous gap in our understanding of ncRNA interactions. To fully evaluate a lncRNA as a therapeutic target, the mechanisms of action must be better understood. Until this gap in knowledge can better be filled, the translational impact of the studies performed may be overlooked. In summary, Chapter 2 demonstrates that Kcnq1ot1 and miR-378a may act as constituents of a regulatory axis that can influence the expression of mitochondrial genome-encoded mt-ATP6 in the T2DM heart. Further, overexpression of Kcnq1ot1 may reduce miR-378a levels and preserve mt-ATP6 protein content, suggesting that Kcnq1ot1 may participate in the regulation of the mitochondrial genome. In totality, these data suggest that dysregulation of the ncRNA network may impact regulation of the mitochondrial genome, with evidence to suggest that miR-378a and lncRNA Kcnq1ot1 may act as regulatory targets in T2DM to rescue mitochondrially-encoded mt-ATP6 protein expression and ATP synthase functionality.

For chapters 3 and 4, our focus shifted to a more macroscale approach; ameliorating mitochondrial dysfunction using mitochondrial transplantation. Mitochondrial transplantation provided a unique macroscale opportunity to ameliorate mitochondrial dysfunction through the replacement of unhealthy mitochondria with undamaged, bioenergetically competent mitochondria, but there are notable differences between treatment of CVD in diabetes mellitus versus ischemia reperfusion and other spontaneous cardiac events. Overall, many barriers impede the application of mitochondrial transplantation in diabetes mellitus, two of the most important being lack of timing and location for cardiac events. The most inhibitory challenges are that when applied in a prophylactic manner, it cannot be performed in response to a cardiac event. Further, there is no pre-determined area of risk to determine location for injections, such as with ischemia reperfusion studies. Therefore, the primary objective of chapter 3 was to determine the efficacy of mitochondrial transplantation as a prophylactic technique for diabetes mellitus. In order to perform the procedure prophylactically, and make it worthwhile clinically, the procedure needed to be performed in a minimally

invasive manner. While many ischemia reperfusion studies provide direct, uninhibited, access to the heart through open-heart surgery, some alternative methods of mitochondrial delivery are available. Coronary artery cannulation, which provides widespread distribution of mitochondria rather than accumulation at an injection site, is one such method. Unfortunately, coronary artery cannulation provides a wide distribution of mitochondria, and may not provide enough localized assistance to the left ventricle in the case of diabetes mellitus (55). These challenges must be met in order to adapt mitochondrial transplantation as a therapeutic approach in the diabetic heart.

Though previous studies suggest that mitochondria are incorporated into host cells, available data are limited. One such report by Masuzawa et al. demonstrated localization and uptake of transplanted mitochondria in the rabbit heart using immunohistochemistry and microscopy methodologies (56). While it appears that mitochondria may be incorporated into the myocardium following transplantation, we believed it was necessary to further assess the behavior of mitochondria following transplantation and the extent of their uptake and localization. We began with *in vitro* assessments of mitochondrial transplantation, which suggest that transplanted mitochondria may bind to the membrane surface of HL-1 cardiomyocytes, and interact with the host cell mitochondrial network, but are not incorporated into the cell by 48 hours. Interestingly, at 24 hours mitochondrial appear connected to the cell membrane, but do not definitively interact with the host cell mitochondrial population. At 48 hours, mitochondria could be identified interacting with host cell mitochondria, but did not appear to penetrate the cellular membrane and become fully localized within the cell. Indeed, microscopy imaging and IMARIS 3D reconstruction of the cardiomyocytes following transplantation suggest that transplanted mitochondria may interact with cardiomyocyte mitochondrial populations without complete incorporation into the cell. These conclusions oppose previous literature suggesting mitochondrial internalization *in vitro*, as it is seemingly unclear if mitochondria are within the cell, or simply attached to the surface (56).

Some limitations of the *in vitro* studies performed include imaging restraints, in which the imaging technique was chosen due to its ability to capture fluorescent signal over its depth and image quality. Because of this, we were able to identify mitochondrial signals, but were not able to acquire close-up and clear images of mitochondrial positioning and integration. Importantly, previous studies suggest that mitochondrial interactions with the cell occur through actin-dependent or micropinocytosis related mechanisms that were not explored in this study (57-59). To more substantially investigate mitochondrial uptake and localization, in depth microscopy, including electron microscopy or alternative methods, would have to be utilized. Further, evaluating mitochondrial uptake *in vitro* presents additional limitations due to time constraints associated with microscopy imaging. HL-1 cardiomyocytes, and the Claycomb media used for their growth, are light-sensitive and cannot be imaged at high frequencies for long periods of time. These limitations suggest that a more thorough evaluation of mitochondrial uptake and localization may be necessary to fully determine their positioning within cells, and their interactions with host mitochondria.

In vivo transplantation of mitochondria using ultrasound-guided echocardiography appeared to be an effective method for the delivery of mitochondria to the left ventricle myocardium, and produced minimal side effects, suggesting it is feasible to use mitochondrial transplantation to deliver healthy mitochondria to the left ventricle myocardium using this method. Ultrasound-guided intracardiac injections in adult recipients (at least 8 weeks of age) did not lead to immediate cardiac abnormalities, and maintained a low risk of mortality. Mouse behavior remained normal and no immediate side effects were observed. A limitation to this study was that mice under certain body weights may have hearts that are too small to safely receive injections, therefore we believe it is necessary for mice be at least 25 g in weight prior to injection. Heart size must be comparable to that of an adult mouse to receive mitochondrial transplantation in the volume described without significantly increasing risk of death. To inject leaner or younger

261

mice, the volume of both respiration buffer and mitochondria would need to be adjusted to body/heart weight in order to reduce risk of death. Further, adaptation for models involving changes to the heart size, weight, or structure may alter the injection protocol. Determining the precise volume and mitochondrial number necessary for each recipient would ameliorate increased risk of mortality. Specifically, the volume of respiration buffer and mitochondrial content may need to be adjusted to account for body weight and age in animal models. While these specific limitations may not apply to human patients, more research is necessary to determine these adjustments. Further, studies to determine the "effective amount" of mitochondria, or the number of mitochondria necessary to observe a beneficial effect, is unknown and would require further elucidation and customization. It should be noted that a limitation to this study is mitochondrial distribution within the myocardium, where mitochondria were located primarily in and around the sites of injection.

Subsequently, transplanted mitochondria were identified in the left ventricle myocardium 24 hours following injection, consistent with previously published literature (56). It should be noted that the accepted mitochondrial half-life is about 14 days (60, 61), and previous studies have demonstrated that transplanted mitochondria maintain viability and function for at least 28 days, therefore the sharing of information, including mtDNA, with recipient mitochondrial networks may provide an explanation for how transplanted mitochondria are acquiring both MitoTracker orange and COX IV signals following cellular interactions (62, 63). Overall, numerous studies demonstrate the ability of mitochondria to influence the host mitochondrial network and increase bioenergetic function through donation of healthy mitochondrial DNA, increased ATP production, and increased respiratory capacity (56, 57, 59, 62). Confocal microscopy images suggest that transplanted mitochondria may not only integrate into recipient mitochondrial networks, but may be integrated is such a way that they are positioned precisely within both subsarcolemmal and interfibullar mitochondrial networks, rather than non-discriminately. These data coincide with a report by Cowan et al, in which they

utilized microscopy to identify exogenous mitochondria within the myocardium following coronary artery cannulation, and suggested that transplanted mitochondria incorporate themselves within cardiac myocytes (55). To further elucidate the localization of transplanted mitochondria within the myocardium requires deeper exploration and perhaps more advanced methods of mitochondrial tracking and imaging. As mentioned above, the microscopy techniques utilized in this paper allowed for mitochondrial tracking through fluorescent signals to identify overlap between host and donor mitochondria, but in turn reduced visual clarity. As a result, mitochondrial localization and integration require further elucidation, as overlap with mitochondrial host signal indicates overlap of signal, but does not confirm interactions. Further, while imaging suggests that mitochondria positioning align with mitochondrial networks, studies segregating mitochondrial populations following injection may be beneficial in confirming the presence of donor mitochondria and these findings. This report suggests that mitochondrial transplantation may be an efficacious method of reducing mitochondrial dysfunction in the diabetic heart when performed using ultrasound-guided echocardiography and intracardiac injections. The deposition of mitochondria within the left ventricular myocardium, which was identified, quantified, and visualized, suggests that mitochondrial transplantation may be able to be utilized as a prophylactic measure in diabetes mellitus.

In summary, mitochondrial transplantation can be performed using ultrasound-guided echocardiography efficiently enough to deposit mitochondria within the left ventricle myocardium, which can be identified, quantified, and visualized, suggesting that mitochondrial transplantation may be able to be utilized as a prophylactic measure in diabetes mellitus. To be beneficial for diabetes mellitus patients, mitochondrial transplantation must be applied in a minimally invasive prophylactic manner, with the intent of preventing future cardiac events and reducing overall risk of mortality. To improve the specificity of mitochondrial transplantation, and improve its efficacy for future use, we determined it would be

of benefit to identify and pinpoint regions of interest, and to adapt mitochondrial transplantation to provide healthy mitochondria to a specific region of the heart.

Regional and segmental analyses provided a logical next step of determining localized impact of CVD on cardiovascular contractile dysfunction, but evaluations are limited by large and complex datasets that require extensive time to assess. With the implementation of machine learning, these large datasets were able to be assessed quickly and efficiently, while simultaneously identifying the features most predictive of cardiac contractile dysfunction associated with the diabetic condition (Chapter 4). Herein, we described the presence of spatial and temporal patterns of cardiac dysfunction in the diabetic heart using machine learning as a tool to analyze large and complex cardiovascular imaging datasets.

The etiology of cardiovascular contractile dysfunction in T2DM remains elusive, and as morbidity and mortality continue to rise, our understanding of its pathophysiology will be critical to produce new and improved diagnostic and treatment opportunities. STE is an invaluable tool for the evaluation of cardiac function, and has been utilized to evaluate changes in contractility and deformation in both murine models of T1DM (64, 65), T2DM (66), and human subjects (67-70). At current, STE has not been utilized to evaluate progressive changes in regional and segmental function as a method of identifying patterns of cardiac contractile dysfunction in the type 2 diabetic heart. Elucidating changes in cardiac function, to the fullest extent possible, may aid in filling this gap in our knowledge, and may provide an alternative method to identify cardiovascular dysfunction in diabetes mellitus patients earlier and with greater specificity than current methods. In this study, we aimed to elucidate if cardiac contractile dysfunction associated with the T2DM condition occurs spatially, and if patterns of regional or segmental dysfunction manifest in a temporal fashion. We further aimed to utilize machine learning to identify the cardiac regions, segments, and features that best described a state of cardiac contractile dysfunction using solely non-invasive echocardiography features.

The use of machine learning enhanced our ability to predict what regions and segments of the heart were most impacted during disease progression, and to further explore those that were best able to identify cardiac contractile dysfunction. Traditional data analyses use descriptive and exploratory methods to provide results and discover patterns in current or past data, but do not make predictions about the future. We aimed to compare traditional data analyses with machine learning methodologies to determine if the regions and segments that were best able to identify cardiac contractile dysfunction also contained the largest number of dysfunctional parameters. By determining the prevalence of a region or segment, we gained insight into the cardiac locales that were likely impacted by T2DM to the greatest extent, and exhibited the largest number of noteworthy changes.

We were able to identify the regions and segments which best identified a state of cardiac contractile dysfunction, and the features which best defined it. The Septal region, and primarily the AntSeptum segment, were determined to be the strongest identifiers of cardiac dysfunction at 5, 20, and 25 weeks. Moreover, the Septal region was identified as a region of interest early in T2DM development, and was maintained into the late stages of disease. These data suggest that the Septal region, and the segments contained within, may provide a new metric for the identification of subclinical cardiac dysfunction. The importance of the Septal region may be explained, in part, by the role of the septum in conduction of the heart. The electrical sequence in the heart follows a pre-defined order in healthy individuals, but may be disrupted in individuals with cardiovascular contractile dysfunction (71). For example, the healthy septum transfers energy between the ventricles, acting as a third pump. Diseases that increase septal elastance, such as diabetes mellitus, can resemble left ventricular diastolic dysfunction (72). Myocardial work, or the contribution by each region to contraction, has been found to be significantly affected by both hypertension and diabetes, with diabetic patients having lower strain values in the septal and lateral segments (73). Further,

the observation of early Septal region dysfunction has been utilized as a method of identifying and monitoring diabetes mellitus (73-75). These reports suggest that alterations in the Septal region may be observable early in the pathophysiology of T2DM, prior to the onset of clinically recognizable symptoms of cardiac dysfunction. The data presented in this study suggest that the Septal region may benefit most from therapeutic interventions aimed at preventing the progression of cardiac contractile dysfunction in T2DM when initiated early in disease.

Interestingly, the Septal region was the second-best classifier of the diabetic condition at week 12, where the Anterior Free region, and the LatWall segment, were able to identify cardiac contractile dysfunction with the greatest accuracy. This shift from the Septal wall to the AntFree region and LatWall segment at 12 weeks, and back to the Septal region again at 20 weeks, may be the result of the cardiac structural and metabolic remodeling preceding, and ultimately leading to the development of overt contractile dysfunction (76-80). Metabolic inflexibility and substrate overload initiate several metabolic and structural changes that manifest during the subclinical stages of cardiac contractile dysfunction as an adaptive mechanism to protect the heart (77, 81-83). In healthy individuals, the LV primarily performs contractile or shortening work, but in patients with cardiomyopathies, the ability of the septum to provide energy for contraction may be decreased, with a greater amount energy being wasted (84). This means that even though the Septal region begins the contractile process, the Free and Anterior regions may overcompensate for the Septal regions lack of energy contribution by contributing additional energy for contraction (85). Metabolically, segments contributing the greatest level of contractile energy also exhibit the highest levels of glucose metabolism, and show a disruption of glucose metabolism, and therefore an ability to produce energy for contraction, with disease (86). This metabolic shift suggests that regions displaying this pattern of energy waste may experience larger amounts of mitochondrial dysfunction, including impaired glucose metabolism, increased reliance on fatty acid oxidation, and changes in mitochondrial DNA (86-89). With this in mind, structural and metabolic alterations may manifest in the

Anterior Free region, prior to the onset of overt contractile dysfunction that temporarily improve its ability to identify animals as diabetic or non-diabetic. As a result, we believe that future directions should include the biochemical analysis of regional and segmental metabolism.

Analysis of our data using traditional methods produced results similar to those observed using machine learning. Subsequently, determining the most prevalent regions and segments, or those containing the largest number of noteworthy, and likely dysfunctional metrics were reflective of the most impacted cardiac locale at each timepoint. We observed that the prevalence of regions and segments overlapped, with the most prevalent region containing the most prevalent segment. Overall, these results suggest the AntSeptum segment may contain the greatest number of features contributing to cardiac contractile dysfunction, and may be a metric to identify and monitor throughout the T2DM pathology. Taken together, these data support assessments of regional and segmental function using feature ranking algorithms as a feasible alternative to traditional data analysis to determine regions or locales of interest for experimental, therapeutic, or clinical purposes.

The healthcare community has largely benefited from the implementation of STE, which has provided a great deal of insight into cardiac contractile dysfunction, and the incorporation of machine learning in the evaluation of echocardiography represents a new and powerful tool for the study (90-92). Further, machine learning and features ranking methodologies with the intention of identifying regions and segments of interest for experimental, clinical, and therapeutic purposes. Combining these techniques may provide a more descriptive and thorough approach to managing large amounts of contractile data, as well as improve the process of analyzing and interpreting cardiovascular contractile data (70, 93, 94). These applications in echocardiography are increasing exponentially, particularly for their ability to develop innovative models of diagnosis and care (34, 70, 95, 96). The initial collection and analysis of data

can be difficult, leading to the interpretation of a small subset of data collected, rather than the data as a whole (94). In clinical settings, the ability to automate data acquisition, processing, and interpretation may help to improve methods of evaluating cardiac dysfunction in the T2DM heart (93, 97, 98). The data presented in this study support that machine learning can be used as a tool to identify cardiac contractile dysfunction by using solely non-invasive echocardiography features in a murine model of T2DM. We demonstrate that feature ranking algorithms can be used to identify regional and segmental patterns of cardiovascular contractile dysfunction in T2DM, suggesting that cardiovascular contractile dysfunction occurs not only in a temporal fashion, but progresses spatially.

Interestingly, despite significant changes in M-mode parameters, STE outperformed conventional echocardiography at all timepoints, and was consistently better at identifying cardiac contractile dysfunction. Prior to the development of overt systolic dysfunction, as at 5 and 12 weeks, the ability of STE to outperform conventional M-mode echocardiography was expected due to its ability to detect subclinical changes in cardiac function. Alternatively, M-mode echocardiography demonstrated significant decreases in EF and FS features at 20 and 25 weeks of age, but was not as strong of an identifier of cardiac contractile dysfunction as STE features. This discrepancy may be due, in part, to the methodology used by machine learning classification. Specifically, M-mode may contain a large number of significantly altered features, but if the STE regions and segments discussed above contain an overall larger number of altered features, it could indirectly increase the ability of STE features to identify cardiac contractile dysfunction. In terms of clinical applicability, numerous altered STE features may be necessary to outperform the ability of EF to identify contractile dysfunction. Moreover, M-mode echocardiography parameters, including EF and FS, may be a stronger indicator of contractile dysfunction once overt dysfunction is present, but M-mode echocardiography remains unable to detect clinical and subclinical measures of dysfunction. Hence, the focus of STE should remain the assessment and diagnosis of subclinical cardiac dysfunction. As discussed above, the Septal

region may provide a metric for clinicians to identify subclinical changes in cardiac deformation, aid in the diagnosis and staging of cardiac contractile dysfunction prior to the presence of overt systolic dysfunction, and monitor, in addition to EF, during late stages of disease. A limitation to this study is the sole use of murine models of T2DM. To fully elucidate the translational value of these data, further evaluation is necessary to determine if the spatial and temporal patterns of STE observed in *Db/Db* mice also occur in T2DM human subjects.

In summary, cardiac contractile dysfunction associated with the T2DM condition manifests spatially, and patterns of regional and segmental dysfunction appear early in the T2DM pathology while progressing in a temporal fashion. Further, the Septal region may provide a metric for the identification of subclinical dysfunction, the diagnosis and staging of cardiac contractile dysfunction prior to the presence of overt systolic dysfunction, and a target for therapeutic interventions aimed at preventing the progression of cardiac contractile dysfunction in T2DM when initiated early in the disease. Additionally, these data support that assessments of regional and segmental function using machine learning and feature ranking algorithms may be a feasible alternative to traditional data analysis and may provide a more descriptive and thorough approach to managing large amounts of contractile data with the intention of identifying regions and segments of interest for experimental, clinical, and therapeutic purposes.

FUTURE DIRECTIONS

Future directions for chapter 2 would be the inclusion of an experimental component aimed at assessing the impact of miR-378a loss or inhibition on mitochondrial respiration. Because of the time and resources necessary to gain fresh murine mitochondrial from KO/*Db/Db* mice, efforts given to the evaluation of mitochondrial respiration will be given to future studies assessing lncRNA-miRNA interactions, and their impact of mitochondrial function. Next, the question of translational repression versus mRNA degradation of mt-ATP6 mRNA was not emphasized in the study, but indicates an area of interest for future experimentation. Current literature emphasizes the ambiguity in our understanding of miR mediated mRNA repression and degradation, with evidence to support the occurrence of both, but minimal evidence available to describe their mechanisms (47-51). Hence, further experimentation is necessary to fully elucidate the fate of mitochondrial mRNAs following RISC interaction. Finally, future experiments will require a deeper evaluation of ncRNA interactions, and a better understanding of the sponging mechanisms and outcomes. On par with the question of mRNA degradation, the mechanisms and outcomes of sponging are not well elucidated, therefore future experiments will focus on the evaluation of sponging mechanisms and ncRNA interactions.

Future directions for chapter 3 would include the incorporation of both fluorescent microscopy as well as electron microscopy for a more thorough evaluation of mitochondrial uptake and localization both *in vivo* and *in vitro*. Additional experimentation would include greater evaluation of mitochondrial behavior *in vivo,* rather than *in vitro* due to the inherent differences of cellular and animal models. Further, adaptation for models involving changes to the heart size, weight, or structure may alter the injection protocol. Determining the precise volume and mitochondrial number necessary for each recipient would ameliorate increased risk of mortality. Specifically, the volume of respiration buffer and mitochondrial content may need to be adjusted to account for body weight and age

in animal models. While these specific limitations may not apply to human patients, more research is necessary to determine these adjustments are necessary. Further, studies aimed at determining the "effective amount" of mitochondria, or the number of mitochondria necessary to observe a beneficial effect, would be necessary prior to studies in diabetic models. To optimize mitochondrial transplantation for the diabetic heart a great deal of personalization will be necessary, prior to implementation in diabetic models. To this end, to fully elucidate the localization of transplanted mitochondria within the myocardium requires deeper exploration and perhaps more advanced methods of mitochondrial tracking and imaging. As mentioned above, the microscopy techniques utilized in this paper allowed for mitochondrial tracking through fluorescent signals to identify overlap between host and donor mitochondria, but in turn reduced visual clarity. As a result, mitochondrial localization and integration require further elucidation, as overlap with mitochondrial host signal indicates overlap of signal, but does not confirm interactions. Further, while imaging suggests that mitochondria positioning align with mitochondrial networks, further studies segregating mitochondrial populations following injection may be beneficial in confirming the presence of donor mitochondria and these findings.

Overall, following *in vivo* and *in vitro* mitochondrial transplantation, mitochondrial localization was consistent with previously published literature (21), but mitochondrial localization and integration will require further elucidation, as overlap with mitochondrial host signal indicates overlap of signal, but does not confirm interactions. In addition, though imaging suggests that mitochondria positioning align with mitochondrial networks, further studies segregating mitochondrial populations following injection may be beneficial in confirming the presence of donor mitochondria and these findings. In summary, mitochondrial transplantation may be applied in a minimally invasive prophylactic manner with the intent of preventing future cardiac events and reducing overall risk of mortality, but would require a great deal of attention to be feasible.

With the intention of improving mitochondrial transplantation in mind, chapter 4 suggests that structural and metabolic alterations may manifest in the Anterior Free region, prior to the onset of overt contractile dysfunction that temporarily improve its ability to identify animals as diabetic or non-diabetic. As a result, we believe that future directions should include the biochemical analysis of regional and segmental metabolism. Further, we aim to determine if the spatial and temporal patterns of STE observed in *Db/Db* mice also occur in T2DM human subjects.

References

1. Taanman JW. The Mitochondrial Genome: Structure, Transcription, Translation and Replication. Biochim Biophys Acta. 1999;1410(2):103-123. doi:10.1016/s0005-2728(98)00161-3

2. Guo R, Nair S. Role of Microrna in Diabetic Cardiomyopathy: From Mechanism to Intervention. Biochim Biophys Acta Mol Basis Dis. 2017;1863(8):2070-2077. doi:10.1016/j.bbadis.2017.03.013

3. Hathaway QA, Pinti MV, Durr AJ, Waris S, Shepherd DL, Hollander JM. Regulating Microrna Expression: At the Heart of Diabetes Mellitus and the Mitochondrion. Am J Physiol Heart Circ Physiol. 2018;314(2):H293-H310. doi:10.1152/ajpheart.00520.2017

4. Geiger J, Dalgaard LT. Interplay of Mitochondrial Metabolism and Micrornas. Cell Mol Life Sci. 2017;74(4):631-646. doi:10.1007/s00018-016-2342-7

5. Bonnet S, Boucherat O, Paulin R, Wu D, Hindmarch CCT, Archer SL, et al. Clinical Value of Non-Coding Rnas in Cardiovascular, Pulmonary, and Muscle Diseases. Am J Physiol Cell Physiol. 2020;318(1):C1-C28. doi:10.1152/ajpcell.00078.2019

6. Dietrich A, Wallet C, Iqbal RK, Gualberto JM, Lotfi F. Organellar Non-Coding Rnas: Emerging Regulation Mechanisms. Biochimie. 2015;117:48-62. doi:10.1016/j.biochi.2015.06.027

7. Jakubik D, Fitas A, Eyileten C, Jarosz-Popek J, Nowak A, Czajka P, et al. Micrornas and Long Non-Coding Rnas in the Pathophysiological Processes of Diabetic Cardiomyopathy: Emerging Biomarkers and Potential Therapeutics. Cardiovascular diabetology. 2021;20(1):55. doi:10.1186/s12933-021-01245-2

8.   Baradan R, Hollander JM, Das S. Mitochondrial Mirnas in Diabetes: Just the Tip of the Iceberg. Can J Physiol Pharmacol. 2017;95(10):1156-1162. doi:10.1139/cjpp-2016-0580

9.   Shepherd DL, Hathaway QA, Pinti MV, Nichols CE, Durr AJ, Sreekumar S, et al. Exploring the Mitochondrial Microrna Import Pathway through Polynucleotide Phosphorylase (Pnpase). J Mol Cell Cardiol. 2017;110:15-25. doi:10.1016/j.yjmcc.2017.06.012

10.   Jagannathan R, Thapa D, Nichols CE, Shepherd DL, Stricker JC, Croston TL, et al. Translational Regulation of the Mitochondrial Genome Following Redistribution of Mitochondrial Microrna in the Diabetic Heart. Circ Cardiovasc Genet. 2015;8(6):785-802. doi:10.1161/CIRCGENETICS.115.001067

11.   Moore JBt, Uchida S. Functional Characterization of Long Noncoding Rnas. Curr Opin Cardiol. 2020;35(3):199-206. doi:10.1097/HCO.0000000000000725

12.   Yang F, Chen Y, Xue Z, Lv Y, Shen L, Li K, et al. High-Throughput Sequencing and Exploration of the Lncrna-Circrna-Mirna-Mrna Network in Type 2 Diabetes Mellitus. Biomed Res Int. 2020;2020:8162524. doi:10.1155/2020/8162524

13.   Yu L, Fu J, Yu N, Wu Y, Han N. Long Noncoding Rna Malat1 Participates in the Pathological Angiogenesis of Diabetic Retinopathy in an Oxygen-Induced Retinopathy Mouse Model by Sponging Mir-203a-3p. Can J Physiol Pharmacol. 2020;98(4):219-227. doi:10.1139/cjpp-2019-0489

14.   Li J, Li M, Bai L. Kcnq1ot1/Mir-18b/Hmga2 Axis Regulates High Glucose-Induced Proliferation, Oxidative Stress, and Extracellular Matrix Accumulation in Mesangial Cells. Molecular and cellular biochemistry. 2021;476(1):321-331. doi:10.1007/s11010-020-03909-1

15.   Shao J, Pan X, Yin X, Fan G, Tan C, Yao Y, et al. Kcnq1ot1 Affects the Progression of Diabetic Retinopathy by Regulating Mir-1470 and Epidermal Growth Factor Receptor. J Cell Physiol. 2019;234(10):17269-17279. doi:10.1002/jcp.28344

16.   Zhang C, Gong Y, Li N, Liu X, Zhang Y, Ye F, et al. Long Noncoding Rna Kcnq1ot1 Promotes Sc5b-9-Induced Podocyte Pyroptosis by Inhibiting Mir-486a-3p and Upregulating Nlrp3. Am J Physiol Cell Physiol. 2021;320(3):C355-C364. doi:10.1152/ajpcell.00403.2020

17.   Shaker OG, Abdelaleem OO, Mahmoud RH, Abdelghaffar NK, Ahmed TI, Said OM, et al. Diagnostic and Prognostic Role of Serum Mir-20b, Mir-17-3p, Hotair, and Malat1 in Diabetic Retinopathy. IUBMB Life. 2019;71(3):310-320. doi:10.1002/iub.1970

18.   Zhang H, Yan Y, Hu Q, Zhang X. Lncrna Malat1/Microrna Let-7f/Klf5 Axis Regulates Podocyte Injury in Diabetic Nephropathy. Life Sci. 2021;266:118794. doi:10.1016/j.lfs.2020.118794

19.   Che H, Wang Y, Li H, Li Y, Sahil A, Lv J, et al. Melatonin Alleviates Cardiac Fibrosis Via Inhibiting Lncrna Malat1/Mir-141-Mediated Nlrp3 Inflammasome and Tgf-Beta1/Smads Signaling in Diabetic Cardiomyopathy. FASEB J. 2020;34(4):5282-5298. doi:10.1096/fj.201902692R

20.   Xia C, Liang S, He Z, Zhu X, Chen R, Chen J. Metformin, a First-Line Drug for Type 2 Diabetes Mellitus, Disrupts the Malat1/Mir-142-3p Sponge to Decrease Invasion and Migration in Cervical Cancer Cells. Eur J Pharmacol. 2018;830:59-67. doi:10.1016/j.ejphar.2018.04.027

21.   Chang W, Wang J. Exosomes and Their Noncoding Rna Cargo Are Emerging as New Modulators for Diabetes Mellitus. Cells. 2019;8(8). doi:10.3390/cells8080853

22.   Leung A, Natarajan R. Long Noncoding Rnas in Diabetes and Diabetic Complications. Antioxidants & redox signaling. 2018;29(11):1064-1073. doi:10.1089/ars.2017.7315

23.   Prokisch MGaH. Ncrnas: New Players in Mitochondrial Health and Disease? Front Genet. 2020;10.3389/fgene.2020.00095. doi:10.3389/fgene.2020.00095

24.   Yang F, Qin Y, Wang Y, Li A, Lv J, Sun X, et al. Lncrna Kcnq1ot1 Mediates Pyroptosis in Diabetic Cardiomyopathy. Cell Physiol Biochem. 2018;50(4):1230-1244. doi:10.1159/000494576

25.   Yang F, Qin Y, Lv J, Wang Y, Che H, Chen X, et al. Silencing Long Non-Coding Rna Kcnq1ot1 Alleviates Pyroptosis and Fibrosis in Diabetic Cardiomyopathy. Cell Death Dis. 2018;9(10):1000. doi:10.1038/s41419-018-1029-4

26.   Wu A, Sun W, Mou F. Lncrnamalat1 Promotes High Glucoseinduced H9c2 Cardiomyocyte Pyroptosis by Downregulating Mir1413p Expression. Mol Med Rep. 2021;23(4). doi:10.3892/mmr.2021.11898

27.   Wang C, Liu G, Yang H, Guo S, Wang H, Dong Z, et al. Malat1-Mediated Recruitment of the Histone Methyltransferase Ezh2 to the Microrna-22 Promoter Leads to Cardiomyocyte Apoptosis in Diabetic Cardiomyopathy. Sci Total Environ. 2021;766:142191. doi:10.1016/j.scitotenv.2020.142191

28.   Sun F, Yuan W, Wu H, Chen G, Sun Y, Yuan L, et al. Lncrna Kcnq1ot1 Attenuates Sepsis-Induced Myocardial Injury Via Regulating Mir-192-5p/Xiap Axis. Exp Biol Med (Maywood). 2020;245(7):620-630. doi:10.1177/1535370220908041

29.   Dong Y, Yoshitomi T, Hu JF, Cui J. Long Noncoding Rnas Coordinate Functions between Mitochondria and the Nucleus. Epigenetics Chromatin. 2017;10(1):41. doi:10.1186/s13072-017-0149-x

30.   Chen G, Guo H, Song Y, Chang H, Wang S, Zhang M, et al. Long Noncoding Rna Ak055347 Is Upregulated in Patients with Atrial Fibrillation and Regulates Mitochondrial Energy Production in Myocardiocytes. Mol Med Rep. 2016;14(6):5311-5317. doi:10.3892/mmr.2016.5893

31.   Sirey TM, Roberts K, Haerty W, Bedoya-Reina O, Rogatti-Granados S, Tan JY, et al. Correction: The Long Non-Coding Rna Cerox1 Is a Post Transcriptional Regulator of Mitochondrial Complex I Catalytic Activity. eLife. 2019;8. doi:10.7554/eLife.50980

32.   Tian T, Lv X, Pan G, Lu Y, Chen W, He W, et al. Long Noncoding Rna Mprl Promotes Mitochondrial Fission and Cisplatin Chemosensitivity Via Disruption of Pre-Mirna Processing. Clin Cancer Res. 2019;25(12):3673-3688. doi:10.1158/1078-0432.CCR-18-2739

33.   Li HJ, Sun XM, Li ZK, Yin QW, Pang H, Pan JJ, et al. Lncrna Uca1 Promotes Mitochondrial Function of Bladder Cancer Via the Mir-195/Arl2 Signaling Pathway. Cell Physiol Biochem. 2017;43(6):2548-2561. doi:10.1159/000484507

34.   Hathaway QA, Roth SM, Pinti MV, Sprando DC, Kunovac A, Durr AJ, et al. Machine-Learning to Stratify Diabetic Patients Using Novel Cardiac Biomarkers and Integrative Genomics. Cardiovascular diabetology. 2019;18(1):78. doi:10.1186/s12933-019-0879-0

35.   Croston TL, Thapa D, Holden AA, Tveter KJ, Lewis SE, Shepherd DL, et al. Functional Deficiencies of Subsarcolemmal Mitochondria in the Type 2 Diabetic Human Heart. Am J Physiol Heart Circ Physiol. 2014;307(1):H54-65. doi:10.1152/ajpheart.00845.2013

36.   Hollander JM, Thapa D, Shepherd DL. Physiological and Structural Differences in Spatially Distinct Subpopulations of Cardiac Mitochondria: Influence of Cardiac Pathologies. Am J Physiol Heart Circ Physiol. 2014;307(1):H1-14. doi:10.1152/ajpheart.00747.2013

37.   Bijkerk R, Esguerra JLS, Ellenbroek JH, Au YW, Hanegraaf MAJ, de Koning EJ, et al. In Vivo Silencing of Microrna-132 Reduces Blood Glucose and Improves Insulin Secretion. Nucleic Acid Ther. 2019;29(2):67-72. doi:10.1089/nat.2018.0763

38.   Zhu L, Zhong Q, Yang T, Xiao X. Improved Therapeutic Effects on Diabetic Foot by Human Mesenchymal Stem Cells Expressing Malat1 as a Sponge for Microrna-205-5p. Aging (Albany NY). 2019;11(24):12236-12245. doi:10.18632/aging.102562

39.   Liu SX, Zheng F, Xie KL, Xie MR, Jiang LJ, Cai Y. Exercise Reduces Insulin Resistance in Type 2 Diabetes Mellitus Via Mediating the Lncrna Malat1/Microrna-382-3p/Resistin Axis. Molecular therapy Nucleic acids. 2019;18(18):34-44. doi:10.1016/j.omtn.2019.08.002

40.   Liang C, Gao L, Liu Y, Liu Y, Yao R, Li Y, et al. Mir-451 Antagonist Protects against Cardiac Fibrosis in Streptozotocin-Induced Diabetic Mouse Heart. Life Sci. 2019;224:12-22. doi:10.1016/j.lfs.2019.02.059

41.   Munusamy S, Saba H, Mitchell T, Megyesi JK, Brock RW, Macmillan-Crow LA. Alteration of Renal Respiratory Complex-Iii During Experimental Type-1 Diabetes. BMC Endocr Disord. 2009;9:2. doi:10.1186/1472-6823-9-2

42.   Wu J, Luo X, Thangthaeng N, Sumien N, Chen Z, Rutledge MA, et al. Pancreatic Mitochondrial Complex I Exhibits Aberrant Hyperactivity in Diabetes. Biochem Biophys Rep. 2017;11:119-129. doi:10.1016/j.bbrep.2017.07.007

43.   Guo X, Wu J, Du J, Ran J, Xu J. Platelets of Type 2 Diabetic Patients Are Characterized by High Atp Content and Low Mitochondrial Membrane Potential. Platelets. 2009;20(8):588-593. doi:10.3109/09537100903288422

44.   Szendroedi J, Schmid AI, Chmelik M, Toth C, Brehm A, Krssak M, et al. Muscle Mitochondrial Atp Synthesis and Glucose Transport/Phosphorylation in Type 2 Diabetes. PLoS Med. 2007;4(5):e154. doi:10.1371/journal.pmed.0040154

45.   Pandya JD, Sullivan PG, Leung LY, Tortella FC, Shear DA, Deng-Bryant Y. Advanced and High-Throughput Method for Mitochondrial Bioenergetics Evaluation in Neurotrauma. Methods Mol Biol. 2016;1462:597-610. doi:10.1007/978-1-4939-3816-2_32

46.   Smolina N, Bruton J, Kostareva A, Sejersen T. Assaying Mitochondrial Respiration as an Indicator of Cellular Metabolism and Fitness. Methods Mol Biol. 2017;1601:79-87. doi:10.1007/978-1-4939-6960-9_7

47.   Freimer JW, Hu TJ, Blelloch R. Decoupling the Impact of Micrornas on Translational Repression Versus Rna Degradation in Embryonic Stem Cells. eLife. 2018;7. doi:10.7554/eLife.38014

48.   Valencia-Sanchez MA, Liu J, Hannon GJ, Parker R. Control of Translation and Mrna Degradation by Mirnas and Sirnas. Genes Dev. 2006;20(5):515-524. doi:10.1101/gad.1399806

49.   Eisen TJ, Eichhorn SW, Subtelny AO, Bartel DP. Micrornas Cause Accelerated Decay of Short-Tailed Target Mrnas. Mol Cell. 2020;77(4):775-785 e778. doi:10.1016/j.molcel.2019.12.004

50.   O'Brien J, Hayder H, Zayed Y, Peng C. Overview of Microrna Biogenesis, Mechanisms of Actions, and Circulation. Front Endocrinol (Lausanne). 2018;9:402. doi:10.3389/fendo.2018.00402

51.   Gao K, Cheng M, Zuo X, Lin J, Hoogewijs K, Murphy MP, et al. Active Rna Interference in Mitochondria. Cell Res. 2021;31(2):219-228. doi:10.1038/s41422-020-00394-5

52.   Jan Krützfeldt NR, Ravi Braich, Kallanthottathil G. Rajeev, Thomas Tuschl, Muthiah Manoharan & Markus Stoffel. Silencing of Micrornas in Vivo with 'Antagomirs'. Nature. 2005;10.1038/nature04303. doi:10.1038/nature04303

53.   Li Feng, Huanqin Li, , Fan Li, Songhua Bei, Xiaohong Zhang. Lncrna Kcnq1ot1 Regulates Microrna-9-Lmx1a Expression and Inhibits Gastric Cancer Cell Progression. Aging. 2020;12(1). doi:10.18632/aging.102651

54.   Wang Y, Xu Z, Jiang J, Xu C, Kang J, Xiao L, et al. Endogenous Mirna Sponge Lincrna-Ror Regulates Oct4, Nanog, and Sox2 in Human Embryonic Stem Cell Self-Renewal. Dev Cell. 2013;25(1):69-80. doi:10.1016/j.devcel.2013.03.002

55.   Cowan DB, Yao R, Akurathi V, Snay ER, Thedsanamoorthy JK, Zurakowski D, et al. Intracoronary Delivery of Mitochondria to the Ischemic Heart for Cardioprotection. PLoS One. 2016;11(8):e0160889. doi:10.1371/journal.pone.0160889

56.   Masuzawa A, Black KM, Pacak CA, Ericsson M, Barnett RJ, Drumm C, et al. Transplantation of Autologously Derived Mitochondria Protects the Heart from Ischemia-Reperfusion Injury. Am J Physiol Heart Circ Physiol. 2013;304(7):H966-982. doi:10.1152/ajpheart.00883.2012

57.   Pacak CA, Preble JM, Kondo H, Seibel P, Levitsky S, Del Nido PJ, et al. Actin-Dependent Mitochondrial Internalization in Cardiomyocytes: Evidence for Rescue of Mitochondrial Function. Biol Open. 2015;4(5):622-626. doi:10.1242/bio.201511478

58.   Kesner EE, Saada-Reich A, Lorberboum-Galski H. Characteristics of Mitochondrial Transformation into Human Cells. Sci Rep. 2016;6:26057. doi:10.1038/srep26057

59.   Kitani T, Kami D, Matoba S, Gojo S. Internalization of Isolated Functional Mitochondria: Involvement of Macropinocytosis. J Cell Mol Med. 2014;18(8):1694-1703. doi:10.1111/jcmm.12316

60.   R A Menzies PHG. The Turnover of Mitochondria in a Variety of Tissues of Young Adult and Aged Rats. J Biol Chem. 1971;246(8):6. doi,

61.   Gottlieb RA, Stotland A. Mitotimer: A Novel Protein for Monitoring Mitochondrial Turnover in the Heart. J Mol Med (Berl). 2015;93(3):271-278. doi:10.1007/s00109-014-1230-6

62.   Cowan DB, Yao R, Thedsanamoorthy JK, Zurakowski D, Del Nido PJ, McCully JD. Transit and Integration of Extracellular Mitochondria in Human Heart Cells. Sci Rep. 2017;7(1):17450. doi:10.1038/s41598-017-17813-0

63.   Katrangi E, D'Souza G, Boddapati SV, Kulawiec M, Singh KK, Bigger B, et al. Xenogenic Transfer of Isolated Murine Mitochondria into Human Rho0 Cells Can Improve Respiratory Function. Rejuvenation Res. 2007;10(4):561-570. doi:10.1089/rej.2007.0575

64.   Shepherd DL, Nichols CE, Croston TL, McLaughlin SL, Petrone AB, Lewis SE, et al. Early Detection of Cardiac Dysfunction in the Type 1 Diabetic Heart Using Speckle-Tracking Based Strain Imaging. J Mol Cell Cardiol. 2016;90:74-83. doi:10.1016/j.yjmcc.2015.12.001

65.   Pappritz K, Grune J, Klein O, Hegemann N, Dong F, El-Shafeey M, et al. Speckle-Tracking Echocardiography Combined with Imaging Mass Spectrometry Assesses Region-Dependent Alterations. Sci Rep. 2020;10(1):3629. doi:10.1038/s41598-020-60594-2

66.   Li R, Yang J, Yang Y, Ma N, Jiang B, Sun Q, et al. Speckle Tracking Echocardiography in the Diagnosis of Early Left Ventricular Systolic Dysfunction in Type Ii Diabetic Mice. BMC Cardiovasc Disord. 2014;14. doi:10.1186/1471-2261-14-141

67.   Liu JH, Chen Y, Yuen M, Zhen Z, Chan CW, Lam KS, et al. Incremental Prognostic Value of Global Longitudinal Strain in Patients with Type 2 Diabetes Mellitus. Cardiovascular diabetology. 2016;15(22):22. doi:10.1186/s12933-016-0333-5

68.　　Hensel KO, Grimmer F, Roskopf M, Jenke AC, Wirth S, Heusch A. Subclinical Alterations of Cardiac Mechanics Present Early in the Course of Pediatric Type 1 Diabetes Mellitus: A Prospective Blinded Speckle Tracking Stress Echocardiography Study. J Diabetes Res. 2016;2016:2583747. doi:10.1155/2016/2583747

69.　　Biering-Sorensen T, Biering-Sorensen SR, Olsen FJ, Sengelov M, Jorgensen PG, Mogelvang R, et al. Global Longitudinal Strain by Echocardiography Predicts Long-Term Risk of Cardiovascular Morbidity and Mortality in a Low-Risk General Population: The Copenhagen City Heart Study. Circ Cardiovasc Imaging. 2017;10(3). doi:10.1161/CIRCIMAGING.116.005521

70.　　František Sabovčik NC, Celine Vens, Tatiana Kuznetsova. Erratum. European Heart Journal - Digital Health. 2022;3(1):115-116. doi:10.1093/ehjdh/ztab098

71.　　Sengupta PP, Korinek J, Belohlavek M, Narula J, Vannan MA, Jahangir A, et al. Left Ventricular Structure and Function: Basic Science for Cardiac Imaging. J Am Coll Cardiol. 2006;48(10):1988-2001. doi:10.1016/j.jacc.2006.08.030

72.　　Luo C, Ware DL, Zwischenberger JB, Clark JW, Jr. A Mechanical Model of the Human Heart Relating Septal Function to Myocardial Work and Energy. Cardiovasc Eng. 2008;8(3):174-184. doi:10.1007/s10558-008-9054-z

73.　　Kaushik A, Kapoor A, Dabadghao P, Khanna R, Kumar S, Garg N, et al. Use of Strain, Strain Rate, Tissue Velocity Imaging, and Endothelial Function for Early Detection of Cardiovascular Involvement in Young Diabetics. Ann Pediatr Cardiol. 2021;14(1):1-9. doi:10.4103/apc.APC_158_19

74.　　Lindner O, Vogt J, Kammeier A, Wielepp P, Holzinger J, Baller D, et al. Effect of Cardiac Resynchronization Therapy on Global and Regional Oxygen Consumption and Myocardial Blood Flow in Patients with Non-Ischaemic and Ischaemic Cardiomyopathy. Eur Heart J. 2005;26(1):70-76. doi:10.1093/eurheartj/ehi046

75.   Iozzo P, Chareonthaitawee P, Rimoldi O, Betteridge DJ, Camici PG, Ferrannini E. Mismatch between Insulin-Mediated Glucose Uptake and Blood Flow in the Heart of Patients with Type Ii Diabetes. Diabetologia. 2002;45(10):1404-1409. doi:10.1007/s00125-002-0917-3

76.   Borghetti G, von Lewinski D, Eaton DM, Sourij H, Houser SR, Wallner M. Diabetic Cardiomyopathy: Current and Future Therapies. Beyond Glycemic Control. Front Physiol. 2018;9:1514. doi:10.3389/fphys.2018.01514

77.   Salvatore T, Pafundi PC, Galiero R, Albanese G, Di Martino A, Caturano A, et al. The Diabetic Cardiomyopathy: The Contributing Pathophysiological Mechanisms. Front Med (Lausanne). 2021;8:695792. doi:10.3389/fmed.2021.695792

78.   Tran DH, Wang ZV. Glucose Metabolism in Cardiac Hypertrophy and Heart Failure. J Am Heart Assoc. 2019;8(12):e012673. doi:10.1161/JAHA.119.012673

79.   Gibb AA, Hill BG. Metabolic Coordination of Physiological and Pathological Cardiac Remodeling. Circ Res. 2018;123(1):107-128. doi:10.1161/CIRCRESAHA.118.312017

80.   Wende AR, Brahma MK, McGinnis GR, Young ME. Metabolic Origins of Heart Failure. JACC Basic Transl Sci. 2017;2(3):297-310. doi:10.1016/j.jacbts.2016.11.009

81.   Chong CR, Clarke K, Levelt E. Metabolic Remodeling in Diabetic Cardiomyopathy. Cardiovasc Res. 2017;113(4):422-430. doi:10.1093/cvr/cvx018

82.   Connor T, Martin SD, Howlett KF, McGee SL. Metabolic Remodelling in Obesity and Type 2 Diabetes: Pathological or Protective Mechanisms in Response to Nutrient Excess? Clin Exp Pharmacol Physiol. 2015;42(1):109-115. doi:10.1111/1440-1681.12315

83.   Yap J, Tay WT, Teng TK, Anand I, Richards AM, Ling LH, et al. Association of Diabetes Mellitus on Cardiac Remodeling, Quality of Life, and Clinical Outcomes in Heart Failure with Reduced and Preserved Ejection Fraction. J Am Heart Assoc. 2019;8(17):e013114. doi:10.1161/JAHA.119.013114

84.   Russell K, Eriksen M, Aaberge L, Wilhelmsen N, Skulstad H, Gjesdal O, et al. Assessment of Wasted Myocardial Work: A Novel Method to Quantify Energy Loss Due to Uncoordinated Left Ventricular Contractions. Am J Physiol Heart Circ Physiol. 2013;305(7):H996-1003. doi:10.1152/ajpheart.00191.2013

85.   Samset E. Evaluation of Segmental Myocardial Work in the Left Ventricle ge healthcare website: GE Healthcare; 2017. Available from: https://www.gehealthcare.com/-/media/8cab29682ace4ed7841505f813001e33.pdf.

86.   Lionetti V, Guiducci L, Simioniuc A, Aquaro GD, Simi C, De Marchi D, et al. Mismatch between Uniform Increase in Cardiac Glucose Uptake and Regional Contractile Dysfunction in Pacing-Induced Heart Failure. Am J Physiol Heart Circ Physiol. 2007;293(5):H2747-2756. doi:10.1152/ajpheart.00592.2007

87.   Larsen CK, Aalen JM, Stokke C, Fjeld JG, Kongsgaard E, Duchenne J, et al. Regional Myocardial Work by Cardiac Magnetic Resonance and Non-Invasive Left Ventricular Pressure: A Feasibility Study in Left Bundle Branch Block. Eur Heart J Cardiovasc Imaging. 2020;21(2):143-153. doi:10.1093/ehjci/jez231

88.   Hicks S, Labinskyy N, Piteo B, Laurent D, Mathew JE, Gupte SA, et al. Type Ii Diabetes Increases Mitochondrial DNA Mutations in the Left Ventricle of the Goto-Kakizaki Diabetic Rat. Am J Physiol Heart Circ Physiol. 2013;304(7):H903-915. doi:10.1152/ajpheart.00567.2012

89.   Wende AR, Schell JC, Ha CM, Pepin ME, Khalimonchuk O, Schwertz H, et al. Maintaining Myocardial Glucose Utilization in Diabetic Cardiomyopathy Accelerates Mitochondrial Dysfunction. Diabetes. 2020;69(10):2094-2111. doi:10.2337/db19-1057

90.   Dinh A, Miertschin S, Young A, Mohanty SD. A Data-Driven Approach to Predicting Diabetes and Cardiovascular Disease with Machine Learning. BMC Med Inform Decis Mak. 2019;19(1):211. doi:10.1186/s12911-019-0918-5

91.   Kusunose K, Haga A, Abe T, Sata M. Utilization of Artificial Intelligence in Echocardiography. Circ J. 2019;83(8):1623-1629. doi:10.1253/circj.CJ-19-0420

92.   Yasmin F, Shah SMI, Naeem A, Shujauddin SM, Jabeen A, Kazmi S, et al. Artificial Intelligence in the Diagnosis and Detection of Heart Failure: The Past, Present, and Future. Rev Cardiovasc Med. 2021;22(4):1095-1113. doi:10.31083/j.rcm2204121

93.   Chang A, Cadaret LM, Liu K. Machine Learning in Electrocardiography and Echocardiography: Technological Advances in Clinical Cardiology. Curr Cardiol Rep. 2020;22(12):161. doi:10.1007/s11886-020-01416-9

94.   Seetharam K, Raina S, Sengupta PP. The Role of Artificial Intelligence in Echocardiography. Curr Cardiol Rep. 2020;22(9):99. doi:10.1007/s11886-020-01329-7

95.   Smole T, Zunkovic B, Piculin M, Kokalj E, Robnik-Sikonja M, Kukar M, et al. A Machine Learning-Based Risk Stratification Model for Ventricular Tachycardia and Heart Failure in Hypertrophic Cardiomyopathy. Comput Biol Med. 2021;135:104648. doi:10.1016/j.compbiomed.2021.104648

96.   Butt UM, Letchmunan S, Ali M, Hassan FH, Baqir A, Sherazi HHR. Machine Learning Based Diabetes Classification and Prediction for Healthcare Applications. J Healthc Eng. 2021;2021:9930985. doi:10.1155/2021/9930985

97.   Seetharam K, Shrestha S, Sengupta PP. Artificial Intelligence in Cardiovascular Medicine. Curr Treat Options Cardiovasc Med. 2019;21(6):25. doi:10.1007/s11936-019-0728-1

98.   Seetharam K, Kagiyama N, Sengupta PP. Application of Mobile Health, Telemedicine and Artificial Intelligence to Echocardiography. Echo Res Pract. 2019;6(2):R41-R52. doi:10.1530/ERP-18-0081

Andrya J. Durr

Office Address

Biomedical Sciences
Division of Exercise Physiology and Division
Of Cardiovascular and Metabolic Disease
West Virginia University School of Medicine
1 Medical Center Drive
P.O. Box 9227
Morgantown, WV 26506
Tel: (724) 984-8114
Email: ajdurr@mix.wvu.edu
Personal Email: andryajean@gmail.com

Education

May 2022	**Doctor of Philosophy, Exercise Physiology**
	Biomedical Sciences, Department of Exercise Physiology, Division of Cardiovascular and Metabolic Diseases
	Laboratory of Dr. John M. Hollander
	West Virginia University School of Medicine
	Morgantown, West Virginia
	Dissertation topic: Amelioration of Mitochondrial Bioenergetic Dysfunction in Diabetes Mellitus: Delving into Specialized and Nonspecific Therapeutics for the Ailing Heart
May 2016	
	Bachelor of Science, Biology-Pre-Dental/Medical/Veterinarian
	Major: Department of Biology, Environmental Science, and Health Science
	Minor: Psychology
	Waynesburg University
	Waynesburg, Pennsylvania

Professional Experience

February 2022 – Present	**Research Specialist** WVU Office of Health and Human Services School of Public Health • Provides support with data management, analytics, evaluation, and quality improvement support to the OHSR in its work with primary care and community-based organizations.
March 2018 – Present	**Women's Health Volunteer and Advocate** Women on Wellness, Morgantown, WV • Human subject's research including females of all ages and health status through project design, implementation, and coordination of health screening volunteers
March 2018 – June 2019	**Director of Behavior Health and Biometric Research** National Center of Excellence in Women's Health, Morgantown, West Virginia • Assistance with human subject research including project design and implementation requiring data collection, organization, and analysis.

Professional Development

Professional Societies

October 2018 – Present	American Association for the Advancement of Science (AAAS)
August 2018 – August 2019	AmeriCorps Member Innovation Service Champion
August 2017 – 2019	American Heart Association (AHA)
December 2017 – August 2021	American Physiology Society (APS)
December 2017 – June 2018	National center for Excellence in Women's Health
December 2017 – Present	West Virginia Women and Women on Wellness Initiative
February 2021 – Present	International Society for the Study of Women's Sexual Health (ISSWSH)

Community Service and Leadership

Public Service

October 2018 – August 2019	**AmeriCorps Member** Collaborative Direct, Morgantown, West Virginia Collaboration with the West Virginia University National Center for Excellence in Women's Health
June 2019 - Present	Behavioral Health and Biometric Research Assistant for the Women on Wellness initiative
November 2018 – February 2019	Health Screenings Operations Coordinator and Director 2019 Women Love Your Heart event
October 2018 - April 2019	Health Screenings Operations Coordinator and Director 2019 Women on Wellness retreat
July 2018 – June 2019	Director of Behavioral Health and Biometric Research for the National Center for Excellence in Women's Health
October 2017 – March 2018	Volunteer coordination and committee member 2018 Women on Wellness retreat
October 2016 - March 2017	Volunteer coordination and committee member 2017 Women on Wellness retreat

Mentoring

Facilitated laboratory skills for new laboratory members

Fall 2017- 2021	Amina Kunovac (Laboratory member)
Fall 2017 – Spring 2018	Shanawar Waris (Undergraduate Research)
Fall 2018 – Present	Andrew Taylor (Laboratory member)
2018	Shruthi Sreekumar (Intermittent Experience)
Summer 2018 – Spring 2019	Garrett Fink (Undergraduate Research)
2020 Fall -Spring 2021	Katelyn Pinti (Undergraduate Research
Fall 2020 – Present	Anna Korol (Research Rotation)
Fall 2020 – Present)	Saira Rizwan (Laboratory member)
Summer 2021 – Spring 2022	Samantha Weaver (Undergraduate Research)
2021- Present	Ethan Meadows (Mitochondrial Metabolism and Bioenergetics Core Director)

Scientific Achievements

Presentations

Invited Podia Presentations

Cortactin's Influence on Mitochondrial Bioenergetics in the Diabetic Heart: A Novel Viewpoint, Campbell award competition, Experimental Biology, San Diego, CA, 2018, Authors: **Andrya J. Durr**, Danielle L. Shepherd, Quincy A. Hathaway, John M. Hollander

Speckle-Tracking Echocardiography Identifies Early Segmental Abnormalities Preceding Cardiac Dysfunction in a *db/db* Mouse Model, Van Liere, West Virginia University, Morgantown West Virginia, March 22-23rd, 2019. Authors: **Andrya J. Durr**, Quincy A. Hathaway, Mark V. Pinti, Danielle L. Shepherd[1], Amina Kunovac, Garrett K. Fink, John M. Hollander

Stress Strain Speckle-Tacking Segmental Analysis Reveals Early Indications of Diastolic Dysfunction in a Type 2 Mouse Model of Diabetes Mellitus, Experimental Biology, Orlando, Fl, April 2019, Authors: **Andrya J. Durr**, Quincy A. Hathaway, Mark V. Pinti, Danielle L. Shepherd, Amina Kunovac, Garrett K. Fink, John M. Hollander

Poster Presentations

Mitochondrial Bioenergetics in the Diabetic Heart and the Influence of Cortactin, Van Liere, West Virginia University, Morgantown West Virginia, March 2018, Authors: **Andrya J. Durr**, Danielle L. Shepherd, Quincy A. Hathaway, John M. Hollander

Cortactin's Influence on Mitochondrial Bioenergetics in the Diabetic Heart: A Novel Viewpoint, Experimental Biology, San Diego, CA, April 2018, Authors: **Andrya J. Durr**, Danielle L. Shepherd, Quincy A. Hathaway, John M. Hollander

Educational Barriers Inhibit LARC Utilization and Promote Teenage Pregnancy, 8th Annual Appalachian Translational Research Network Summit, Lexington, KY, September 2018, Authors: **A. J. Durr, Graduate Student, Department of Biomedical Sciences, West Virginia University, Director of Behavioral Health and Biometric Research, WV National Center of Excellence in Women's Health**, P. M. Fitzgerald, Nathan Haddad Professor of Business Administration, Marketing Department, West Virginia University College of Business and Economics, Faculty Liaison, WV National Center of Excellence in Women's Health, E. A. Critch, Executive Director, WV National Center of Excellence in Women's Health, R. R. Cain, Obstetrics and Gynecology, West Virginia University, Director, WV National Center of Excellence in Women's Health.

Speckle-Tracking Echocardiography Identifies Early Segmental Abnormalities Preceding Cardiac Dysfunction in a *db/db* Mouse Model, Van Liere, West Virginia University, Morgantown, West Virginia, March 22-23rd, 2019. Authors:

Andrya J. Durr, Quincy A. Hathaway, Mark V. Pinti, Danielle L. Shepherd, Amina Kunovac, Garrett K. Fink, John M. Hollander

Stress Strain Speckle-Tracking Segmental Analysis Reveals Early Indications of Diastolic Dysfunction in a Type 2 Mouse Model of Diabetes Mellitus, Experimental Biology, Orlando, Fl, April 2019, Authors: **Andrya J. Durr**, Quincy A. Hathaway, Mark V. Pinti, Danielle L. Shepherd, Amina Kunovac, Garrett K. Fink, John M. Hollander

Stress Strain Speckle-Tracking Segmental Analysis Reveals Early Indications of Diastolic Dysfunction in a Type 2 Mouse Model of Diabetes Mellitus, Cardiology Grand Rounds, West Virginia University, Morgantown, West Virginia, June 2019, Authors: **Andrya J. Durr**, Quincy A. Hathaway, Mark V. Pinti, Danielle L. Shepherd, Amina Kunovac, Garrett K. Fink, John M. Hollander

LOSS OF MICRORNA-378A FUNCTION RESTORES MITOCHONDRIAL BIOENERGETICS IN A TYPE 2 DIABETIC MOUSE MODEL, NHLBI Mitochondrial Biology Symposium, Bethesda, Maryland, September 2019, Authors: **Andrya Durr**, Quincy Hathaway, Andrew Taylor, Amina Kunovac, Mark Pinti, Danielle Shepherd, Garrett Fink, John Hollander

MicroRNA-378a Loss Enhances Mitochondrial Bioenergetics and Lessens Cardiac Contractile Dysfunction in the Type 2 Diabetic Heart, Experimental Biology, Virtual due to COVID-19, April 2020, Authors: **Andrya J. Durr**, Quincy A. Hathaway, Amina Kunovac, Andrew D. Taylor, Mark V. Pinti, Sarah L. McLaughlin, Danielle L. Shepherd, Garrett K. Fink, and John M. Hollander

Published Abstracts

Cortactin's Influence on Mitochondrial Bioenergetics in the Diabetic Heart: A Novel Viewpoint, Experimental Biology, San Diego, CA, April 2018, Authors: **Andrya J. Durr**, Danielle L. Shepherd, Quincy A. Hathaway, John M. Hollander

Nuclear-mitochondrial crosstalk in the heart during diabetes mellitus – the impact on RNA in mitochondrial subpopulations, Experimental Biology, San Diego, CA, April 2018, Authors: Q. A. Hathaway, D. L. Shepherd, **A. J. Durr**, and J. M. Hollander

Stress Strain Speckle-Tacking Segmental Analysis Reveals Early Indications of Diastolic Dysfunction in a Type 2 Mouse Model of Diabetes Mellitus, Experimental Biology, Orlando, Fl, April 2019, Authors: **Andrya J. Durr**, Quincy A. Hathaway, Mark V. Pinti, Danielle L. Shepherd, Amina Kunovac, Garrett K. Fink, John M. Hollander

MicroRNA Changes in Diabetic Cardiac Mitochondria: What are they doing there?, Experimental Biology, Orlando, Fl, April 2019. M.V. Pinti, Q.A. Hathaway, A. Kunovac, **A.J. Durr**, C.C. Cook, H.G. Roberts, M. Salman, J.M. Hollander

Elevated ROS and Epigenetic Remodeling Disrupt Cardiac Function in Offspring Following Maternal Engineered Nanomaterial (ENM) Exposure, Experimental Biology, Orlando, Fl, April 2019. A. Kunovac, Q.A. Hathaway, M.V. Pinti, **A.J. Durr**, G.K. Fink, W.T. Goldsmith, T.R. Nurkiewicz, J.M. Hollander

Using Machine Learning to Predict the Development of Diabetes and Potential Biomarkers Linked to Cardiac Risk, Experimental Biology, Orlando, Fl, April 2019. Q.A. Hathaway, M.V. Pinti, S.M. Roth, D.C. Sprando, A. Kunovac, **A.J. Durr**, C.C. Cook, G.K. Fink, T.B. Cheuvront, J.H. Grossman, G.A. Aljahli, H.G. Roberts, M. Salman, A.P. Giromini, J.M. Hollander

MicroRNA-378a Loss Enhances Mitochondrial Bioenergetics and Lessens Cardiac Contractile Dysfunction in the Type 2 Diabetic Heart, Experimental Biology, San Diego, CA, (Virtual due to COVID-19), April 2020, Authors: **Andrya J. Durr**, Quincy A. Hathaway, Amina Kunovac, Andrew D. Taylor, Mark V. Pinti, Sarah L. McLaughlin, Danielle L. Shepherd, Garrett K. Fink, and John M. Hollander

Glutathione Peroxidase Influence on Cardiac Remodeling in Progeny of Dams Exposed to Engineered Nanomaterials during Gestation, Experimental Biology, San Diego, CA, (Virtual due to COVID-19), April 2020, Authors: Amina Kunovac[1], Quincy A. Hathaway, Andrew D. Taylor, **Andrya J. Durr**, William T. Goldsmith, Mark V. Pinti, Garrett K. Fink, Timothy R. Nurkiewicz, and John M. Hollander

Loss of Functional Non-Coding RNA Diversity in Diabetic Cardiac Mitochondria, Experimental Biology, San Diego, CA, (Virtual due to COVID-19), April 2020, Authors: Andrew D. Taylor, Quincy A. Hathaway, Amina Kunovac, Mark V. Pinti, Chris C. Cook, Garrett K. Fink, **Andrya J. Durr**, John M. Hollander

LncRNAs imported into mitochondria possess distinct features stratified by machine learning that promote interaction with the mitochondrial import protein PNPase, Experimental Biology, Philadelphia, PA, April 2022, Authors: Andrew Taylor, Quincy Hathaway, Aaron Robart, Chris Cook, Amina Kunovac, **Andrya Durr**, Saira Rizwan, Evan Cramer, Sarah Starcovic, John Hollander

Targeting Diabetic Cardiomyopathy: LncRNA Kcnq1ot1 Rescues Mitochondrial ATP Synthase via Sponging of MiR-378a-5p, Experimental Biology, Philadelphia, PA, April 2022, Authors: **Andrya J. Durr**, Quincy A. Hathaway, Amina Kunovac, Andrew D. Taylor, Saira Rizwan, Chris C. Cook, and John M. Hollander

Machine Learning to Identify Regional and Segmental Dysfunction during Type 2 Diabetes Mellitus Progression, Experimental Biology, Philadelphia, PA, April 2022, Authors: Saira Rizwan, **Andrya J. Durr**, Anna Korol, Quincy A. Hathaway, Amina Kunovac, Andrew D. Taylor, Mark V. Pinti, and John M. Hollander

Non-published Abstracts

FpvA Peptide Vaccine Confers Protection against P. aeruginosa Infections in Acute Murine Pneumonia. American Society of Microbiologists (ASM), 2016. Emel Sen Kilic, Catherine Blackwood, Shelby Bradford, Dylan Boehm, Melinda Varney, Ting Wong, Katherine DeRoos, Justin Bevere, **Andrya Jean Durr**, William Witt, Matthew Epperly, F. Heath Damron, Mariette Barbier

Engineered Nanomaterial Exposure: Effects on Epigenetic and MiR Regulation of Cardiac Mitochondria, Society of Toxicology, San Antonio, TX, March 2018. Q.A. Hathaway, C.E. Nichols, D.L. Shepherd, **A.J. Durr**, P.A. Stapleton, A.B. Abukabda, T.R. Nurkiewicz, and J.M. Hollander

Epigenetics in Diabetes, Van Liere, West Virginia University, Morgantown West Virginia, March 2018. Bethany Noble BS, Quincy Hathaway BS, **Andrya Durr BS**, Danielle Shepherd PhD

Non-coding RNA and the Mitochondrion – Function and Pathology in the Heart, Van Liere, West Virginia University, Morgantown West Virginia, March 2018. Q. A. Hathaway, M. V. Pinti, **A. J. Durr**, D. L. Shepherd, and J. M. Hollander

Educational Barriers Inhibit LARC Utilization and Promote Teenage Pregnancy, 8th Annual Appalachian Translational Research Network Summit, Lexington, KY, September 2018, Authors: **A. J. Durr,** Graduate Student, Department of Biomedical Sciences, West Virginia University, Director of Behavioral Health and Biometric Research, WV National Center of Excellence in Women's Health, P. M. Fitzgerald, Nathan Haddad Professor of Business Administration, Marketing Department, West Virginia University College of Business and Economics, Faculty Liaison, WV National Center of Excellence in Women's Health, E. A. Critch, Executive Director, WV National Center of Excellence in Women's Health, R. R. Cain, Obstetrics and Gynecology, West Virginia University, Director, WV National Center of Excellence in Women's Health.

Speckle-Tracking Echocardiography Identifies Early Segmental Abnormalities Preceding Cardiac Dysfunction in a *db/db* Mouse Model, Van Liere, West Virginia University, Morgantown West Virginia, March 22-23, 2019. Authors: **Andrya J. Durr**, Quincy A. Hathaway, Mark V. Pinti, Danielle L. Shepherd, Amina Kunovac, Garrett K. Fink, John M. Hollander

LOSS OF MICRORNA-378A FUNCTION RESTORES MITOCHONDRIAL BIOENERGETICS IN A TYPE 2 DIABETIC MOUSE MODEL, NHLBI Mitochondrial Biology Symposium, Bethesda, Maryland, September 2019, Authors: **Andrya Durr**, Quincy Hathaway, Andrew Taylor, Amina Kunovac, Mark Pinti, Danielle Shepherd, Garrett Fink, John Hollander

Applying Machine-Learning to Disease Diagnosis through Patient-Matched Omics Profiles, NHLBI Mitochondrial Biology Symposium, Bethesda, Maryland, September 2019, Authors: Quincy Hathaway, Skyler Roth, Mark Pinti, Daniel Sprando, Amina Kunovac, **Andrya Durr**, Chris Cook, Garrett Fink, Tristen Cheuvront, Jasmine Grossman, Ghadah Aljahli, Andrew Taylor, Andrew Giromini, Jessica Allen, John Hollander

ANTIOXIDANT PROTECTION ATTENUATES CARDIAC AND MITOCHONDRIAL DYSFUNCTION IN OFFSPRING FOLLOWING MATERNAL ENGINEERED NANOMATERIAL EXPOSURE, NHLBI Mitochondrial Biology Symposium, Bethesda, Maryland, September 2019, Authors: Amina Kunovac, Quincy Hathaway, **Andrya Durr**, William Goldsmith, Andrew Taylor, Mark Pinti, Garrett Fink, Timothy Nurkiewicz, John Hollander

IMPACT OF DIABETES MELLITUS ON MITOCHONDRIAL MIR DIVERSITY AND RELATED CELLULAR PATHWAYS, NHLBI Mitochondrial Biology Symposium, Bethesda, Maryland, September 2019, Authors: Andrew Taylor, Quincy Hathaway, Amina Kunovac, Mark Pinti, Chris Cook, Garrett Fink, **Andrya Durr**, Danielle Shepherd, Aaron Robart, John Hollander

Interstitial Mitochondria Localize to Cellular membrane following transplantation in HL-1 Cardiomyocytes, Undergraduate Research Symposium West Virginia University, Morgantown, West Virginia, April 2020, Authors: Katelyn G. Pinti, **Andrya Durr**, John M. Hollander

Identifying Mitochondrial Localization Patterns Following Transplantation in Murine Models, Van Liere, West Virginia University, Morgantown, West Virginia, April 2020, Authors: Katelyn G. Pinti, **Andrya J. Durr**, Andrew D. Taylor, Amina Kunovac and John M. Hollander

Publications

Manuscripts

Exploring the mitochondrial microRNA import pathway through Polynucleotide Phosphorylase (PNPase), *Journal of Molecular and Cellular Cardiology.* 2017 Sep. Shepherd DL, Hathaway QA, Pinti MV, Nichols CE, **Durr AJ**, Sreekumar S, Hughes KM, Stine SM, Martinez I, Hollander JM.

Regulating MicroRNA Expression: At the Heart of Diabetes Mellitus and the Mitochondrion, *Am J Physiol Heart Circ Physiol*. 2017 Oct 6. Hathaway QA, Pinti MV, **Durr AJ**, Waris S, Shepherd DL, Hollander JM.

Reactive Oxygen Species Damage Drives Cardiac and Mitochondrial Dysfunction Following Acute Nano-Titanium Dioxide Inhalation Exposure, *Nanotoxicology*. 2018 Feb 12. Nichols, Cody E; Shepherd, Danielle L; Hathaway, Quincy A; **Durr, Andrya J**; Thapa, Dharendra; Abukabda, Alaeddin; Yi, Jinghai; Nurkiewicz, Tim; Hollander, John M

Mitochondrial Proteome Disruption in the Diabetic Heart Through Targeted Epigenetic Regulation at the Mitochondrial Heat Shock Protein 70 (mtHsp70) Nuclear Locus, *Journal of Molecular and Cellular Cardiology*. 2018 Jun. Danielle L. Shepherd, Quincy A. Hathaway, Cody E. Nichols, **Andrya J. Durr**, Mark V. Pinti, Kristen M. Hughes, Amina Kunovac, Seth M. Stine, and John M. Hollander

Mitochondria dysfunction in type 2 diabetes mellitus: an organ-based analysis, *AJP-Endocrinology and Metabolism*. 2019 Feb 1. Mark V Pinti, Garrett K Fink, Quincy A Hathaway, **Andrya J Durr**, Amina Kunovac, and John M Hollander

Machine-learning to stratify diabetic patients using novel cardiac biomarkers and integrative genomics, *Cardiovascular Diabetology*. 2019 Jun 11. Quincy A Hathaway; Skyler M Roth; Mark V Pinti; Dan C Sprando; Amina Kunovac; **Andrya J Durr**; Chris C Cook; Garrett K Fink; Tristen B Cheuvront; Jasmine H Grossman; Ghadah A Aljahli; Andrew D Taylor; Andrew P Giromini; Jessica L Allen; John Michael Hollander

MiR-378a as a Key Regulator of Cardiovascular Health Following Engineered Nanomaterial Inhalation Exposure, *Nanotoxicology*. 2019 Jun 13. Hathaway, Quincy A; **Durr, Andrya J**; Shepherd, Danielle L; Pinti, Mark V; Brandebura, Ashley N; Nichols, Cody E; Kunovac, Amina; Goldsmith, William T; Friend, Sherri; Abukabda, Alaeddin; Fink, Garrett K; Nurkiewicz, Tim; Hollander, John M

The role of SIRT1 in skeletal muscle function and repair of older mice, *Journal of Cachexia, Sarcopenia and Muscle.* 2019 Aug 10. Myers MJ, Shepherd DL, **Durr AJ**, Stanton DS, Mohamed JS, Hollander JM, Alway SE

ROS Promote Epigenetic Remodeling and Cardiac Dysfunction in Offspring Following Maternal Engineered Nanomaterial (ENM) Exposure, *Particle and fibre toxicology*. 2019 Jun 18. Amina Kunovac; Quincy A. Hathaway; Mark V. Pinti; William T. Goldsmith; **Andrya J. Durr**; Garrett K. Fink; Timothy R. Nurkiewicz; John M. Hollander, Ph.D.

Untangling the Roots of the West Virginia Opioid Crisis: Relationships in Adolescent Pregnancy, Drug Abuse, and Future Outcomes, *J Osteopath Med.* 2021 February 12. **Andrya J. Durr**, BS, Elizabeth A. Critch, MBA, M. Paula Fitzgerald, PhD, BS, Kylie A. Fuller, MD, Kelly M. Devlin, MD, Roberta I. Renzelli-Cain, DO, MHS

Enhanced antioxidant capacity prevents epitranscriptomic and cardiac alterations in adult offspring gestationally-exposed to ENM. Nanotoxicology. 2021 May 8:1-20. doi: 10.1080/17435390.2021.1921299. Kunovac A, Hathaway QA, Pinti MV, **Durr AJ**, Taylor AD, Goldsmith WT, Garner KL, Nurkiewicz TR, Hollander JM.

What Providers Know vs. What Providers Do: Barriers to Contraception in Adolescents. West Virginia Medical Journal. 2021 June. Authors: **Andrya J. Durr**, BS, Elizabeth A. Critch, MBA, M. Paula Fitzgerald, PhD, Kylie A. Fuller, BS, Kelly M. Devlin, MD, Roberta I. Renzelli-Cain, DO, MHS

Manipulation of the MiR-378a/mt-ATP6 Regulatory Axis Rescues ATP Synthase in the Diabetic Heart and Offers a Novel Role for LncRNA Kcnq1ot1. *Am J Physiol Cell Physiol.* 2022 Feb 2. **Andrya J Durr**, Quincy A Hathaway, Amina Kunovac, Andrew D Taylor, Mark V Pinti, Saira Rizwan, Danielle L Shepherd, Chris C Cook, Garrett K Fink, John M Hollander

Awards and Recognition

2018-Present

Grant Co-investigator
Ruby Memorial Hospital Heart and Vascular Institute Research Collaboration
Project title: Quantitative Myocardial Blood Flow assessment by Adenosine Stress Cardiac Magnetic Resonance Imaging in Perimenopausal Women with and without Hormone Replacement Therapy (HRT) in the Contemporary Era: A Pilot Study
- Funded March 2020 – WVU CTSI pilot grant